

South Dakota  
Department of Transportation  
Office of Research



U.S. Department  
of Transportation  
Federal Highway  
Administration

SD2007-04-F



# **Structural Performance of Prestressed Self-Consolidating Concrete Bridge Girders Made with Limestone Aggregates**

**Study SD2007-04  
Final Report**

Prepared by  
Nadim Wehbe, Arden Sigl, Zachary Gutzmer, and Chad Stripling

South Dakota State University  
Department of Civil & Environmental Engineering  
Brookings, SD 57007

May 2009

## DISCLAIMER

The contents of this report reflect the views of the authors who are responsible for the facts and accuracy of the data presented herein. The contents do not necessarily reflect the official views or policies of the South Dakota Department of Transportation, the State Transportation Commission, the South Dakota Highway Patrol, or the Federal Highway Administration. This report does not constitute a standard, specification, or regulation.

## ACKNOWLEDGEMENTS

This work was performed under the supervision of the SD2007-04 Technical Panel:

Mark Clausen.....	Federal Highway Administration	Hadly Eisenbeisz .....	Bridge Design
Ron Dahme .....	Mitchell Region	Paul Oien .....	Roadway Design
Phil Graham.....	BASF Construction Chemicals	Terry Coomes .....	W. R. Grace
Corey Haeder.....	Cretex West	Pat Sweetman .....	Concrete Materials
Darin Hodges.....	Materials & Surfacing	Matt Stone .....	Rapid City Region
Dan Johnston .....	Research		

Funding for the work presented in this report was provided by the South Dakota Department of Transportation, the Mountain-Plains Consortium University Transportation Center, and Cretex Concrete Products West, Inc.



## TECHNICAL REPORT STANDARD TITLE PAGE

1. Report No. <b>SD2007-04-F</b>		2. Government Accession No.		3. Recipient's Catalog No.	
4. Title and Subtitle <b>Structural Performance of Prestressed Self-Consolidating Concrete Bridge Girders Made with Limestone Aggregates</b>				5. Report Date <b>May 4, 2009</b>	
				6. Performing Organization Code	
7. Author(s) <b>Nadim Wehbe, Arden Sigl, Zachary Gutzmer, and Chad Stripling</b>				8. Performing Organization Report No.	
9. Performing Organization Name and Address <b>South Dakota State University Department of Civil &amp; Environmental Engineering Brookings, SD 57007</b>				10. Work Unit No.	
				11. Contract or Grant No.	
12. Sponsoring Agency Name and Address <b>South Dakota Department of Transportation Office of Research 700 East Broadway Avenue Pierre, SD 57501-2586</b>				13. Type of Report and Period Covered <b>Final Report July 2007 to April 2009</b>	
				14. Sponsoring Agency Code <b>310976</b>	
15. Supplementary Notes					
16. Abstract <p>This study was designed to investigate the structural performance of prestressed SCC bridge girders made with limestone aggregates and to develop draft specifications, acceptance criteria, mix qualifications, and guidelines for use by SDDOT for prestressed SCC applications. The study covered in this report involved material testing of SCC mixtures and structural testing of full-scale prestressed bridge girders. Three SCC mix mixtures (w/c ratios of 0.33, 0.35, and 0.37) and one conventional concrete mixture (w/c ratio of 0.33) were developed and investigated, and three full-scale prestressed girders were fabricated and tested to failure. Two of the girders were cast with SCC and one was cast with conventional concrete to serve as a control specimen. The control specimen and one of the SCC specimens were tested under increasing monotonic load until failure. The other SCC specimen was tested under increasing cyclic loading until failure. The evaluation of SCC for use in prestressed bridge girder applications included analysis of transfer length, prestress losses, camber, flexural behavior and strength, flexural rigidity, and shear strength.</p> <p>The results indicated that the strength growth, shrinkage, modulus of rupture, and modulus of elasticity of SCC can be determined using existing empirical equations that are used for conventional concrete. The transfer length, strength, stiffness, and prestress losses of the SCC girders were similar to those of the conventional concrete girders and were predictable using current code equations and methods. Special provisions for the use of SCC for prestressed/precast elements were developed.</p>					
17. Keywords <b>Bridges; Bridge Girders; Prestressed Concrete; Self-Consolidating Concrete; SCC</b>			18. Distribution Statement <b>No restrictions. This document is available to the public from the sponsoring agency.</b>		
19. Security Classification (of this report) <b>Unclassified</b>		20. Security Classification (of this page) <b>Unclassified</b>		21. No. of Pages <b>220</b>	
				22. Price	

## TABLE OF CONTENTS

<b>1</b>	<b>EXECUTIVE SUMMARY</b>	<b>1</b>
<b>2</b>	<b>PROBLEM DESCRIPTION</b>	<b>3</b>
<b>3</b>	<b>OBJECTIVES AND SCOPE</b>	<b>5</b>
<b>3.1</b>	<b>OBJECTIVES</b>	<b>5</b>
<b>3.2</b>	<b>SCOPE</b>	<b>5</b>
3.2.1	Study of Concrete Mixtures	6
3.2.2	Study of Full-Scale Bridge Girders	6
<b>4</b>	<b>TASK DESCRIPTION</b>	<b>7</b>
<b>5</b>	<b>LITERATURE REVIEW</b>	<b>10</b>
<b>5.1</b>	<b>INTRODUCTION</b>	<b>10</b>
<b>5.2</b>	<b>SCC CONSTITUENT MATERIALS AND PROPERTIES</b>	<b>10</b>
5.2.1	Constituent Materials	10
5.2.2	Fresh Properties	11
5.2.3	Hardened Properties	13
5.2.4	Shrinkage	14
<b>5.3</b>	<b>SCC PROVISIONS BY DEPARTMENTS OF TRANSPORTATION</b>	<b>15</b>
5.3.1	North Carolina DOT	16
5.3.2	Illinois DOT	16
5.3.3	Michigan DOT	16
5.3.4	South Dakota DOT	16
<b>5.4</b>	<b>TRANSFER LENGTH OF PRESTRESSING STRANDS</b>	<b>17</b>
5.4.1	Code Provisions for Transfer Length	17
5.4.2	Buckner	17
5.4.3	Russell and Burns	18
5.4.4	Barnes, Grove, and Burns	19
5.4.5	Girgis and Tuan	20
<b>5.5</b>	<b>PRESTRESS LOSSES</b>	<b>20</b>
5.5.1	AASHTO Standard Specifications for Highway Bridges Methods	21
5.5.2	AASHTO LRFD Approximate Method	22
5.5.3	PCI Design Handbook Method	23
5.5.4	PCI Committee on Prestress Losses Method	25
<b>5.6</b>	<b>CAMBER</b>	<b>28</b>
<b>5.7</b>	<b>FLEXURAL STRENGTH OF PRESTRESSED CONCRETE GIRDERS</b>	<b>29</b>
5.7.1	ACI Code Provisions for Flexural Strength	30
5.7.2	AASHTO-LRFD Provisions for Flexural Strength	31
<b>5.8</b>	<b>SHEAR STRENGTH OF PRESTRESSED CONCRETE GIRDERS</b>	<b>31</b>
5.8.1	ACI Code Provisions	31
5.8.2	AASHTO-LRFD Provisions for Shear Strength	33
<b>5.9</b>	<b>PREVIOUS TESTS OF FULL-SCALE PRESTRESSED SCC GIRDERS</b>	<b>35</b>
5.9.1	Hamilton, Labonte, and Ansley	35

5.9.2	Naito, Parent, and Brunns	36
<b>6</b>	<b>EVALUATION OF SCC MIXTURES WITH LIMESTONE AGGREGATE</b>	<b>37</b>
<b>6.1</b>	<b>AGGREGATES MEASURED PROPERTIES</b>	<b>37</b>
6.1.1	Sieve Analysis	37
6.1.2	Density, Specific Gravity, and Absorption	38
6.1.3	Bulk Density	39
<b>6.2</b>	<b>LABORATORY CONCRETE MIXTURES</b>	<b>39</b>
6.2.1	Mix Design	39
6.2.2	Mixing and Batching	41
6.2.3	Curing Methods	41
<b>6.3</b>	<b>FRESH PROPERTIES</b>	<b>42</b>
6.3.1	Slump Flow	42
6.3.2	Visual Stability Index (VSI) and $T_{20}$	45
6.3.3	J-Ring Spread	45
6.3.4	L-Box	47
6.3.5	Column Segregation	48
6.3.6	Air Content	49
6.3.7	Mix Temperature	50
<b>6.4</b>	<b>HARDENED PROPERTIES</b>	<b>50</b>
6.4.1	Compressive Strength	50
6.4.2	Flexural Strength (Modulus of Rupture)	53
6.4.3	Modulus of Elasticity	57
6.4.4	Hardened Visual Stability Index (HVSF)	61
<b>6.5</b>	<b>SHRINKAGE</b>	<b>61</b>
<b>7</b>	<b>STRUCTURAL PERFORMANCE OF PRESTRESSED SCC GIRDERS</b>	<b>66</b>
<b>7.1</b>	<b>INTRODUCTION</b>	<b>66</b>
<b>7.2</b>	<b>DESIGN OF TEST SPECIMENS</b>	<b>66</b>
<b>7.3</b>	<b>INSTRUMENTATION</b>	<b>70</b>
7.3.1	Strain Gages	70
7.3.2	Detachable Mechanical Points	72
7.3.3	Extensometers	73
<b>7.4</b>	<b>SPECIMEN FABRICATION AND DELIVERY</b>	<b>75</b>
<b>7.5</b>	<b>TEST SET UP AND PROCEDURE</b>	<b>78</b>
7.5.1	Test Set Up	78
7.5.2	Test Procedure	78
<b>7.6</b>	<b>MEASURED MATERIAL PROPERTIES</b>	<b>80</b>
7.6.1	Fresh Concrete Properties	81
7.6.2	Concrete Compressive Strength	81
7.6.3	Prestressing Strands	82
<b>7.7</b>	<b>TRANSFER LENGTH</b>	<b>83</b>
7.7.1	Measured Transfer Length	83
7.7.2	Comparison of Measured and Calculated Transfer Length	85



<b>7.8</b>	<b>PRESTRESS LOSSES</b>	<b>86</b>
7.8.1	Measured Prestress Losses	86
7.8.2	Theoretical Prestress Losses	89
7.8.3	Comparison of Measured and Calculated Prestress Losses	92
<b>7.9</b>	<b>CAMBER</b>	<b>93</b>
<b>7.10</b>	<b>LOAD TESTING RESULTS</b>	<b>94</b>
7.10.1	Girder AL Experimental Results	94
7.10.2	Girder BL Experimental Results	103
7.10.3	Girder CL Experimental results	112
<b>7.11</b>	<b>ANALYSIS OF FLEXURAL BEHAVIOR AND STRENGTH</b>	<b>121</b>
7.11.1	Measured Load-Deflection Characteristics	121
7.11.2	Effective Stiffness under Cyclic Loading	122
7.11.3	Analytical Evaluation of Flexural Behavior	123
<b>7.12</b>	<b>ANALYSIS OF CONCRETE SHEAR STRENGTH</b>	<b>131</b>
7.12.1	Experimental Evaluation of Concrete Shear Strength	131
7.12.2	Comparison of Experimental and Analytical Concrete Shear Strength	133
<b>8</b>	<b>PRESTRESSED QUARTZITE-AGGREGATE SCC GIRDERS</b>	<b>135</b>
<b>8.1</b>	<b>INTRODUCTION</b>	<b>135</b>
<b>8.2</b>	<b>SPECIMEN DESCRIPTION, INSTRUMENTATION, AND TEST SET UP</b>	<b>135</b>
<b>8.3</b>	<b>EXPERIMENTAL RESULTS</b>	<b>137</b>
8.3.1	Measured Material Properties	137
8.3.2	Transfer Length	138
8.3.3	Load Testing Results	139
<b>9</b>	<b>EVALUATION OF SCC FOR PRESTRESSED BRIDGE GIRDERS</b>	<b>148</b>
<b>9.1</b>	<b>CONSTRUCTABILITY</b>	<b>148</b>
<b>9.2</b>	<b>FINISHED PRODUCT</b>	<b>148</b>
<b>9.3</b>	<b>MATERIAL AND STRUCTURAL PERFORMANCE</b>	<b>149</b>
<b>9.4</b>	<b>ECONOMIC EVALUATION</b>	<b>149</b>
<b>9.5</b>	<b>SPECIAL PROVISIONS</b>	<b>150</b>
<b>10</b>	<b>SUMMARY, CONCLUSIONS, AND RECOMMENDATIONS</b>	<b>151</b>
<b>10.1</b>	<b>SUMMARY</b>	<b>151</b>
<b>10.2</b>	<b>CONCLUSIONS</b>	<b>152</b>
<b>10.3</b>	<b>IMPLEMENTATION AND RECOMMENDATIONS</b>	<b>153</b>
	<b>REFERENCES</b>	<b>154</b>
	<b>APPENDIX A: AGGREGATE TESTING DATA</b>	<b>157</b>
	<b>APPENDIX B: ADMIXTURE LITERATURE</b>	<b>167</b>
	<b>APPENDIX C: GIRDER DETAILS</b>	<b>177</b>
	<b>APPENDIX D: GIRDER INSTRUMENTATION DETAILS</b>	<b>178</b>
	<b>APPENDIX E: CRACK MAPS</b>	<b>183</b>
	<b>APPENDIX F: SPECIAL PROVISIONS</b>	<b>197</b>

## LIST OF FIGURES

FIGURE 2.1: MEASUREMENT METHODS OF CONCRETE FLOWABILITY.....	3
FIGURE 5.1: SLUMP FLOW TEST.....	11
FIGURE 5.2: J-RING TEST.....	12
FIGURE 5.3: L-BOX TEST.....	12
FIGURE 5.4: COLUMN SEGREGATION TEST.....	13
FIGURE 6.1: $\frac{3}{8}$ " LIMESTONE CHIP COARSE AGGREGATE.....	37
FIGURE 6.2: COARSE AGGREGATE GRAIN DISTRIBUTION.....	38
FIGURE 6.3: FINE AGGREGATE GRAIN DISTRIBUTION.....	38
FIGURE 6.4: HEAT (ACCELERATED) CURING BOX.....	41
FIGURE 6.5: HEAT CURING STEP-UP AND SOAK .....	42
FIGURE 6.6: MEASURED AVERAGE SLUMP SPREAD VERSUS W/C AND AMOUNT OF SUPERPLASTICIZER.....	44
FIGURE 6.7: MEASURED AVERAGE SLUMP SPREAD VERSUS NORMALIZED AMOUNT OF SUPERPLASTICIZER.....	44
FIGURE 6.8: $T_{20}$ VERSUS NORMALIZED AMOUNT OF SUPERPLASTICIZER.....	45
FIGURE 6.9: MEASURED BLOCKING POTENTIAL .....	46
FIGURE 6.10: BLOCKING POTENTIAL VERSUS AMOUNT OF SUPERPLASTICIZER AND W/C RATIO.....	46
FIGURE 6.11: BLOCKING POTENTIAL VERSUS NORMALIZED AMOUNT OF SUPERPLASTICIZER .....	47
FIGURE 6.12: MEASURED L-BOX RATIOS.....	47
FIGURE 6.13: MEASURED L-BOX RATIO VERSUS AMOUNT OF SUPERPLASTICIZER AND W/C RATIO .....	48
FIGURE 6.14: MEASURED COLUMN SEGREGATION .....	48
FIGURE 6.15: MEASURED AIR CONTENT .....	49
FIGURE 6.16: AMOUNT OF AIR ENTRAINER VERSUS NORMALIZED AMOUNT OF SUPERPLASTICIZER FOR AIR CONTENT = 7.6% .....	50
FIGURE 6.17: COMPRESSIVE STRENGTH VERSUS AGE OF CONCRETE .....	51
FIGURE 6.18: MEASURED AND THEORETICAL STRENGTH GAIN FOR S33 .....	52
FIGURE 6.19: MEASURED AND THEORETICAL STRENGTH GAIN FOR S35 .....	52
FIGURE 6.20: MEASURED AND THEORETICAL STRENGTH GAIN FOR S37 .....	53
FIGURE 6.21: MEASURED AND THEORETICAL STRENGTH GAIN FOR S33-A .....	53
FIGURE 6.22: MEASURED FLEXURAL STRENGTH VERSUS AGE OF CONCRETE .....	54
FIGURE 6.23: MEASURED FLEXURAL STRENGTH AT 18 HOURS.....	55
FIGURE 6.24: MEASURED FLEXURAL STRENGTH AT 3 DAYS.....	55
FIGURE 6.25: MEASURED FLEXURAL STRENGTH AT 7 DAYS.....	56
FIGURE 6.26: MEASURED FLEXURAL STRENGTH AT 14 DAYS.....	56
FIGURE 6.27: MEASURED FLEXURAL STRENGTH AT 28 DAYS.....	57
FIGURE 6.28: MEASURED FLEXURAL STRENGTH AT ALL AGES.....	57
FIGURE 6.29: MEASURED MODULUS OF ELASTICITY VERSUS AGE OF CONCRETE .....	58
FIGURE 6.30: MEASURED AND THEORETICAL MODULUS OF ELASTICITY FOR S33 .....	59
FIGURE 6.31: MEASURED AND THEORETICAL MODULUS OF ELASTICITY FOR S35 .....	59



FIGURE 6.32: MEASURED AND THEORETICAL MODULUS OF ELASTICITY FOR S37 .....	60
FIGURE 6.33: MEASURED AND THEORETICAL MODULUS OF ELASTICITY FOR S33-A .....	60
FIGURE 6.34: MODULUS OF ELASTICITY VERSUS AGE OF CONCRETE.....	61
FIGURE 6.35: SAWN CYLINDER FOR HVSI EVALUATION.....	61
FIGURE 6.36: SHRINKAGE BEAM MOLD .....	62
FIGURE 6.37: MEASURED AND CALCULATED SHRINKAGE STRAIN FOR S33.....	63
FIGURE 6.38: MEASURED AND CALCULATED SHRINKAGE STRAIN FOR S35.....	63
FIGURE 6.39: MEASURED AND CALCULATED SHRINKAGE STRAIN FOR S37.....	64
FIGURE 6.40: MEASURED AND CALCULATED SHRINKAGE STRAIN FOR CC33 .....	64
FIGURE 6.41: MEASURED SHRINKAGE STRAIN FOR ALL MIXES .....	65
FIGURE 7.1: SCHEMATIC CROSS SECTION OF THE HYPOTHETICAL BRIDGE.....	66
FIGURE 7.2: GIRDER CROSS SECTION AND STRAND LAYOUT .....	67
FIGURE 7.3: DETAILS OF TRANSVERSE AND NON-PRESTRESSED LONGITUDINAL REINFORCEMENT .....	68
FIGURE 7.4: CROSS SECTION OF THE TEST SPECIMENS .....	69
FIGURE 7.5: COORDINATE SYSTEM AND STRAND NUMBERING METHOD.....	70
FIGURE 7.6: STRAND STRAIN GAGE .....	71
FIGURE 7.7: TRANSFER LENGTH STRAIN GAGES.....	71
FIGURE 7.8: EMBEDDED STRAIN GAGE .....	72
FIGURE 7.9: LINE OF DEMEC POINTS .....	73
FIGURE 7.10: WHITTEMORE GAGE, BRASS INSERT, CONTACT SEAT, AND CONTACT POINT.....	73
FIGURE 7.11: LVDT FOR DEFLECTION MEASUREMENT AT MID-SPAN.....	74
FIGURE 7.12: CABLE-EXTENSION TRANSDUCER .....	74
FIGURE 7.13: STRAIN MEASUREMENT LVDTs.....	75
FIGURE 7.14: FABRICATION OF THE GIRDER SPECIMENS .....	76
FIGURE 7.15: DECK FORMWORK AND REINFORCEMENT .....	77
FIGURE 7.16: GIRDER DELIVERY AND UNLOADING .....	78
FIGURE 7.17: SCHEMATIC OF TEST SET UP .....	79
FIGURE 7.18: TEST SET UP OF A GIRDER SPECIMEN.....	79
FIGURE 7.19: STEEL SEATING PLATE.....	80
FIGURE 7.20: CRACK MARKING.....	80
FIGURE 7.21: PRESTRESSING STRAND LOAD VERSUS STRAIN.....	83
FIGURE 7.22: MEASURED CONCRETE STRAIN ALONG POTENTIAL TRANSFER LENGTH.....	84
FIGURE 7.23: MEASURED TRANSFER LENGTH FOR GIRDER AL.....	84
FIGURE 7.24: MEASURED TRANSFER LENGTH FOR GIRDER BL.....	85
FIGURE 7.25: MEASURED TRANSFER LENGTH FOR GIRDER CL.....	85
FIGURE 7.26: MEASURED PRESTRESS LOSSES FOR GIRDER AL .....	87
FIGURE 7.27: MEASURED PRESTRESS LOSSES FOR GIRDER BL .....	87
FIGURE 7.28: MEASURED PRESTRESS LOSSES FOR GIRDER CL .....	87
FIGURE 7.29: AVERAGE MEASURED PRESTRESS LOSSES FOR GIRDER AL AND GIRDER CL .....	88



FIGURE 7.30: COMPARISON OF MEASURED AND CALCULATED EFFECTIVE PRESTRESS.....	93
FIGURE 7.31: COMPARISON OF MEASURED AND CALCULATED CAMBER.....	94
FIGURE 7.32: GIRDER AL AT DIFFERENT STAGES DURING THE TEST .....	95
FIGURE 7.33: MEASURED LOAD-DEFLECTION – GIRDER AL .....	96
FIGURE 7.34: MEASURED STRAND STRAIN AT MID-SPAN RESULTING FROM EXTERNAL LOAD – GIRDER AL.....	96
FIGURE 7.35: MEASURED STRAND STRAIN AT MID-SPAN RESULTING FROM ALL LOADS – GIRDER AL..	97
FIGURE 7.36: MEASURED STRAND STRAIN AT QUARTER-SPAN RESULTING FROM EXTERNAL LOAD – GIRDER AL .....	98
FIGURE 7.37: MEASURED STRAND STRAIN AT QUARTER-SPAN RESULTING FROM ALL LOADS – GIRDER AL.....	98
FIGURE 7.38: MEASURED CONCRETE STRAIN AT MID-SPAN RESULTING FROM EXTERNAL LOAD – GIRDER AL.....	99
FIGURE 7.39: MEASURED CONCRETE STRAIN AT MID-SPAN RESULTING FROM ALL LOADS – GIRDER AL .....	99
FIGURE 7.40: MEASURED CONCRETE STRAIN AT QUARTER-SPAN RESULTING FROM EXTERNAL LOAD – GIRDER AL .....	100
FIGURE 7.41: MEASURED CONCRETE STRAIN AT QUARTER-SPAN RESULTING FROM ALL LOADS – GIRDER AL.....	100
FIGURE 7.42: MEASURED COMPRESSIVE STRAIN ALONG TOP HORIZONTAL LVDT AT MID-SPAN – GIRDER AL .....	101
FIGURE 7.43: MEASURED TENSILE STRAIN ALONG BOTTOM HORIZONTAL LVDT AT MID-SPAN – GIRDER AL.....	101
FIGURE 7.44: MEASURED STRAIN ALONG STIRRUP @ 22.5" – GIRDER AL .....	102
FIGURE 7.45: MEASURED STRAIN ALONG STIRRUP @ 52.5" – GIRDER AL .....	102
FIGURE 7.46: MEASURED STRAIN ALONG STIRRUP @ 82.5" – GIRDER AL .....	103
FIGURE 7.47: MEASURED STRAIN ALONG STIRRUP @ 112.5" – GIRDER AL .....	103
FIGURE 7.48: GIRDER BL AT DIFFERENT STAGES DURING THE TEST .....	104
FIGURE 7.49: MEASURED LOAD-DEFLECTION – GIRDER BL .....	105
FIGURE 7.50: MEASURED STRAND STRAIN AT MID-SPAN RESULTING FROM EXTERNAL LOAD – GIRDER BL.....	105
FIGURE 7.51: MEASURED STRAND STRAIN AT MID-SPAN RESULTING FROM ALL LOADS – GIRDER BL	106
FIGURE 7.52: MEASURED STRAND STRAIN AT QUARTER-SPAN RESULTING FROM EXTERNAL LOAD – GIRDER BL .....	107
FIGURE 7.53: MEASURED STRAND STRAIN AT QUARTER-SPAN RESULTING FROM ALL LOADS – GIRDER BL.....	107
FIGURE 7.54: MEASURED CONCRETE STRAIN AT MID-SPAN RESULTING FROM EXTERNAL LOAD – GIRDER BL.....	108
FIGURE 7.55: MEASURED CONCRETE STRAIN AT MID-SPAN RESULTING FROM ALL LOADS – GIRDER BL .....	108
FIGURE 7.56: MEASURED CONCRETE STRAIN AT QUARTER-SPAN RESULTING FROM EXTERNAL LOAD – GIRDER BL .....	109

FIGURE 7.57: MEASURED CONCRETE STRAIN AT QUARTER-SPAN RESULTING FROM ALL LOADS – GIRDER BL.....	109
FIGURE 7.58: MEASURED COMPRESSIVE STRAIN ALONG BOTTOM HORIZONTAL LVDT AT MID-SPAN – GIRDER BL .....	110
FIGURE 7.59: MEASURED STRAIN ALONG STIRRUP @ 22.5" – GIRDER BL.....	110
FIGURE 7.60: MEASURED STRAIN ALONG STIRRUP @ 52.5" – GIRDER BL.....	111
FIGURE 7.61: MEASURED STRAIN ALONG STIRRUP @ 82.5" – GIRDER BL.....	111
FIGURE 7.62: MEASURED STRAIN ALONG STIRRUP @ 112.5" – GIRDER BL.....	112
FIGURE 7.63: GIRDER CL AT DIFFERENT STAGES DURING THE TEST .....	113
FIGURE 7.64: MEASURED CYCLIC LOAD-DEFLECTION – GIRDER CL .....	114
FIGURE 7.65: MEASURED LOAD-DEFLECTION ENVELOPE – GIRDER CL.....	114
FIGURE 7.66: MEASURED STRAND STRAIN AT MID-SPAN RESULTING FROM EXTERNAL LOAD – GIRDER CL.....	115
FIGURE 7.67: MEASURED STRAND STRAIN AT MID-SPAN RESULTING FROM ALL LOADS – GIRDER CL .....	115
FIGURE 7.68: MEASURED STRAND STRAIN AT QUARTER-SPAN RESULTING FROM EXTERNAL LOAD – GIRDER CL .....	116
FIGURE 7.69: MEASURED STRAND STRAIN AT QUARTER-SPAN RESULTING FROM ALL LOADS – GIRDER CL.....	116
FIGURE 7.70: MEASURED CONCRETE STRAIN AT MID-SPAN RESULTING FROM EXTERNAL LOAD – GIRDER CL.....	117
FIGURE 7.71: MEASURED CONCRETE STRAIN AT MID-SPAN RESULTING FROM ALL LOADS – GIRDER CL .....	117
FIGURE 7.72: MEASURED CONCRETE STRAIN AT QUARTER-SPAN RESULTING FROM EXTERNAL LOAD – GIRDER CL .....	118
FIGURE 7.73: MEASURED CONCRETE STRAIN AT QUARTER-SPAN RESULTING FROM ALL LOADS – GIRDER CL.....	118
FIGURE 7.74: MEASURED COMPRESSIVE STRAIN ALONG TOP HORIZONTAL LVDT AT MID-SPAN – GIRDER CL .....	119
FIGURE 7.75: MEASURED TENSILE STRAIN ALONG BOTTOM HORIZONTAL LVDT AT MID-SPAN – GIRDER CL.....	119
FIGURE 7.76: MEASURED STRAIN ALONG STIRRUP @ 22.5" – GIRDER CL.....	120
FIGURE 7.77: MEASURED STRAIN ALONG STIRRUP @ 52.5" – GIRDER CL.....	120
FIGURE 7.78: MEASURED STRAIN ALONG STIRRUP @ 82.5" – GIRDER CL.....	121
FIGURE 7.79: MEASURED STRAIN ALONG STIRRUP @ 112.5" – GIRDER CL.....	121
FIGURE 7.80: COMPARISON OF MEASURED LOAD-DEFLECTION RELATIONSHIPS .....	122
FIGURE 7.81: ANALYTICAL AND EXPERIMENTAL LOAD-DEFLECTION – GIRDER AL .....	124
FIGURE 7.82: ANALYTICAL AND EXPERIMENTAL LOAD-DEFLECTION – GIRDER BL .....	124
FIGURE 7.83: ANALYTICAL AND EXPERIMENTAL LOAD-DEFLECTION – GIRDER CL .....	125
FIGURE 7.84: ANALYTICAL AND EXPERIMENTAL MOMENT-CURVATURE – GIRDER AL .....	126
FIGURE 7.85: ANALYTICAL AND EXPERIMENTAL MOMENT-CURVATURE – GIRDER BL.....	126
FIGURE 7.86: ANALYTICAL AND EXPERIMENTAL MOMENT-CURVATURE – GIRDER CL.....	127

FIGURE 7.87: ANALYTICAL AND EXPERIMENTAL FLEXURAL RIGIDITY – GIRDER AL .....	130
FIGURE 7.88: ANALYTICAL AND EXPERIMENTAL FLEXURAL RIGIDITY – GIRDER BL .....	130
FIGURE 7.89: ANALYTICAL AND EXPERIMENTAL FLEXURAL RIGIDITY – GIRDER CL .....	131
FIGURE 7.90: INCLINATION ANGLE OF A SHEAR CRACK .....	132
FIGURE 8.1: CROSS SECTION OF THE QUARTZITE-AGGREGATE GIRDER .....	136
FIGURE 8.2: MEASURED TRANSFER LENGTH FOR GIRDER A .....	138
FIGURE 8.3: MEASURED TRANSFER LENGTH FOR GIRDER B .....	139
FIGURE 8.4: GIRDER A AT DIFFERENT STAGES DURING THE TEST .....	140
FIGURE 8.5: MEASURED LOAD-DEFLECTION – GIRDER A .....	140
FIGURE 8.6: GIRDER C AT DIFFERENT STAGES DURING THE TEST .....	141
FIGURE 8.7: MEASURED LOAD-DEFLECTION – GIRDER C .....	142
FIGURE 8.8: MEASURED STIFFNESS UNDER FATIGUE LOADING – GIRDER C .....	143
FIGURE 8.9: GIRDER STIFFNESS DEGRADATION – GIRDER C .....	144
FIGURE 8.10: GIRDER B AT DIFFERENT STAGES DURING THE MONOTONIC LOAD TEST .....	145
FIGURE 8.11: MEASURED LOAD-DEFLECTION – GIRDER B .....	145
FIGURE 8.12: MEASURED LOAD-DEFLECTION – QUARTZITE-AGGREGATE GIRDERS .....	146
FIGURE 8.13: MEASURED LOAD-DEFLECTION – QUARTZITE-AGGREGATE AND LIMESTONE-AGGREGATE GIRDERS .....	147



## LIST OF TABLES

TABLE 5.1: PCI VALUES FOR $K_{RE}$ AND $J$ .....	25
TABLE 5.2: PCI VALUES FOR $C$ .....	25
TABLE 5.3: VALUES OF $SCF$ FOR VARIOUS VOLUME-TO-SURFACE RATIOS.....	27
TABLE 5.4: VALUES OF $AUC$ FOR VARIOUS PRESTRESS DURATIONS.....	27
TABLE 5.5: VALUES OF $SSF$ FOR VARIOUS VOLUME-TO-SURFACE RATIOS.....	28
TABLE 5.6: VALUES OF $AUS$ FOR VARIOUS PRESTRESS DURATIONS.....	28
TABLE 5.7: PCI SIMPLE SPAN MULTIPLIERS FOR LONG-TERM CAMBER AND DEFLECTION.....	29
TABLE 5.8: ACI VALUES FOR $\Gamma_p$ .....	30
TABLE 5.9: AASHTO VALUES FOR $K$ .....	31
TABLE 6.1: MEASURED FINENESS MODULUS OF THE FINE AGGREGATE.....	38
TABLE 6.2: AGGREGATE SSD DENSITY, SSD SPECIFIC GRAVITY, AND ABSORPTION.....	39
TABLE 6.3: AGGREGATE SSD DENSITY, SSD SPECIFIC GRAVITY, AND ABSORPTION.....	39
TABLE 6.4: MIX DESIGN MATRIX.....	40
TABLE 6.5: MIX DESIGN MATRIX.....	40
TABLE 6.6: DESIGN AND ACTUAL SUPERPLASTICIZER AND AIR ENTRAINER QUANTITIES.....	40
TABLE 6.7: HEAT CURING PROTOCOL.....	42
TABLE 6.8: MEASURED SCC FRESH PROPERTIES.....	43
TABLE 6.9: MEASURED AVERAGE CONCRETE COMPRESSIVE STRENGTH.....	51
TABLE 6.10: THEORETICAL CONCRETE COMPRESSIVE STRENGTH.....	52
TABLE 6.11: MEASURED AVERAGE CONCRETE FLEXURAL STRENGTH.....	54
TABLE 6.12: MEAN AND STANDARD DEVIATION OF MEASURED FLEXURAL STRENGTH.....	55
TABLE 6.13: MEASURED AVERAGE MODULUS OF ELASTICITY.....	58
TABLE 6.14: MEASURED AND CALCULATED MODULUS OF ELASTICITY.....	58
TABLE 6.15: AVERAGE MEASURED SHRINKAGE STRAIN.....	65
TABLE 7.1: CONTROL AND SCC MIX DESIGNS.....	68
TABLE 7.2: DECK CONCRETE MIX DESIGN.....	69
TABLE 7.3: MEASURED PROPERTIES OF FRESH CONCRETE USED FOR THE TEST SPECIMENS.....	81
TABLE 7.4: MEASURED GIRDER CONCRETE COMPRESSIVE STRENGTH.....	82
TABLE 7.5: MEASURED DECK CONCRETE COMPRESSIVE STRENGTH.....	82
TABLE 7.6: MEASURED AND CALCULATED TRANSFER LENGTH.....	86
TABLE 7.7: AVERAGE MEASURED PRESTRESS LOSSES.....	89
TABLE 7.8: AVERAGE MEASURED STRAND STRESS.....	89
TABLE 7.9: CALCULATED PRESTRESS LOSSES—AASHTO STANDARD SPECIFICATIONS.....	90
TABLE 7.10: CALCULATED INITIAL AND EFFECTIVE PRESTRESS—AASHTO STANDARD SPECIFICATIONS.....	90
TABLE 7.11: CALCULATED PRESTRESS LOSSES—AASHTO LRFD.....	90
TABLE 7.12: CALCULATED INITIAL AND EFFECTIVE PRESTRESS—AASHTO LRFD.....	90
TABLE 7.13: CALCULATED PRESTRESS LOSSES—PCI DESIGN HANDBOOK.....	91
TABLE 7.14: CALCULATED INITIAL AND EFFECTIVE PRESTRESS—PCI DESIGN HANDBOOK.....	91

TABLE 7.15: CALCULATED PRESTRESS LOSSES—PCI COMMITTEE ON PRESTRESS LOSSES .....	91
TABLE 7.16: CALCULATED INITIAL AND EFFECTIVE PRESTRESS— PCI COMMITTEE ON PRESTRESS LOSSES .....	92
TABLE 7.17: RATIO OF MEASURED TO CALCULATED EFFECTIVE PRESTRESS .....	92
TABLE 7.18: CAMBER MEASUREMENTS .....	93
TABLE 7.19: CALCULATED CAMBER (PCI DESIGN HANDBOOK METHOD).....	94
TABLE 7.20: COMPARISON OF MEASURED CRACKING MOMENTS AND FLEXURAL STRENGTHS .....	122
TABLE 7.21: MEASURED EFFECTIVE STIFFNESS.....	123
TABLE 7.22: COMPARISON OF THEORETICAL <sup>†</sup> AND MEASURED PRE-CRACKING EFFECTIVE STIFFNESS .....	125
TABLE 7.23: COMPARISON OF THEORETICAL <sup>†</sup> AND MEASURED ULTIMATE LOADS .....	125
TABLE 7.24: ANALYTICAL AND MEASURED CRACKING MOMENT .....	127
TABLE 7.25: ANALYTICAL AND MEASURED FLEXURAL STRENGTH .....	128
TABLE 7.26: ANALYTICAL AND MEASURED FLEXURAL STRENGTH .....	131
TABLE 7.27: CONCRETE EXPERIMENTAL SHEAR CAPACITY – GIRDER AL.....	132
TABLE 7.28: CONCRETE EXPERIMENTAL SHEAR CAPACITY – GIRDER BL.....	132
TABLE 7.29: CONCRETE EXPERIMENTAL SHEAR CAPACITY – GIRDER CL.....	133
TABLE 7.30: CHANGE IN STIRRUP FORCE FOLLOWING DEVELOPMENT OF WEB-SHEAR CRACKING – GIRDER AL .....	133
TABLE 7.31: CHANGE IN STIRRUP FORCE FOLLOWING DEVELOPMENT OF WEB-SHEAR CRACKING – GIRDER BL .....	133
TABLE 7.32: CHANGE IN STIRRUP FORCE FOLLOWING DEVELOPMENT OF WEB-SHEAR CRACKING – GIRDER CL .....	133
TABLE 7.33: COMPARISON OF EXPERIMENTAL <sup>†</sup> AND ANALYTICAL SHEAR STRENGTH.....	134
TABLE 8.1: CONTROL AND SCC QUARTZITE-AGGREGATE MIX PROPORTIONS.....	136
TABLE 8.2: DECK CONCRETE MIX PROPORTIONS .....	136
TABLE 8.3: MEASURED GIRDER CONCRETE COMPRESSIVE STRENGTH – QUARTZITE-AGGREGATE GIRDERS .....	137
TABLE 8.4: MEASURED DECK CONCRETE COMPRESSIVE STRENGTH – QUARTZITE-AGGREGATE GIRDERS .....	138
TABLE 8.5: FATIGUE LOADING PROTOCOL AND CORRESPONDING STRAND STRESSES .....	142
TABLE 8.6: AVERAGE FATIGUE STIFFNESS AND STIFFNESS DEGRADATION.....	144
TABLE 8.7: MEASURED CRACKING MOMENT, FLEXURAL STRENGTH, AND SHEAR FORCE AT FIRST WEB-SHEAR CRACK .....	146
TABLE D.1 GIRDER AL STRAIN GAGE LOCATIONS.....	180
TABLE D.2 GIRDER BL STRAIN GAGE LOCATIONS .....	181
TABLE D.3 GIRDER CL STRAIN GAGE LOCATIONS .....	182



# 1 EXECUTIVE SUMMARY

Recent studies have shown that the use of self-consolidating concrete (SCC) results in improved finished quality, increased production efficiency, and reduced labor cost. Because of the favorable properties that SCC exhibits, the Federal Highway Administration and the precast concrete industry have been promoting the research and development of SCC for structural applications in bridges.

The use of SCC for prestressed applications is relatively new to local designers and producers in South Dakota. Because of the lack of data on the performance of SCC using South Dakota aggregates, there is hesitancy by local engineers and producers to design and fabricate prestressed SCC bridge girders. If SCC is properly specified and used, it has the potential to yield more economical and higher quality prestressed concrete products than conventional concrete. To take advantage of this new technology, there was a need to study production feasibility and structural performance of prestressed SCC bridge girders made with South Dakota aggregates. Proportioning, behavior, and properties of SCC are highly dependent on the coarse aggregates physical properties. Two types of aggregates, crushed limestone and quartzite, are frequently used in preparing concrete for SDDOT bridges.

In 2007 researchers at South Dakota State University (SDSU) concluded an experimental study on three full-scale prestressed bridge girders. One of the three girders was cast using conventional concrete and served as a control specimen, while the other two girders were cast using SCC. The SCC mix was made with quartzite coarse aggregate that is commonly used in eastern South Dakota. The results of the study showed that the structural performance of the prestressed SCC girders was similar to that of the control prestressed girder. It was also observed that the SCC girders had a better finished surface than the conventional concrete girder.

Crushed limestone is commonly used for concrete production in western South Dakota. In order to assure the applicability of prestressed SCC concrete statewide, a study was designed to investigate the performance of prestressed SCC bridge girders made with limestone aggregates and to develop draft specifications, acceptance criteria, mix qualifications, and guidelines for use by SDDOT for prestressed SCC applications. The study covered in this report involved material testing of SCC mixtures and structural testing of full-scale prestressed bridge girders.

Three mix designs were developed based on varying the w/c ratio and using different curing methods. The design mix was provided by Cretex Concrete Products West, Inc. The design mix had a w/c ratio of 0.33. The three w/c ratios used in this research were 0.33, 0.35, and 0.37. The three mixes were moist cured and the design mix was also heat cured. The fresh properties of the three SCC mix designs were measured to evaluate the feasibility of producing SCC made with limestone coarse aggregate. The fresh SCC properties that were measured in this study include slump flow, visual stability index (VSI), T20, J-ring spread, L-box, and column segregation. The hardened properties of the SCC mixes were measured to evaluate the performance of SCC made with limestone coarse aggregate. The hardened SCC properties that were measured in this study include compressive strength, flexural strength, modulus of elasticity, hardened visual stability index (HVSI), and shrinkage.

Three full-scale prestressed girders were fabricated at Cretex Concrete Products West, Inc. in Rapid City, SD. Two of the girders were cast with SCC and one was cast with conventional concrete to serve as a control specimen. Design of the girders included instrumentation capable of measuring instantaneous and



time-dependent structural responses. The girders were tested until failure. The control specimen and one of the SCC specimens were tested under increasing monotonic load until failure. The other SCC specimen was tested under increasing cyclic loading until failure. The evaluation of SCC for use in prestressed bridge girder applications included analysis of transfer length, prestress losses, camber, flexural behavior and strength, flexural rigidity, and shear strength.

The results of the study can be summarized in the following main conclusions:

1. SCC mixtures were successfully produced using local South Dakota aggregates. Some of the concrete producers in South Dakota were well equipped to produce SCC on a commercial scale.
2. The laboratory tests showed that the behavior of SCC was similar to or better than conventional concrete of the same strength. The current code empirical equations for determining the engineering properties of hardened conventional concrete were found to be also applicable to SCC.
3. The structural performance of full-scale prestressed SCC bridge girders were similar to that of prestressed concrete girders made with conventional concrete. The current code equations for determining strength and stiffness of prestressed concrete girders were applicable to prestressed SCC girders.
4. The material cost of SCC was approximately 26% more than that of conventional concrete. However, the enhanced finished quality and the production efficiency of SCC girders made SCC an attractive choice among concrete producers. This may result in better finished product at no additional cost to the client.

Based on the results of this study, the following recommendations are made:

1. The South Dakota Department of Transportation should permit the use of SCC for the production of prestressed bridge girders and probably for other cast-in-place and precast applications.
2. The concrete producer should be responsible for the design of a SCC mix to meet the client's stated performance levels. The special provisions that were developed in this study set performance levels and acceptance criteria for SCC mixtures when used for the fabrication of prestressed/precast elements for bridge structures in South Dakota.
3. It is recommended that a showcase bridge be constructed by SDDOT using SCC for parts of the substructure and the superstructure. The bridge can be instrumented for data collection over an extended period of time. Monitoring of such a bridge would provide valuable information on the long-term performance of SCC bridge structures.

## 2 PROBLEM DESCRIPTION

In 2001 it was reported that 29% of the nation's bridges were structurally deficient or functionally obsolete (ASCE 2001). The cost of eliminating all of the reported deficiencies was estimated at \$10.6 billion a year for 20 years. The high cost of replacing and/or upgrading the deficient bridges has prompted engineers to investigate the feasibility of constructing new bridges using innovative materials that possess enhanced engineering properties.

Recent studies have shown that the use of self-consolidating concrete (SCC) results in improved finished quality, increased production efficiency, and reduced labor cost (Goodier 2003; PCI 2003). Because of the favorable properties that SCC exhibits, the Federal Highway Administration and the precast concrete industry have been promoting the research and development of SCC for structural applications in bridges (FHWA 2005).

ACI committee 237 (2007) defines SCC as "highly flowable, non-segregating concrete that can spread into place, fill the formwork, and encapsulate the reinforcement without any mechanical consolidation." ASTM C 09.91 (2006) defines SCC as "concrete that can flow around reinforcement and consolidates under its own weight without additional effort and without exceeding specified limits of segregation." Figure 2.1 shows a comparison between the methods used for measuring the flowability of conventional concrete and SCC. For conventional concrete, the flowability is measured by the slump of a concrete cone, whereas for SCC, the flowability is measured by the spread of the concrete after being discharged from the steel cone mold.



(a) Slump Test of Conventional Concrete



(b) Slump Spread Test of SCC

Figure 2.1: Measurement Methods of Concrete Flowability

The use of SCC for prestressed applications is relatively new to local designers and producers in South Dakota. Because of the lack of data on the performance of SCC using South Dakota aggregates, there is hesitancy by local engineers and producers to design and fabricate prestressed SCC bridge girders. If SCC is properly specified and used, it has the potential to yield more economical and higher quality prestressed concrete products than conventional concrete. To take advantage of this new technology, there is a need to study production feasibility and structural performance of prestressed SCC bridge girders made with



South Dakota aggregates. Proportioning, behavior, and properties of SCC are highly dependent on the coarse aggregates physical properties. Two types of aggregates, crushed limestone and quartzite, are frequently used in preparing concrete for SDDOT bridges.

In 2007 researchers at South Dakota State University (SDSU) concluded an experimental study on three full-scale prestressed bridge girders (Wehbe et al. 2007a). One of the three girders was cast using conventional concrete and used as a control specimen, while the other two girders were cast using SCC. The SCC mix was made with quartzite coarse aggregate that is commonly used in eastern South Dakota. The study was designed to investigate the structural performance of prestressed SCC bridge girders and to compare the strength and serviceability of such girders to those of prestressed girders made with conventional concrete. Funding for the study was provided by the College of Engineering at SDSU and Gage Brothers Concrete Products Inc., a local precast concrete producer in Sioux Falls. The results showed that the structural performance of the prestressed SCC girders was similar to that of the control prestressed girder. It was also observed that the SCC girders had a better finished surface than the conventional concrete girder.

In western South Dakota, limestone aggregate is used in the production of concrete. Previous research efforts at SDSU have focused on the structural performance of prestressed SCC bridge girders made with quartzite aggregates. In order to assure the applicability of prestressed SCC concrete statewide, a similar fabrication and testing regimen needed to be conducted on girders made with limestone aggregate. Therefore, research was needed to study the performance of prestressed SCC bridge girders made with limestone aggregates in order to develop draft specifications, acceptance criteria, mix qualifications, and guidelines for use by SDDOT for prestressed SCC applications.



## 3 OBJECTIVES AND SCOPE

### 3.1 OBJECTIVES

The study covered in this report was undertaken to address the following two main objectives.

1. *Evaluate the feasibility and performance of SCC using limestone coarse aggregate in prestressed concrete products.*

The work was initiated with a thorough search of the available literature not only within the structural area but in the broader area of materials. This search included results of research projects on SCC mix designs and structural behavior of prestressed bridge girders made with conventional and with self-consolidating concretes. The search for material went beyond the published literature and included contacts and discussions with industry representatives.

Once the literature search was completed, trial mix proportions for SCC made with limestone aggregates were developed for use in prestressed concrete applications. The base mix design was first determined in collaboration with the industry partner, Cretex Concrete Products West, Inc., on this project. Following the development of the base mix, the materials and additives required to produce different SCC mixes were determined. With the acquisition of the mix constituents an experimental study was conducted to evaluate the fresh and hardened properties of the different SCC mixtures.

After the mixes have been developed, three full-scale prestressed bridge girders (one control specimen and two SCC specimens) were fabricated at Cretex Concrete Products West Inc. fabrication facility in Rapid City. The girders were tested until failure at SDSU's Lohr Structures Laboratory. The girders were instrumented with an array of embedded strain gages and external sensors to capture prestress losses, transfer length, and the flexural and shear responses of the girders. The information obtained from the literature search, the data collected from the laboratory study of the trial SCC mixtures, and the field construction and structural testing of the full-scale girders were used to evaluate the feasibility and performance of prestressed SCC bridge girders made limestone aggregates.

2. *Develop draft specifications, acceptance criteria, mix qualifications, and guidelines for use of SCC by SDDOT.*

The data gathered through the progress of this project on prestressed limestone SCC girders, the data obtained from a previous SDSU study on prestressed quartzite SCC girders, the expected data from the literature search, and the input from the industry representatives and SDDOT personnel were incorporated into the writing of a specifications document. The document covers performance standards for the use of SCC made with either quartzite or limestone coarse aggregates in prestressed SCC girders. The performance standard includes acceptance criteria for the plastic concrete as well as acceptance criteria based on the properties of the hardened concrete.

### 3.2 SCOPE

This study involved material testing of SCC mixtures and structural testing of full-scale prestressed bridge girders.

### **3.2.1 STUDY OF CONCRETE MIXTURES**

Three mix designs were developed based on varying the w/c ratio and using different curing methods. The design mix was provided by Cretex Concrete Products West, Inc. The design mix had a w/c ratio of 0.33. The three w/c ratios used in this research were 0.33, 0.35, and 0.37. The three mixes were moist cured and the design mix was also heat cured.

The fresh properties of the three SCC mix designs were measured to evaluate the feasibility of producing SCC made with limestone coarse aggregate. The fresh SCC properties that were measured in this study include slump flow, visual stability index (VSI), T20, J-ring spread, L-box, and column segregation.

The hardened properties of the SCC mixes were measured to evaluate the performance of SCC made with limestone coarse aggregate. The hardened SCC properties that were measured in this study include compressive strength, flexural strength, modulus of elasticity, hardened visual stability index (HVSF), and shrinkage.

### **3.2.2 STUDY OF FULL-SCALE BRIDGE GIRDERS**

Three full-scale prestressed girders were fabricated at Cretex Concrete Products West, Inc. in Rapid City, SD. Two of the girders were cast with SCC and one was cast with conventional concrete to serve as a control specimen. Design of the girders included instrumentation capable of measuring instantaneous and time-dependent structural responses. The girders were tested until failure. The control specimen and one of the SCC specimens were tested under increasing monotonic load until failure. The other SCC specimen was tested under increasing cyclic loading until failure.

The evaluation of SCC for use in prestressed bridge girder applications included analysis of transfer length, prestress losses, camber, flexural behavior and strength, flexural rigidity, and shear strength. The codes that were used to assess the performance of the test specimens include: the American Association of State and Highway Transportation Officials LRFD Bridge Design Specifications (AASHTO 2007), the AASHTO Standard Specifications for Highway Bridges (AASHTO 2002), the American Concrete Institute Building Code (ACI 2008), and the Precast/Prestressed Concrete Institute Design Handbook (PCI 2004).



## 4 TASK DESCRIPTION

In the following text, when reference is made to the standard laboratory tests that are used to evaluate the fresh properties of an SCC mix, it is understood that the tests performed included slump flow with visual stability index (VSI), J-ring, L-box, column segregation evaluation, and the visual examination of cut cylinders to evaluate the distribution of the coarse aggregate in the concrete matrix. When reference is made to the standard acceptance tests that were used to evaluate the fresh properties of an SCC mix, it is understood that the tests performed included slump flow with visual stability index (VSI) and J-ring.

**Task 1:** *Review literature regarding SCC practices for prestressed concrete in other state transportation departments and industry.*

Through direct search in the relevant literature, contacts with industry experts and state departments of transportation that have had experience with SCC, and the previous experience of the researchers on SCC material and structural behavior, documents and research papers were located and utilized as the knowledge base for the study covered in this report. (See Chapter 5)

**Task 2:** *Develop concrete mixture designs for SCC containing limestone coarse aggregate factoring in both release and 28-day compressive strength.*

The researchers at SDSU, in collaboration with representatives from the concrete admixtures and the precast concrete industries, developed SCC mix designs using sand and limestone aggregates from western South Dakota for the SCC prestressed girders in this study. Refinement of the mix design was done, as needed, in consultation with concrete admixtures and the precast concrete industries to obtain acceptable release and 28-days compressive strengths. (See Chapter 6)

**Task 3:** *Conduct concrete testing on selected SCC and control mixtures, using both conventional and accelerated curing, as appropriate, including compressive and flexural strengths at 16-18 hours, 3, 7, 14, and 28 days, modulus of elasticity at 16-18 hours, 14 and 28 days, and shrinkage.*

Small batch mixes were prepared at the concrete materials laboratory at SDSU. Fine and limestone coarse aggregates from western South Dakota were employed in preparing the trial mixes. The trial SCC mixes had water/cement ratios of 0.33, 0.35, and 0.37. Standard 6"x12" concrete cylinders and 6"x6"x22" concrete beams were made to evaluate the trial mixes. The concrete specimens were divided into two groups. One group was cured using conventional (moist) curing the other was cured using accelerated (heat) curing. The cylinders were used to measure the compressive strength and the modulus of elasticity while the beams will be used to measure the flexural strength (modulus of rupture). The compressive and flexural strength measurements were made at 16-18 hours, 3 days, 7 days and 28 days. The modulus of elasticity measurements were made at 16-18 hours, 14 days and 28 days.

Shrinkage of the SCC mix with w/c of 0.33 was measured and compared to that of a conventional concrete (conventional) mix having the same w/c ratio. The shrinkage measurements were made on standard 6"x6"x22" beams that were moist cured. The beams were instrumented with embedded strain gages and kept under the same ambient conditions in the Lohr Structures Laboratory at SDSU. Strain measurements were made at short time intervals over the first 24 hours, then at increasingly higher time intervals afterwards over the following three months. (See Chapter 6)



**Task 4:** *Develop an instrumentation plan for three girders capable of measuring both instantaneous and time-dependent structural responses.*

The researchers developed and implemented an instrumentation plan that consisted of an array of strain gages attached to the prestressing tendons and shear reinforcement, embedded strain gages in the concrete, and linear variable differential transformers (LVDTs) to measure the instantaneous and time-dependent strains and deflections of the girders. (See Chapter 7)

**Task 5:** *Verify through small batch production the mix designs identified in Task 2 using slump flow with VSI (visual stability index), J-Ring, L-Box, column segregation, and hardened cut cylinders in addition to standard fresh concrete property tests, as suitable for each mix.*

The concrete materials laboratory at SDSU was utilized to produce the small batch mixes that were used to evaluate trial mixes proposed in task 2. Fine and limestone coarse aggregates from western South Dakota were employed in preparing the trial mixes. The physical properties of the aggregates were determined. All of the standard tests that are routinely performed on SCC plastic concrete, including Slump Flow,  $T_{50}$ , VSI, J-Ring, L-Box, and Column Segregation, were performed in this study. Hardened visual stability index rating was performed on hardened cut cylinders to evaluate the segregation extent of the proposed mix. Whenever applicable, the ASTM standard test methods were followed. (See Chapter 6)

**Task 6:** *Install instrumentation for each of the three girders, two fabricated using SCC and a control.*

Three 40-ft long Mn/DOT 36M girders were constructed at Cretex Concrete Products West, Inc. fabrication facility in Rapid City, South Dakota. One of the girders was cast using conventional concrete and served as the control specimen. The other two girders will be cast using SCC. Composite deck slabs were added to the girders after they were removed from the prestressing bed. The research team installed all of the embedded gages prior to concrete placement. The prestressing strands strain gages were attached after the strands were laid on the prestressing bed and starched to eliminate slack. The shear stirrups were instrumented at SDSU and then installed at the required location within the girders. The embedded concrete gages in the girders and the decks were installed in-situ prior to concrete placement. Following the stripping of the forms, brass DEMEC inserts were epoxy glued to the bottom flange of each girder along the potential transfer length. (See Chapter 7)

**Task 7:** *Conduct slump flow with VSI (visual stability index), J-Ring, and wet concrete property tests during fabrication, as appropriate, demonstrating these procedures to appropriate SDDOT personnel while documenting fabrication process.*

During the concrete placement for the three girders, the SDSU research team was present at Cretex fabrication facility. The team performed and documented the fresh SCC standard acceptance tests (slump flow,  $T_{50}$ , VSI, and J-Ring) provided training on conducting the standard tests to the SDDOT personnel that were present. Still and video images of the fabrication and testing process were captured and made available to SDDOT personnel for future reference. (See Chapter 7)

**Task 8:** *Conduct monotonic increasing load testing on two girders (one control specimen and one SCC specimen) and incrementally increasing cyclic load testing on one SCC girder while collecting data on stress-strain responses in both flexure and shear. Meet with the Technical Panel at the Lohr Structural Laboratory during the testing to discuss interim results and demonstrate the testing procedures.*

The girders were transported from the fabrication facility in Rapid City to the Lohr Structures Laboratory. The control girder and one of the SCC girders were tested under monotonic increasing load until failure. The other SCC girder was tested under incrementally increasing cyclic load until failure. The increasing cyclic load allowed for the determination of the effect of the service load level on the girder stiffness. Data collected from the sensors (load cell, strain gages, LVDTs) provided substantial information on the shear and flexural behavior throughout the entire loading process.

Members of the technical panel and a number of SDDOT engineers attended the testing of one of the SCC girders at the Lohr Structures Laboratory. The attendees were briefed on the testing procedure and the data acquisition process. (See Chapter 7)

**Task 9:** *Provide an analysis of data for the limestone girder test results along with the results obtained with quartzite girders in prior testing, especially with respect to shear response.*

The data were reduced and analyzed to determine strength and serviceability properties of the SCC prestressed girders made with limestone aggregate. The structural behavior of the limestone SCC girders was compared with those of conventional concrete girders and quartzite SCC girders (tested previously). An evaluation of the applicability of current code equations for determining flexural and shear strengths of prestressed girders to girders made with SCC was conducted. (See Chapter 7)

**Task 10:** *Evaluate criteria—including constructability, cost, quality, safety, durability, and other appropriate factors—for using SCC in prestressed bridge members in South Dakota and provide a cost/benefit comparison with conventional girder fabrication.*

The evaluation criteria were obtained from two main sources. One source came through discussion and input from the industry representatives involved in the project. The other source came from the data collected and experience gained through this and the prior research project on SCC bridge girders. (See Chapter 8)

**Task 11:** *Develop a Special Provision for Prestressed Concrete using Self-Consolidating Concrete.*

In collaboration with industry representatives and SDDOT personnel, the researchers developed special provisions for prestressed SCC. The provisions were based on the test results of the small batch production in the lab, the full scale production at the fabrication facility in Rapid City, and the structural performance of the SCC girders. (See Chapter 8)

**Task 12:** *Prepare a final report and executive summary of the literature review, research methodology, findings, conclusions and recommendations.*

This task is met through this report.

**Task 13:** *Make an executive presentation to the SDDOT Research Review Board at the conclusion of the project.*

An executive presentation was given on June 10, 2009.

## 5 LITERATURE REVIEW

### 5.1 INTRODUCTION

Many studies have been conducted to evaluate the engineering properties of SCC and the performance of SCC structural elements. A large number of recent studies can be found in the proceedings of the first and second North American Conference on the Design and Use of SCC (ACBM 2003, 2005). Most of the studies indicate that the engineering properties of SCC are equal to or better than equivalent conventional concrete mixes.

This chapter covers a review of previous literature regarding material performance of SCC and conventional concrete, use of SCC for prestressed bridge girders, and code provisions for transfer length, prestress losses, flexural strength, and shear strength of prestressed girders.

A previous study on proportioning SCC mixtures for precast and cast-in-place box culverts in South Dakota was conducted at SDSU and co-funded by SDDOT and the Mountain-Plains Consortium (MPC) University Transportation Center. The study included a comprehensive literature review on the effects of constituent materials on SCC wet and dry properties, testing methods, and previous work done by others. The results of that study can be found in Wehbe et al. (2007b). To avoid duplication in reporting some of the literature, this report makes several references to the previous study.

### 5.2 SCC CONSTITUENT MATERIALS AND PROPERTIES

#### 5.2.1 CONSTITUENT MATERIALS

Similar to conventional concrete, the main ingredients of SCC are coarse aggregate, fine aggregate, cement, and water. Admixtures are used to achieve special fresh and hardened performance characteristics. A detailed review of the constituent materials, the different admixtures used to prepare SCC, and the effects of the constituent materials and admixtures on the properties of SCC is presented in Wehbe et al. (2007b).

To achieve high flowability, SCC typically has larger paste volume, higher sand-to-aggregate ratio (S/A), and smaller maximum coarse aggregate size than conventional concrete. The shape and texture of the coarse aggregate affect the filling ability, passing ability, and stability of SCC. Coarse aggregate having a large maximum size or aggregate with high volume-to-surface ratio are prone to segregation during placement. Spherical coarse aggregate with relatively smooth surface is preferable for SCC mixtures (Mindness et al. 2003).

Self-consolidating concrete can be produced in one of three main types: powder-type, viscosity modifying admixture (VMA)-type, and combination-type. Powder-type SCC has high powder content. The powder may be cement and fillers such as fly ash, limestone powder, slag, and silica fume. High range water reducing (HRWR) admixtures, also called superplasticizers, are used to achieve high flowability. Segregation resistance is achieved by using high powder content, VMA, or a combination of the two (Bonen and Shah 2005; Berke et al. 2003).

Plasticizers are added to freshly mixed SCC to improve the workability for a short period of time. Plasticizers typically have a workability window of 30-60 minutes. Plasticizers are added to decrease the water demand of concrete and create fluidity in the mix (Kosmatka et al. 2002). Plasticizers can increase



the compressive strength of concrete by 10-25%. Shrinkage may increase slightly due to use of plasticizer. Viscosity modifying admixtures (VMA) raise the viscosity of the mix and increase cohesiveness of freshly mixed concrete. VMA reduce bleeding, segregation, and the pumping pressures for placement using a pump truck (Kosmatka et al. 2002). Air entraining admixtures are added to freshly mixed SCC to raise the air content. The main goal of increasing the air content in concrete is to improve durability. The amount of air in the fresh mix will increase in the short term but will decrease gradually over longer periods of time. The addition of the air entrainer will improve workability, improve cohesiveness, provide bleeding and segregation resistance, and decrease strength by 10-20% (Mindness et al. 2003). Set controlling agents, or retardants, are added to SCC to delay setting and prolong the plasticity of the fresh concrete. The set retardant is added midway through the mixing process. Retardants can cause increase in compressive and flexural strengths, drying shrinkage, and creep (Kosmatka et al. 2002).

### 5.2.2 ***FRESH PROPERTIES***

The performance of fresh SCC is evaluated based on filling ability, passing ability, and stability. Test methods have been developed specifically to evaluate the fresh properties of SCC. Some of those tests are standardized ASTM tests (ASTM 2006). A detailed review of the testing methods used to evaluate the fresh properties of SCC is presented in Wehbe et al. (2007b).

The *filling ability* of SCC is the ability to flow and completely fill all spaces under its self weight. The slump spread test is performed to evaluate filling ability. This test is performed in accordance with ASTM C 1611 and measures the flow distance of the SCC mix when it is discharged from a standard cone under free flow conditions. Figure 5.1 shows a slump flow test being done. The spread is measured as the average of two orthogonal diameters. Acceptable values are typically in the range of 18 to 30 in. (ACI 2007). It is recommended that the slump spread test be performed for every batch to ensure consistency of the SCC. The SCC slump spread should not differ by more than 2 in. between batches (ACI 2007). The  $T_{20}$  test is performed simultaneously with the slump spread. The  $T_{20}$  is the time, measured in seconds, for the slump spread to reach a diameter of 20 in. after the cone mold is lifted. The  $T_{20}$  measures the flow rate of the SCC under free flow conditions. The relative viscosity influences on the flow rate of the mix can be determined by the  $T_{20}$  time. A SCC mix with a  $T_{20}$  less than 2 seconds is categorized as a low viscosity mix, and a  $T_{20}$  time of more than 5 seconds is a high viscosity mix (ACI 2007).



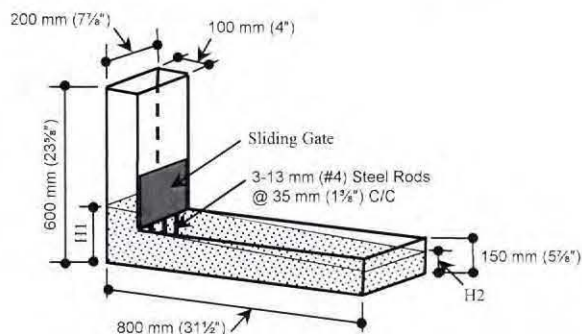
Figure 5.1: Slump Flow Test

The *passing ability* is defined as the ease with which the fresh concrete can pass through various obstacles and spaces without blocking or segregating. The passing ability of freshly mixed SCC can be evaluated by the J-ring test in accordance with ASTM C 1621. The test is similar to the slump spread but the J-ring is placed around the slump cone and the SCC is forced to pass through the legs of the J-ring. Figure 5.2 shows a J-ring test. The average of two orthogonal diameters is measured as the J-ring spread. The difference between the slump spread and J-ring spread assesses the blocking potential of the SCC mix. A difference between the spreads of less than 1 in. indicates no visible blocking while a difference of greater than 2 in. indicates noticeable to extreme blocking. A high J-ring spread indicates that the SCC mix can travel farther from discharge under its own weight and the faster it can fill formwork (ACI 2007).



Figure 5.2: J-Ring Test

The L-box test is another way to evaluate the passing ability of SCC. The L-box test is not an ASTM standard test, but is sometimes used in laboratory studies to evaluate blocking potential. The test can be performed in accordance with the PCI interim guidelines (2003). Figure 5.3 shows an L-Box test. The vertical segment of the L-box is filled with concrete then the concrete is allowed to flow through an opening at the bottom and spread into the horizontal trough of the box. The measured L-Box results are expressed in terms of the ratio  $H_2/H_1$ , where  $H_2$  is the height of the concrete at the downstream end and  $H_1$  is the height of the concrete at the upstream end of the L-Box trough.



(a) Schematic



(b) Completed Test

Figure 5.3: L-Box Test



*Stability* is the ability of SCC mix to resist segregation of the coarse aggregate from the paste. The stability characteristic considers the dynamic and static stability of freshly mixed SCC. *Dynamic stability* would be demonstrated during SCC placement and static stability would be demonstrated after SCC placement. The dynamic stability is evaluated by the visual stability index (VSI). The VSI is performed immediately following the slump spread. Once the mix is subjected to the free flow condition from the slump spread, the slump patty is visually inspected for signs of segregation and bleeding. The visual stability of the mix is assigned a value of 0, 1, 2, or 3. A stable mix would have a VSI rating of 0-1, and a rating of 2-3 indicates possible segregation problems. Since the VSI is a visual inspection, the test is subjective and the results are best used as quality control for SCC mixes (ACI 2007). Static stability is measured using the column segregation test in accordance with ASTM C 1610. Figure 5.4 shows a column segregation test set up. In the column segregation test a three-segment tube is filled with SCC and left undisturbed for 15 minutes. The concrete in the top and bottom segments of the concrete column in the tube are then removed and washed over a U.S. No. 4 sieve so that only the coarse aggregate remains. The column segregation test result is expressed as the percentage ratio of the difference of aggregate mass between the bottom and the top segments of the column to the total aggregate mass in the two segments. This percentage measures the segregation of the aggregate under confined flow conditions. No set point has been established to determine when SCC surpasses tolerable segregation, but an acceptable percent segregation is 10% or less (ACI 2007).



(a) Test Apparatus



(b) Test Set Up

Figure 5.4: Column Segregation Test

The air content and the mix temperature are measured in accordance with ASTM C 231 and ASTM C 1064, respectively.

### 5.2.3 HARDENED PROPERTIES

The hardened SCC properties that are of interest for prestressed concrete applications include compressive strength, flexural strength (modulus of rupture), modulus of elasticity, and shrinkage. In some cases, the Hardened Visual Stability Index (HVSI) is measured to establish the extent of static segregation. The HVSI is evaluated in accordance with AASHTO draft "Standard Method of Test for Static Segregation of Hardened Self-Consolidating Concrete Cylinders." (AASHTO 2005). A detailed review of the HVSI procedure and rating is presented in Wehbe et al. (2007b).



Studies by Attiogbe et al. (2005) and Collepardi et al. (2005) concluded that the compressive strength of SCC is comparable to that of conventional concrete of the same w/c ratio. Collepardi et al. (2005) also reported that SCC forms a better bond with reinforcement than conventional concrete.

Hegger (2005) and Walraven (2005) reported that the tensile strength of SCC is higher than that for conventional concrete, due to the homogeneous interface between the aggregates and paste. The flexural strength of SCC depends on the w/c ratio and coarse aggregate content (ACI 2007). An accepted theoretical value for the flexural strength of conventional concrete is determined using the following empirical equation (ACI 2008):

$$f_r = 7.5 \sqrt{f'_c} \quad (5.1)$$

where

$f_r$  = flexural strength (modulus of rupture), psi

$f'_c$  = 28 day compressive strength, psi

Bonen et al. (2005), Hegger et al. (2005), and Walraven (2005) reported that the modulus of elasticity of SCC is lower than that of conventional concrete of the same compressive strength. The ACI empirical code equation for determining the modulus of elasticity of conventional concrete is (ACI 2008):

$$E_c = 33 w_c^{1.5} \sqrt{f'_c} \quad (5.2)$$

where

$E_c$  = modulus of elasticity, psi

$w_c$  = unit weight of concrete, pcf

$f'_c$  = 28 day compressive strength, psi

#### 5.2.4 SHRINKAGE

Shrinkage is a phenomenon that is the result of moisture loss in concrete. A volume change occurs as concrete loses water. Concrete can lose water to its surroundings through evaporation or the pore water may be consumed through the hydration process. When the internal water evaporates, negative capillary pressures are formed that cause the paste to contract. Shrinkage involves a moisture exchange and depends on the shape and size of the specimen. A volume-to-surface area ratio (V/S) is used in shrinkage prediction equations; higher V/S ratios lead to less shrinkage. A higher V/S ratio indicates the internal water must travel farther to reach a point on the exposed surface to evaporate. Shrinkage is a three dimensional volume change that is measured as the strain on a load free specimen (Kosmatka et al. 2002).

Plastic shrinkage occurs as the surface of fresh concrete rapidly loses moisture. The loss of moisture causes volume change while the concrete is still fresh and before hardening begins. Plastic shrinkage appears as tears in the finish of fresh concrete. Plastic shrinkage can be slowed or prevented by providing external moist curing to the concrete or by misting/fogging as the surface is being finished (Kosmatka et al. 2002). SCC can be prone to plastic shrinkage because the mixes typically have no surface bleeding. High plastic shrinkage can occur in SCC without proper curing (ACI 2007).

Autogeneous shrinkage occurs when concrete begins to dry internally and a volume reduction of paste occurs due to the hydration process (Kosmatka et al. 2002). The internal drying is called self-desiccation

and causes the drying sections of the specimen to undergo tension while the moist section experiences compression. Autogeneous shrinkage can only occur if the concrete is sealed, when no external water is present, or if low w/c concrete is being used. The autogeneous shrinkage will increase with a decrease in the w/c ratio. Autogeneous shrinkage is most applicable to high performance concretes that utilize low w/c ratios for strength and admixtures for workability (Mindness et al. 2003). For a concrete with w/c of 0.30, autogeneous shrinkage can account for up to half of the total drying shrinkage (Kosmatka et al. 2002).

Drying shrinkage is the strain that is caused by water loss from hardened concrete when it is exposed to the environment. The part of total shrinkage that occurs upon first drying is irreversible (Kosmatka et al. 2002). Lower autogeneous and higher drying shrinkage have been reported for SCC (ACI 2007).

A model that had been recommended by ACI committee 209 (ACI 2005) for calculating the shrinkage of concrete is given by Equation 5.3. Due to its relative simplicity, the ACI 209 model is limited in its accuracy. In the ACI 209 model, shrinkage is dependent on the curing method, relative humidity, type of cement, specimen shape, ultimate shrinkage strain, and age of concrete after casting.

$$\varepsilon_s(t) = \frac{t}{b+t} K_{ss} K_{sh} (\varepsilon_{sh})_u \quad (5.3)$$

where

- $\varepsilon_s(t)$  = shrinkage strain at time  $t$
- $t$  = age of concrete after casting, days
- $b$  = constant in determining shrinkage strain, based on curing method  
 $b = 35$  for moist cured concrete, and  $55$  for heat cured concrete
- $K_{ss}$  = shape and size correction factor for shrinkage given by Equation 5.4
- $K_{sh}$  = relative humidity correction factor for shrinkage given by Equation 5.5
- $(\varepsilon_{sh})_u$  = ultimate shrinkage strain =  $780 \times 10^{-6}$  in./in.

$$K_{ss} = 1.14 - 0.0035 \left( \frac{V}{S} \right) \quad (5.4)$$

where

- $V$  = volume of specimen,  $\text{mm}^3$
- $S$  = area of specimen,  $\text{mm}^2$

$$K_{sh} = 1.40 - 0.01 H \quad (5.5)$$

where

- $H$  = relative humidity, %

### 5.3 SCC PROVISIONS BY DEPARTMENTS OF TRANSPORTATION

Some departments of transportation (DOT), including SDDOT, have developed special provisions for the use of SCC in their states. This section presents a summary of some of such special provisions. Most of the following information was reported by Wehbe et al. (2007).



### **5.3.1 NORTH CAROLINA DOT**

Following is a listing of the North Carolina DOT requirements for materials used to produce SCC (North Carolina 2005):

- Cement – Use a minimum of 639 lb/yd<sup>3</sup> and a maximum of 850 lb/yd<sup>3</sup>.
- Pozzolan – A pozzolan such as fly ash, ground granulated blast furnace slag, silica fume or limestone powder may be substituted for a portion of the cement.
- Coarse and fine aggregate – Use a fine aggregate content of 40% to 60% of the combined coarse and fine aggregate weight.
- Water – (for precast concrete) Use a quantity of water such that w/cm is no greater than 0.48.
- Admixtures – Use of a VMA is recommended to enhance homogeneity.
- 

The North Carolina DOT requires a slump spread of 24 inches to 30 inches using an inverted cone, a difference in spread between slump flow and J-ring tests not to exceed 2 inches, and, an L-Box ratio of H<sub>2</sub>/H<sub>1</sub> between 0.8 and 1.0. The North Carolina DOT requires also that concrete delivery be timed such that consecutive lifts will combine without segregation, the time between consecutive lifts not to exceed 20 minutes, the horizontal flow distance not to exceed 30 feet, and the vertical free fall distance not to exceed 10 feet.

### **5.3.2 ILLINOIS DOT**

The Illinois DOT requires that the maximum VSI value be 1, the maximum Hardened Visual Stability Index (HVS<sub>I</sub> by the cut cylinder method) be 1, the maximum J-ring value be 4 inches, the L-box blocking ratio be a minimum of 60%, and the slump flow be between 20 and 28 inches (Illinois 2004).

### **5.3.3 MICHIGAN DOT**

The Michigan DOT specifies the following SCC fresh properties requirements (Michigan 2005):

- Slump flow equal to 27 in  $\pm$  1.0 in
- VSI rating equal to or less than 1
- J-ring value between 0.5 in and 0.6 in (procedure from PCI)
- L-box ratio greater than 0.8 (80%)

### **5.3.4 SOUTH DAKOTA DOT**

South Dakota DOT developed the following SCC mix guidelines for use in box culverts (Wehbe et al. 2007).

- Minimum cement content of 700 lb/yd<sup>3</sup>
- Maximum w/c of 0.46
- Minimum coarse aggregate content of 40%
- Entrained air range of 5 to 7.5%

The acceptance criteria for use of SCC in box culverts are as follows

- Slump flow range of 22 to 28 in.
- VSI range of 0 to 1

- J-ring spread maximum difference of 2 in.
- 28 day compressive strength of at least 4500 psi

## 5.4 TRANSFER LENGTH OF PRESTRESSING STRANDS

Transfer length is defined by the ACI code (ACI 2008) as the “length of embedded pretensioned strand required to transfer the effective prestress to the concrete.” Various models are available for determining the required transfer length of embedded strands. Following is a presentation of the various models.

### 5.4.1 CODE PROVISIONS FOR TRANSFER LENGTH

The American Concrete Institute’s Building Code (ACI 2008) provides two methods for determining the transfer length of prestressing strands. When determining the concrete web-shear strength,  $V_{cw}$ , Section 11.3.5 of the ACI code defines the transfer length,  $L_t$ , in terms of the given strand diameter,  $d_b$ , as

$$L_t = 50d_b \quad (5.6)$$

where  $L_t$  and  $d_b$  are of the same length units.

When determining the development length of prestressing seven-wire strands, Section 12.9.1 of the ACI code defines the transfer length,  $L_t$ , in terms of strand diameter,  $d_b$ , and the effective stress in the prestressing strand,  $f_{se}$ , as is shown in Equation 5.7.

$$L_t = \left( \frac{f_{se}}{3} \right) d_b \quad (5.7)$$

where  $L_t$  and  $d_b$  are of the same length units and  $f_{se}$  is in ksi units. The transfer length in Equation 5.7 reduces to approximately 50 strand diameters when Grade 270 strands are prestressed to 75% of ultimate strength and 25% prestress loss is assumed.

The American Association of State Highway and Transportation Officials (AASHTO) Standard Specifications for Highway Bridges (AASHTO 2002) specifies a transfer length similar to that given by Equation 5.6. AASHTO LRFD Bridge Design Specifications (AASHTO 2007) specifies a transfer length,  $L_t$ , in terms of strand diameter,  $d_b$ , as

$$L_t = 60d_b \quad (5.8)$$

where  $L_t$  and  $d_b$  are of the same length units.

### 5.4.2 BUCKNER

In 1988, the Federal Highway Administration (FHWA) issued a memorandum (FHWA 1988) that placed restrictions on the use of seven-wire strands in bridge applications. The restrictions were placed in response to research at North Carolina State University which found development lengths to be significantly longer than those required by ACI and AASHTO. The FHWA prohibited the use of 0.6 in.-diameter prestressing strands, required a minimum strand spacing of  $4d_b$ , and introduced a factor of 1.6 on the ACI and AASHTO expressions for development length of smaller diameter strands. Several research programs on strand transfer and development lengths were initiated as a result of the FHWA memorandum, often resulting in a variety of design recommendations.

Buckner (1995) conducted a study sponsored by the FHWA to resolve conflicting design recommendations from numerous research studies. The goal of this study was to review literature,



rationalize differences among conclusions from recent studies, and recommend design criteria for strand transfer and development lengths. Buckner recommended a 20% increase (from  $50d_b$  to  $60d_b$ ) in the required transfer length. He also recommended the following expression for determining the transfer length

$$L_t = \left( \frac{f_{st}}{3} \right) d_b \quad (5.9)$$

where  $L_t$  and  $d_b$  are of the same length units and  $f_{st}$  is the initial strand stress in ksi units. Equation 5.6 is similar to the ACI expression with the exception that  $f_{st}$  is used in place of  $f_{se}$ . Buckner reported that the use of the term  $f_{st}$  is more rational because transfer length is established at release of the prestress and does not change significantly with time. The recommendations apply to prestressed members with normal weight concrete having a minimum release strength of 3500 psi, a minimum compressive strength of 5000 psi, and Grade 270 seven-wire low-relaxation uncoated strands (Buckner 1995).

#### 5.4.3 RUSSELL AND BURNS

A study by Russell and Burns (1997) investigated the ability of 0.6 in.-diameter seven wire strands to transfer prestress forces within a reliable transfer length. For this study, 18 single-strand prestressed specimens were prepared using Grade 270, seven-wire, low relaxation strands. The specified release strength and 28-day strength were 4000 psi and 6000 psi, respectively. The strands were tensioned to about 75% of  $f_{pu}$ , where  $f_{pu}$  is the specified tensile strength of the prestressing strands, or approximately 202.5 ksi. The strands were detensioned after two days and transfer length measurements were recorded.

Concrete surface strains, end slip, and strand strain were measured during this study to determine the transfer length for each specimen. Concrete surface strains were measured with detachable mechanical strain gages (demec gages). The strand end slip was determined by placing a tape marker on the strand outside the concrete specimen and measuring the distance the tape slipped toward the concrete during release of the strand. Electrical resistance strain gages were attached to the strands to monitor strains, but were reported to be ineffective due to multiple problems.

Transfer lengths were determined by evaluating the concrete strain profiles and using the 95% average maximum strain (95% AMS) method. According to Russell and Burns, the procedure for the 95% AMS method is as follows

- Plot the strain profile against the potential transfer length of the strand.
- Determine the AMS for the specimen by computing the numerical average of all the strains contained within the strain plateau of the fully effective prestress force.
- Scale the AMS value by 0.95 and construct a line on the plot corresponding to 0.95AMS.
- The transfer length is determined as the length between zero strain and the intersection of the strain profile with the 0.95AMS line.

The reported average transfer length for fully bonded 0.5 in.-diameter strands was 33.6 in. with a standard deviation of 8.66 in. The reported average transfer length for fully bonded 0.6 in.-diameter strands was 39.7 in. with a standard deviation of 7.95 in. Data from this study suggests that longer transfer lengths are required for 0.6 in.-diameter strands than those required for 0.5 in. strands. The results also show that the ratio of the strand diameters is approximately equal to the ratio of the two average transfer lengths. Therefore, the results suggest that the transfer lengths can be represented as a linear function of the strand diameters.

The average transfer length for all data obtained from this study was equal to  $66.6d_b$  with a standard deviation of  $14.1d_b$ . The transfer length provision of  $50d_b$  is considerably less than the average of  $66.6d_b$  measured by Russell and Burns. The researchers recommended the following transfer length expression

$$L_t = \left( \frac{f_{se}}{2} \right) d_b \quad (5.10)$$

For an effective prestress of 160 ksi, the transfer length becomes  $80d_b$  which is approximately equal to the mean value of the measured transfer length plus one standard deviation. An  $80d_b$  requirement would be much more conservative than current code provisions (Russell and Burns 1997)

#### 5.4.4 BARNES, GROVE, AND BURNS

Barnes, Grove, and Burns (2003) studied transfer length in 36 plant-cast AASHTO Type I girders with 0.6 in.-diameter strands at 2 in. spacing. One third of the specimens featured fully bonded strands. The remaining two thirds of the strands were subjected to varying debonding lengths. A total of 192 different transfer zones were created. Transfer lengths were determined for 184 of the 192 total transfer zones.

The researchers investigated several factors that influence transfer length including concrete strength, time, strand surface condition, and the prestress release method. Three concrete mixture designs were used and designated as L, M, and H. Mix L had a target release strength of 4000 psi and a target range of 5000 to 7000 psi for 28 day strength. Mix M had a target release strength of 7000 psi and a target range of 9500 to 11,500 psi for 28 day strength. Mix H had a target release strength of 9000 psi and a target range of 13,000 to 15,000 psi for 28 day strength. To determine the time dependence of transfer length, measurements were taken at various time frames after casting. The strand surface condition was considered during testing by using weathered strands for some specimens and clean strands for others. Finally, two release methods were used to determine their effect on transfer length, the live release method and the dead release method. In the live release method, each strand was cut simultaneously with torches at both ends of the member to introduce the full prestress force from that strand prior to cutting subsequent strands. The dead release method involved cutting all of the strands at only one end of a member, thus the prestress force was gradually introduced at the opposite end.

According to results of this study, all transfer lengths were less than the AASHTO LRFD value of  $60d_b$  and only three of the 184 transfer lengths exceeded  $50d_b$ . Based on their measured results, the researchers developed the following transfer length expression

$$L_t = \alpha \left( \frac{f_{pt}}{\sqrt{f'_{ci}}} \right) d_b \quad (5.11)$$

where  $L_t$  and  $d_b$  are of the same length units,  $\alpha$  is a proportionality constant in units of  $(\text{ksi})^{-0.5}$ ,  $f_{pt}$  is the stress in the prestressing strand after release in ksi units, and  $f'_{ci}$  is the initial compressive strength of concrete in ksi units.

Equation 5.11 indicates that the transfer length is inversely proportional to the square root of the concrete compressive strength. Based on the experimental results, upper and lower values for  $\alpha$  were set such that approximately 95% of the data would fall within the upper and lower bounds of Equation 5.11. The upper-and the lower-bound lines corresponded to  $\alpha = 0.57 (\text{ksi})^{-0.5}$  and  $\alpha = 0.17 (\text{ksi})^{-0.5}$ , respectively. The results also indicated that the transfer length increased with time. The average ratio of long-term transfer



length to initial transfer length was 1.13 and 1.17 for bright strands and rusted strands, respectively. A majority of this increase occurred within 28 days of prestress release. The strand surface condition did affect the measured transfer length. In concrete with lower compressive strengths, the transfer length of weathered strands was 13% shorter than that of bright strands. In higher strength concretes, the effect of the surface condition was negligible as the weathered strand transfer lengths varied and were sometimes longer than those for bright strands. The researchers concluded that surface weathering should not be a basis for reducing transfer length. The prestress release method had little effect on the performance of bright strands. Conversely, the live release method resulted in transfer lengths 30 to 50% longer than the dead release method for the weathered strand specimens. The researchers recommended using a lower-bound estimate of the transfer length when checking allowable stresses.

#### **5.4.5 GIRGIS AND TUAN**

Girgis and Tuan (2005) studied the bond strength of SCC with 0.6 in.-diameter prestressing strands. The transfer lengths of three prestressed bridge girders were measured. Two of the test specimens were cast with SCC and the third was cast with a conventional concrete mix.

This study consisted of three projects, each consisting of a different girder shape and concrete mixture. The girder tested in Project I was cast with an SCC mix, had a depth of 43.3 in., a web width of 5.9 in., and was 72.5 ft long. Fourteen 0.6 in.-diameter straight strands at 2 in. spacing, two harped strands, and four top strands were placed in the girder tested in Project I. For Project II, the bridge girder was also cast with an SCC mix, but had a depth of 35.4 in., a web width of 5.9 in., and was 90.2 ft long. A total of 26, 0.6 in.-diameter straight strands at 2 in. spacing, eight harped strands, and four top strands were placed in the girder tested in Project II. The bridge girder of Project III was cast with a conventional concrete mix, had a depth of 53.6 in., a web width of 5.9 in., and was 124.0 ft long. A total of 44, 0.5 in.-diameter straight strands at 2 in. spacing, ten harped strands, and four top strands were placed in the girder tested in Project III. The one-day concrete compressive strengths for Project I, Project II, and Project III were 6,492, 5,977, and 6,970 psi, respectively. The 28 day concrete compressive strengths for Projects I, II, and III were 10,887, 8,033, and 9,523 psi, respectively.

Demec point measurements were taken with a caliper gage and recorded at release and at 3, 7, 14, and 28 days after casting the concrete. The 95% average maximum strain method was used to determine transfer lengths. Average measured transfer lengths of Projects I, II, and III were determined to be 36, 43, and 20 in., respectively. Due to the difference in compressive strengths of each girder, transfer lengths were normalized with respect to compressive strength using Equation 5.8 as recommended by Barnes et al. (2003). The transfer lengths normalized with respect to compressive strengths were 38, 46, and 21 in. for Project I, Project II, and Project III, respectively. The researchers concluded that the transfer lengths of SCC mixtures may be longer than those of conventional concrete mixtures. The results also indicated that SCC experienced lower early concrete strengths than conventional concrete mixtures which may have led to longer transfer lengths (Girgis and Tuan 2005).

### **5.5 PRESTRESS LOSSES**

Prestress losses occur in pretensioned concrete elements due to several sources including prestressing steel seating at transfer, elastic shortening of concrete, creep of concrete, shrinkage of concrete, and relaxation of prestressing steel.

Several methods are available for calculating prestress losses. Some methods provide simplified lump sum estimates while others provide a more detailed time step estimate. AASHTO Standard Specifications for Highway Bridges (2002) and the PCI Design Handbook (2004) provide simplified estimates. AASHTO LRFD Bridge Design Specifications (2007) provides two methods for determining time-dependent prestress losses. One method is an approximate estimate while the other provides a refined estimate based on a time step analysis. Due to the relatively short service life of the specimens, only the approximate estimate of AASHTO LRFD will be discussed in this study. The PCI Committee on Prestress Losses (1975) provides a time step method for estimation of prestress losses.

#### 5.5.1 AASHTO STANDARD SPECIFICATIONS FOR HIGHWAY BRIDGES METHODS

The AASHTO Standard Specifications for Highway Bridges (2002) uses a simplified method to estimate prestress losses. In this method, the total prestress loss,  $\Delta f_s$ , is equal to the sum of four prestress loss components as is shown in Equation 5.12.

$$\Delta f_s = SH + ES + CR_c + CR_s \quad (5.12)$$

where

- $\Delta f_s$  = total loss excluding friction, psi
- $SH$  = loss due to concrete shrinkage, psi
- $ES$  = loss due to elastic shortening, psi
- $CR_c$  = loss due to creep of concrete, psi
- $CR_s$  = loss due to relaxation of prestressing steel, psi

The following are the methods used to compute each of the prestress loss components.

##### 5.5.1.1 Concrete Shrinkage, $SH$

$$SH = 17,000 - RH \quad (5.13)$$

where

$RH$  = mean ambient relative humidity (%)

##### 5.5.1.2 Elastic Shortening, $ES$

$$ES = \frac{E_s}{E_{ci}} f_{cir} \quad (5.14)$$

where

- $E_s$  = modulus of elasticity of prestressing steel strand, which can be taken as  $28 \times 10^6$  psi
- $E_{ci}$  = modulus of elasticity of concrete at stress transfer, psi
- $f_{cir}$  = concrete stress at the center of gravity of the prestressing steel due to the prestressing force and dead load of the beam immediately after transfer, psi

##### 5.5.1.3 Creep of Concrete, $CR_c$

$$CR_c = 12 f_{cir} - 7 f_{cds} \quad (5.15)$$

where

- $f_{cir}$  = concrete stress at the center of gravity of the prestressing steel due to the prestressing force and dead load of the beam immediately after transfer, psi



$f_{eds}$  = concrete stress at the center of gravity of the prestressing steel due to all dead loads except the dead load present at the time the prestressing force is applied, psi

#### 5.5.1.4 Steel Relaxation, $CR_s$

$$CR_s = 5000 - 0.10 ES - 0.05(SH + CR_c) \quad (5.16)$$

where

$SH$  = loss due to concrete shrinkage, psi

$ES$  = loss due to elastic shortening, psi

$CR_c$  = loss due to creep of concrete, psi

#### 5.5.2 AASHTO LRFD APPROXIMATE METHOD

The AASHTO LRFD Bridge Design Specifications (2007) prescribes two methods for determining prestress loss: an approximate method and a refined time step method. Only the approximate method of time-dependent losses will be discussed in this study. In the approximate method, prestress losses are divided into: (1) initial losses due to elastic shortening and (2) long-term losses due to shrinkage of concrete, creep of concrete, and relaxation of prestressing steel. In pretensioned members, the total prestress loss is determined using Equation 5.17.

$$\Delta f_{pT} = \Delta f_{pES} + \Delta f_{pLT} \quad (5.17)$$

where

$\Delta f_{pT}$  = total loss, ksi

$\Delta f_{pES}$  = sum of all losses due to elastic shortening, ksi

$\Delta f_{pLT}$  = loss due to long-term concrete shrinkage, creep of concrete, and relaxation of steel, ksi

The prestress loss due to elastic shortening is determined as

$$\Delta f_{pES} = \frac{E_p}{E_{ct}} f_{cgp} \quad (5.18)$$

where

$E_p$  = modulus of elasticity of the prestressing steel, ksi

$E_{ct}$  = modulus of elasticity of concrete at transfer or time of load application, ksi

$f_{cgp}$  = concrete stress at the center of gravity of the prestressing tendons due to the prestressing force immediately after transfer and the self-weight of the member at the section of maximum moment, ksi

The change in the prestressing steel stress due to time-dependent prestress losses,  $\Delta f_{pLT}$ , is determined as

$$\Delta f_{pLT} = 10.0 \frac{f_{pi} A_{ps}}{A_g} \gamma_h \gamma_{st} + 12.0 \gamma_h \gamma_{st} + \Delta f_{pR} \quad (5.19)$$

$$\gamma_h = 1.7 - 0.01 H \quad (5.20)$$

$$\gamma_{st} = \frac{5}{(1 + f'_{ct})} \quad (5.21)$$

where

- $f_{pt}$  = prestressing steel stress immediately prior to transfer, ksi  
 $A_{ps}$  = area of prestressing steel, in<sup>2</sup>  
 $A_g$  = gross area of concrete section, in<sup>2</sup>  
 $\gamma_h$  = correction factor for relative humidity of ambient air  
 $\gamma_{st}$  = correction factor for specified concrete strength at time of prestress transfer  
 $H$  = average annual ambient relative humidity, %  
 $f'_{ci}$  = initial concrete compressive strength, ksi  
 $\Delta f_{pR}$  = an estimate of relaxation loss taken as 2.4 ksi for low relaxation strand, 10.0 ksi for stress relieved strand, and in accordance with manufacturers recommendation for other types of strands, ksi

The estimate of time-dependent losses given by Equation 5.16 was derived from approximations of the refined method prescribed by AASHTO. The terms in the approximate method were developed for members of common shapes. This method was calibrated with full-scale test results and results of the refined method. The first, second, and third terms of Equation 5.16 represent creep losses, shrinkage losses, and relaxation losses, respectively (AASHTO 2007).

### 5.5.3 PCI DESIGN HANDBOOK METHOD

The prestress losses in the PCI Design Handbook (2004) method are based on a report of a task group sponsored by Joint ACI-ASCE Committee 423, Prestressed Concrete. Using this method, the total prestress loss,  $TL$ , is equal to the sum of four prestress loss components as follows.

$$TL = ES + CR + SH + RE \quad (5.22)$$

where

- $TL$  = total loss, psi  
 $ES$  = loss due to elastic shortening, psi  
 $CR$  = loss due to creep of concrete, psi  
 $SH$  = loss due to shrinkage of concrete, psi  
 $RE$  = loss due to relaxation of tendons, psi

The following equations are used to compute each of the prestress loss components in Equation 5.22.

#### 5.5.3.1 Elastic Shortening, $ES$

$$ES = K_{es} f_{cir} \left( \frac{E_{ps}}{E_{ci}} \right) \quad (5.23)$$

where

- $K_{es}$  = 1.0 for pretensioned members  
 $E_{ps}$  = modulus of elasticity of prestressing tendons, which can be taken as  $28.5 \times 10^6$  psi  
 $E_{ci}$  = modulus of elasticity of concrete at the time the prestress force is applied, psi  
 $f_{cir}$  = net compressive stress in concrete at the center of gravity of prestressing force immediately after the prestress has been applied to the concrete, psi

$$f_{cir} = K_{cir} \left( \frac{P_i}{A_g} \right) - \frac{M_g e}{I_g} \quad (5.24)$$



where

- $K_{cir}$  = 0.9 for pretensioned members
- $P_i$  = initial prestress force (after seating and before release), lb
- $e$  = eccentricity of center of gravity of tendons with respect to center of gravity of the concrete section, in.
- $A_g$  = area of gross concrete section, in<sup>2</sup>
- $I_g$  = moment of inertia of the gross concrete section, in<sup>4</sup>
- $M_g$  = bending moment due to self weight of member and any other permanent loads in place at time of prestressing, lb-in

#### 5.5.3.2 Creep of Concrete, $CR$

$$CR = K_{cr} \left( \frac{E_{ps}}{E_c} \right) (f_{cir} - f_{cds}) \quad (5.25)$$

where

- $K_{cr}$  = 2.0 for normal weight concrete
- $E_c$  = modulus of elasticity of concrete at 28 days, psi
- $E_{ci}$  = modulus of elasticity of concrete at the time the prestress force is applied, psi
- $f_{cds}$  = compressive stress in concrete at the center of gravity of the prestressing steel due to all dead loads applied to the member after it has been prestressed, psi

$$f_{cds} = \frac{M_{sd} e}{I_g} \quad (5.26)$$

where

- $M_{sd}$  = moment due to superimposed permanent dead loads applied after prestressing, lb-in

#### 5.5.3.3 Shrinkage of Concrete, $SH$

$$SH = (8.2 \times 10^{-6}) K_{sh} E_{ps} \left( 1 - 0.06 \frac{V}{S} \right) (100 - RH) \quad (5.27)$$

where

- $K_{sh}$  = 1.0 for pretensioned members
- $V/S$  = volume to surface area, in.
- $RH$  = mean ambient relative humidity, %

#### 5.5.3.4 Steel Relaxation, $RE$

$$RE = [K_{re} - J(SH + CR + ES)]C \quad (5.28)$$

where  $K_{re}$  and  $J$  are dependent on the type of the prestressing tendon, and  $C$  is dependent on the ratio of the prestressing steel stress immediately prior to transfer,  $f_{pi}$ , to the ultimate stress of the tendon,  $f_{pu}$ . The values of  $K_{re}$  and  $J$  are given in Table 5.1, and the values of  $C$  are given in Table 5.2.

**Table 5.1: PCI Values for  $K_{re}$  and  $J$** 

Type of Tendon	$K_{re}$	$J$
270 Grade stress-relieved strand or wire	20,000	0.15
250 Grade stress-relieved strand or wire	18,500	0.14
240 or 235 Grade stress-relieved wire	17,600	0.13
270 Grade low-relaxation strand	5,000	0.040
250 Grade low-relaxation wire	4,630	0.037
240 or 235 Grade low-relaxation wire	4,400	0.035
145 or 160 Grade stress-relieved bar	6,000	0.050

**Table 5.2: PCI Values for  $C$** 

$f_{pi} / f_{pu}$	Stress-Relieved Stand or Wire	Stress-Relieved Bar or Low-Relaxation Strand or Wire
0.80	-	1.28
0.79	-	1.22
0.78	-	1.16
0.77	-	1.11
0.76	-	1.05
0.75	1.45	1.00
0.74	1.36	0.95
0.73	1.27	0.90
0.72	1.18	0.85
0.71	1.09	0.80
0.70	1.00	0.75
0.69	0.94	0.70
0.68	0.89	0.66
0.67	0.83	0.61
0.66	0.78	0.57
0.65	0.73	0.53
0.64	0.68	0.49
0.63	0.63	0.45
0.62	0.58	0.41
0.61	0.53	0.37
0.60	0.49	0.33

The PCI Design Handbook recommends the use of its prestress loss model for practical design applications and indicates that the model provides realistic values for normal design conditions. A more detailed analysis may be necessary for unusual design applications and special structures (PCI 2004).

#### **5.5.4 PCI COMMITTEE ON PRESTRESS LOSSES METHOD**

The PCI Committee on Prestress Losses (1975) prescribes a time-dependent method to estimate prestress losses. Although this method is over thirty years old, the ACI building code (2008) still recognizes it as



an acceptable method for estimating prestress losses. In this model, the total prestress loss,  $TL$ , is equal to the sum of four prestress loss components including elastic shortening, concrete creep, concrete shrinkage, and steel relaxation as shown in Equation 5.29 (PCI 1975).

$$TL = ES + \sum_{t1}^t (CR + SH + RET) \quad (5.29)$$

where

$TL$  = total loss, psi

$ES$  = loss due to elastic shortening, psi

$CR$  = loss due to creep of concrete, psi

$RET$  = compressive stress in concrete at the center of gravity of the prestressing steel due to all dead loads applied to the member after it has been prestressed, psi

$t1$  = beginning time, days

$t$  = end time, days

The prestress loss components in Equation 5.29 are determined as follows.

#### 5.5.4.1 Elastic Shortening, $ES$

$$ES = f_{cr} \left( \frac{E_s}{E_{ci}} \right) \quad (5.30)$$

where

$f_{cr}$  = concrete stress at center of gravity of the prestressing force immediately after transfer, psi

$E_s$  = modulus of elasticity of prestressing tendons, psi

$E_{ci}$  = modulus of elasticity of concrete at the time the prestress force is applied, psi

#### 5.5.4.2 Creep of Concrete, $CR$

$$CR = (UCR)(SCF)(MCF)(PCR)(f_c) \quad (5.31)$$

where

$UCR = 63 - 20E_c/10^6$ ;  $UCR \geq 11$  for normal weight accelerated cured concrete

$SCF$  = member size and shape factor

$MCF$  = age at prestress and length of cure factor

$PCR = (AUC)_t - (AUC)_{t1}$  = portion of ultimate creep over the time interval  $t1$  to  $t$  in which  $AUC$  is the estimated variation of creep with time

$f_c$  = net concrete compressive stress at prestress centroid at time  $t1$ , taking into account the loss of prestress force occurring over the preceding time interval, psi

Values for  $SCF$  and  $AUC$  are given Table 5.3 and Table 5.4, respectively.

Table 5.3: Values of *SCF* for Various Volume-to-Surface Ratios

Volume-to-Surface Ratio	<i>SCF</i>
1	1.05
2	0.96
3	0.87
4	0.77
≥ 5	0.68

Table 5.4: Values of *AUC* for Various Prestress Durations

Time after Prestress (Days)	<i>AUC</i>
1	0.08
2	0.15
5	0.18
7	0.23
10	0.24
20	0.30
30	0.35
60	0.45
90	0.51
180	0.61
365	0.74
End of Service Life	1.00

#### 5.5.4.3 Shrinkage of Concrete, *SH*

$$SH = (USH)(SSF)(PSH) \quad (5.32)$$

where

*USH* = ultimate shrinkage loss in normal weight concrete, psi

$$= 27,000 - 3000E_c / 10^6 \geq 12,000 \text{ psi}$$

*SSF* = member size and shape factor

*MCF* = age at prestress and length of cure factor

*PSH* =  $(AUS)_t - (AUS)_{t1}$  = portion of ultimate shrinkage over the time interval  $t1$  to  $t$  in which *AUS* is the estimated variation of shrinkage with time

Values for *SSF* and *AUS* are given Table 5.5 and Table 5.6, respectively.



Table 5.5: Values of SSF for Various Volume-to-Surface Ratios

Volume-to-Surface Ratio	SSF
1	1.04
2	0.96
3	0.86
4	0.77
5	0.69
6	0.60

Table 5.6: Values of AUS for Various Prestress Durations

Time after Prestress (Days)	AUS
1	0.08
2	0.15
5	0.20
7	0.22
10	0.27
20	0.36
30	0.42
60	0.55
90	0.62
180	0.68
365	0.86
End of Service Life	1.00

#### 5.5.4.4 Steel Relaxation, $RET$

$$RET = f_{st} \left( \frac{\log(24 t) - \log(24 t_1)}{45} \right) \left( \frac{f_{st}}{f_{py}} - 0.55 \right) \quad (5.33)$$

where

- $f_{pu}$  = guaranteed ultimate tensile strength of prestressing steel, psi
- $f_{py}$  = stress at 1% elongation of prestressing steel, psi, may be taken as  $0.90 f_{pu}$
- $f_{st}$  = stress in prestressing steel at time  $t$ , psi
- $f_{st}/f_{py} - 0.55 \geq 0.05$

## 5.6 CAMBER

Camber is a net upward deflection due to the eccentric compression applied to prestressed concrete members. A significant amount of camber often occurs after release of the prestressing force. Many variables affect camber including concrete mix proportions, time of prestress release, placement of superimposed loads, and relative humidity. Therefore, long-term values are only estimates and should not be specified, but should instead be recognized (PCI 2004).

The PCI Design Handbook (2004) provides methods for estimating the both initial and long-term camber. The equation used for determining the initial camber includes the effects of the prestressing force and the self weight as follows

$$\Delta = \frac{P_0 e l^2}{8 E_{ci} I} - \frac{5 w l^4}{384 E_{ci} I} \quad (5.34)$$

where

- $\Delta$  = mid-span deflection, in.
- $P_0$  = prestress force at transfer, kips
- $e$  = eccentricity of prestressing force, in.
- $l$  = span length, in.
- $E_{ci}$  = modulus of elasticity at time of initial prestress, ksi
- $I$  = moment of inertia of the beam section, in<sup>4</sup>
- $w$  = self weight per unit length, kip/in.

Long-term camber estimates are more complex than initial estimates due to the effect of prestress loss over time and increase in concrete strength after release of prestress. The PCI Design Handbook (PCI 2004) suggests that long-term camber be determined by multiplying the initial calculated deflections by a given multiplier. The PCI Design Handbook recommended multipliers are given in Table 5.7.

**Table 5.7: PCI Simple Span Multipliers for Long-Term Camber and Deflection**

Cause of Deflection	Multiplier	
	Without Composite Topping	With Composite Topping
Deflection (downward) due to member weight at release	2.70	2.40
Camber (upward) due to prestress release	2.45	2.20
Deflection (downward) due to superimposed dead load	3.00	3.00
Deflection (downward) due to composite topping	-	2.30

## 5.7 FLEXURAL STRENGTH OF PRESTRESSED CONCRETE GIRDERS

The nominal flexural strength of a section can be determined using strain compatibility and static equilibrium (ACI 2005).

For a rectangular section or a T-section where the equivalent rectangular stress block falls within the flange, and assuming the compression steel, if any, to be yielding at the strength limit state, the nominal flexural strength of a prestressed concrete member can be determined using Equation 5.35 (Nawy 2006).

$$M_n = A_{ps} f_{ps} \left( d_p - \frac{a}{2} \right) + A_s f_y \left( d - \frac{a}{2} \right) + A'_s f_y \left( \frac{a}{2} - d' \right) \quad (5.35)$$

where

- $M_n$  = nominal flexural strength, lb-in.
- $A_{ps}$  = area of prestressed reinforcement, in<sup>2</sup>
- $f_{ps}$  = stress in prestressing steel at nominal flexural strength, psi



- $d_p$  = depth from extreme compression fiber of concrete to centroid of prestressing steel, in.  
 $a$  = depth of compressive stress block, in.  
 $A_s$  = area of tension reinforcement, in<sup>2</sup>  
 $f_y$  = yield strength of non-prestressed reinforcement, psi  
 $d$  = depth from extreme compression fiber of concrete to centroid of tension reinforcement, in.  
 $A'_s$  = area of compression reinforcement, in<sup>2</sup>  
 $d'$  = depth from extreme compression fiber of concrete to centroid of compression reinforcement ( $d' \leq 0.15d_p$ ), in.

### 5.7.1 ACI CODE PROVISIONS FOR FLEXURAL STRENGTH

ACI (2008) defines the prestressing steel stress at nominal flexural strength,  $f_{ps}$ , based on strain compatibility using the following expression for fully bonded strands

$$f_{ps} = f_{pu} \left\{ 1 - \frac{\gamma_p}{\beta_1} \left[ \rho_p \frac{f_{pu}}{f'_c} + \frac{d}{d_p} (\omega - \omega') \right] \right\} \quad (5.36)$$

$$\text{with } \left[ \rho_p \frac{f_{pu}}{f'_c} + \frac{d}{d_p} (\omega - \omega') \right] \geq 0.17$$

where

- $f_{ps}$  = stress in prestressing steel at nominal flexural strength, psi  
 $f_{pu}$  = ultimate stress of prestressing steel, psi  
 $\gamma_p$  = factor for type of prestressing steel  
 $\beta_1$  = factor relating depth of equivalent rectangular compressive stress block to neutral axis depth  
 $\rho_p$  =  $A_{ps}/b d_p$   
 $f'_c$  = 28-day concrete compressive strength, psi  
 $d$  = depth from extreme compression fiber of concrete to centroid of tension reinforcement, in.  
 $d_p$  = depth from extreme compression fiber of concrete to centroid of prestressing steel, in.  
 $\omega$  = tension reinforcement index =  $\rho f_y/f'_c$   
 $\omega'$  = compression reinforcement index =  $\rho' f_y/f'_c$   
 $\rho$  = non-prestressed tension reinforcement ratio =  $A_s/bd$   
 $\rho'$  = compression reinforcement ratio =  $A'_s/bd$   
 $b$  = section width in the compression zone

The value of  $\gamma_p$  used in Equation 5.36 is dependent on the type of prestressing steel. ACI (2008) prescribes values of  $\gamma_p$  based on the ratio  $f_{py}/f_{pu}$ . Values of  $\gamma_p$  are shown in Table 5.8.

Table 5.8: ACI Values for  $\gamma_p$

Type of Tendon	$f_{py}/f_{pu}$	$\gamma_p$
Low Relaxation Strand	0.90	0.28
Stress-Relieved Strand	0.85	0.40
High-Strength Prestressing Bar	0.80	0.55

### 5.7.2 AASHTO-LRFD PROVISIONS FOR FLEXURAL STRENGTH

AASHTO-LRFD (2007) prescribes the same method as ACI for determining nominal flexural strength of a prestressed member. However, AASHTO uses the following expression for determining the stress in the prestressing steel,  $f_{ps}$ .

$$f_{ps} = f_{pu} \left( 1 - k \frac{c}{d_p} \right) \quad (5.37)$$

where

- $f_{ps}$  = stress in prestressing steel at nominal flexural strength, psi
- $f_{pu}$  = ultimate stress of prestressing steel, psi
- $k$  = factor for type of prestressing steel
- $c$  = distance of outermost compressive fiber to the neutral axis
- $d_p$  = depth from extreme compression fiber of concrete to centroid of prestressing steel, in.

The value of  $k$  used in Equation 2.33 is dependent on the type of prestressing steel. Similar to ACI, AASHTO prescribes values of  $k$  based on the ratios of  $f_{py}/f_{pu}$ . Values of  $k$  are shown in Table 5.9.

Table 5.9: AASHTO Values for  $k$

Type of Tendon	$f_{py}/f_{pu}$	$V_u$
Low Relaxation Strand	0.90	0.28
Stress-Relieved Strand	0.85	0.38
Type 1 High-Strength Bar	0.85	0.38
Type 2 High-Strength Bar	0.80	0.48

## 5.8 SHEAR STRENGTH OF PRESTRESSED CONCRETE GIRDERS

This section presents a brief review of code provisions regarding shear strength of prestressed concrete girders.

### 5.8.1 ACI CODE PROVISIONS

In the ACI code (2008), the nominal shear strength of a concrete member to be equal to the sum of the nominal shear strength provided by concrete and the nominal shear strength provided by shear reinforcement as shown in Equation 5.38.

$$V_n = V_c + V_s \quad (5.38)$$

where

- $V_n$  = nominal shear strength
- $V_c$  = nominal shear strength provided by concrete
- $V_s$  = nominal shear strength provided by shear reinforcement

Section 11.3 of the ACI Code (2008) provides detailed expressions for determining the nominal shear strength provided by concrete for prestressed members.  $V_c$  is taken as the lesser of  $V_{ci}$  and  $V_{cw}$  where  $V_{ci}$  is the shear strength provided by concrete when flexure-shear cracking results from combined shear and



moment, and  $V_{cw}$  is the shear strength provided by concrete when web-shear cracking results from principal tensile stresses in the web.

$V_{ci}$  is determined using Equation 5.39.

$$V_{ci} = 0.6 \lambda \sqrt{f'_c} b_w d_p + V_d + \frac{V_i M_{cre}}{M_{max}} \quad (5.39)$$

with  $V_{ci} \geq 1.7 \sqrt{f'_c} b_w d_p$

where

- $V_{ci}$  = nominal shear strength provided by concrete when diagonal cracking results from combined shear and moment, lb
- $f'_c$  = concrete compressive strength, psi
- $\lambda$  = modification factor for lightweight concrete = 1 for normal weight concrete
- $b_w$  = web width, in
- $d_p$  = depth from extreme compression fiber of concrete to centroid of prestressing steel where  $d_p \geq 0.80h$ , in.
- $h$  = section depth
- $V_i$  = maximum factored shear force at section due to externally applied loads, lb
- $M_{cre}$  = moment causing flexural cracking at section due to externally applied loads, in-lb
- $M_{max}$  = maximum factored moment at section due to externally applied loads, in-lb

$M_{cre}$  is determined as follows.

$$M_{cre} = \left( \frac{1}{y_t} \right) (6 \sqrt{f'_c} + f_{pe} - f_d) \quad (5.40)$$

where

- $I$  = moment of inertia of section about centroidal axis, in<sup>4</sup>
- $y_t$  = distance from centroidal axis to tension face, in.
- $f'_c$  = concrete compressive strength, psi
- $f_{pe}$  = compressive stress in concrete due to effective prestress forces only at extreme tensile fiber of section, psi
- $f_d$  = stress due to unfactored dead load at extreme tensile fiber of section, psi

$V_{cw}$  is determined using Equation 5.41.

$$V_{cw} = (3.5 \sqrt{f'_c} + 0.3 f_{pc}) b_w d_p + V_p \quad (5.41)$$

where

- $V_{cw}$  = nominal shear strength provided by concrete when diagonal cracking results from high principal tensile stress in the web, lb
- $f'_c$  = concrete compressive strength, psi
- $f_{pc}$  = resultant compressive stress at centroid of composite section due to prestress and moments resisted by precast member alone, psi
- $b_w$  = web width, in.

- $d_p$  = depth from extreme compression fiber of concrete to centroid of prestressing steel where  $d_p \geq 0.80h$ , in.  
 $h$  = section depth, in.  
 $V_p$  = vertical component of effective prestress force at section, lb

The ACI Code (2008) provides expressions for determining the nominal shear strength provided by the shear reinforcement. When  $V_u$ , the factored shear force at a section, exceeds  $\phi V_c$ , where  $\phi$  is the strength reduction factor, shear reinforcement is required to satisfy Equation 5.38. When the shear reinforcement is placed perpendicular to the axis of the member, the shear strength provided by the reinforcement may be determined using Equation 5.42 (ACI 2005).

$$V_s = \frac{A_v f_{yt} d}{s} \quad (5.42)$$

with  $V_s \leq 8 \sqrt{f'_c} b_w d$

where

- $V_s$  = nominal shear strength provided by the shear reinforcement, lb  
 $A_v$  = area of shear reinforcement within spacing  $s$ , in.  
 $f_{yt}$  = yield strength of transverse reinforcement, psi  
 $d$  = depth from extreme compression fiber of concrete to centroid of longitudinal tension reinforcement, where  $d \geq 0.80h$ , in.  
 $s$  = center-to-center spacing of transverse reinforcement, in.

### 5.8.2 AASHTO-LRFD PROVISIONS FOR SHEAR STRENGTH

The AASHTO-LRFD (2007) provisions indicate that the nominal shear strength of a prestressed concrete member,  $V_n$ , be equal to the lesser of the two expressions given by Equation 5.43 and Equation 5.44.

$$V_n = V_c + V_s + V_p \quad (5.43)$$

where

- $V_c$  = nominal shear strength provided by concrete  
 $V_s$  = nominal shear strength provided by the transverse reinforcement  
 $V_p$  = vertical component of effective prestress force at the section

$$V_n = 0.25 f'_c b_v d_v + V_p \quad (5.44)$$

where

- $b_v$  = effective web width  
 $d_v$  = effective shear depth

AASHTO-LRFD Bridge Design Specifications Article 5.8.3.4.3, "Simplified Procedure for Prestressed and Nonprestressed Sections," provides a simplified method for determining the nominal shear strength of a prestressed concrete member. The concepts of this procedure are similar to those prescribed by the ACI Code and AASHTO Standard Specifications for Highway Bridges. With this method,  $V_p$  in Equations 5.39 and 5.40 shall be taken as zero and  $V_c$  shall be taken as the lesser of  $V_{ci}$  and  $V_{cw}$  as provided in Equation 5.41 and Equation 5.43.  $V_{ci}$  is the shear strength provided by concrete when flexural-shear cracking results from combined shear and moment.  $V_{cw}$  is the shear strength provided by concrete when web-shear cracking results from principal tensile stresses in the web.

$$V_{ci} = 0.02 \sqrt{f'_c} b_v d_v + V_d + \frac{V_i M_{cre}}{M_{max}} \quad (5.45)$$

where

- $V_{ci}$  = shear resistance provided by concrete when diagonal cracking results from combined shear and moment, kip
- $f'_c$  = concrete compressive strength, ksi
- $b_v$  = effective web width, in
- $d_v$  = effective depth, in.
- $h$  = section depth
- $V_d$  = shear force at the section due to unfactored dead load, lb
- $V_i$  = maximum factored shear force at section due to externally applied loads, kip
- $M_{cre}$  = moment causing flexural cracking at section due to externally applied loads, kip-in.
- $M_{max}$  = maximum factored moment at section due to externally applied loads, kip-in.

$M_{cre}$  is determined as follows.

$$M_{cre} = S_c \left( f_r + f_{cpe} - \frac{M_{dnc}}{S_{nc}} \right) \quad (5.46)$$

where

- $f_r$  = modulus of rupture of concrete, ksi
- $f_{cpe}$  = compressive stress in concrete due to effective prestress forces only at extreme tensile fiber of section, ksi
- $M_{dnc}$  = total unfactored dead load moment acting on the non-composite section, kip-in
- $S_c$  = section modulus for the extreme tensile fiber of the composite section, in<sup>3</sup>
- $S_{nc}$  = section modulus for the extreme tensile fiber of the non-composite section, in<sup>3</sup>

$$V_{cw} = (0.06 \sqrt{f'_c} + 0.30 f_{pc}) b_v d_v + V_p \quad (5.47)$$

where

- $V_{cw}$  = nominal shear strength provided by concrete when diagonal cracking results from high principal tensile stress in the web, kip
- $f'_c$  = concrete compressive strength, ksi
- $f_{pc}$  = resultant compressive stress at centroid of composite section due to prestress and moments resisted by precast member alone, ksi
- $b_v$  = effective web width, in.
- $d_v$  = effective shear depth, in.
- $V_p$  = vertical component of effective prestress force at section, lb

The shear strength provided by the shear reinforcement is given by Equation 5.48.

$$V_s = \frac{A_v f_y d_v (\cot \theta + \cot \alpha) \sin \alpha}{s} \quad (5.48)$$

where

- $V_s$  = shear resistance provided by the shear reinforcement, kip
- $A_v$  = area of shear reinforcement within spacing  $s$ , in<sup>2</sup>



- $f_y$  = yield strength of transverse reinforcement, ksi
- $d_v$  = effective shear depth, in.
- $\theta$  = angle of inclination of diagonal compressive stresses
- $\alpha$  = angle of inclination of transverse reinforcement to longitudinal axis
- $s$  = center-to-center spacing of transverse reinforcement, in.

When  $V_{ci} < V_{cw}$ ,  $\cot \theta$  shall be taken as 1.0. However, if  $V_{ci} > V_{cw}$ , then (AASHTO 2007)

$$\cot \theta = 1.0 + 3 \left( \frac{f_{pc}}{\sqrt{f'_c}} \right) \leq 1.8 \quad (5.49)$$

## 5.9 PREVIOUS TESTS OF FULL-SCALE PRESTRESSED SCC GIRDERS

A summary of previous investigations regarding full-scale prestressed SCC girders is presented in this section. Although research regarding the use of SCC for prestressed applications exists, very few studies analyze the performance of full-scale specimens.

### 5.9.1 HAMILTON, LABONTE, AND ANSLEY

Hamilton, Labonte, and Ansley (2005) conducted a study comparing the structural performance of AASHTO Type II bridge girders constructed with SCC with those cast with a standard concrete mix. The objectives of the research were to compare the fresh and hardened material properties, construction process, transfer length, camber, and shear and flexural structural behavior. After optimizing trial mix designs, six 42 ft prestressed AASHTO Type II bridge girders were constructed. Three of the girders were cast with SCC and three were cast with standard concrete mixes. Four of the girders (two SCC and two standard concrete) included a composite cap to simulate the composite action of a deck and were tested in flexure and shear. The remaining girders were tested in shear without composite action from the deck.

Shear tests were performed on each end of two girders for a total of four tests. Two different test setups were used on each end of the girders. The test results of the first test setup indicated that the girder cast with standard concrete carried 8.7% more load and deflected about 22% more than that cast with SCC concrete. The test results of the second test setup indicated that the girder cast with standard concrete and that cast with SCC concrete had nearly identical failure loads and deflections.

Shear-flexure tests were performed on each end of two girders to compare the flexural performance of SCC with that of standard concrete. In all four shear-flexure tests, failure occurred in the composite cap due to flexural compressive stresses. The researchers concluded that the flexural capacity of the SCC and standard concrete girders were similar, but the ductility of the standard concrete girder was greater than that of the SCC girder.

The final two girders were tested for shear-slip on both ends. During the test, failure in the SCC girder was due to premature strand slip at the end of the girder. The strands at that particular end of the girder were torch cut abruptly during prestress transfer. The researchers believe the abrupt prestress transfer may have contributed to the early strand slip and resulted in reduced load capacity (Hamilton et al. 2005).

### **5.9.2 *NAITO, PARENT, AND BRUNNS***

Naito, Parent, and Brunn (2006) studied the performance of full-scale SCC girders. Four 35 ft prestressed bulb-tee girders were constructed. Two of the girders were cast with SCC and two were cast with a conventional high-early strength concrete (HESC). Three failure modes were addressed during this study: compressive-flexural failure, shear-flexural failure, and tensile-flexural failure. To achieve the desired failure modes, the girders were tested in two different simply supported arrangements.

All test specimens reached theoretical flexural and shear capacities calculated with actual material properties. HESC girders achieved between 101% and 104% of the theoretical moment capacities. The SCC girders achieved between 101% and 102% of the theoretical moment capacities. The results also indicated that the measured shear capacity of the SCC and HESC girders exceeded the shear strength estimates by 6% and 7%, respectively. In all cases, the SCC girders were more ductile than the HESC girders. The researchers concluded that responses of the SCC and HESC girders were comparable and that both reached the flexural and shear capacities estimated by the ACI code (Naito et al. 2006).



## 6 EVALUATION OF SCC MIXTURES WITH LIMESTONE AGGREGATE

This chapter covers the experimental and analytical study that was carried out to evaluate the performance of SCC mixtures made with limestone aggregate. The limestone aggregate used in this study was obtained from Rapid City, SD. The purpose of this study was to assess the SCC mix properties for use in prestressed bridge girder fabrication in western South Dakota and to prepare special provisions for use by SDDOT when specifying SCC for prestressed girders. Standard tests were performed to measure the aggregate properties and the fresh and hardened SCC properties. The measured SCC properties were compared to theoretical models that are normally used to represent the performance of conventional concrete.

### 6.1 AGGREGATES MEASURED PROPERTIES

The coarse aggregate used in the SCC mix was a  $\frac{3}{8}$ " limestone chip from Rapid City, SD. The coarse aggregate is shown in Figure 6.1. The fine aggregate used in the SCC mix was Pete Lein Sand from Rapid City, SD.

The aggregates used for the SCC in this research were received at the laboratory in large bins. Aggregate samples were then reduced and tested. The aggregate sampling and testing were done in accordance with ASTM standards (ASTM 2007). Sampling of the aggregate was performed according to ASTM C 702-98: "Standard Practice for Reducing Samples of Aggregate to Testing Size." The aggregate testing data can be found in Appendix A. Following are summaries of the measured results.

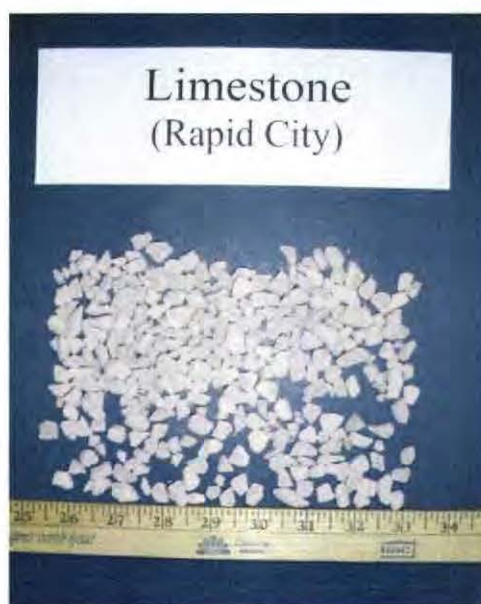


Figure 6.1:  $\frac{3}{8}$ " Limestone Chip Coarse Aggregate

#### 6.1.1 SIEVE ANALYSIS

The aggregate gradation was determined in accordance with ASTM C 117: "Standard Test Method for Materials Finer than 75- $\mu$ m (No. 200) Sieve by Washing" and ASTM C 136: "Standard Test Method for Sieve Analysis of Fine and Coarse Aggregates." The grain size distributions for the coarse and fine aggregates are presented in Figure 6.2 and 6.3, respectively. The sieve analysis showed that the grain size



distributions were within the SDDOT acceptable upper and lower limits. The fineness modulus of the fine aggregate is given in Table 6.1.

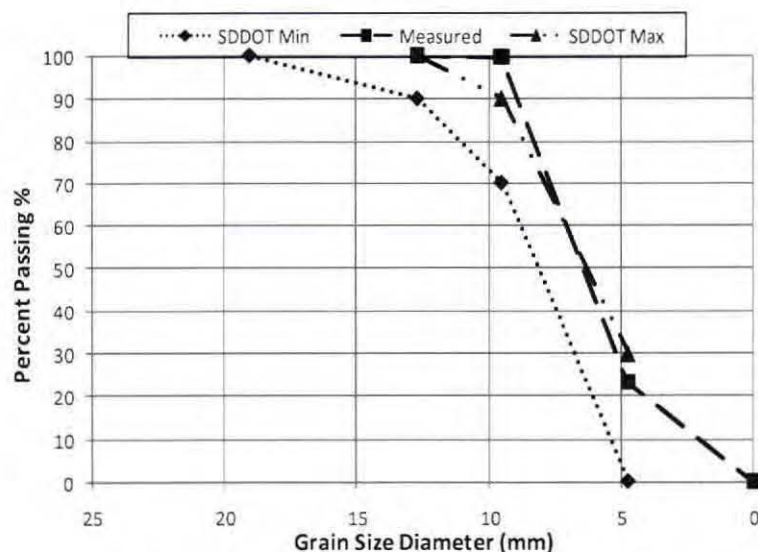


Figure 6.2: Coarse Aggregate Grain Distribution

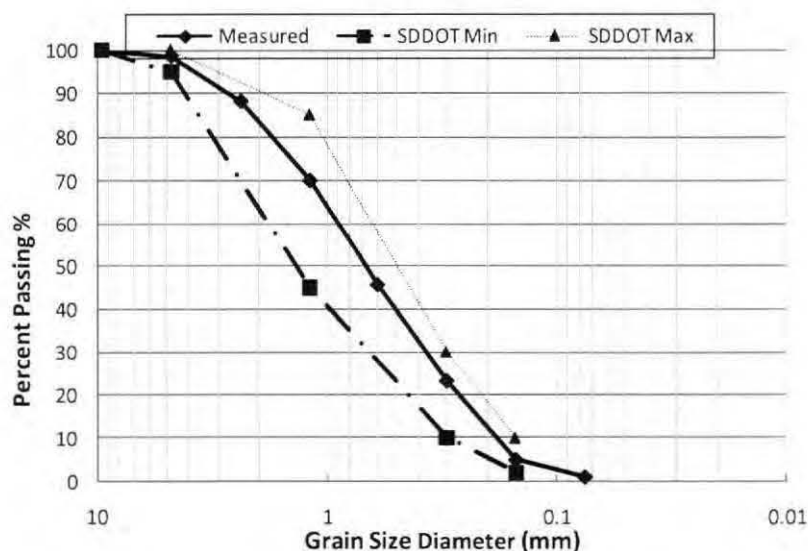


Figure 6.3: Fine Aggregate Grain Distribution

Table 6.1: Measured Fineness Modulus of the Fine Aggregate

Aggregate	Fineness Modulus
Rapid City Sand	2.69

### 6.1.2 DENSITY, SPECIFIC GRAVITY, AND ABSORPTION

Three samples of each aggregate were tested for saturated surface dry (SSD) density, SSD specific gravity, and absorption. The tests were performed according to ASTM C 127-04: "Standard Test Method for Density, Relative Density (Specific Gravity), and Absorption of Coarse Aggregate" and ASTM C 128-04a: "Standard Test Method for Density, Relative Density (Specific Gravity), and

Absorption of Fine Aggregate”: The average measured SSD densities, SSD specific gravities, and absorptions for the coarse and fine aggregate are presented in Table 6.2. The values fell within the expected ranges for the aggregate properties. Typically, the specific gravity of aggregate is between 2.4 and 2.9. The absorption of coarse aggregate normally ranges between 0.2% and 4%, and that of fine aggregates ranges between 0.2% and 2% (Kosmatka et al. 2002).

**Table 6.2: Aggregate SSD Density, SSD Specific Gravity, and Absorption**

Aggregate	SSD Density (lb/ft <sup>3</sup> )	SSD Specific Gravity	Absorption (%)
Rapid City Limestone	158.2	2.54	0.66
Rapid City Sand	164.1	2.64	1.19

### 6.1.3 **BULK DENSITY**

The bulk density was measured according to ASTM C 29-97: “Standard Test Method for Bulk Density (“Unit Weight”) and Voids in Aggregate.” The values for each test were averaged and recorded. The measured bulk densities of the oven dried aggregates are listed in Table 6.3. The measured values were reasonable and within expected results.

**Table 6.3: Aggregate SSD Density, SSD Specific Gravity, and Absorption**

Aggregate	Dry Bulk Density (lb/ft <sup>3</sup> )
Rapid City Limestone	96.7
Rapid City Sand	101.3

## 6.2 **LABORATORY CONCRETE MIXTURES**

### 6.2.1 **MIX DESIGN**

One conventional concrete and four SCC mixtures were studied in this research. The main variables among the SCC mixtures were the w/c ratio and the method of curing. A w/c ratio of 0.33 was used for the conventional concrete mix and for the control SCC mix. The conventional concrete and the control SCC mix designs were prepared by Cretex Concrete Products West in Rapid City, SD. Three w/c ratios were implemented in the SCC mixtures: 0.33, 0.35, and 0.37. All of the concrete mixtures were moist cured. Specimens from the SCC control mix were also heat cured in order to study the effect of accelerated curing on SCC hardened properties. To identify the different mixes, the prefixes “S” and “CC” were used for SCC and conventional concrete, respectively. A numeric suffix was used to identify the w/c ratio used in the mix. For the heat cured mix, the letter “A” was added to the suffix. The mix design matrix is shown in Table 6.4.



**Table 6.4: Mix Design Matrix**

Mix ID	S33	S35	S37	S33-A	CC33
w/c Ratio	0.33	0.35	0.37	0.33	0.33
Concrete Type	SCC	SCC	SCC	SCC	Conventional
Coarse Aggregate	Rapid City Limestone	Rapid City Limestone	Rapid City Limestone	Rapid City Limestone	Rapid City Limestone
Fine Aggregate	Rapid City Sand	Rapid City Sand	Rapid City Sand	Rapid City Sand	Rapid City Sand
Curing Method	Moist	Moist	Moist	Heat	Moist

The cement used to produce the concrete mixtures was GCC Dacotah Type I/II. Three admixtures were added to the SCC mixtures: Daravair® M air entrainer, ADVA® Cast 555 superplasticizer, and Daratard® 17 set retardant. The ADVA® Cast 555 superplasticizer contains a viscosity modifying agent. For the conventional concrete mix, Daracem® 19 instead of ADVA® Cast 555 was used as superplasticizer. Grace Construction Products developed and provided all of the admixtures. Literature on the admixtures can be found in Appendix B. The mix design proportions are shown in Table 6.5. Based on observed behavior of the fresh SCC during mixing, the quantities of the superplasticizer and the air entrainer had to be adjusted to create the desired SCC characteristics. Typically, the mixes required less superplasticizer and more air entrainer than the quantities required in the original mix designs. The design quantities and actual quantities used in preparing the SCC mixtures are shown in Table 6.6.

**Table 6.5: Mix Design Matrix**

Mix Designation	S33	S35	S37	CC33
Coarse (lb/cu yd)	1499	1499	1499	1875
Fine (lb/cu yd)	1343	1343	1343	1200
Cement (lb/cu yd)	832	795.6	772.4	667.0
W/C Ratio	0.33	0.35	0.37	0.33
Water (lb/cu yd)	274.6	278.5	285.8	220.0
Daravair® M (oz/cwt)	1.76	1.76	1.76	1.43
Daratard® 17 (oz/cwt)	3.01	3.01	3.01	2.00
ADVA® 555 (oz/cwt)	29.10	29.10	29.10	-
Daracem® 19 (oz/cwt)	-	-	-	18.57

**Table 6.6: Design and Actual Superplasticizer and Air Entrainment Quantities**

	ADVA 555 (oz/cwt)		Daravair M (oz/cwt)	
	Design	Actual	Design	Actual
S33	29.1	22.35	1.76	1.71
S35	29.1	21.25	1.76	1.57
S37	29.1	20.81	1.76	1.40



### 6.2.2 MIXING AND BATCHING

The mixer used to produce the concrete was a portable tilt-drum mixer. The mixer had a rotating drum with three interior paddles. The angle of the mixer drum was adjustable. The mixer capacity was one third of a cubic yard. However, the batch size was limited to one tenth of a cubic yard due to the fluidity of the SCC mixtures. By limiting the batch size, the drum could be tilted so the SCC would mix well without spilling.

The same mixing regimen was used for all the mixes developed in this research. First, the drum of the mixer was moistened to prevent any absorption of water from the mix to the drum. All of the dry ingredients (coarse aggregate, fine aggregate, and cement) were added and well mixed before adding the water. The batch quantity of water was split into 80% and 20%. The air entrainer was added to the 80% of the batch quantity water. The 80% water and air entrainer were mixed with the dry ingredients. The set retardant was added next, followed by the remaining 20% water. The superplasticizer was added last and the batch was then mixed for eight minutes. The eight minutes mixing period was found to be an optimum duration to ensure the dispersion of the superplasticizer and the development of the appropriate viscosity.

### 6.2.3 CURING METHODS

Concrete specimens consisting of standard 6"×12" cylinders and 6"×6"×22" beams were cast and cured in the Materials Laboratory at SDSU. Specimens from S33, S35, S37, and CC33 were moist cured in a moisture room for the intended specimen age. Additional specimens from the SCC mix with w/c ratio of 33% were heat cured for accelerated curing (high early strength). The mix corresponding to the heat cured specimens was labeled S33-A.

Two heat curing boxes were used to cure the S33-A concrete cylinders and beams. The exterior and interior views of one of the curing boxes are shown in Figure 6.4. The curing box had a single heating element installed beneath a raised wire grid floor. A fan circulated the heated air inside the curing box. The interior temperature was monitored by a thermocouple. The heating element was controlled by a microprocessor on the outside of the box. The microprocessor was programmable to control the temperature level and duration inside the box.



(a) Exterior View



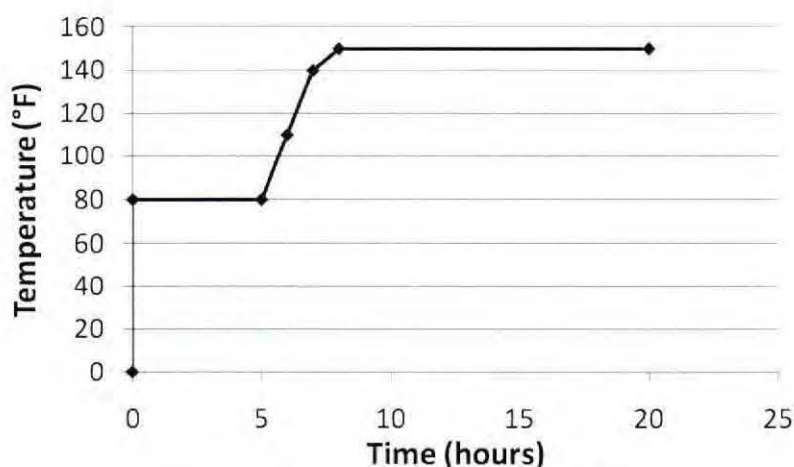
(b) Interior View

Figure 6.4: Heat (Accelerated) Curing Box

The heating program that was used to cure the specimens in this study is listed in Table 6.7 and shown in Figure 6.5. The three types of functions used in the heat program were “Step-Up”, “Soak”, and “End-Hold”. A Step-Up function raises the temperature to the set point in the programmed amount of time. The Soak function holds the temperature constant for the programmed amount of time. The End-Hold function ends the program and holds the final temperature until the processor is switched off. The microprocessor had two digital display screens. The top displayed the current temperature inside the box, and the bottom displayed the set point for the current phase of the program.

**Table 6.7: Heat Curing Protocol**

Step	Function	Temperature (°F)	Duration
1	Step-Up	80	-
2	Soak	80	5 hours
3	Step-Up	110	1 hour
4	Step-Up	140	1 hour
5	Step-Up	150	1 hour
6	Soak	150	12 hours
7	End-Hold	150	1 hour



**Figure 6.5: Heat Curing Step-Up and Soak**

## 6.3 FRESH PROPERTIES

The fresh SCC was discharged from the mixer into a wheelbarrow. Test samples were made for measuring the fresh and hardened properties of the SCC and mixtures. The fresh concrete was sampled according to ASTM C 172-04: “Standard Practice for Sampling Freshly Mixed Concrete” (ASTM 2006). The results of the SCC fresh properties are summarized in Table 6.8.

### 6.3.1 SLUMP FLOW

The flowability of the SCC mix was measured according to ASTM C 1611: “Standard Test Method for Slump Flow of Self-Consolidating Concrete”. In this study, the slump flow was measured for every SCC



batch. The average measured slump spread values versus the w/c ratio and the amount of superplasticizer are shown in Figure 6.6. The average slump spread values were approximately 25.1", 24.2", and 23.5" for S33, S35, and S37, respectively. These values were well within the normally accepted slump spread range of 20" to 28".

**Table 6.8: Measured SCC Fresh Properties**

Mix ID	Slump Flow (in)	J-Ring Spread (in)	T20 (sec)	VSI	L-Box			Unit Weight (pcf)	Air Content (%)	Temperature (°F)
					H1	H2	H2/H1			
RC-PS-S33-1		-----Failed Slump Flow (> 28")-----								
RC-PS-S33-2	27.75	27	2.35	0	5	1.5	0.30	138.5	7.40%	77
RC-PS-S33-3	21.50		3.27	0						
RC-PS-S33-4		-----Failed Slump Flow (=18")-----								
RC-PS-S33-5	24.00		2.23	0						
RC-PS-S33-6	24.00		2.66	0						
RC-PS-S33-7	27.50		1.76	0						
RC-PS-S33-8	27.50		1.77	0						
RC-PS-S33-9	26.00		2.03	1						
RC-PS-S33-10	22.50		2.08	0						

Mix ID	Slump Flow (in)	J-Ring Spread (in)	T20 (sec)	VSI	L-Box			Unit Weight (pcf)	Air Content (%)	Temperature (°F)
					H1	H2	H2/H1			
RC-PS-S35-1	22.00		2.58	0						
RC-PS-S35-2	24.00	22.5	1.19	0	4	2.5	0.63	141.1	6.20%	77
RC-PS-S35-3	24.50		1.67	0						
RC-PS-S35-4	28.00		1.01	1						
RC-PS-S35-5	28.00		1.91	1					7.80%	
RC-PS-S35-6	24.00		1.76	0						
RC-PS-S35-7	22.00		2.1	0						
RC-PS-S35-8	21.50		2.39	0						

Mix ID	Slump Flow (in)	J-Ring Spread (in)	T20 (sec)	VSI	L-Box			Unit Weight (pcf)	Air Content (%)	Temperature (°F)
					H1	H2	H2/H1			
RC-PS-S37-1	21.75		1.76	0						
RC-PS-S37-2	21.00		1.84	0						
RC-PS-S37-3	21.00	18.25	2.13	0	5	3.25	0.65	136.4	7.80%	79
RC-PS-S37-4	26.50		1.46	0						
RC-PS-S37-5	21.50		2.19	0						
RC-PS-S37-6	28.00		2.43	0.5						
RC-PS-S37-7	28.00		1.72	0						
RC-PS-S37-8	20.00		2.97	0						

Mix ID	Slump Flow (in)	J-Ring Spread (in)	T20 (sec)	VSI	L-Box			Unit Weight (pcf)	Air Content (%)	Temperature (°F)
					H1	H2	H2/H1			
RC-PS-S33A-3	27.00		1.98	0						
RC-PS-S33A-4	28.00		1.89	1						
RC-PS-S33A-5	26.50		1.53	0						
RC-PS-S33A-6	22.00		3.09	0						
RC-PS-S33A-7	27.50		1.67	0						
RC-PS-S33A-8	26.50		1.89	0	3.75	2.38	0.63			



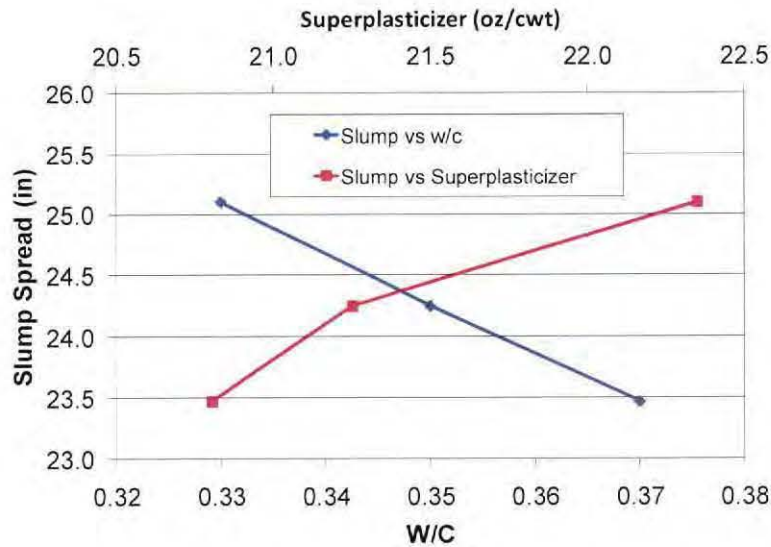


Figure 6.6: Measured Average Slump Spread versus W/C and Amount of Superplasticizer

Figure 6.6 indicates that the slump spread increased with an increase in the amount of the superplasticizer, but decreased with an increase in the w/c ratio. Since the ratio of the superplasticizer to the w/c was not kept the same for all of the mixes, the trend of the slump spread relative to the change in the w/c ratio would be misleading in this case. A better parameter to gauge the variation of the slump spread would be a normalized value of the amount of superplasticizer with respect to w/c. Figure 6.7 shows a plot of the slump spread versus the ratio of the superplasticizer to w/c. The figure also shows the best fit line of the data points with a coefficient of determination  $R^2$  of 0.99 (correlation coefficient =  $R = 0.99$ ). It is clear from Figure 6.7 that, for the data range and mix proportions considered in this study, the slump spread varied linearly with the normalized amount of superplasticizer. The measured results indicate that for a 1 oz/cwt increase in the normalized amount of superplasticizer, the slump spread increases by 0.14".

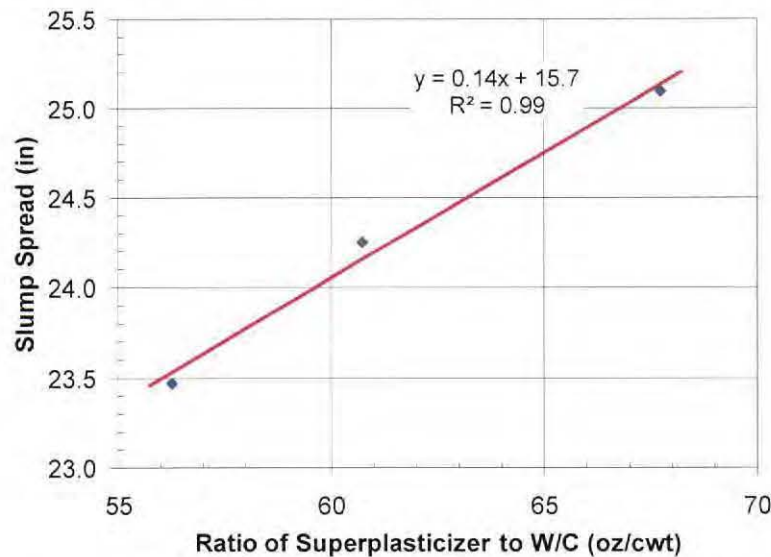


Figure 6.7: Measured Average Slump Spread versus Normalized Amount of Superplasticizer

### 6.3.2 VISUAL STABILITY INDEX (VSI) AND $T_{20}$

The VSI test was performed immediately following the slump flow test according to ASTM C 1611: “Standard Test Method for Slump Flow of Self-Consolidating Concrete.” The VSI was evaluated for every batch of SCC. All three mixes were rated an average VSI of 0. A rating of 0 indicates high dynamic stability and absence of segregation.

The  $T_{20}$  test results varied between 1 and 3.3 seconds with an average of approximately 2 seconds. The  $T_{20}$  measurements are plotted against the normalized amount of superplasticizer in Figure 6.8. Nowak et al. (2005) suggested an acceptable  $T_{20}$  range of 2 to 5 seconds. However, the  $T_{20}$  results are seldom used as acceptance criteria. A previous study on the performance of SCC materials showed that SCC batches with  $T_{20}$  less than 2 seconds were still robust and acceptable (Wehbe et al. 2007b). The  $T_{20}$  results in this study were too scattered to be able to draw any significant correlations.

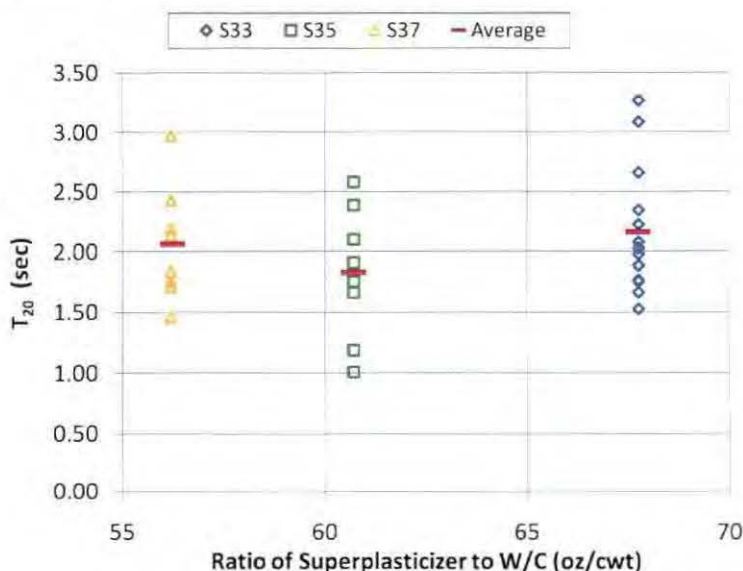


Figure 6.8:  $T_{20}$  versus Normalized Amount of Superplasticizer

### 6.3.3 J-RING SPREAD

The blocking potential was measured using the J-ring test. The test was performed according to ASTM C 1621: “Standard Test Method for Passing Ability of Self-Consolidating Concrete by J-Ring”. The blocking potential is evaluated as the difference in spread between the slump flow and J-ring tests. A difference of less than 1" indicates no visible blocking. A difference between 1" and 2" indicates minimal to noticeable blocking. A difference of more than 2" indicates noticeable to extreme blocking. The average measured slump and J-Ring spreads results are shown and compared in Figure 6.9. The results suggest that S33 had no visible blocking, S35 had minimal blocking, and S37 had noticeable blocking.

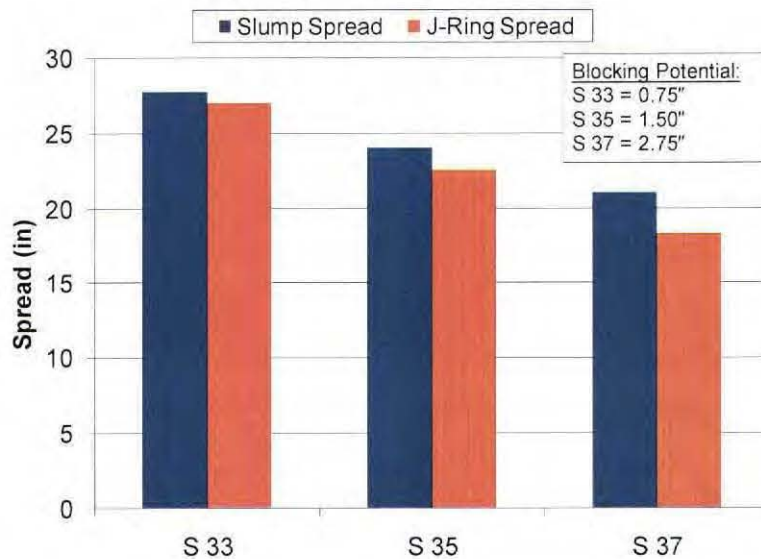


Figure 6.9: Measured Blocking Potential

The blocking potential was plotted versus the amount of superplasticizer and the w/c ratio. The plots are shown in Figure 6.10. Similar to the trends exhibited by the slump spread (Section 6.3.1), the blocking potential increased with an increase in the amount of the superplasticizer, but decreased with an increase in the w/c ratio. A better parameter to gauge the variation of the blocking potential would be the normalized value of the amount of superplasticizer with respect to w/c ratio. Figure 6.11 shows a plot of the blocking potential versus the ratio of the superplasticizer to w/c. The figure also shows the best fit line of the data points with a coefficient of determination  $R^2$  of 0.93 (correlation coefficient =  $R = 0.96$ ). It is clear from Figure 6.11 that, for the data range and mix proportions considered in this study, the blocking potential varied approximately linearly with the normalized amount of superplasticizer. The measured results indicate that for a 1 oz/cwt increase in the normalized amount of superplasticizer, the blocking potential decreases by 0.17".

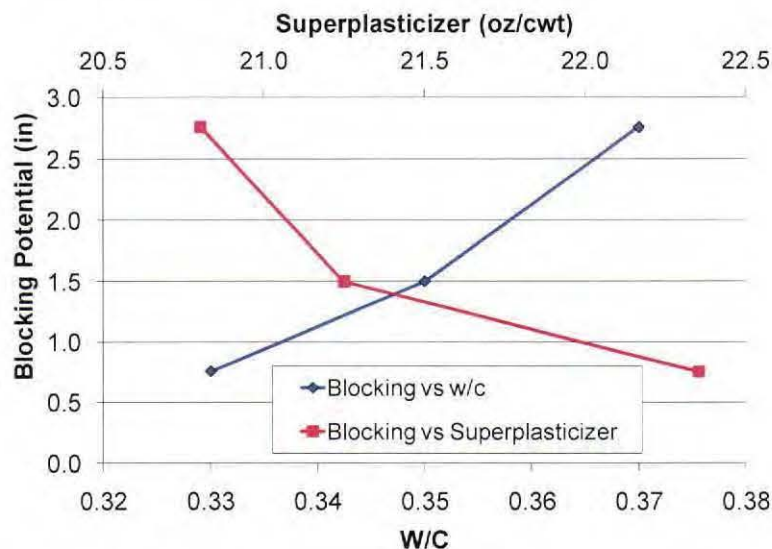


Figure 6.10: Blocking Potential versus Amount of Superplasticizer and W/C Ratio



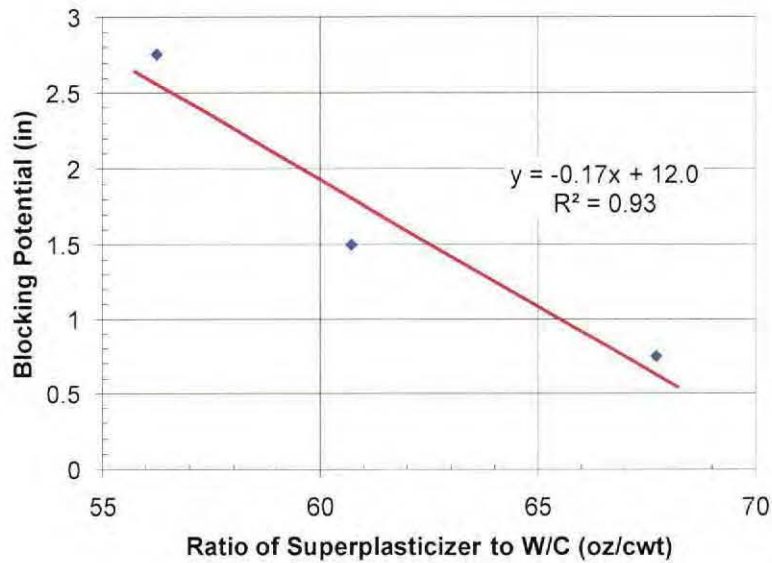


Figure 6.11: Blocking Potential versus Normalized Amount of Superplasticizer

#### 6.3.4 L-Box

The filling ability was measured using the L-Box test. The test was performed in accordance with the PCI interim guidelines (2003). The measured L-Box results were expressed in terms of the ratio  $H_2/H_1$ , where  $H_2$  is the height of the concrete at the downstream end and  $H_1$  is the height of the concrete at the upstream end of the L-Box trough. Figure 6.12 shows the averaged test results. The average L-Box ratios were 0.62, 0.61, and 0.63 for S33, S35, and S37, respectively. EFNARC (2002) recommends the L-Box ratio to be in the vicinity of 0.8. Although the measured values were below that recommended by EFNARC, the L-Box test is not considered by ASTM as a standard test for SCC.

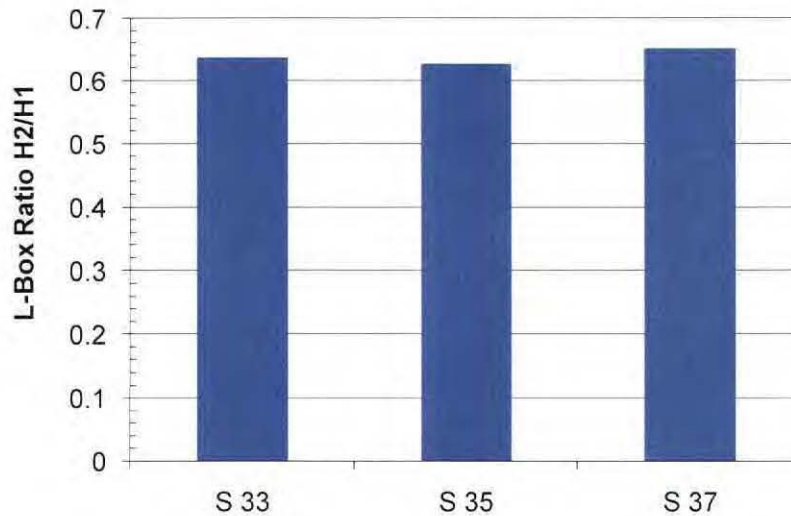


Figure 6.12: Measured L-Box Ratios

Figure 6.13 shows a plot of the L-Box ratios versus the amount of the superplasticizer and the w/c ratio. The plots indicate that the L-Box ratio was insensitive to both the w/c ratio and the amount of

superplasticizer. Therefore, the L-Box ratio will also be insensitive to the ratio of the amount of superplasticizer to the w/c ratio. Hence, no conclusive trends could be established.

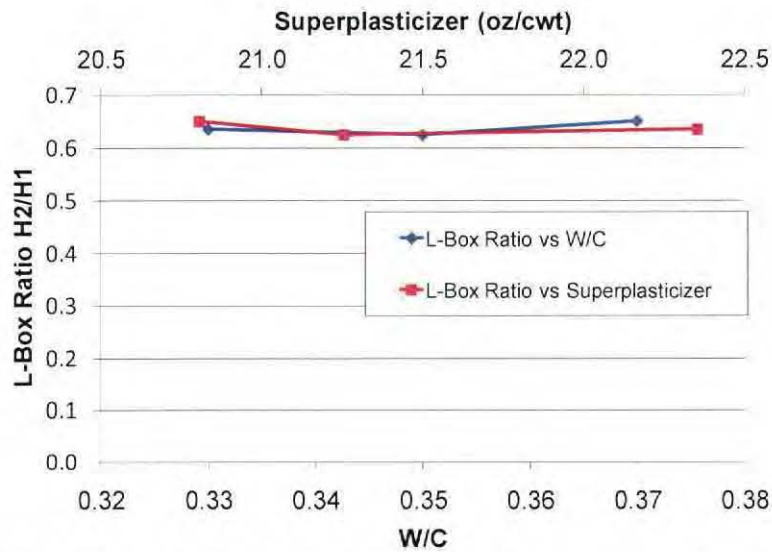


Figure 6.13: Measured L-Box Ratio versus Amount of Superplasticizer and W/C Ratio

### 6.3.5 COLUMN SEGREGATION

The static stability of the SCC mixes was measured using the column segregation test. The test was performed according to ASTM C 1610: "Standard Test Method for Static Segregation of Self-Consolidating Concrete Using Column Technique." The column segregation test result is expressed as the percentage ratio of the difference of aggregate mass between the bottom and the top segments of the column to the total aggregate mass in the two segments. For the mixes considered in this study, the column segregation was 6.5% for the S37 mix, and nonexistent for the S33 and S35 mixes. The results indicate that the columns segregation of the SCC mixes was insignificant. The column segregation test results are shown in Figure 6.14.

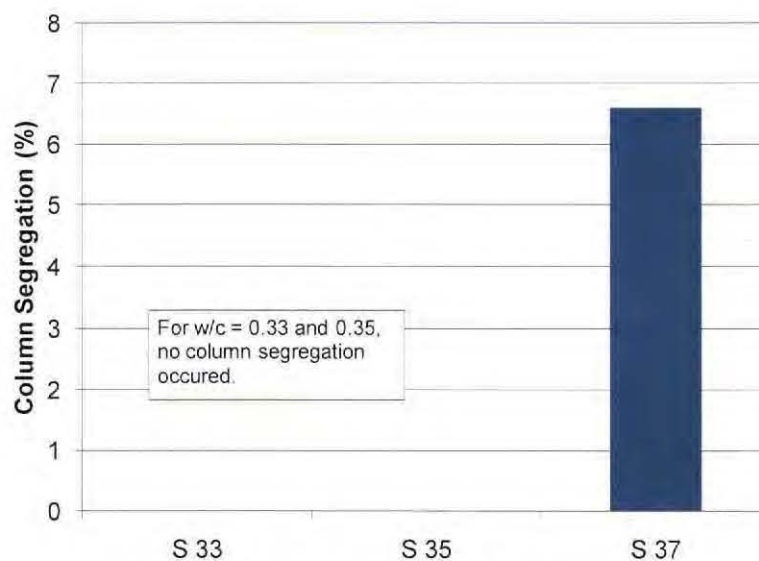


Figure 6.14: Measured Column Segregation

### 6.3.6 AIR CONTENT

The air content was measured according to ASTM C 231: "Standard Test Method for Air Content of Freshly Mixed Concrete by the Pressure Method." The amount of air entrainer was altered from the mix design for each mix in order to achieve acceptable air content between 6% and 8%. The averaged measured air content was 7.4%, 7.8%, and 7.8% for S33, S35, and S37, respectively. The measured values are shown in Figure 6.15.

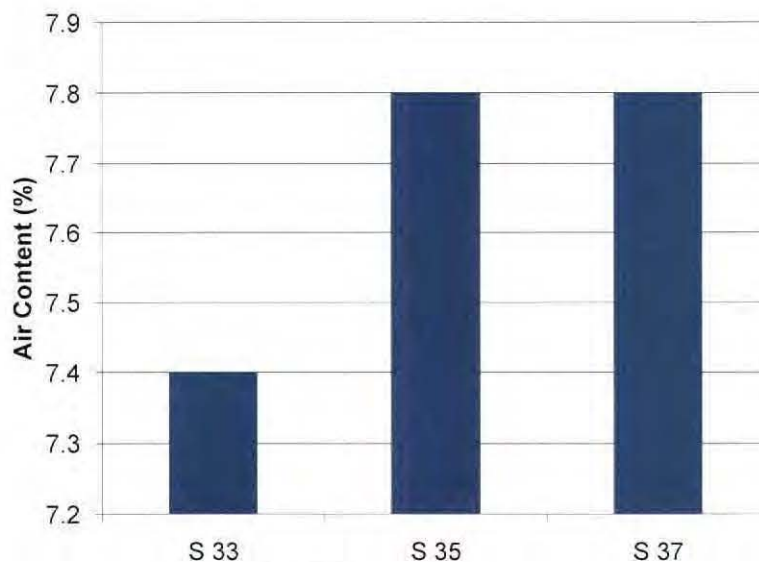


Figure 6.15: Measured Air Content

The measured air content was practically the same for all three SCC mixes. Therefore, the results were used to determine a parametric relationship between the amount of air entrainer and the normalized amount of superplasticizer for a constant air content value. For all practical purposes, the average measured air content was approximately 7.6%. Figure 6.16 shows the measured amount of air entrainer versus the normalized amount of superplasticizer for an air content of approximately 7.6%. The figure also shows the best fit line of the data points with a coefficient of determination  $R^2$  of 0.97 (correlation coefficient =  $R = 0.98$ ). The plot indicates that to maintain an air content of 7.6% in the SCC mixes considered in this study, the air entrainer amount would have to be increased by 0.026 oz/cwt when the normalized amount of superplasticizer is increased by 1 oz/cwt.



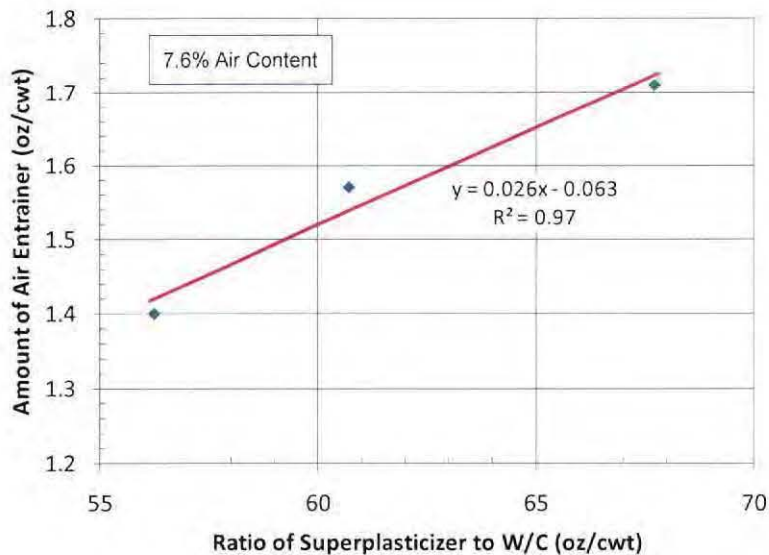


Figure 6.16: Amount of Air Entrainment versus Normalized Amount of Superplasticizer for Air Content = 7.6%

#### 6.3.7 MIX TEMPERATURE

The mix temperatures were 77°F, 77°F, and 79°F for S33, S35, and S37, respectively. These values were within the SDDOT acceptable temperature range of 50 – 80 °F (Wehbe et al. 2007).

### 6.4 HARDENED PROPERTIES

Standard 6"×12" cylinders and 6"×6"×22" beams were prepared according to ASTM C 192-06 "Standard Practice for Making and Curing Concrete Test Specimens in the Laboratory" with two exceptions: the SCC specimens were not rodded and they were filled in one lift when possible. This section covers the measured hardened properties of the concrete mixes considered in this study.

#### 6.4.1 COMPRESSIVE STRENGTH

The concrete compression tests were performed according to ASTM C 39. Compressive strength measurements were done at 18 hours and at 3, 7, 14, and 28 days. Each measurement consisted of the average of at least three compression tests. The compression test results are summarized in Table 6.9 and plotted in Figure 6.17. In general, the measured compressive strength followed expected trends. The compressive strength increased with time, decreased with increasing w/c ratio, and had earlier gains under heat curing conditions. At 18 hours, the compressive strength of the heat cured mix (S33-A) was 80% higher than the similar but moist cure mix (S33). At 3 days, the compressive strength of the heat cured mix was 43% higher than that of the moist cure mix.

Table 6.9: Measured Average Concrete Compressive Strength

Age	Compressive Strength, $f'_c$ (psi)			
	S33	S35	S37	S33-A
18 hours	2,736	1,640	1,071	4,919
3 days	3,951	4,170	3,291	5,644
7 days	6,169	4,332	4,030	6,399
14 days	6,759	4,671	4,657	6,670
28 days	8,280	5,286	5,007	7,260

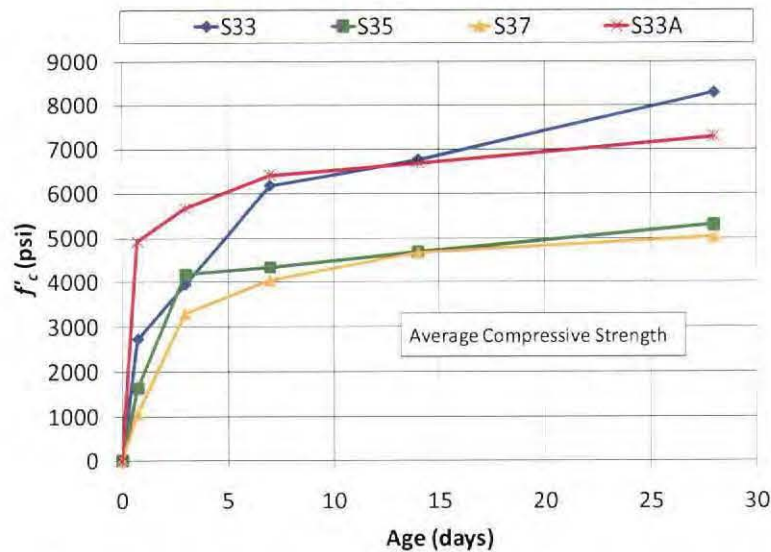


Figure 6.17: Compressive Strength versus Age of Concrete

The rate of strength gain was analyzed using a model that was developed for conventional concrete. The concrete strength at a given age  $t$ , where  $t$  is in days, is given by (Nawy 2006)

$$f'_{ct} = \frac{t}{\alpha + \beta t} f'_c \quad (6.1)$$

where

- $f'_{ct}$  = compressive strength at time  $t$
- $f'_c$  = 28-day compressive strength
- $\alpha$  = factor based on cement type and curing method
- $\beta$  = factor based on curing method and curing method

For moist-cured Type I cement,  $\alpha$  is 4.0 and the  $\beta$  is 0.85. For steam-cured Type I cement,  $\alpha$  is 1.0 and the  $\beta$  is 0.95. The calculated compressive strength results are summarized in Table 6.10. The theoretical and measured (experimental) results for S33, S35, S37, and S33-A are presented in Figures 6.18, 6.19, 6.20, and 6.21, respectively. The plots show a generally good agreement between the experimental and the theoretical results for both S33 and S33-A. However, the theoretical model seems to underestimate the early strength of S35 and S37.

Table 6.10: Theoretical Concrete Compressive Strength

Age	Compressive Strength, $f'_c$ (psi)			
	S33	S35	S37	S33-A
18 hours	1,339	855	810	3,180
3 days	3,792	2,421	2,293	5,657
7 days	5,825	3,719	3,523	6,643
14 days	7,291	4,654	4,409	7,108
28 days	8,280	5,286	5,007	7,365

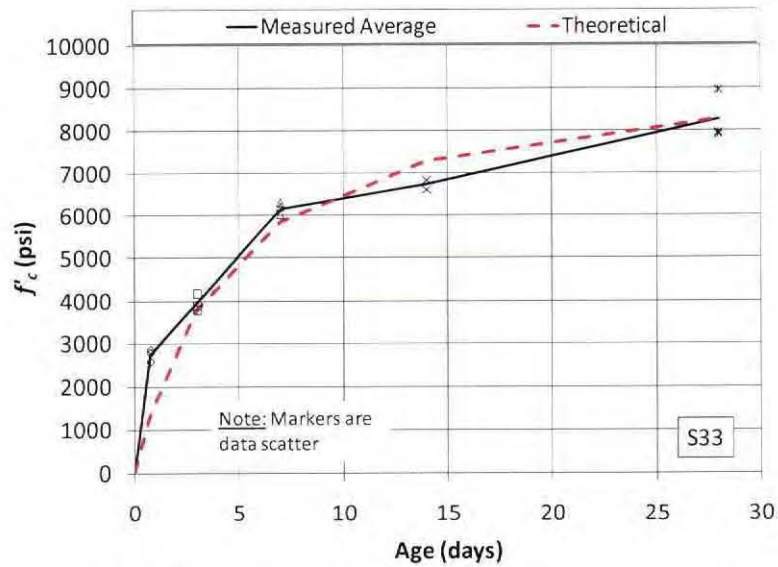


Figure 6.18: Measured and Theoretical Strength Gain for S33

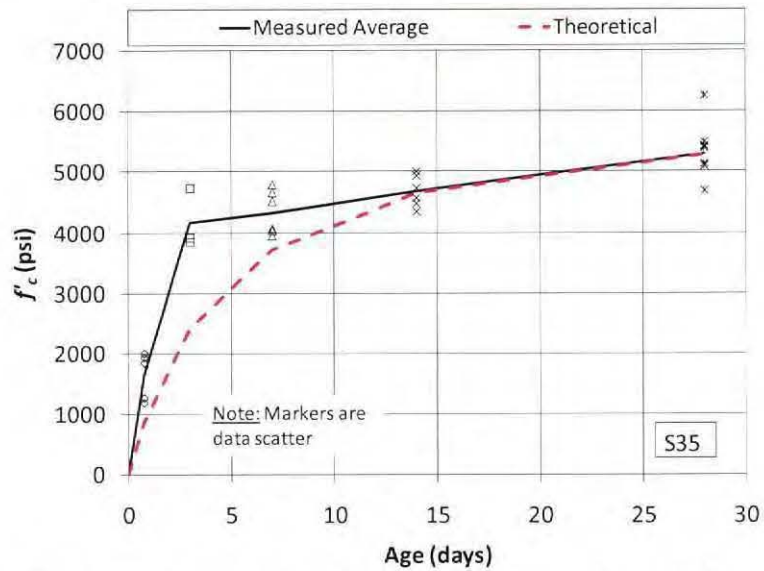


Figure 6.19: Measured and Theoretical Strength Gain for S35



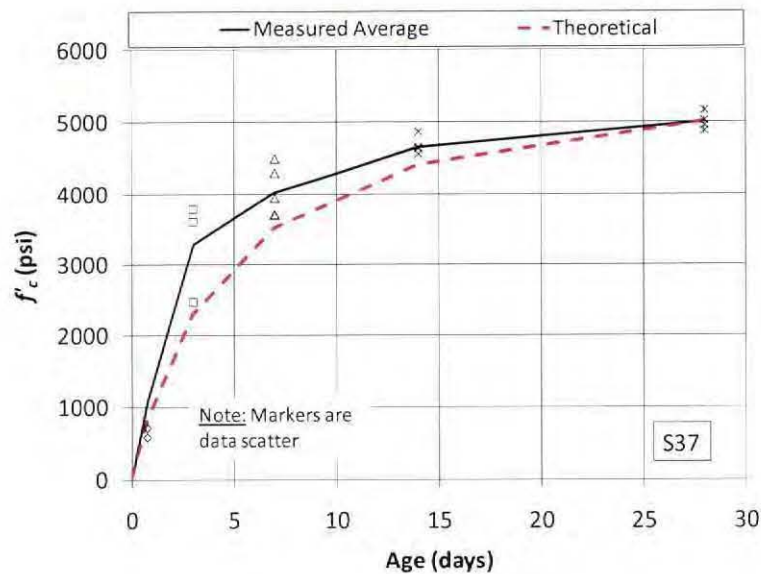


Figure 6.20: Measured and Theoretical Strength Gain for S37

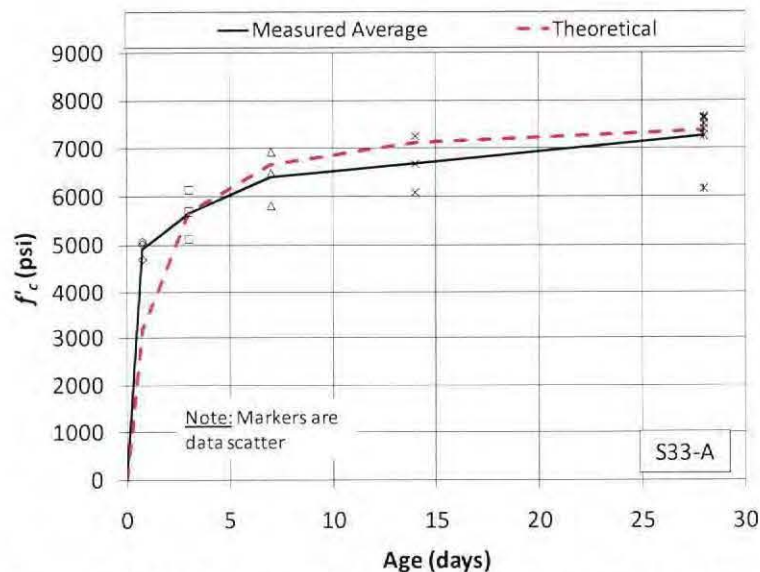


Figure 6.21: Measured and Theoretical Strength Gain for S33-A

#### 6.4.2 FLEXURAL STRENGTH (MODULUS OF RUPTURE)

The concrete flexural tests were performed according to ASTM C 78. Flexural strength measurements were done at 18 hours and at 3, 7, 14, and 28 days. Each measurement consisted of the average of at least three flexural tests. The flexural test results are summarized in Table 6.11 and plotted in Figure 6.22.

Some of the measurements did not follow the expected trends. For S33, the 3 days measured flexural was 67% higher than the 7 days flexural strength, and the 7 days flexural strength was 53% higher than the 14 days flexural strength. Moreover, the flexural strength of S37 was higher than that of S35 at 7, 14, and 28 days and higher than that of S 33 at 7 and 28 days. The reason for such unpredictable results was unknown at the time of writing of this report.

Table 6.11: Measured Average Concrete Flexural Strength

Age	Flexural Strength, $f_r$ (psi)			
	S33	S35	S37	S33-A
18 hours	261	106	314	472
3 days	583	628	533	661
7 days	679	375	543	592
14 days	444	414	539	592
28 days	565	546	638	697

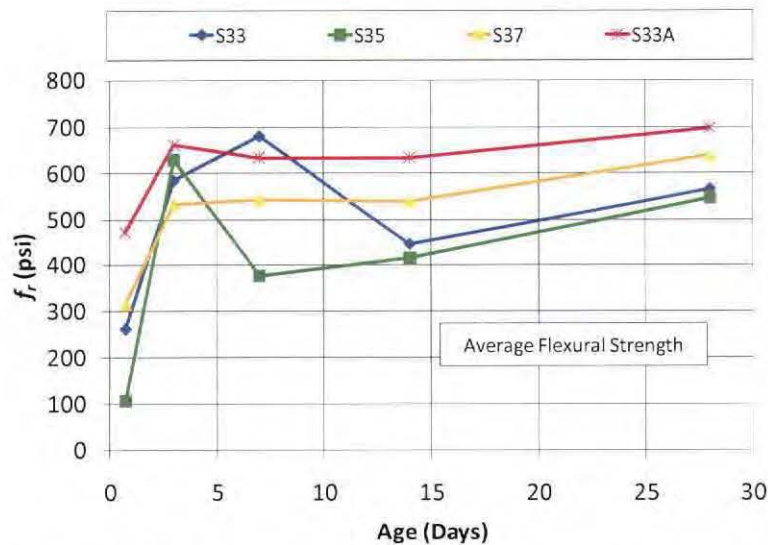


Figure 6.22: Measured Flexural Strength versus Age of Concrete

Table 6.12 presents a summary of the mean and standard deviation of the measured flexural strength values in terms of  $\sqrt{f'_c}$ . The measured flexural strength values at 18 hours, 3 days, 7 days, 14 days, and 28 days are plotted versus  $\sqrt{f'_c}$  in Figures 6.23, 6.24, 6.29, 6.26, and 6.27, respectively. The plots also show the mean and the standard deviation of the measurements as functions of  $\sqrt{f'_c}$ . The line labeled  $7.5 \sqrt{f'_c}$  represents the empirical code equation for determining the modulus of rupture (Equation 5.1). In some cases, the measurements had a wide scatter (e.g. at 18 hours), while in other cases the measurement scatter was tight (e.g. at 3 days). The mean varied between a lower value of  $9.8 \sqrt{f'_c}$  (at 18 hours) and an upper value of  $9.27 \sqrt{f'_c}$  (at 3 days).

The entire flexural strength data set is plotted in Figure 6.28. When all of the measurements are combined, the overall mean is  $7.49 \sqrt{f'_c}$ . Although the overall mean is practically equal to the value obtained from the code empirical equation, the standard deviation of  $1.85 \sqrt{f'_c}$  indicates a wide scatter. However, the flexural strength of concrete has been reported to vary between  $7 \sqrt{f'_c}$  and  $13 \sqrt{f'_c}$  (Park and Paulay 1975).

Table 6.12: Mean and Standard Deviation of Measured Flexural Strength

Age	Measured Flexural Strength, $f_r$ (psi)	
	Mean	Standard Dev.
18 hours	$5.98 \sqrt{f'_c}$	$2.94 \sqrt{f'_c}$
3 days	$9.27 \sqrt{f'_c}$	$0.38 \sqrt{f'_c}$
7 days	$7.70 \sqrt{f'_c}$	$1.38 \sqrt{f'_c}$
14 days	$6.78 \sqrt{f'_c}$	$1.24 \sqrt{f'_c}$
28 days	$7.73 \sqrt{f'_c}$	$1.19 \sqrt{f'_c}$
Overall	$7.49 \sqrt{f'_c}$	$1.85 \sqrt{f'_c}$

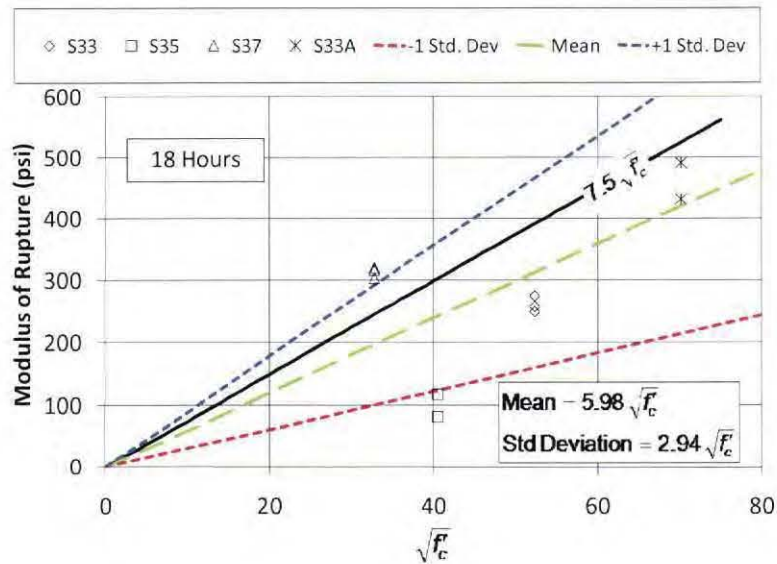


Figure 6.23: Measured Flexural Strength at 18 Hours

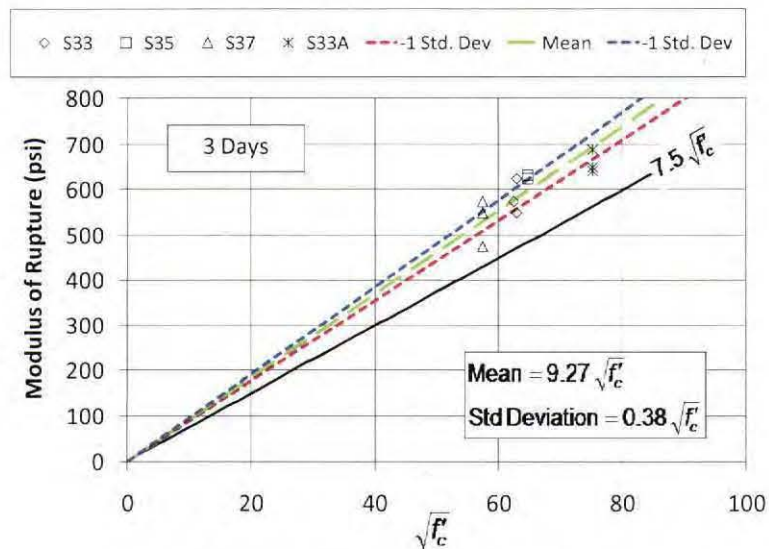


Figure 6.24: Measured Flexural Strength at 3 Days



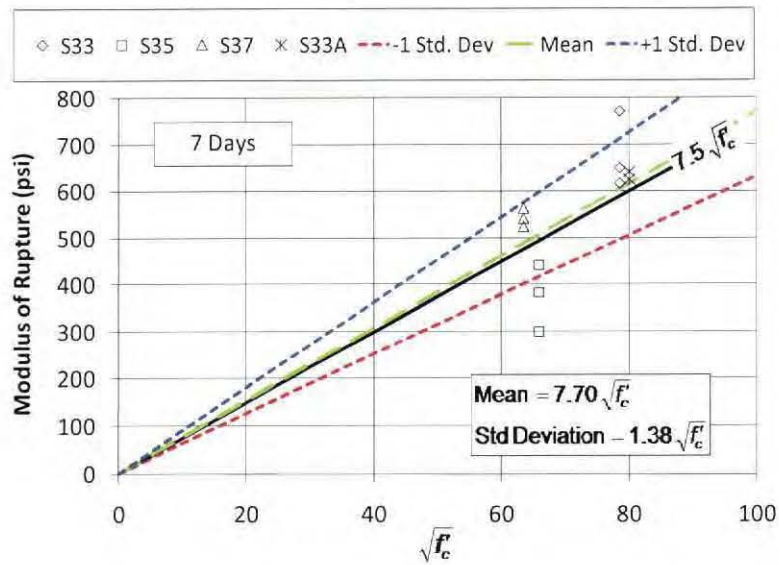


Figure 6.25: Measured Flexural Strength at 7 Days

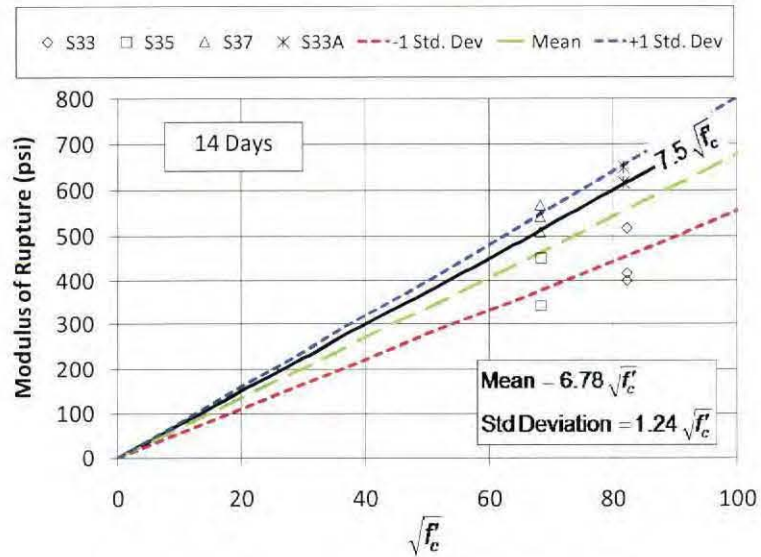


Figure 6.26: Measured Flexural Strength at 14 Days

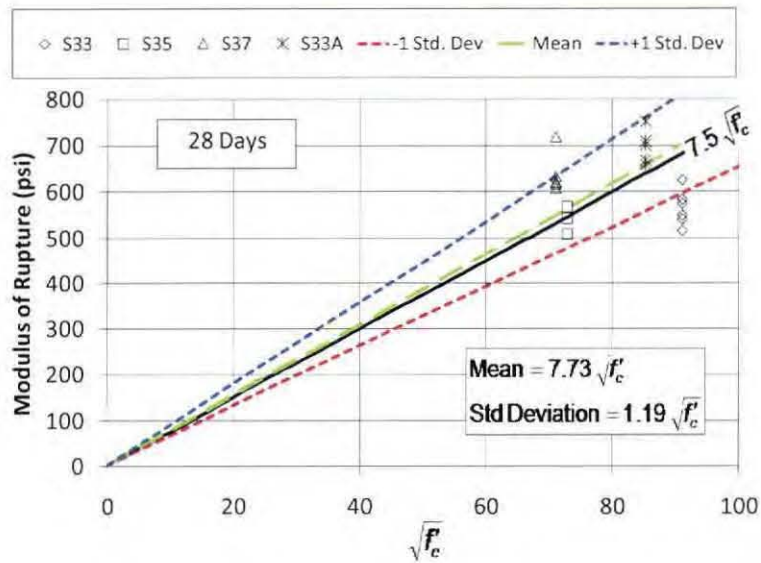


Figure 6.27: Measured Flexural Strength at 28 Days

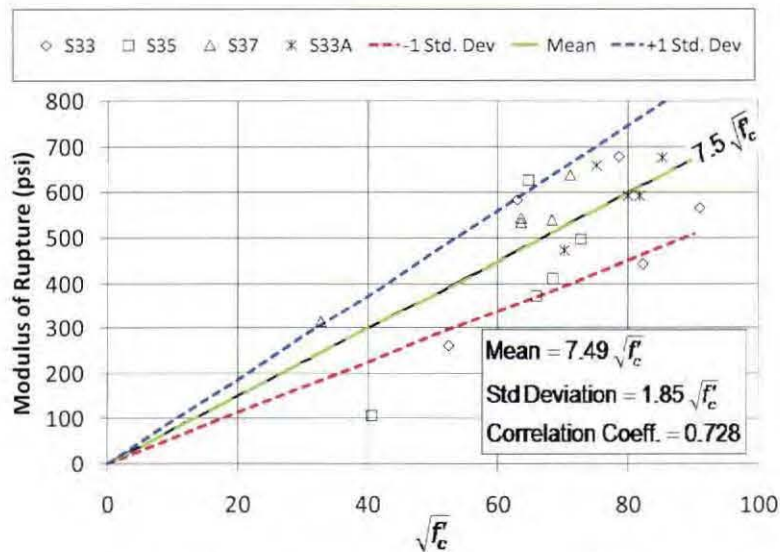


Figure 6.28: Measured Flexural Strength at All Ages

#### 6.4.3 MODULUS OF ELASTICITY

The elastic modulus tests were performed according to ASTM C 469-02. Modulus of elasticity measurements were done at 18 hours, 14 days, and 28 days. Each measurement consisted of the average of at least three flexural tests. The flexural test results are summarized in Table 6.13 and plotted in Figure 6.29. In general, the measured modulus of elasticity was in agreement with the expected trend; it increased with an increase in compressive strength.

**Table 6.13: Measured Average Modulus of Elasticity**

Age	Modulus of Elasticity, $E_c$ (ksi)			
	S33	S35	S37	S33-A
18 hours	2,885	2,367	1,093	3,704
14 days	4,470	3,430	3,557	4,438
28 days	4,785	3,740	3,683	4,522

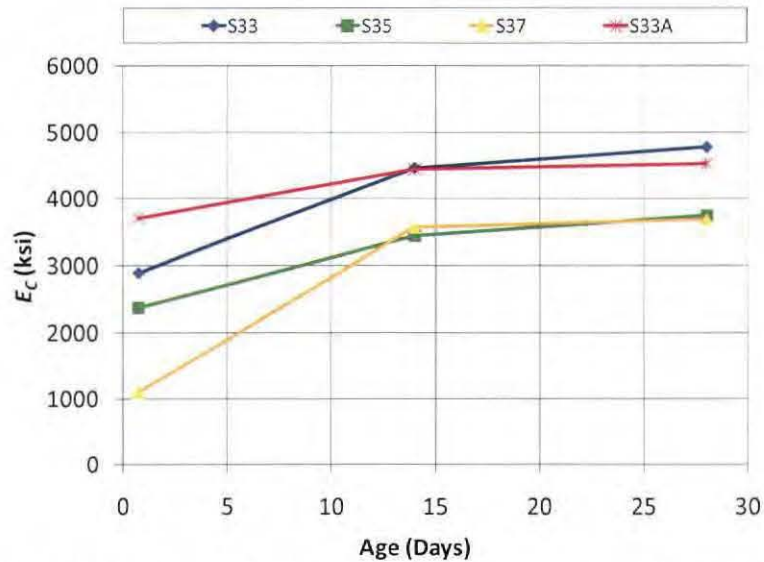


**Figure 6.29: Measured Modulus of Elasticity versus Age of Concrete**

Table 6.14 presents a summary of calculated (theoretical) and the mean and standard deviation of the measured elastic modulus values in terms of  $\sqrt{f'_c}$ . The calculated values were based on the ACI empirical equation (Equation 5.2). The results show excellent agreement between the experimental measurements and the empirical code equation. The ratio of the measured to the calculated elastic modulus varied between 0.94 and 1.01.

**Table 6.14: Measured and Calculated Modulus of Elasticity**

Mix	Measured $E_c$		Calculated $E_c$	Ratio of Measured to Calculated $E_c$
	Mean	Standard Dev.		
S33	$54.5 \sqrt{f'_c}$	$1.76 \sqrt{f'_c}$	$53.8 \sqrt{f'_c}$	1.01
S35	$53.1 \sqrt{f'_c}$	$1.84 \sqrt{f'_c}$	$53.3 \sqrt{f'_c}$	1.00
S37	$49.5 \sqrt{f'_c}$	$4.64 \sqrt{f'_c}$	$52.6 \sqrt{f'_c}$	0.94
S33-A	$53.8 \sqrt{f'_c}$	$2.45 \sqrt{f'_c}$	$53.8 \sqrt{f'_c}$	1.00

The measured modulus of elasticity values for S33, S35, S37, and S33-A are plotted versus  $\sqrt{f'_c}$  in Figures 6.30, 6.31, 6.32, and 6.33, respectively. The plots also show the mean and the standard deviation of the measurements and the calculated elastic modulus as functions of  $\sqrt{f'_c}$ .



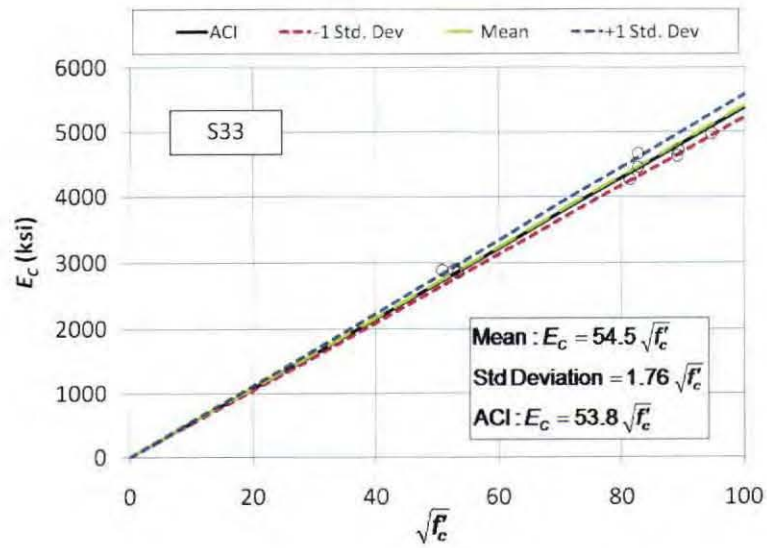


Figure 6.30: Measured and Theoretical Modulus of Elasticity for S33

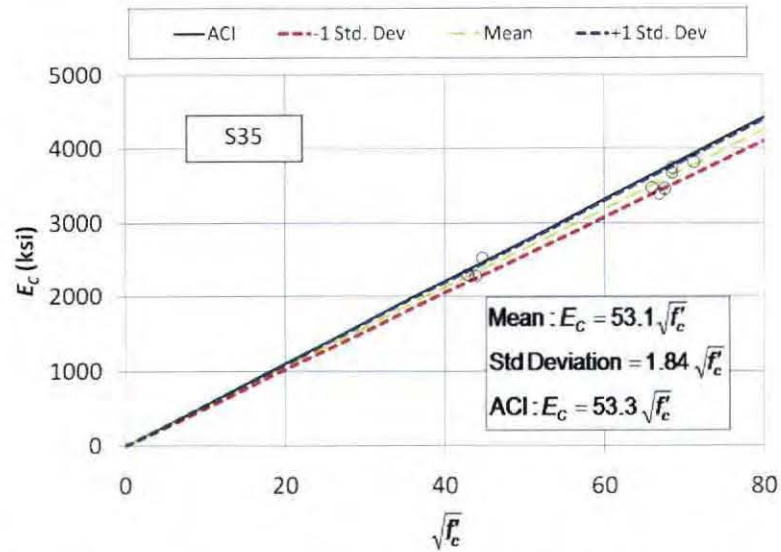


Figure 6.31: Measured and Theoretical Modulus of Elasticity for S35

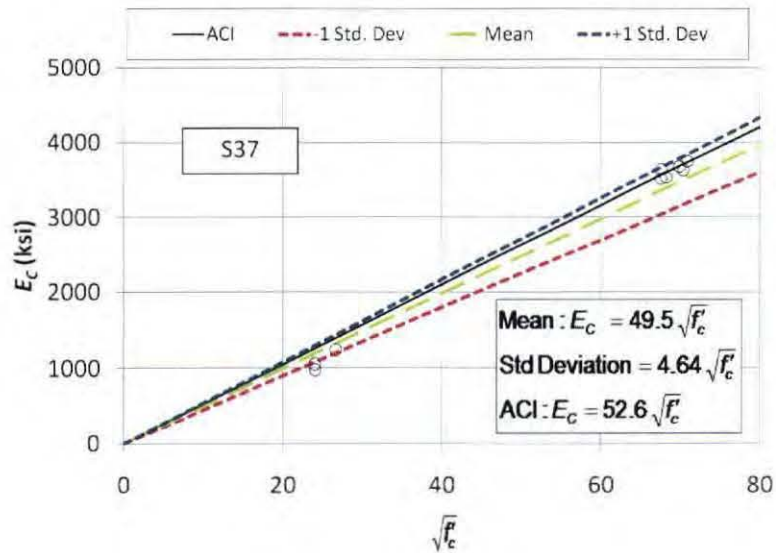


Figure 6.32: Measured and Theoretical Modulus of Elasticity for S37

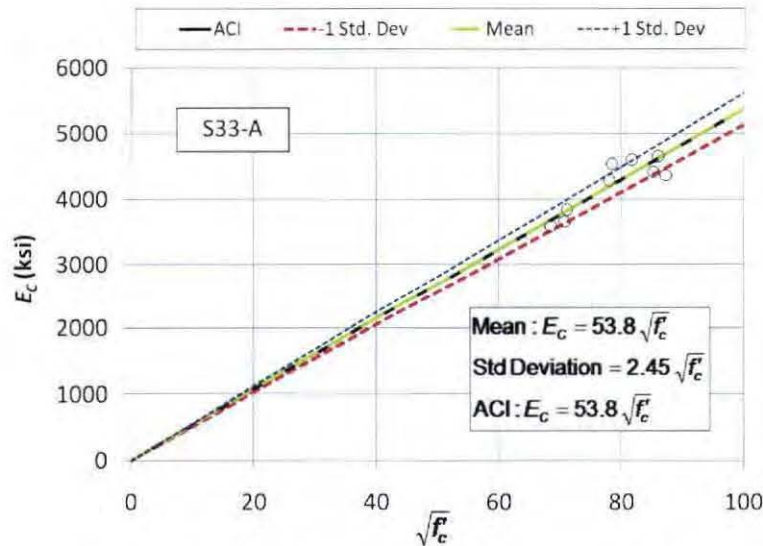


Figure 6.33: Measured and Theoretical Modulus of Elasticity for S33-A

The entire measured modulus of elasticity data set is plotted against the calculated values in Figure 6.34. A perfect agreement between measured and calculated values would be represented by points on the 1:1 line labeled “Em = Et”. The data points had a mean of 0.98, a standard deviation of 0.059, and a correlation coefficient of 0.99. The results indicate excellent agreement between the measured values and the code empirical equation (Equation 5.2).

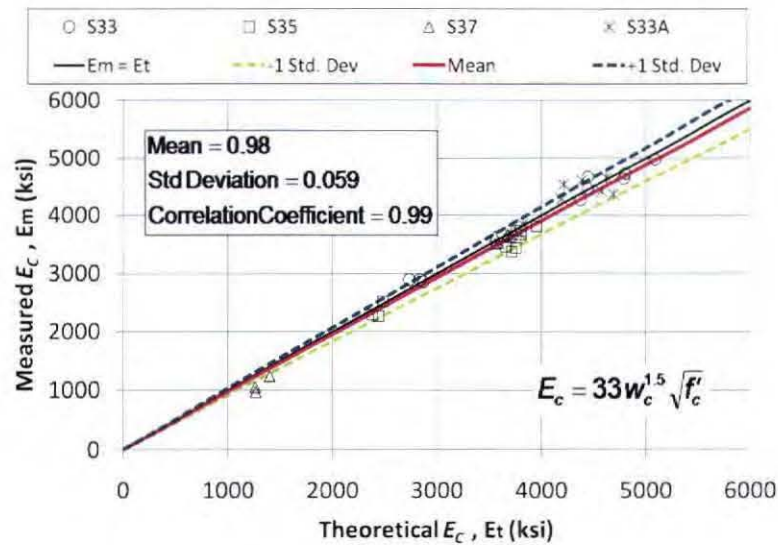


Figure 6.34: Modulus of Elasticity versus Age of Concrete

#### 6.4.4 HARDENED VISUAL STABILITY INDEX (HVSI)

The hardened visual stability index (HVSI) was evaluated according to AASHTO draft “Standard Method of Test for Static Segregation of Hardened Self-Consolidating Concrete Cylinders” (AASHTO 2005). Two cylinders from each SCC mix were sawn in half longitudinally. The sawn cylinders were visually inspected for the distribution of aggregate throughout the height of the cylinders. All of the mixes had a HVSI rating of 0. A typical cut cylinder is shown in Figure 6.35.



Figure 6.35: Sawn Cylinder for HVSI Evaluation

### 6.5 SHRINKAGE

Shrinkage tests were performed according to ASTM C 426-07 “Standard Test Method for Linear Drying Shrinkage of Concrete Masonry Units.” Shrinkage measurements were made on concrete beam specimens that were sampled from all three SCC mixes (S33, S35, S37) and the conventional concrete mix (CC33).



The shrinkage specimens consisted of standard 6"×6"×22" beams. An embedded concrete strain gauge was placed at the center of the beam. The strain gauge was held in place using wires tied to the beam mold. Figure 6.36 shows a beam specimen mold with a strain gage in place. Three beam specimens were cast from each mix.



Figure 6.36: Shrinkage Beam Mold

The molds were stripped after 24 hours and the shrinkage beams were carefully transferred to a cart. The beams were not lifted from the mold but rather slid onto the cart so that the beam experienced no significant flexure during the transfer. Each beam was placed on ¼" wooden dowels to prevent the development of frictional forces between the beam and the cart that may hinder the shrinkage of the beam. The beam specimens were stored for 90 days in a controlled environment. Strain readings were recorded periodically. The ambient temperature and relative humidity were recorded concurrently with the strain measurements. A complete record of the strain readings can be found elsewhere (Gutzmer 2008). The ambient temperature ranged between 65°F and 70°F with an average of 67.9°F while the humidity ranged between 20% and 38% with an average of 27.1%.

Initially after casting, the strain was measured at approximately 1 hour intervals for about 4 hours, 4 hours intervals for the next 8 hours, and 6 hours intervals for next 12 hours. After the first 24 hours, the strain measurement interval was increased to approximately 24 hours, and eventually to 7 days until at least 90 days had elapsed since casting.

The measured shrinkage strain versus time is shown in Figures 6.37, 6.38, 6.39, and 6.40 for S33, S35, S37, and CC33, respectively. Each figure shows the strain measurements of three beam specimens and a plot of the theoretical shrinkage strain as calculated by Equation 5.4. Figure 6.41 shows plots of the average measured shrinkage strain for all four mixes. While the strain measurements did continue until the ultimate strain, the collected data was sufficient to capture most of the shrinkage strain in the specimens. The measured shrinkage at 24 hours, 8 days, 94 days, and 115 days are summarized in Table 6.15. It should be noted that no readings were taken for CC33 after the age of 94 days.

The experimental results indicate the following:

1. The shrinkage strain of the SCC mixes increased with an increase in the w/c ratio. At 24 hours, the average shrinkage strain of S37 was 88% and 122% higher than those of S33 and S35, respectively. At 115 days, the shrinkage strain of S37 was 23% and 3% higher than those of S33 and S35, respectively.

2. The conventional concrete mix (CC33) exhibited significant shrinkage during the first 24 hours. The measured shrinkage strain at 24 hours was 42% of the total measured shrinkage strain at 94 days. The significant initial shrinkage may be attributed to autogenous shrinkage which normally occurs in concrete mixtures with w/c ratios below that required for complete hydration (Mindness et al. 2003). Normally, a w/c of 0.42 is considered to be the minimum ratio for complete hydration. The high fluidity and set retarding properties of the SCC mixtures may have prevented autogenous shrinkage from taking place at the same rate experienced by CC33.
3. At a w/c ratio of 0.33, the conventional concrete mix (CC33) exhibited higher shrinkage strain than the SCC mix (S33). The main difference was the result of the initial strains during the first 24 hours. However, at higher ages, the rates of strain increase with time for the two mixtures were practically similar.
4. The ACI 209 shrinkage model (Equation 5.4) was generally in good agreement with the measured shrinkage strain of the SCC mixes. However, it underestimated the strains of S35 and S37 during the initial 24 hours. For CC33, the model resulted in significant underestimation of the initial shrinkage strains, but was in good agreement with the measured strain at 94 days.

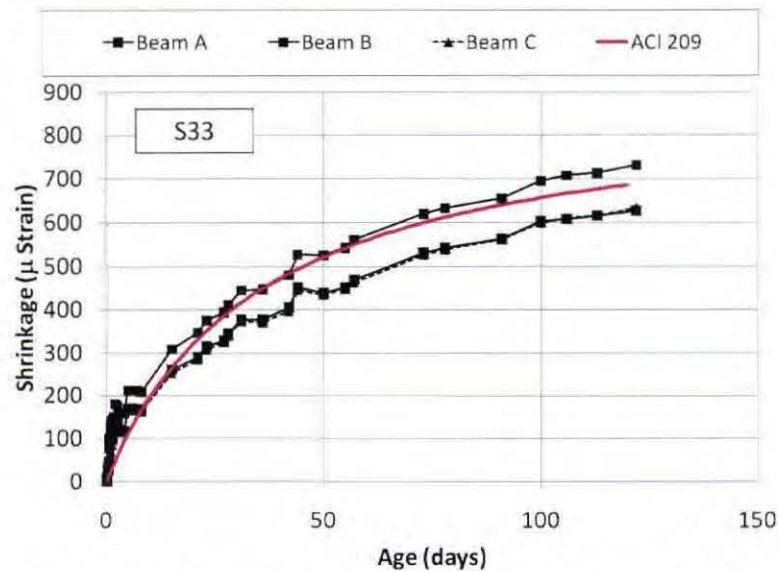


Figure 6.37: Measured and Calculated Shrinkage Strain for S33

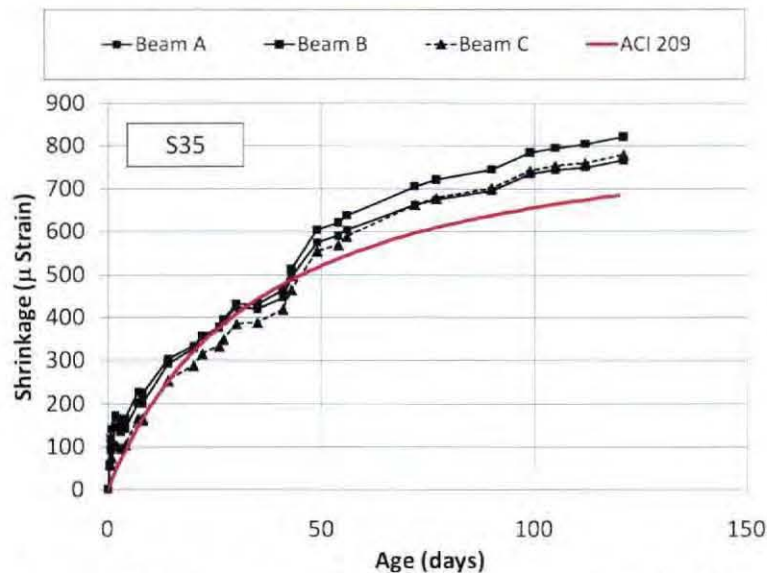


Figure 6.38: Measured and Calculated Shrinkage Strain for S35

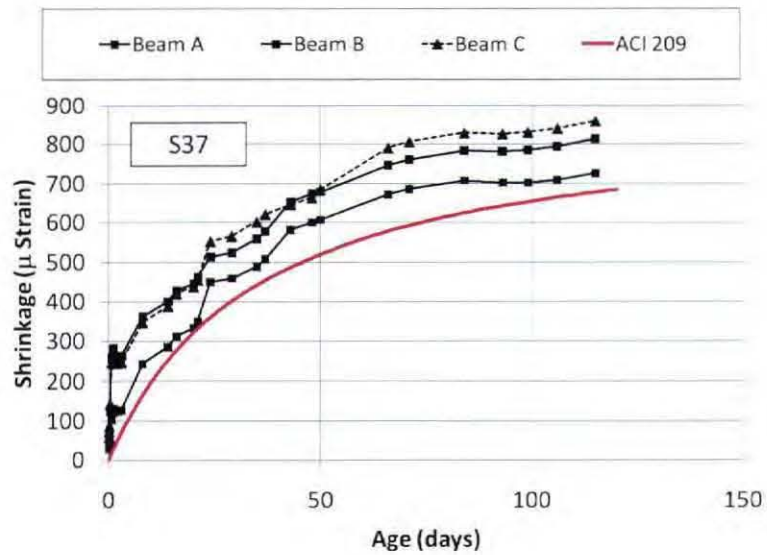


Figure 6.39: Measured and Calculated Shrinkage Strain for S37

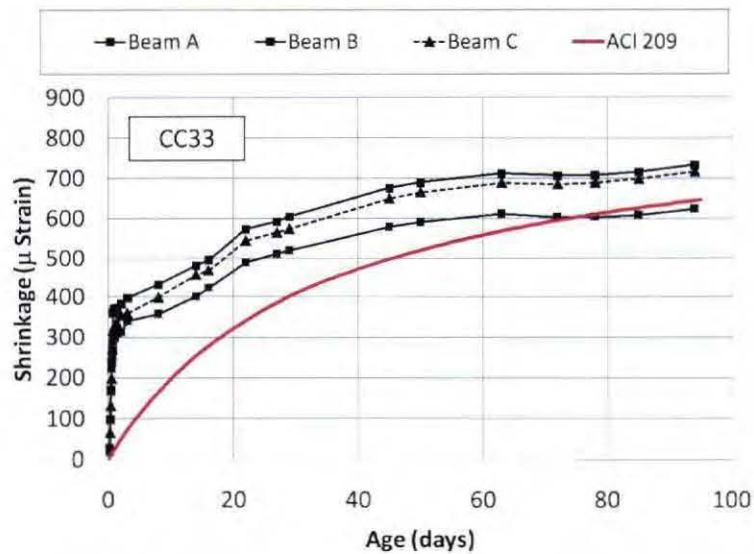


Figure 6.40: Measured and Calculated Shrinkage Strain for CC33



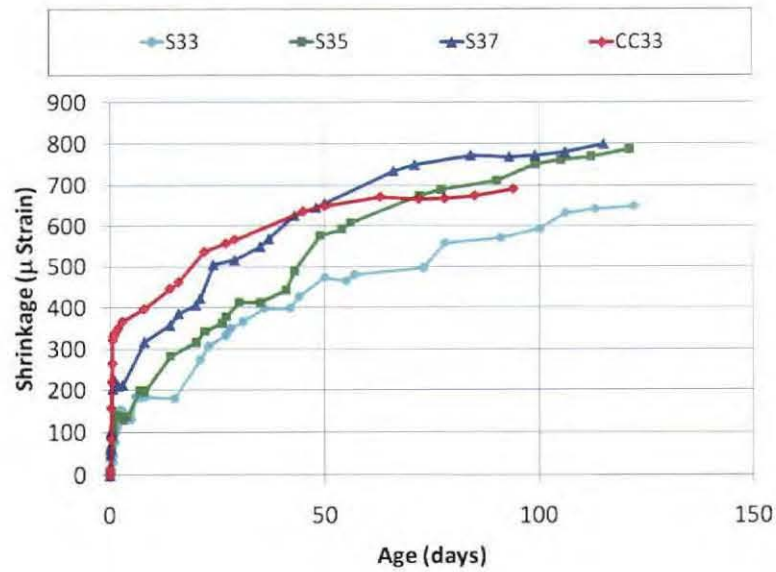


Figure 6.41: Measured Shrinkage Strain for All Mixes

Table 6.15: Average Measured Shrinkage Strain

Age	Shrinkage Strain ( $\mu$ Strain)			
	S33	S35	S37	CC33
24 hours	99	117	220	334
8 Days	179	200	318	397
94 days	606	730	772	692
115 days	652	777	801	N.A.

## 7 STRUCTURAL PERFORMANCE OF PRESTRESSED SCC GIRDERS

### 7.1 INTRODUCTION

This chapter covers the experimental and analytical work that was undertaken in this study to assess the structural performance of full-scale prestressed SCC bridge girders made with limestone coarse aggregate. The subsequent sections contain information on the design, instrumentation, fabrication, testing, and analysis of three 40'-long full-scale prestressed concrete bridge girder specimens. Two of the girders were cast using SCC. The third girder was cast with conventional concrete and used as a control specimen. Each specimen incorporated a composite concrete top layer to simulate a bridge deck.

The girder specimens were loaded at their mid-spans until failure. The collected data, which included load, deflection, and strain measurements, allowed for the evaluation of transfer length, prestress losses, flexural strength and stiffness, and shear strength of the girder specimens. The experimental results were compared to current code provisions and some analytical models to assess the applicability of those provisions and models to prestressed SCC girders.

### 7.2 DESIGN OF TEST SPECIMENS

The girder design in this study was similar to that of a previous study that had been performed on prestressed SCC bridge girders using quartzite coarse aggregate (Wehbe et al. 2007a). Only a minor difference pertaining to the distribution of the prestressing strands existed between the cross sections used in the previous and the current studies.

In selecting the cross-section for the test specimens, the vertical clearance of the Lohr Structures Laboratory and the lifting capacity of the overhead crane inside the laboratory had to be taken into consideration. The cross-section also had to be selected from standard sections that the SDDOT normally uses for short to medium span bridges. Therefore, a MnDOT 36M section was selected. This cross section allowed for sufficient clearance beneath the girder during the test, and the weight of the specimen was well within the lifting capacity of the 15 ton overhead crane when used to lift one end of the girder.

A hypothetical two lanes bridge was considered for the girder design. The girders were assumed to have a span of 40 feet and a center-to-center spacing of 8 feet. A schematic cross sectional view of the hypothetical bridge is shown in Figure 7.1. The minimum composite deck thickness of 8¼" required by the SDDOT was assumed for the hypothetical bridge.

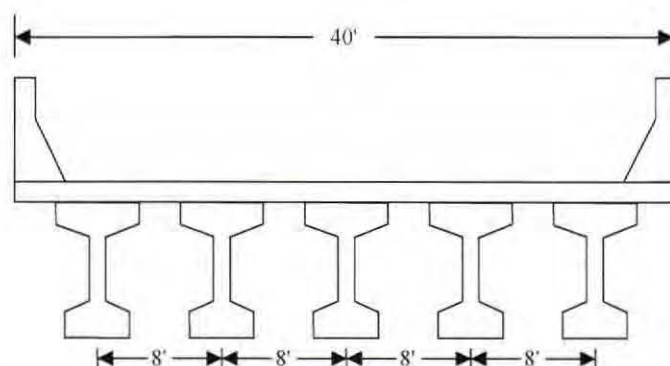
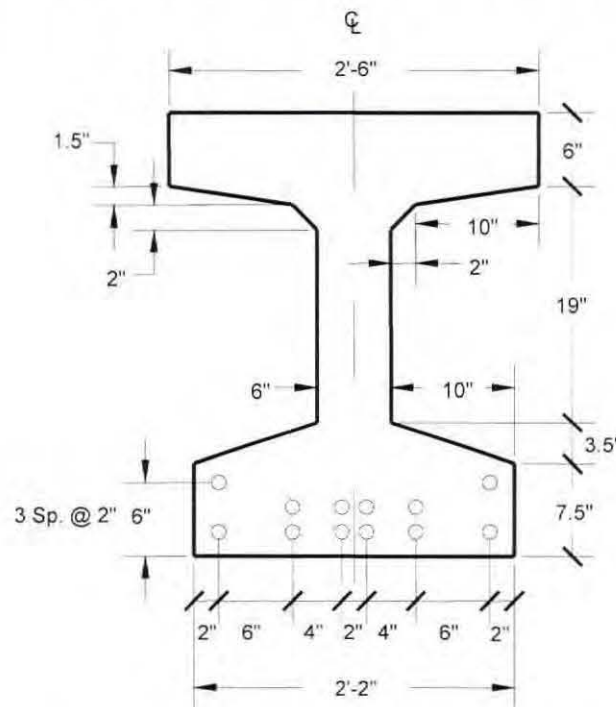


Figure 7.1: Schematic Cross Section of the Hypothetical Bridge

The girder design was performed according to the 17th Edition of the AASHTO Standard Specifications for Highway Bridges (AASHTO, 2002). The AASHTO Standard Specifications were in use by SDDOT at the time the previous study was started. Unshored construction was assumed. Therefore, the deck self weight was considered as a non-composite load.

The final girder design resulted in a MnDOT 36M section containing 12-0.6" diameter, seven-wire, low-relaxation prestressing strands that were distributed within the bottom flange of the girder. The specified jacking force per strand was 40,500 lbs, for a total initial jacking force of 486,000 lbs. The relatively short span allowed the prestressing strands to be straight. The theoretical tensile stress in the top of the girder at strand release was 520 psi. This exceeded the allowable tensile stress of 502 psi as prescribed by the AASHTO Standard Specifications for Highway Bridges (AASHTO, 2002). In order to prevent cracking at strand release, four #4 bars were placed in the top flange of the girder to carry the excess tensile stress. The girder cross-section and strand layout is shown in Figure 7.2.



**Figure 7.2: Girder Cross Section and Strand Layout**

Shear reinforcement, consisting of #5 Grade 60 U-stirrups, was provided along the entire girder span. The stirrups were 3'-4" long and extended 5" into the composite deck, providing continuity between the girder and the composite deck. The stirrups were placed at a center-to-center spacing of 7.5". Transverse reinforcement was also placed in the top and bottom flanges. A minimum of 1" concrete cover was provided around all reinforcement. The transverse reinforcement details are shown in Figure 7.3.



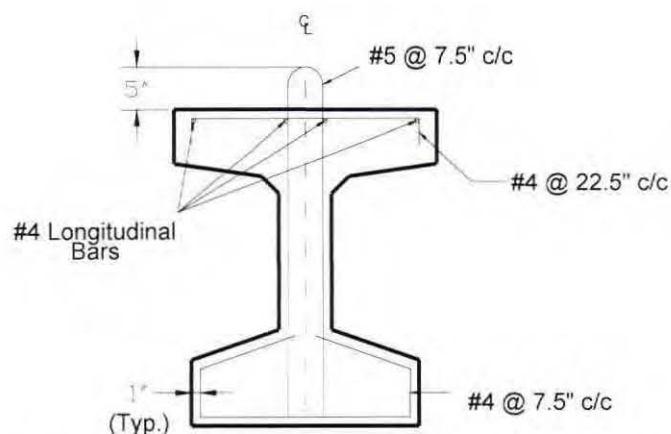


**Figure 7.3: Details of Transverse and non-prestressed Longitudinal Reinforcement**

For this study, a total of three girders were fabricated. One girder was cast with a conventional concrete mix used by the SDDOT for prestressed bridge girders while the other two were cast with an SCC mix. The girder cast with the conventional concrete served as the control specimen. Both concrete mixes used for casting the girders had a specified minimum compressive strength of 6,500 psi at strand release and a specified minimum 28-day compressive strength of 7,000 psi. The control concrete mix and SCC mix are shown in Table 7.1. Product literature for the admixtures used is presented in Appendix B. Complete girder plans are shown in Appendix C.

**Table 7.1: Control and SCC Mix Designs**

	Control Mix	SCC Mix
GCC Dacotah Type I/II Cement (lbs)	700	800
Fine Aggregate (lbs)	1200	1343
3/8" Limestone (lbs)	-	1454
3/4" Limestone (lb)	1875	-
Water (Gal.)	26.4	28.7
Daravair® M (oz)	10	15
Daracem® 19 (oz)	130	-
Daratard® 17 (oz)	14	24
ADVA 555 (oz)	-	224
Water/Cement Ratio	0.34	0.33

The hypothetical bridge girder had an 8' wide by 8 1/4" thick effective composite deck. To simulate the effect of the composite deck, a 36" wide by 10" thick equivalent concrete deck was cast on top of each girder specimen. The width of the equivalent deck was selected to simplify the construction and handling of the test specimens. The depth of the equivalent deck was determined so that the theoretical nominal flexural strength of the test specimen would be equal to that of the hypothetical girder. Figure 7.4 shows the cross section of the test specimens.

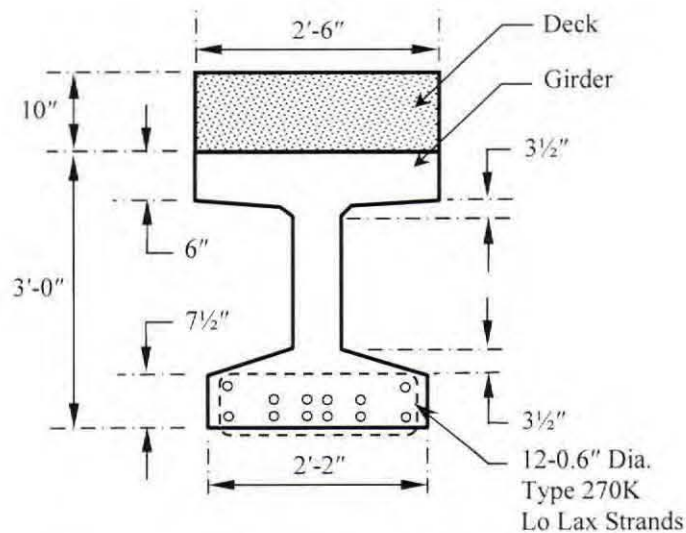


Figure 7.4: Cross Section of the Test Specimens

The deck was reinforced with the minimum amount of steel required by the ACI code for shrinkage and temperature effects (ACI 2008). The reinforcement was placed in two layers within the deck. The top layer was placed 7" above the top of the girder and consisted of D11 standard wire reinforcement with a center-to-center spacing of 4". For the bottom layer, four #4 longitudinal bars were placed 2" above the top of the girder. Individual bars, instead of steel mesh, were used in the bottom layer because a steel mesh would intersect the top segment of the U-stirrup, and therefore, would be difficult to place. The deck was cast using conventional concrete with specified 28-day strength of 5,000 psi. The mix design for the deck concrete is shown in Table 7.2.

Table 7.2: Deck Concrete Mix Design

	Deck Mix
GCC Dacotah Type I/II Cement (lbs)	544
Class F Flyash (lbs)	96
Fine Aggregate (lbs)	1150
¾" Limestone (lb)	1873
Water (Gal.)	27.5
Daravair® M (oz)	8
Daracem® 19 (oz)	100
Water/Cement Ratio	0.35

All three girders were cast on the same prestressing bed. The prestressing bed used for fabrication was oriented in the east-west direction. Each girder was marked on its west end with an identification label. The girders were labeled "A", "B", and "C" followed by the letter "L". The letter "L" was included in the label to indicate that the specimens were cast with *limestone* aggregates. This was necessary to distinguish the specimens from those in a prior study that were cast with quartzite aggregates. The furthest west girder was labeled AL. The middle girder was labeled BL. The east girder was labeled CL. Girder AL was the control girder and was cast with conventional concrete.

### 7.3 INSTRUMENTATION

The girder specimens were instrumented with a variety of strain gages, detachable mechanical (demec) points, linear variable differential transformers (LVDTs), and cable-extension transducers. The strain gages were installed during the fabrication of the girder specimens. Due to the limited capacity of data acquisition equipment, only one half of each specimen was instrumented with strain gages. Details regarding the instrumentation and the data acquisition equipment used in this study are provided in the following sub-sections.

#### 7.3.1 STRAIN GAGES

The specimens were instrumented with surface mounted and embedded resistance strain gages. The surface mounted strain gages were used to measure strain in the prestressing tendons and the shear reinforcement, while the embedded gages were used to measure strain in the concrete. In order to identify the location of each strain gage after fabrication, each lead wire was labeled with an identification tag. The first portion of the identification label represented the type of strain gage. The strain gage type was given a two letter abbreviation. Strain gages that were attached to the prestressing strands were labeled PS. The gages attached to the shear stirrups were labeled ST. The strain gages that were embedded in the concrete were labeled EM. The second portion of the identification label represented the number of the strain gage and the corresponding girder. For example, PS-5AL indicated prestressed strand strain gage number 5 in girder AL. All gages were numbered using the sequence discussed hereafter.

Following the placement of the strain gages, the exact location of each gage was measured and recorded prior to casting the girder. A three-dimensional coordinate system was adopted for recording the gage location. The origin of the coordinate system was located at the bottom of the cross-section centerline on the west end of the girder. The positive X-axis extended longitudinally along the girder length, the positive Y-axis extended vertically upward from the bottom of the girder, and the positive Z-axis followed the right-hand-rule. To aid in documenting the strain gage locations, the strands were numbered sequentially as shown in Figure 7.5. Appendix D shows detailed mapping of the strain gage locations.

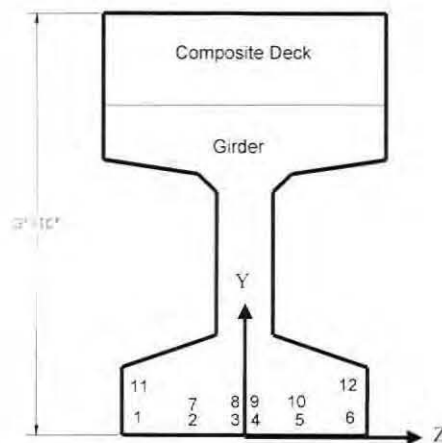


Figure 7.5: Coordinate System and Strand Numbering Method

A total of twenty strain gages were attached to the prestressing strands at predetermined locations to monitor the strain in the strands before and during testing. The strand gage was only 2 mm long to allow for mounting of the gage on one of the strand wires. Figure 7.6 shows one of the mounted strand strain



gages. Two sets of four strain gages were mounted on four strands with one set placed at quarter-span and the other set at placed mid-span. The use of multiple gages at the same location provided redundancy and allowed for the comparison of strain between different prestressing strands at the same location. Four strain gages were used to instrument the strands at two additional sections. The sections were located between the quarter span and the mid-span at 12" intervals from the quarter-span. At each section, two strain gages were attached to two strands.



**Figure 7.6: Strand Strain Gage**

For measuring the transfer length, two strands were each instrumented with four strain gages along the potential transfer length. The first strain gage was placed at 2" from the end of the girder and the remaining strain gages were placed at 12" intervals along the strand. The purpose of these strain gages was to measure the change in strain that occurred during release. The measured strains would then be used to calculate the transfer length for each girder. Figure 7.7 shows a series of strain gages that were installed for transfer length measurement.



**Figure 7.7: Transfer Length Strain Gages**

The shear reinforcement was instrumented using 6 mm long strain gages. Four stirrups were instrumented in each girder. The first instrumented stirrup was located at 22.5" from the girder end while the other three were placed at 30" intervals thereafter (at 52.5", 82.5", and 112.5" from the girder end).

Each instrumented stirrup was fitted with three gages placed on one leg. The top strain gage was placed at the level where the girder's top flange intersects the web. The middle strain gage was positioned at the web's mid-height. The bottom strain gage was placed at the level where the girder's bottom flange intersects the web. The primary purpose for stirrup strain gages was to measure the strain in the shear reinforcement at different locations along the span of each girder. The reason for using three strain gages on one stirrup was to help determine when and where a shear crack intersected a stirrup during the loading sequence.

Thirteen 60 mm long embedded strain gages were placed in each girder. Each strain gage was suspended in place 24 gauge steel wire as shown in Figure 7.8. The sections at the quarter span and at the mid-span were each instrumented with six embedded gages. Three of the six gages were placed at three different elevations within the girder and remaining three gages were placed within the composite deck. The purpose for these embedded gages was to measure strain in the concrete and to determine the strain gradient in the section. The section at 7.5' from the girder end was also instrumented with one embedded gage that was placed at the theoretical neutral axis. The purpose for this gage was to monitor the shrinkage strain in the concrete where the flexural stresses are approximately equal to zero.



Figure 7.8: Embedded Strain Gage

### 7.3.2 DETACHABLE MECHANICAL POINTS

Detachable mechanical points (demec points) were used in this study to measure concrete strain along the potential transfer length. A demec point consists of a small brass insert with a threaded hole. A fast-setting two-part epoxy was used to mount the brass inserts to the surface of the bottom flange of each girder. Seven demec points were mounted on each side at the west end of each girder. The first point was placed at 2" from the end of the girder and the remaining points were placed at 6" intervals. The demec line extended 38" from the end of each girder and was placed at the elevation of the centroid of the prestressing strands. A line of installed demec points is shown in Figure 7.9.





Figure 7.9: Line of Demec Points

After mounting the line of demec points, contact seats were threaded into place in each brass insert. A Whittemore gage was used to measure the distance between successive demec points. Initial measurements were taken prior to release of the prestressing strands. After release of prestress, the distance between consecutive demecs was measured again to determine concrete surface strains. The concrete surface strains were then used to calculate the transfer length. The Whittemore gage, brass inserts, contact seats, and contact points that were used to take measurements are shown in Figure 7.10.



Figure 7.10: Whittemore Gage, Brass Insert, Contact Seat, and Contact Point

### 7.3.3 EXTENSOMETERS

Mid-span deflections were measured using a combination of two linear variable differential transducers (LVDTs) and two cable-extension transducers. The LVDTs had  $\pm 1.0"$  range and were used to measure pre-cracking deflections. The cable-extension transducers had a working range of 30" and were used to measure post-cracking deflections. Prior to flexural cracking, the girder specimens were relatively stiff and the deflections were relatively small. Hence, the short-range LVDTs with high resolution were needed to monitor deflections that occur prior to cracking. Each LVDT was suspended above the girder with mounting brackets that were attached to side braces. A steel disc was placed beneath the tip of each LVDT plunger to ensure a smooth contact surface. The average of the two LVDT measurements was



used in order to eliminate inaccuracies that could be caused by girder rotation during loading. A deflection LVDT is shown in position beside the actuator in Figure 7.11. The long-range cable-extension transducers were placed on each side of the girder at mid-span. Similar to the LVDT deflection measurements, the average of the two cable-extension deflection measurements was considered as the measured mid-span deflection. The cable-extension transducer units were mounted to side braces while the cables were attached to brackets that were mounted to each side of the girder's top flange. A cable-extension transducer is shown mounted to a side brace in Figure 7.12.

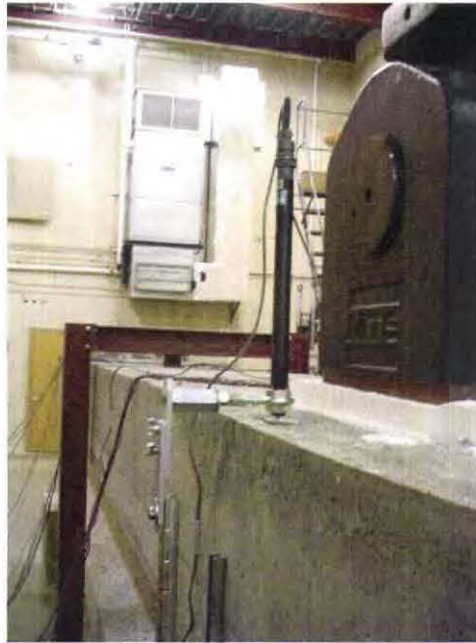


**Figure 7.11: LVDT for Deflection Measurement at Mid-Span**



**Figure 7.12: Cable-Extension Transducer**

Top and bottom concrete strains at the girder's mid-span were measured using a pair of LVDTs. The LVDTs had a working range of  $\pm 0.5$ ". Each LVDT was mounted to the girder with screws that were tapped into the concrete. A  $\frac{1}{2}$ " threaded rod was used to provide the required gage length. Due to the location of other instrumentation within each girder, the gage lengths were not always the same for each

test. Prior to each test, the gage length for each threaded rod was measured and recorded. During the test, changes in length measured by each LVDT were used in conjunction with the initial gage length to determine the strain in the concrete. Strain readings could then be used to determine the strain profile of the mid-span section. The LVDTs used to monitor concrete strains are shown in Figure 7.13.

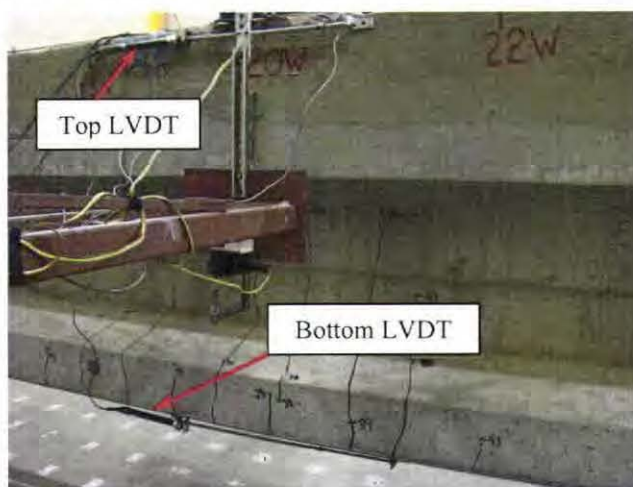


Figure 7.13: Strain Measurement LVDTs

## 7.4 SPECIMEN FABRICATION AND DELIVERY

The girder specimens were fabricated in August of 2007 at Cretex Concrete Products West, Inc. fabrication facility in Rapid City, SD. The construction activities were performed by Cretex West employees and South Dakota State University staff. This section provides an overview of the fabrication process and transportation of the girders to the Lohr Structures Laboratory.

Prior to the installation of the strain gages, the strands were laid on the prestressing bed. On August 13, 2007 the strands were each tensioned to 4000 lbs to remove some of the slack and to allow for the installation of the strain gages. The strain gages were attached to the strands by SDSU personnel. On August 14, 2007, the installation of the strand strain gages was completed and each strand was then tensioned to 44,300 lbs. Strand strain gage readings were recorded before and after full tensioning. Following the strand tensioning, the shear reinforcement was installed. After placement of the shear stirrups, the embedded strain gages were placed in position. The actual gage location and initial strain readings were recorded for each of the embedded strain gages. On August 15, 2007, the formwork was installed and the concrete was placed. The control girder was cast first, followed by the two SCC girders. The SDSU personnel on site tested the fresh concrete properties and cast concrete cylinders. Immediately after casting, the girders were covered with tarp and heat curing was started. Figure 7.14 shows a sequence of pictures during the fabrication process.





(a) Prestressing Bed



(b) Marking Strain Gage Locations



(c) Recording Strain Gage Readings



(d) Installation of Shear Reinforcement



(e) Installation of Formwork



(f) Casting of Girders

**Figure 7.14: Fabrication of the Girder Specimens**

Concrete cylinders were tested on August 16, 2007 to determine the concrete strength. The cylinder breaks showed that Girders AL and BL had met the release strength, but Girder CL had not. De-tensioning was delayed until August 17, 2007 due to the low concrete strength for Girder CL. Prior to de-tensioning, the formwork was removed and the demec points were installed. Measurements between demec points and the initial strain in the strain gages were recorded prior to prestress transfer. The



prestress transfer to the girders was accomplished by torch cutting the strands simultaneously between the three girders. Immediately after de-tensioning, the girders were lifted slightly and then placed back on the prestressing bed to release the friction between the girders and the bed. The distance between the demec points were then measured again in order to determine the transfer length for each girder. Strains in the concrete-embedded strain gages and strand strain gages were also recorded. Camber in each girder was measured using a surveyor's level and a ruler graduated with decimal inches.

Following the completion of the measurements at de-tensioning, the formwork, reinforcement, and instrumentation of the deck were installed. The deck instrumentation consisted of embedded strain gages. The same concrete mix was used for casting the decks of all three girder specimens. SDSU personnel tested the fresh concrete properties and cast standard concrete cylinders. The deck formwork and reinforcement is shown in Figure 7.15.



**Figure 7.15: Deck Formwork and Reinforcement**

On August 27, 2007, the three girder specimens were transported on semi-truck trailers to the Lohr Structures Laboratory (LSL) at SDSU. Each girder specimen weighed in excess of 18 tons. Since the capacity of the overhead crane in the LSL is limited to 15 tons, a 10-ton chain hoist was also used to help unload the girders. The chain hoist was suspended from the loading steel frame that was positioned in the middle of the laboratory floor. Each girder was lifted off of the trailer using the overhead crane on one end and the chain hoist on the other end of the girder. After lifting the girder off of the trailer, the truck drove out and the girder was placed at each end on steel roller dollies to allow for the movement of the girder within the laboratory. Figure 7.16 shows the delivery and unloading of the specimens.



(a) Delivery



(b) Unloading

Figure 7.16: Girder Delivery and Unloading

## 7.5 TEST SET UP AND PROCEDURE

The structural testing for this study was performed at the Lohr Structures Laboratory (LSL) at South Dakota State University in Brookings, SD. The LSL is furnished with a loading steel frame, hydraulic actuators, hydraulic control system, and a data acquisition system. This section discusses the experimental set up and procedures.

### 7.5.1 TEST SET UP

The test setup was the same for all three girders. Each girder was tested as a simply supported beam with a point load applied at mid-span. The load was applied by means of an MTS hydraulic actuator having a load capacity of 328 kips in compression and a stroke of 30". The actuator was suspended from the cross beam of the steel loading frame which was securely anchored to the strong floor. The specimen was supported at its ends by means of two 24" tall  $\times$  30" wide  $\times$  36" long concrete reaction blocks. A 4" diameter  $\times$  20" long solid stainless steel shaft was placed on top of each reaction block to serve as a roller support. The shaft was positioned at 6" from the face of the girder directly beneath a steel bearing plate that was built into the girders at the time of fabrication. Thus, the clear span was approximately equal to 38.5'. Figure 7.17 shows a schematic of the test set up. Figure 7.18 shows a picture of specimen immediately before testing. Prior to the day of testing, a 2" thick steel plate was centered on top of the girder at the mid-span and embedded in plaster of Paris. The purpose of the steel plate was to provide a smooth and level surface for seating the actuator. This also allowed for a more uniform load distribution directly beneath the actuator. After the plaster of Paris had cured, the actuator was seated on the plate. Figure 7.19 shows the steel plate in place prior to seating of the actuator.

### 7.5.2 TEST PROCEDURE

Although the test setup was identical for all three girders, the test procedure was not the same for the SCC specimens. The control girder (Girder AL) and one of the SCC girders (Girder BL) were tested under increasing *monotonic* load until failure. The other SCC specimen (Girder CL) was tested under increasing *cyclic* load until failure. The loading was load-controlled during the elastic response range, and displacement controlled afterwards.



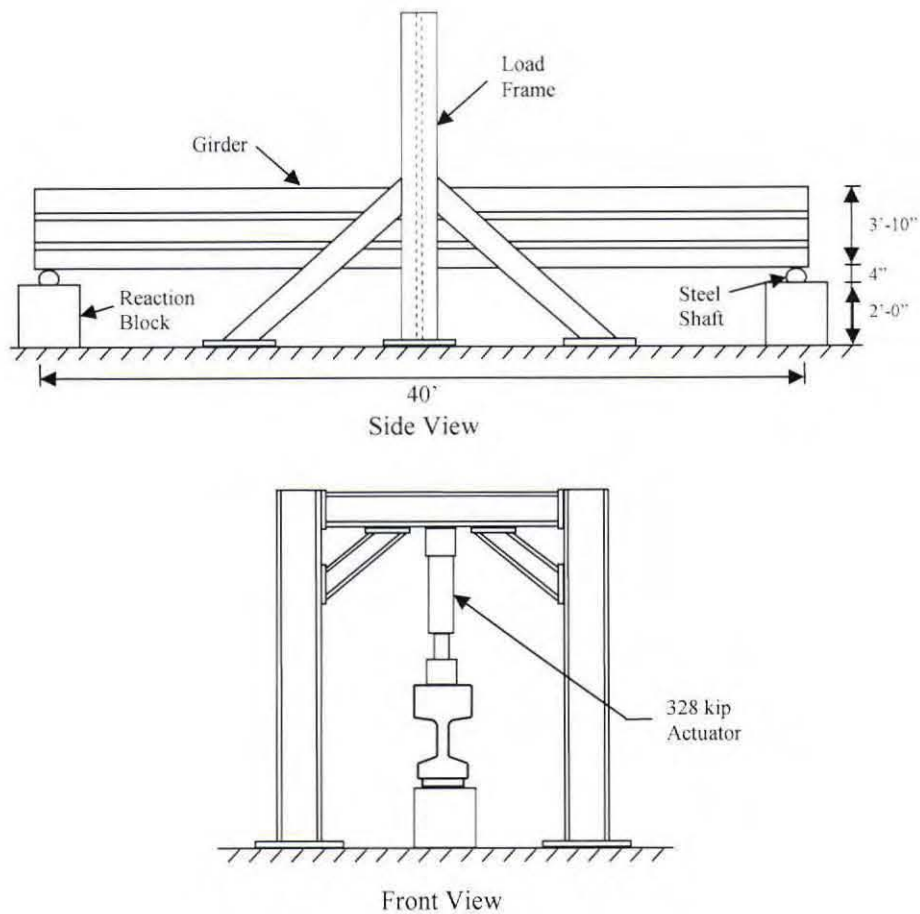


**Figure 7.17: Schematic of Test Set Up**



**Figure 7.18: Test Set Up of a Girder Specimen**





**Figure 7.19: Steel Seating Plate**

After each load increment, data readings from the strain gages, LVDTs, cable-extension transducers, actuator load cell, and actuator displacement transducer were recorded. Data acquisition was done using a MEGADAC 3415AC/DC that was manufactured by the currently defunct OPTIM Electronics Corporation of Germantown, MD. The data acquisition system was set to scan the sensors at a rate of two sets of readings per second. The data was recorded only at the end of each load increment. Recording was maintained for at least two seconds (four sets of readings) each time a data recording was initiated.

During the tests, the girders were visually monitored for cracking. Crack propagation was traced on the specimen using permanent markers. The end of each crack trace was marked with a number indicating the load number at which the crack tracing was being done. Figure 7.20 shows an example of the crack marking on the surface of the girder. The cracks of each girder were mapped following the end of the test. The crack maps for the three girders are presented in Appendix E.

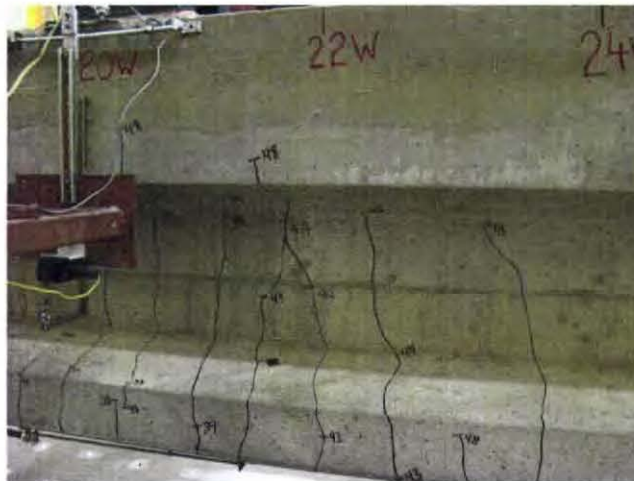


**Figure 7.20: Crack Marking**

## **7.6 MEASURED MATERIAL PROPERTIES**

This section presents the measured fresh and hardened properties of the concrete and the stress-strain relationship of the strands used for the construction of the girder test specimens. .

### 7.6.1 FRESH CONCRETE PROPERTIES

The fresh concrete properties were measured at the fabrication facility for the concrete used to cast the girders and the decks. The conventional concrete used to cast Girder AL was tested for temperature, air content, unit weight, and slump. The SCC used to cast Girders BL and CL was tested for temperature, air content, unit weight, slump flow, J-ring,  $T_{20}$ , and Visual Stability Index (VSI). Conventional concrete was also used to cast the decks on top of the girders. The conventional concrete used for the decks was subjected to tests similar to those applied to the conventional concrete of Girder AL. The fresh concrete properties are summarized in Table 7.3.

**Table 7.3: Measured Properties of Fresh Concrete Used for the Test Specimens**

	Temperature (°F)	Air Content (%)	Unit Weight (lb/ft <sup>3</sup> )	Slump (in.)	Slump Flow (in.)	J-Ring (in.)	$T_{20}$	VSI
AL-Girder	90	6.3	147.2	7.4	N.A.	N.A.	N.A.	N.A.
BL-Girder	90	4.7	145.6	N.A.	25.5	21.5	2.57	0
CL-Girder	88	5.0	146.4	N.A.	24.5	22.75	6.06	0
AL-Deck	83	5.3	146.4	7.5	N.A.	N.A.	N.A.	N.A.
BL-Deck	85	5.0	147.2	7.5	N.A.	N.A.	N.A.	N.A.
CL-Deck	83	5.1	146.4	8.0	N.A.	N.A.	N.A.	N.A.

### 7.6.2 CONCRETE COMPRESSIVE STRENGTH

The specified minimum concrete strength for the girder specimens was 6,500 psi at release and 7,000 psi at 28 days. During construction of the specimens, concrete cylinders were cast for each of the girders and each composite deck. The concrete cylinders that were made from the girder concrete were heat-cured for 24 hours to be representative of the curing procedures used for the girders. One cylinder for each girder was tested 24 hours after casting to determine if the release strength had been met. At 24 hours, the cylinders tested for Girder AL and Girder BL met the release strength, but that for Girder CL did not. Therefore, the strand release was delayed one day until the concrete strength for Girder CL exceeded the specified release strength. The remaining concrete cylinders were transported to the materials laboratory at South Dakota State University and stored at room temperature.

Three cylinders were tested for each girder at 7 days, 28 days, and on the day of testing of the girder. The 7-day cylinders were standard 4" × 8" cylinders while the remaining cylinders were standard 6" × 12". The average 7-day strengths were 9,072 psi, 8,051 psi, and 9,019 psi for Girder AL, Girder BL, and Girder CL, respectively. The average 28-day strengths were 9,455 psi, 7,492 psi, and 9,803 psi for Girder AL, Girder BL, and Girder CL, respectively. The average compressive strengths on the day of testing were 10,192 psi, 8,099 psi, and 10,410 psi for Girder AL, Girder BL, and Girder CL, respectively. A summary of the measured concrete compressive strengths is shown in Table 7.4. The unexpected decrease in strength between the 7-day and 28-day strengths for Girder BL could be due to the difference in the cylinder sizes.



Table 7.4: Measured Girder Concrete Compressive Strength

	Measured Concrete Strength (psi)		
	Girder AL (Control)	Girder BL (SCC)	Girder CL (SCC)
@ Release	6,963 <sup>†</sup>	7,140 <sup>†</sup>	8,162
@ 7 Days	9,072	8,051	9,019
@ 28 Days	9,455	7,492	9,803
@ Day of Testing	10,192 <sup>‡</sup>	8,099 <sup>*</sup>	10,410 <sup>**</sup>

<sup>†</sup> Tested 24 hours before release

<sup>‡</sup> Tested 83 days after casting

<sup>\*</sup> Tested 48 days after casting

<sup>\*\*</sup> Tested 69 days after casting

The deck concrete for each specimen was measured at 28 days and on the day of testing. Each measurement consisted of the average strength obtained from testing two standard 6" × 12" cylinders. The measured 28-day strengths were 6,367 psi, 6,747 psi, and 6,570 psi for the composite deck of Girder AL, Girder BL, and Girder CL, respectively. The measured strengths on the day of testing of the girder specimens were 7,392 psi, 7,171 psi, and 7,578 psi for the composite deck of Girder AL, Girder BL, and Girder CL, respectively. A summary of the measured concrete compressive strengths is shown in Table 7.5.

Table 7.5: Measured Deck Concrete Compressive Strength

	Measured Concrete Strength (psi)		
	Girder AL (Control)	Girder BL (SCC)	Girder CL (SCC)
@ 7 Days	6,367	6,747	6,570
@ Day of Testing	7,392 <sup>†</sup>	7,171 <sup>‡</sup>	7,578 <sup>*</sup>

<sup>†</sup> Tested 81 days after casting

<sup>‡</sup> Tested 46 days after casting

<sup>\*</sup> Tested 67 days after casting

### 7.6.3 PRESTRESSING STRANDS

The prestressing strands used in constructing the girder specimens were 0.6"-diameter, seven-wire, Grade 270, low relaxation strands. The engineering properties of the strands were not measured in this study. However, the properties were obtained from the mill certificate that was provided by the strand manufacturer, Insteel Wire Products of Gallatin, TN. Figure 7.21 shows the load versus strain diagram as provided in the mill certificate. Based on the information provided on the mill certificate, the strand had an area of 0.2169 in<sup>2</sup>, an average modulus of elasticity of 29,000 ksi, a yield force of 54,057 lbs at 1% elongation, and an ultimate breaking force of 59,880 lbs at 6.75% elongation. The corresponding yield stress and ultimate stress were 246,225 psi and 276,072 psi, respectively.



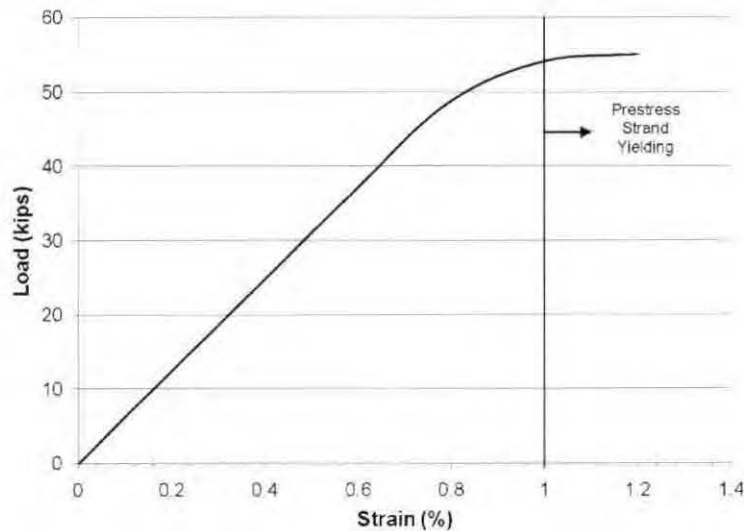


Figure 7.21: Prestressing Strand Load versus Strain

## 7.7 TRANSFER LENGTH

### 7.7.1 MEASURED TRANSFER LENGTH

As discussed in Sections 7.3.1 and 7.3.2, each girder was instrumented in two different ways to measure the transfer length. The first method used demec points attached to the surface of the concrete along the potential transfer length. The second method used strain gages attached to the prestressing strands near the end of each girder.

The attempt to measure strain along the concrete surface was not successful. Figure 7.22 shows the measured strain versus the distance from the girder end for all three girders. It is clear that the readings were erratic. The shock induced by and the uneven sequence of prestress transfer may have affected the demec adhesion to the concrete surface. Therefore, the demec points measurements were not used to draw any conclusions regarding the transfer length.

The measured strand strain versus the distance from the girder end for Girder AL, Girder BL, and Girder CL are shown in Figures 7.23, 7.24, and 7.25, respectively. Also shown are the 95% AMS lines as explained by Russell and Burns (1997) and presented in Section 5.4.3 of this report. In this study, the strain gages were not placed far enough from the end of each specimen to clearly identify the strain plateau. Therefore, strain measurements from quarter-span and mid-span were used to identify the strain measurements along the potential transfer length that had reached the strain plateau. Using the 95% AMS method, the transfer lengths for Girder AL, Girder BL, and Girder CL were determined to be 30.0", 34.5", and 25.5", respectively.

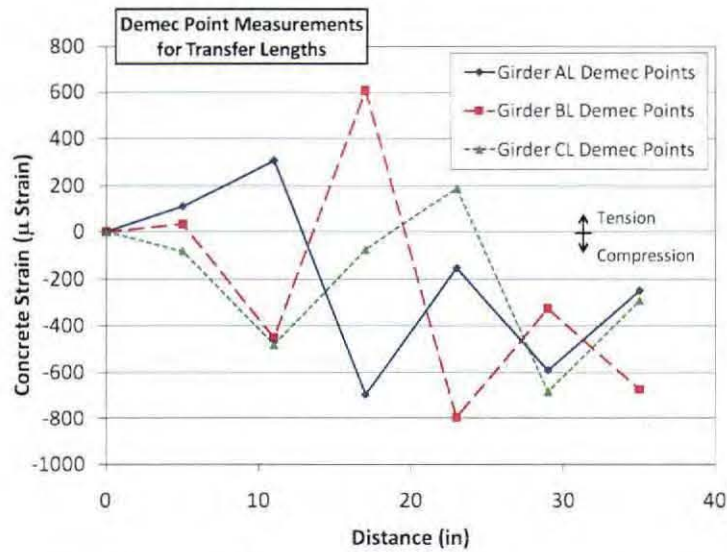


Figure 7.22: Measured Concrete Strain along Potential Transfer Length

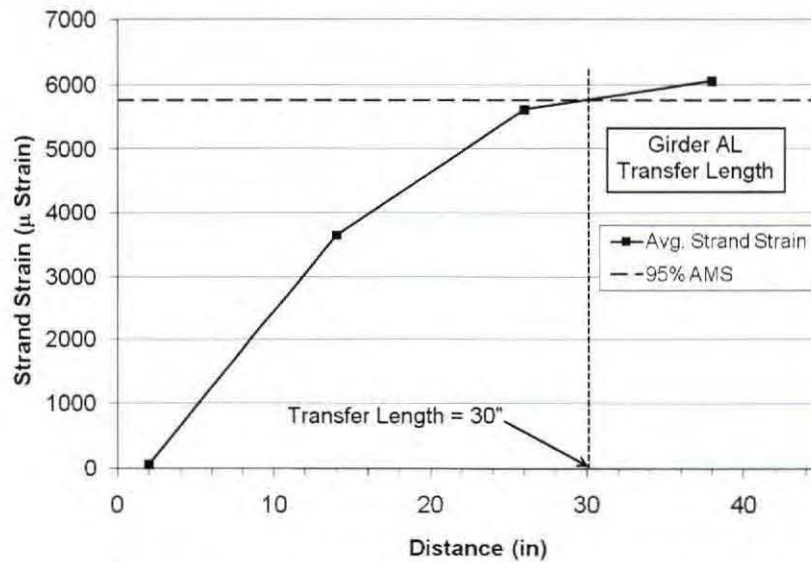


Figure 7.23: Measured Transfer Length for Girder AL

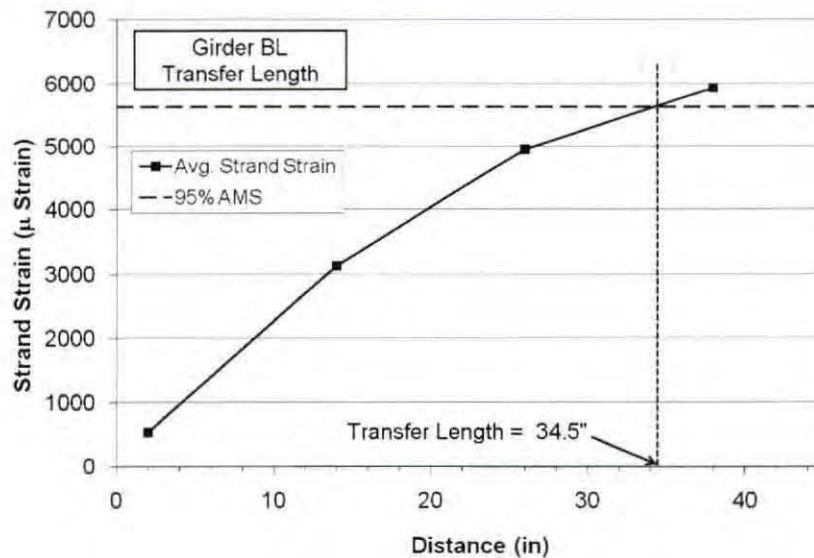


Figure 7.24: Measured Transfer Length for Girder BL

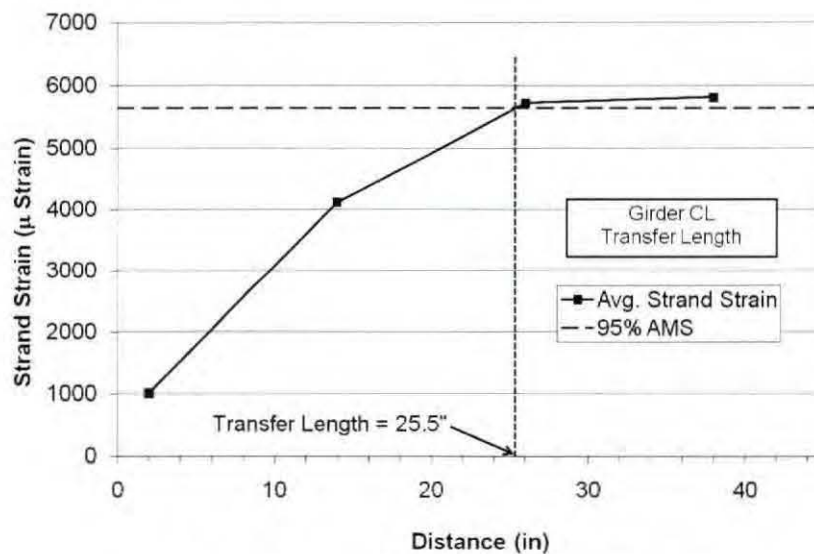


Figure 7.25: Measured Transfer Length for Girder CL

The measured transfer lengths of the SCC specimens are comparable to that of the control specimen. Girder BL had a 15% longer transfer length and Girder CL had a 15% shorter transfer length than that of the control specimen. Although transfer lengths differ by 15%, the average transfer length of the SCC girders is equal to that of the control girder. Therefore, the transfer length in SCC is not significantly different from that in conventional concrete.

### 7.7.2 COMPARISON OF MEASURED AND CALCULATED TRANSFER LENGTH

Several methods provide minimum transfer length requirements. These methods were discussed in details in Section 5.4. The measured and calculated transfer lengths for all three specimens are summarized in Table 7.6.



**Table 7.6: Measured and Calculated Transfer Length**

	Transfer Length (in.)		
	Girder AL	Girder BL	Girder CL
Measured	30.0	34.5	25.5
AASHTO Standard Specifications	30.0	30.0	30.0
AASHTO LRFD	36.0	36.0	36.0
ACI 318-08, Section 11.3.5	30.0	30.0	30.0
ACI 318-08, Section 12.9.1	35.2	32.8	35.0
Buckner	37.9	37.8	38.3
Russell and Burns	52.8	49.1	52.6
Barns, Grove, and Burns	40.0	36.8	36.8

When computing the theoretical transfer lengths, the average strand stress was determined using the measured strain in the prestressing strands at the time of prestress transfer. For models requiring the initial strand stress, the strain values recorded just prior to release were used. For models requiring the effective strand stress, the strain values recorded immediately after release were used.

The measured transfer length in each of the three specimens was less than that required by AASHTO LRFD Bridge Design Specifications. Only Girder BL had a measured transfer length greater than that required by AASHTO Standard Specifications for Highway Bridges and ACI 318. The measured transfer lengths for all three specimens were less than the transfer lengths estimated by the models developed by Buckner et al. and Barnes et al. Based on the test results in this study, it appears that the AASHTO LRFD Bridge Design Specifications provides a more adequate transfer length requirement than the ACI 318 and AASHTO Standard Specifications for Highway Bridges.

## 7.8 PRESTRESS LOSSES

In this study, the instantaneous and the time-dependent prestress losses were both measured. This section discusses the measured prestress losses and compares the measured and the calculated values. The theoretical models for prestress losses were discussed in details in Section 5.5 of this report.

### 7.8.1 MEASURED PRESTRESS LOSSES

Prestress losses were measured for each specimen by monitoring and recording strain in the prestressing strands prior to load testing. Since Girder BL was the first girder to be tested, only a limited amount of long-term prestress loss data was collected from Girder BL. The average measured prestress losses versus time for Girder AL, Girder BL, and Girder CL are shown in Figure 7.26, Figure 7.27, and Figure 7.28, respectively. The two plots on each figure represent the average prestress losses recorded from two sets of four strain gages. The first set of strain gages was placed at quarter-span (120" from the end of the girder) and the second set of strain gages was placed at mid-span (240" from the end of the girder). In each figure, the Y-intercept represents the instantaneous prestress loss due to elastic shortening of the concrete at the time of prestress transfer. The increase in prestress losses after release is due to the combination of time-dependent losses including creep of concrete, shrinkage of concrete, and relaxation of prestressing steel.

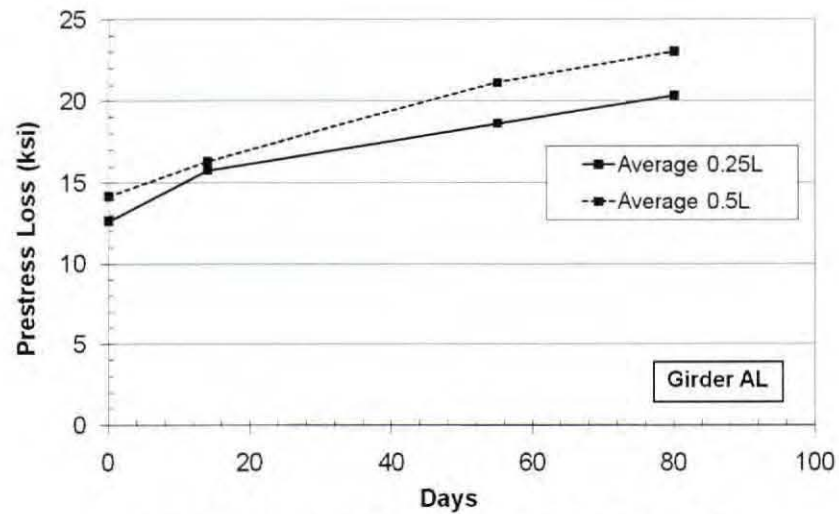


Figure 7.26: Measured Prestress Losses for Girder AL

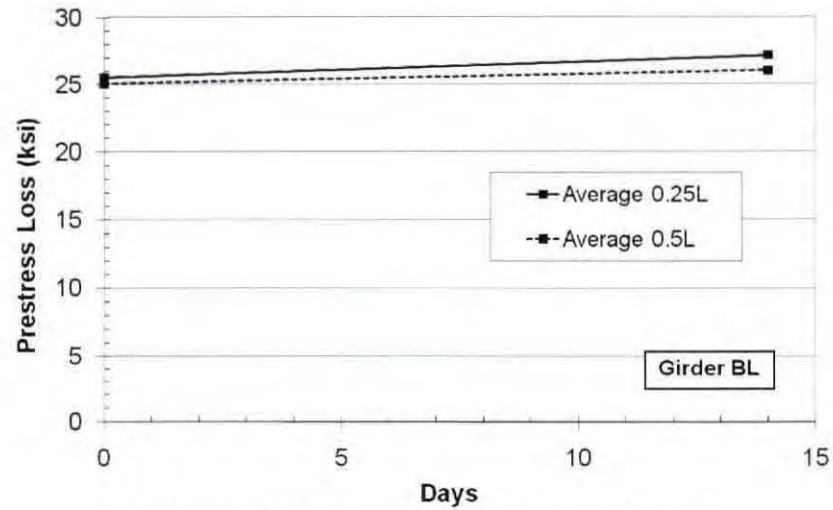


Figure 7.27: Measured Prestress Losses for Girder BL

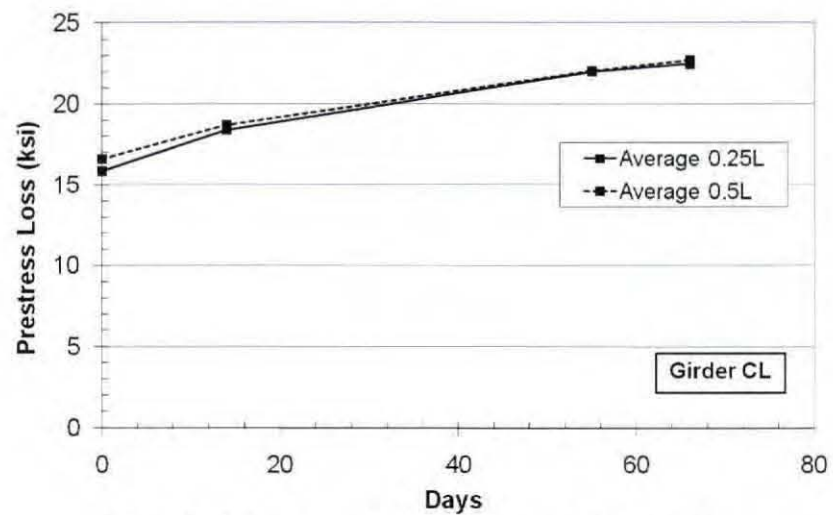


Figure 7.28: Measured Prestress Losses for Girder CL

For Girder AL, the measured average instantaneous prestress losses due to elastic shortening were 12.65 ksi and 14.22 ksi at quarter-span and mid-span, respectively, and the measured average total prestress losses were 20.36 ksi and 23.04 ksi at quarter-span and mid-span, respectively.

For Girder BL, the measured average instantaneous prestress losses due to elastic shortening were 25.55 ksi and 25.07 ksi at quarter-span and mid-span, respectively, and the measured average total prestress losses were 27.21 ksi and 26.06 ksi at quarter-span and mid-span, respectively.

For Girder CL, the measured average instantaneous prestress losses due to elastic shortening were 15.85 ksi and 16.61 ksi at quarter-span and mid-span, respectively, and the measured average total prestress losses were 22.501 ksi and 22.77 ksi at quarter-span and mid-span, respectively.

Due to the limited amount of time-dependent prestress loss data obtained for Girder BL, only the prestress losses of Girder AL and Girder CL are compared. The averages of all strand strain gage readings are plotted for Girder AL and Girder CL in Figure 7.29. The nearly parallel curves suggest that the time-dependent losses are nearly identical for Girder AL and Girder CL. The main difference in the total prestress losses is due to instantaneous losses. The average instantaneous losses were 13.55 ksi and 16.23 ksi for Girder AL and Girder CL, respectively.

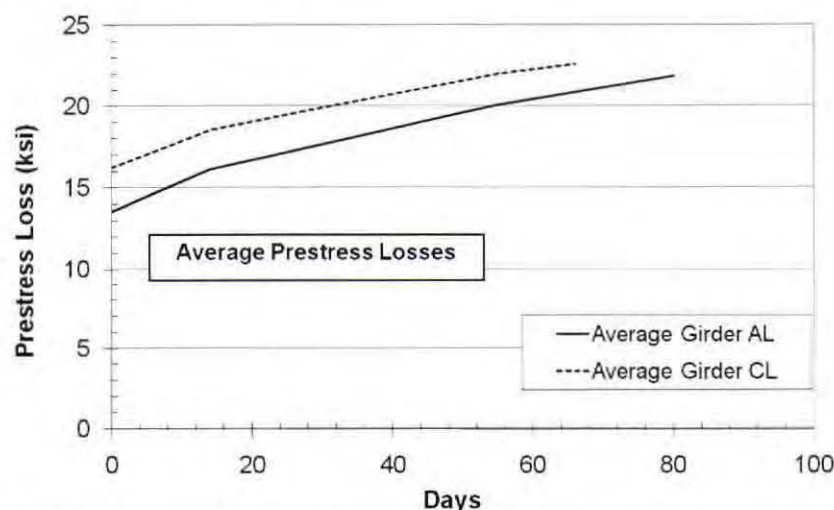


Figure 7.29: Average Measured Prestress Losses for Girder AL and Girder CL

A summary of the average instantaneous and time-dependent prestress losses is shown in Table 7.7. Girder AL, Girder BL, and Girder CL had time-dependent losses based on time spans of 80 days, 14 days, and 66 days, respectively. Girder AL experienced the least amount of prestress loss due to elastic shortening. The prestress losses in Girder BL and Girder CL due to elastic shortening were 86.8% and 19.8%, respectively, greater than that for Girder AL. The time-dependent prestress losses, however, were lower in the SCC specimens than in the control specimen. After 14 days, time-dependent losses for Girder BL and Girder CL were 48.6% and 8.9%, respectively less than the time-dependent losses for Girder AL.



**Table 7.7: Average Measured Prestress Losses**

	Prestress Loss (ksi)		
	Girder AL	Girder BL	Girder CL
<b>Instantaneous Loss</b>	13.55	25.31	16.23
<b>Time-Dependent Losses</b>	8.34 <sup>1</sup>	1.32 <sup>2</sup>	6.40 <sup>3</sup>
<b>Total Losses</b>	21.89	26.63	22.63

<sup>1</sup> @ 80 days after prestress transfer<sup>2</sup> @ 14 days after prestress transfer<sup>3</sup> @ 66 days after prestress transfer

The jacking stress,  $f_{pj}$ , and the initial prestress,  $f_{pi}$ , were determined from measured strand strain before and after prestress release, respectively. The effective prestress,  $f_{pe}$ , was then determined by subtracting the time-dependent losses from the initial prestress. Based on the prestress losses in Table 7.7, the prestressing strand stresses at  $f_{pj}$ ,  $f_{pi}$ , and  $f_{pe}$ , are shown in Table 7.8.

**Table 7.8: Average Measured Strand Stress**

	Strand Stress (ksi)		
	Girder AL	Girder BL	Girder CL
<b>Jacking Stress, <math>f_{pj}</math></b>	189.5	189.1	191.4
<b>Initial Prestress, <math>f_{pi}</math></b>	176.0	163.8	175.2
<b>Effective Prestress, <math>f_{pe}</math></b>	167.6 <sup>1</sup>	162.5 <sup>2</sup>	168.8 <sup>3</sup>

<sup>1</sup> @ 80 days after prestress transfer<sup>2</sup> @ 14 days after prestress transfer<sup>3</sup> @ 66 days after prestress transfer

### 7.8.2 THEORETICAL PRESTRESS LOSSES

In this section, the theoretical prestress losses are calculated and compared to the experimental prestress losses. The prestress loss models considered in this study were discussed in details in Section 5.5 of this report.

For this study, the measured material properties were used to determine the theoretical prestress losses. Since relative humidity was not monitored during this study, a relative humidity of 60% was used for determining the theoretical prestress losses as recommended by AASHTO Standard Specifications for Highway Bridges (2002). When applicable, the age of each specimen at load testing was used to determine time-dependent prestress losses. The calculated prestress losses were used for determining the theoretical effective prestress in each girder. The jacking stress,  $f_{pj}$ , was determined as the measured stress in the prestressing strands just prior to release. The initial prestress,  $f_{pi}$ , was determined as the jacking stress minus the prestress loss due to elastic shortening. The effective prestress,  $f_{pe}$ , was then determined by subtracting the time-dependent losses from the initial prestress.

#### 7.8.2.1 AASHTO Standard Specifications for Highway Bridges (2002)

Table 7.9 summarizes the itemized and the total prestress losses as determined by the AASHTO Standard Specifications method. Table 7.10 shows the calculated initial and effective prestress corresponding to the prestress losses presented in Table 7.9.

**Table 7.9: Calculated Prestress Losses–AASHTO Standard Specifications**

	Prestress Loss (ksi)		
	Girder AL <sup>1</sup>	Girder BL <sup>2</sup>	Girder CL <sup>3</sup>
Elastic Shortening ( <i>ES</i> )	10.80	10.64	10.09
Concrete Shrinkage ( <i>SH</i> )	8.00	8.00	8.00
Concrete Creep ( <i>CR<sub>c</sub></i> )	20.44	20.39	20.68
Strand Relaxation ( <i>CR<sub>s</sub></i> )	2.50	2.52	2.56
Total ( $\Delta f_s$ )	41.74	41.55	41.33

<sup>1</sup> Age at testing = 83 days. Prestress transfer @ 3 days

<sup>2</sup> Age at testing = 48 days. Prestress transfer @ 3 days

<sup>3</sup> Age at testing = 69 days. Prestress transfer @ 3 days

**Table 7.10: Calculated Initial and Effective Prestress–AASHTO Standard Specifications**

	Strand Stress (ksi)		
	Girder AL	Girder BL	Girder CL
Jacking Stress, $f_{pj}$ (measured)	189.5	189.1	191.4
Initial Prestress, $f_{pi}$	178.7	178.5	181.3
Effective Prestress, $f_{pe}$	147.8	147.6	150.1

#### 7.8.2.2 AASHTO LRFD Bridge Design Specifications (2007)

The AASHTO LRFD Bridge Design Specifications prescribes an approximate estimate and a refined time step method for determining prestress losses. Only the approximate estimate of the time-dependent losses is discussed in this study. Table 7.11 summarizes the calculated prestress losses. Table 7.12 shows the calculated initial and effective prestress corresponding to the prestress loss values presented in Table 7.11.

**Table 7.11: Calculated Prestress Losses–AASHTO LRFD**

	Prestress Loss (ksi)		
	Girder AL <sup>1</sup>	Girder BL <sup>2</sup>	Girder CL <sup>3</sup>
Elastic Shortening ( $\Delta f_{pES}$ )	10.80	10.78	10.93
Long-Term Losses ( $\Delta f_{pLT}$ )	16.57	16.26	14.71
Total ( $\Delta f_{pT}$ )	27.37	27.04	25.64

<sup>1</sup> Age at testing = 83 days. Prestress transfer @ 3 days

<sup>2</sup> Age at testing = 48 days. Prestress transfer @ 3 days

<sup>3</sup> Age at testing = 69 days. Prestress transfer @ 3 days

**Table 7.12: Calculated Initial and Effective Prestress–AASHTO LRFD**

	Strand Stress (ksi)		
	Girder AL	Girder BL	Girder CL
Jacking Stress, $f_{pj}$ (measured)	189.5	189.1	191.4
Initial Prestress, $f_{pi}$	178.7	178.3	180.5
Effective Prestress, $f_{pe}$	162.1	162.0	165.8



### 7.8.2.3 PCI Design Handbook (2004)

Table 7.13 summarizes the calculated prestress losses based on the PCI Design Handbook method. Table 7.14 shows the calculated initial and effective prestress corresponding to the prestress loss values presented in Table 7.13.

**Table 7.13: Calculated Prestress Losses—PCI Design Handbook**

	Prestress Loss (ksi)		
	Girder AL <sup>1</sup>	Girder BL <sup>2</sup>	Girder CL <sup>3</sup>
Elastic Shortening (ES)	10.28	10.12	9.60
Concrete Creep (CR)	16.41	18.39	16.31
Concrete Shrinkage (SH)	7.51	7.51	7.51
Strand Relaxation (RE)	2.54	2.49	2.56
Total (TL)	36.74	38.51	35.98

<sup>1</sup> Age at testing = 83 days. Prestress transfer @ 3 days

<sup>2</sup> Age at testing = 48 days. Prestress transfer @ 3 days

<sup>3</sup> Age at testing = 69 days. Prestress transfer @ 3 days

**Table 7.14: Calculated Initial and Effective Prestress—PCI Design Handbook**

	Strand Stress (ksi)		
	Girder AL	Girder BL	Girder CL
Jacking Stress, $f_{pj}$ (measured)	189.5	189.1	191.4
Initial Prestress, $f_{pi}$	178.7	178.3	180.5
Effective Prestress, $f_{pe}$	162.1	162.0	165.8

### 7.8.2.4 PCI Committee on Prestress Losses (1975)

Table 7.15 summarizes the calculated prestress losses based on the report by the PCI committee on Prestress Losses. Table 7.16 shows the calculated initial and effective prestress corresponding to the prestress loss values presented in Table 7.15.

**Table 7.15: Calculated Prestress Losses—PCI Committee on Prestress Losses**

	Prestress Loss (ksi)		
	Girder AL <sup>1</sup>	Girder BL <sup>2</sup>	Girder CL <sup>3</sup>
Elastic Shortening (ES)	10.80	10.64	10.09
Concrete Creep (CR)	7.40	6.10	7.07
Concrete Shrinkage (SH)	5.91	4.95	5.58
Conc. Comp. Stress (RET)	1.72	1.51	1.65
Total (TL)	25.83	23.20	24.39

<sup>1</sup> Age at testing = 83 days. Prestress transfer @ 3 days

<sup>2</sup> Age at testing = 48 days. Prestress transfer @ 3 days

<sup>3</sup> Age at testing = 69 days. Prestress transfer @ 3 days



**Table 7.16: Calculated Initial and Effective Prestress– PCI Committee on Prestress Losses**

	Strand Stress (ksi)		
	Girder AL	Girder BL	Girder CL
Jacking Stress, $f_{pj}$ (measured)	189.5	189.1	191.4
Initial Prestress, $f_{pi}$	178.7	178.5	181.3
Effective Prestress, $f_{pe}$	163.7	165.9	167.0

### 7.8.3 COMPARISON OF MEASURED AND CALCULATED PRESTRESS LOSSES

The calculated prestress loss values varied amongst the four prestress loss models. Depending on the method used, the calculated total prestress loss varied between 12.3% and 22.0% of the jacking stress. The AASHTO Standard Specifications for Highway Bridges and the PCI Design Handbook methods resulted in similar prestress loss values, with variations of no more than 2.8% of the jacking stress between the two models. On the other hand, the AASHTO LRFD Bridge Design Specifications and the 1975 PCI Committee on Prestress Losses yielded similar prestress loss values, with variations of no more than 2.0% of the jacking stress between the two models. The AASHTO Standard Specifications for Highway Bridges resulted in the largest prestress loss. The 1975 PCI Committee on Prestress Losses model resulted in the smallest prestress losses.

The measured and calculated effective prestress values are compared. The comparison is also illustrated in Figure 7.30. The ratio of the measured effective prestress to the calculated effective prestress varied between 0.98 and 1.13. All four models resulted in reasonable estimates of the total prestress losses. However, the calculated prestress losses based on the AASHTO LRFD Bridge Design Specifications and the 1975 PCI Committee on Prestress Losses were virtually identical to the measured prestress losses.

**Table 7.17: Ratio of Measured to Calculated Effective Prestress**

	Girder AL	Girder BL	Girder CL
Measured $f_{pe} / \bar{f}_{pe}$ , AASHTO 2002	1.13	1.10	1.12
Measured $f_{pe} / \bar{f}_{pe}$ , AASHTO LRFD	1.03	1.00	1.02
Measured $f_{pe} / \bar{f}_{pe}$ , PCI Handbook	1.10	1.08	1.09
Measured $f_{pe} / \bar{f}_{pe}$ , PCI 1975	1.02	0.98	1.01

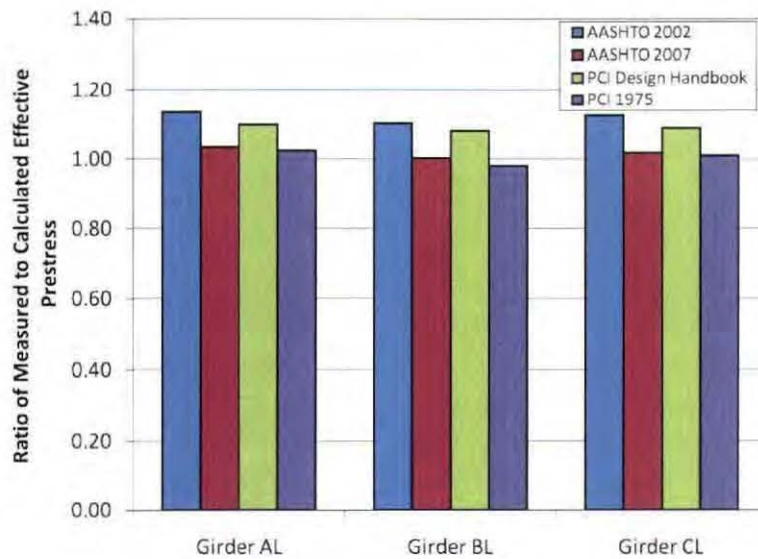


Figure 7.30: Comparison of Measured and Calculated Effective Prestress

## 7.9 CAMBER

The initial camber was measured in each girder following the release of the prestressing strands. Immediately after release, each specimen was lifted slightly off the prestressing bed in order to relieve the friction between the bottom of the specimen and the prestressing bed. A surveyor's level and a ruler graduated with decimal inches were used to measure the camber in each specimen. Elevations were measured on both sides at both ends and at mid-span of each specimen to determine the camber. The camber was also measured in the same manner just prior to load testing each specimen. The average camber measurements are summarized in Table 7.18.

Table 7.18: Camber Measurements

	Camber (in)		
	Girder AL <sup>1</sup>	Girder BL <sup>2</sup>	Girder CL <sup>3</sup>
Initial Camber	0.18	0.60	0.35
Final Camber	0.31 <sup>1</sup>	0.63 <sup>2</sup>	0.49 <sup>3</sup>

<sup>1</sup> 81 days after release

<sup>2</sup> 46 days after release

<sup>3</sup> 67 days after release

The measured camber was larger in the SCC specimens than in the control specimen. Girder BL had the largest measured camber and Girder AL had the smallest measured camber. Camber measurements in all three specimens were consistent with the instantaneous prestress losses due to elastic shortening. The largest amount of camber occurred in the member with the largest amount of prestress loss due to elastic shortening. As the elastic shortening increases, the member experiences an increase in camber.

Using the PCI Design Handbook (2004) methods as described in Section 5.6, the initial and final camber values were calculated for each girder. The measured material properties were used in the calculations. Table 7.19 shows the calculated camber values for the three girders.



Table 7.19: Calculated Camber (PCI Design Handbook Method)

	Camber (in)		
	Girder AL <sup>1</sup>	Girder BL <sup>2</sup>	Girder CL <sup>3</sup>
Initial Camber	0.39	0.38	0.37
Final Camber	0.76	0.74	0.71

The ratios of the measured to the calculated camber are shown in Figure 7.31. The initial camber ratios for Girder AL, Girder BL, and Girder CL were 0.46, 1.56, and 0.96, respectively. The final camber ratios for Girder AL, Girder BL, and Girder CL were 0.41, 0.85, and 0.69, respectively. The results indicate that there is a significant difference between the measured and the calculated results. Except for the initial camber of Girder BL, the calculated always exceeded the measured camber. The method for determining the long-term camber is highly empirical and may not always result in accurate estimates of the camber.

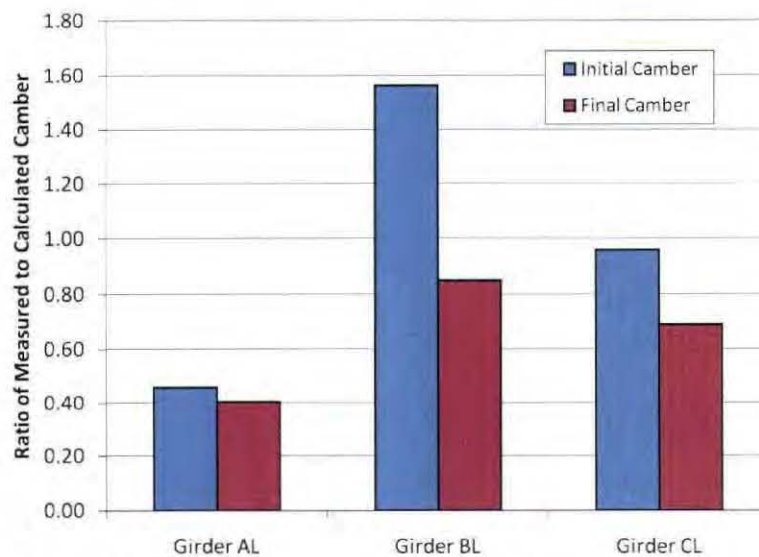


Figure 7.31: Comparison of Measured and Calculated Camber

## 7.10 LOAD TESTING RESULTS

This section presents the experimental results that were obtained from load testing of the girder specimens. The reported experimental results include general observations, development of concrete cracks, measured load–deflection relationships, and measured strain in the prestressing strands, concrete, and shear reinforcement.

### 7.10.1 GIRDER AL EXPERIMENTAL RESULTS

Girder AL was cast with conventional concrete and served as the control specimen. The load testing of Girder AL was performed on November 6, 2007. Figure 7.32 shows Girder AL at different stages during the test. The first flexural tension crack occurred at mid-span at a load of 156.9 Kips and mid-span deflection of 0.346". The corresponding cracking moment was 1540 Kip-ft. As the load was increased, additional flexural and flexural–shear cracks developed within approximately the middle third of the girder, causing significant reduction in stiffness. It was observed that the flexural cracks occurred at the locations of the transverse reinforcement. At a load of 235 Kips and a corresponding mid-span deflection



of 2.90", shear cracks were detected in the girder web. The shear cracks were located between 2 and 10 feet from the north end of the specimen. Girder AL failed in flexure at an ultimate load of 243.6 Kips and a corresponding mid-span deflection of 5.46". The flexural failure was manifested by crushing of the compression concrete at mid-span. Following the conclusion of the test, the cracks were surveyed and mapped. The crack maps of Girder AL are provided in Appendix E.



(a) Before Loading



(b) First Flexural Crack at Load = 157 Kips



(c) Flexural and Flexural-Shear Cracks



(d) Diagonal Shear Cracks at Load = 235 Kips



(e) Girder AL Shortly before Failure



(f) Crushing of Compression Concrete at Failure

Figure 7.32: Girder AL at Different Stages during the Test

### 7.10.1.1 Measured Load-Deflection

Figure 7.33 shows the measured load-deflection plot. The load-deflection response was almost linear up to the point corresponding to the first flexural crack. As the load was increased, the additional flexural and flexural-shear cracks caused significant reduction in stiffness. Past the point of first flexural crack, the load-deflection response became non-linear.

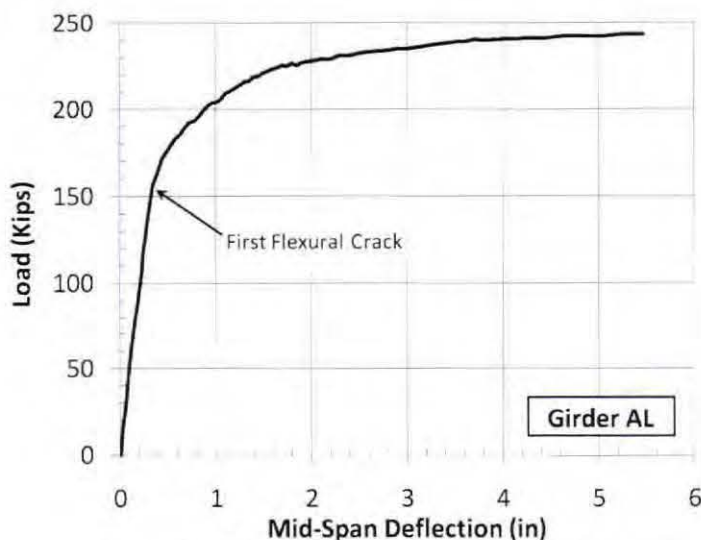


Figure 7.33: Measured Load-Deflection – Girder AL

### 7.10.1.2 Measured Strand Strain

Strand strains were measured at mid-span and at quarter-span. Figure 7.34 shows a plot of the measured strand strain at mid-span resulting from the externally applied load only. The plot does not include strain due to the prestressing force, the girder dead load, or the composite deck dead load. Prior to initiation of the first crack, the strand strain increased approximately linearly with an increase in the applied moment. At the cracking moment of 1540 Kip-ft, the measured strand strain increased significantly.

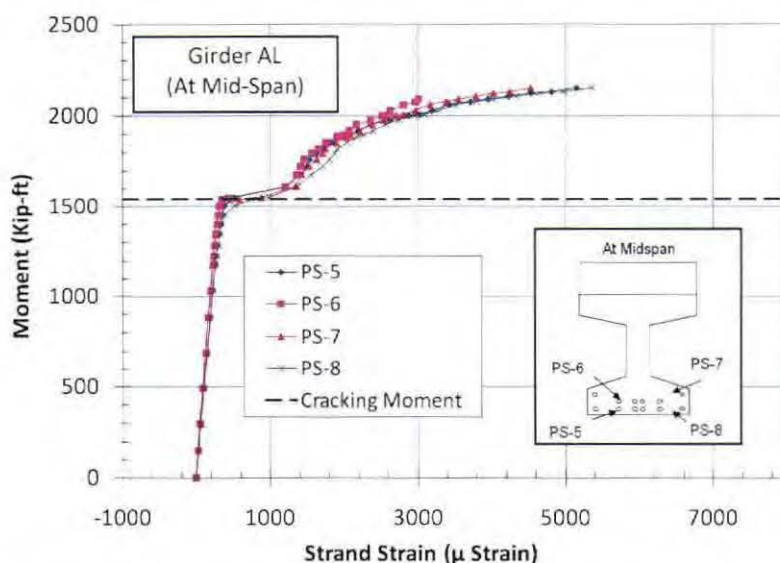
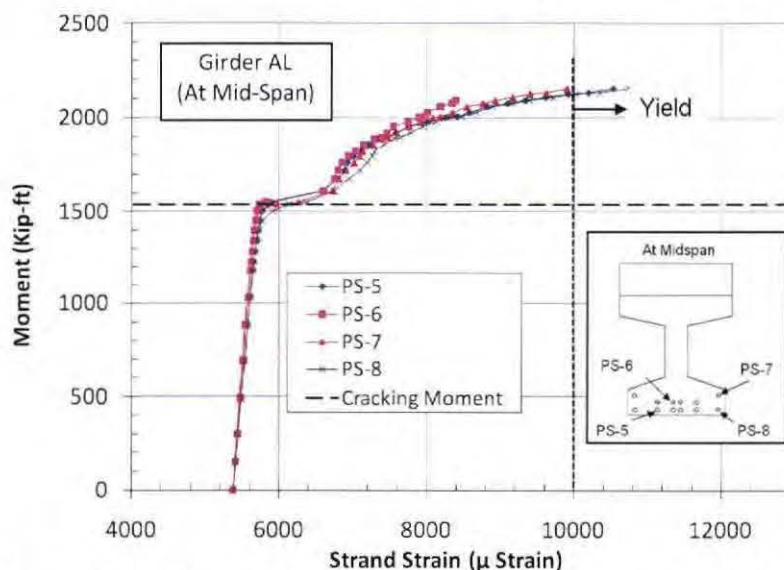


Figure 7.34: Measured Strand Strain at Mid-Span Resulting from External Load – Girder AL



Prior to the application of the actuator's load, the average measured strain in the prestressing strands was 5378 micro-strain. Therefore, the measured strain values shown in Figure 7.34 were increased by 5378 micro-strain to account for the strain due to prestressing and self-weight. Figure 7.35 shows a plot of the externally applied moment versus the measured strand strain at mid-span, including the strain due to prestressing and self-weight at. The prestressing strands had a yield strain of 1% or 10,000 micro-strain. As shown in Figure 7.35, the strain in some of the prestressing strands reached the yield strain at a moment of 2125 Kip-ft, corresponding to an actuator load of approximately 217 Kips.



**Figure 7.35: Measured Strand Strain at Mid-Span Resulting from All Loads – Girder AL**

The strain gages at quarter-span were placed on the same four strands that were instrumented at mid-span. Figure 7.36 shows a plot of the measured strand strain at quarter-span resulting from the externally applied moment only. This plot does not include strain due to the prestressing force, the girder dead load, or the composite deck dead load. The measured results indicate the following

1. The strain increased approximately linearly with an increase in the bending moment.
2. Gage PS-1 exhibited erratic readings above a moment of 760 Kip-ft. Since no cracks had developed across the location of PS-1, the erratic readings may have been the result of a gage malfunction.
3. The measured strain values were consistent with the location of the strands relative to the bottom of the girder. For the same load, higher strain values were exhibited by the strands that were located closer to the outermost tensile fiber.
4. At a moment of approximately 1157 Kip-ft, corresponding to an actuator load of 235 Kips, the strands at quarter-span experienced a sudden increase in strain. This increase in the strain coincided with the formation of the diagonal shear cracks at and close to the quarter-span. The increase in the tensile strain reflects the shear-flexure interaction. Park and Paulay (1975) showed that the formation of diagonal shear cracks increase the tension in the flexural reinforcement.



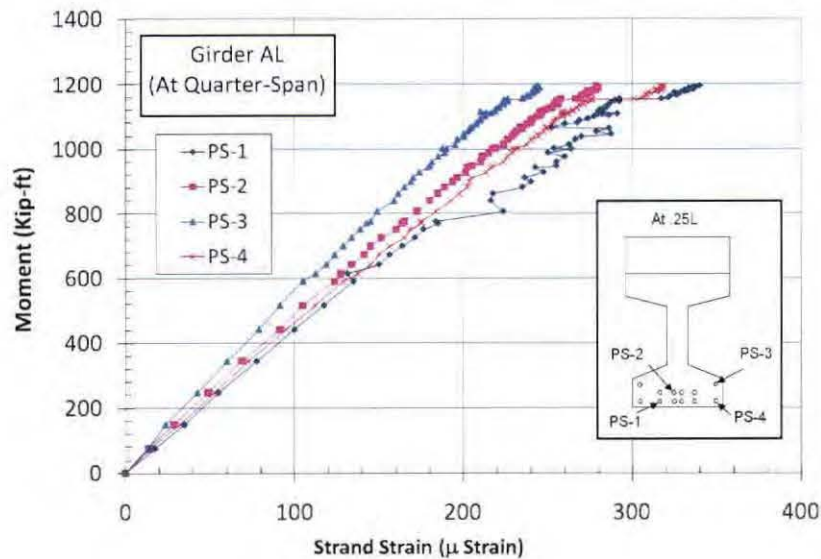


Figure 7.36: Measured Strand Strain at Quarter-Span Resulting from External Load – Girder AL

Figure 7.37 shows the measured strand strain at quarter span after the initial strain due to prestress and the specimen's self-weight are added to the strain resulting from the externally applied load. The maximum strain at quarter-span was approximately 5720 micro-strain which indicates that the strands at quarter-span remained significantly below the yield strain during the test.

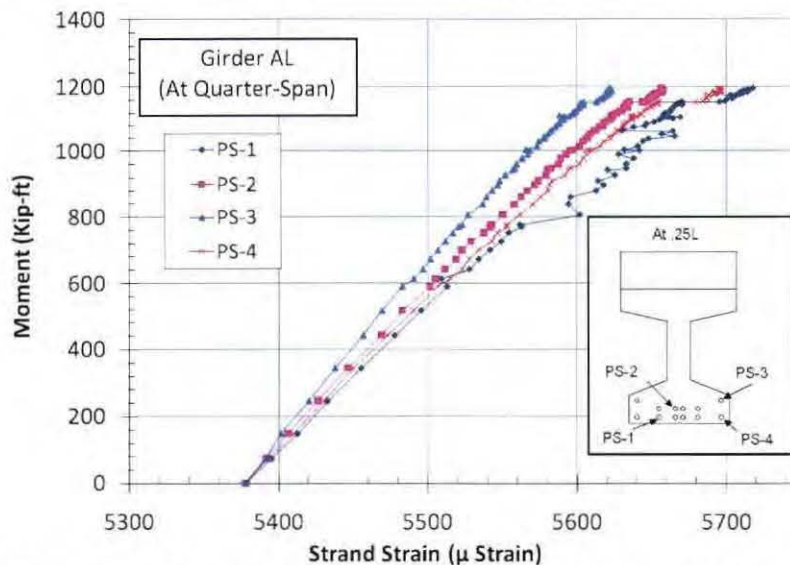


Figure 7.37: Measured Strand Strain at Quarter-Span Resulting from All Loads – Girder AL

#### 7.10.1.3 Measured Concrete Strain

Figure 7.38 shows a plot of the measured concrete strain at mid-span resulting from the externally applied moment only. Figure 7.39 shows the measured concrete strain after the initial strains due to prestressing and self-weight were calculated and added to the measured strain. The concrete strains due to prestressing and self-weight were relatively small compared to the strains due to the applied moment at mid-span. At the first flexural crack, which occurred at a load of 157 Kips (or moment of 1540 Kip-ft), gages EM-8 and EM-9 measured significant tensile strains. As the moment increased, the neutral axis

moved upward and the tensile strains in EM-8, EM-9, EM-10, and EM-11 increased. Gages EM-12 and EM-13, which were placed at 3.5" below the top of the deck, remained in compression throughout the test.

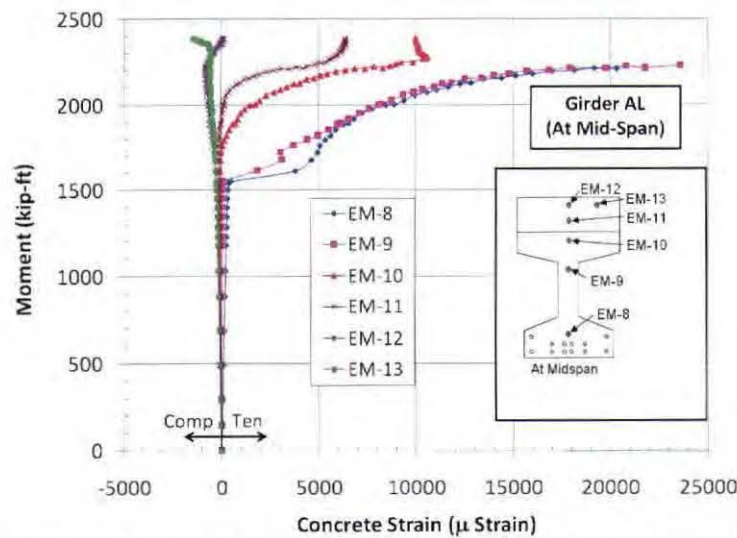


Figure 7.38: Measured Concrete Strain at Mid-Span Resulting from External Load – Girder AL

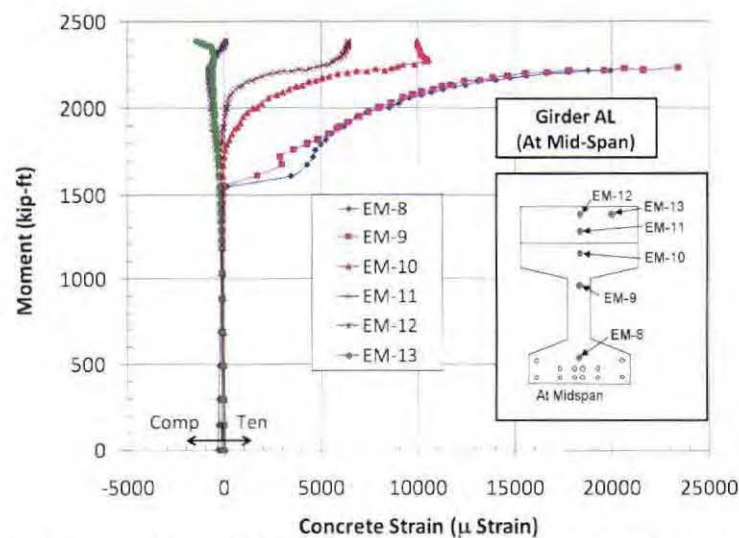


Figure 7.39: Measured Concrete Strain at Mid-Span Resulting from All Loads – Girder AL

The embedded strain gages at quarter-span were placed at the same relative locations as the embedded strain gages at mid-span. Figure 7.40 shows a plot of the measured concrete strain at quarter-span resulting from the externally applied moment only. Figure 7.41 shows the measured concrete strain after the initial strains due to prestressing and self-weight were calculated and added to the measured strain. The measured strain increased approximately linearly with an increase in the moment. This suggests that flexural cracking did not occur at quarter-span. The variation among the strain gage readings was consistent with the locations of the gages. Gages EM-6 and EM-7, which were located at the same depth, exhibited nearly identical compressive strains.

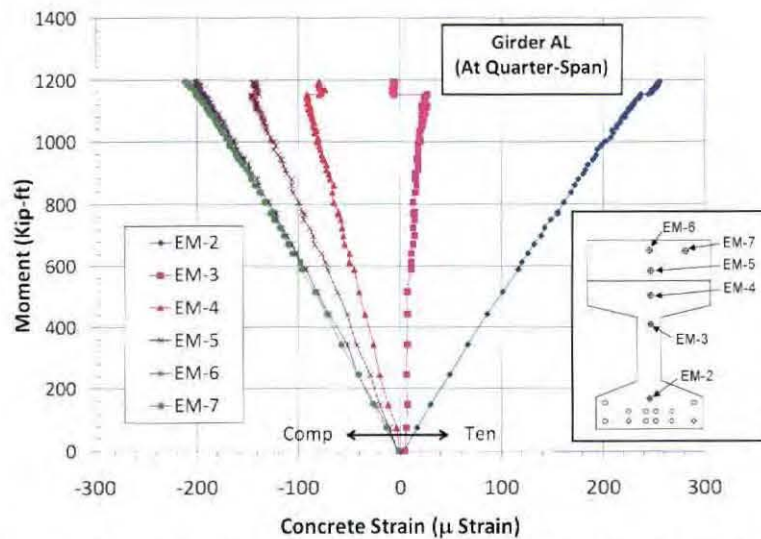


Figure 7.40: Measured Concrete Strain at Quarter-Span Resulting from External Load – Girder AL

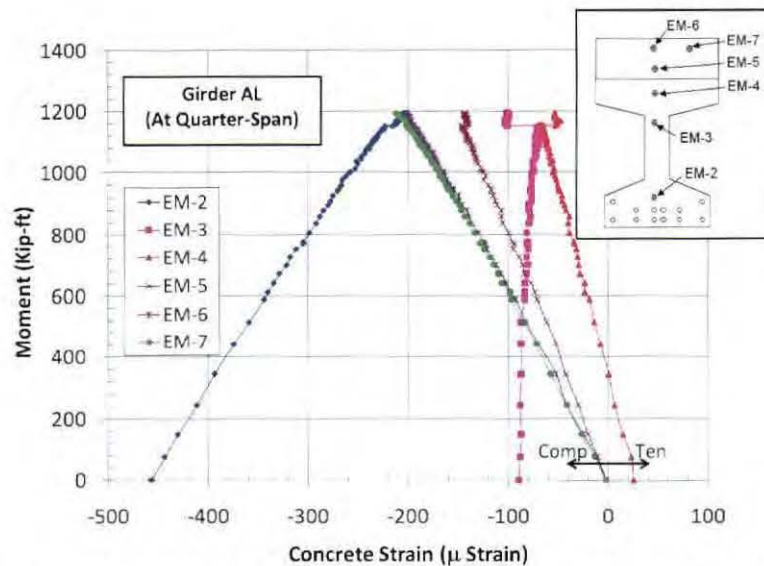


Figure 7.41: Measured Concrete Strain at Quarter-Span Resulting from All Loads – Girder AL

#### 7.10.1.4 Measured Top and Bottom Strains at Mid-Span

Girder AL was instrumented with LVDTs attached horizontally to the top and bottom of the girder at mid-span. The measurements obtained from the LVDTs were used to evaluate the section curvature, monitor the outermost compressive concrete strain, and detect the first flexural crack at the bottom of the section. Figure 7.42 and Figure 7.43 show the applied moment versus the strain at the top and the bottom LVDT locations, respectively. Both curves show approximately linear Moment-Strain relationships until the point of first flexural crack.



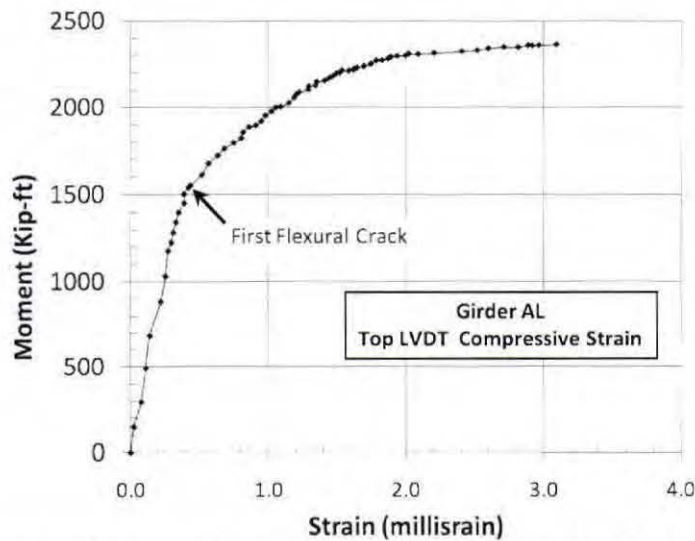


Figure 7.42: Measured Compressive Strain along Top Horizontal LVDT at Mid-Span – Girder AL

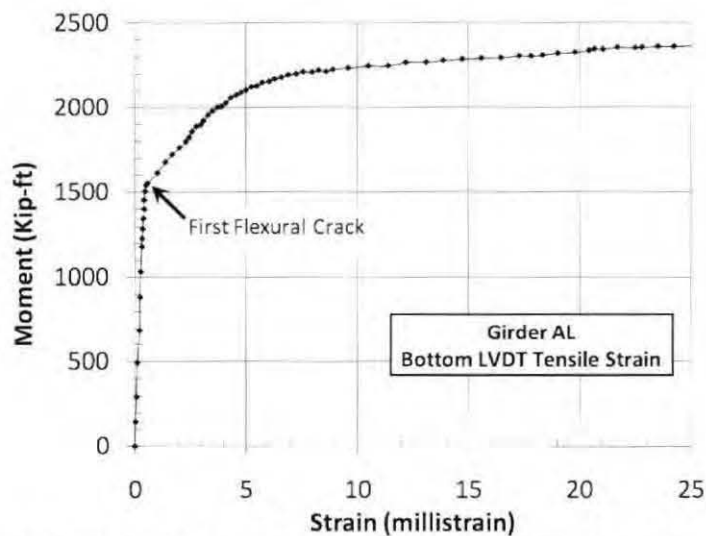


Figure 7.43: Measured Tensile Strain along Bottom Horizontal LVDT at Mid-Span – Girder AL

#### 7.10.1.5 Measured Strain in the Shear Reinforcement

The plots of applied shear force versus stirrup strain are shown in Figure 7.44, Figure 7.45, Figure 7.46, and Figure 7.47 for the stirrups at 22.5", 52.5", 82.5", and 112.5" from the north end of the girder, respectively. The applied shear force does not include the shear due to self-weight of the specimen. For each stirrup, readings from three strain gages were collected. A sharp increase in at least one strain gage indicates the development of a web-shear crack that crosses the stirrup. All four plots indicate that web-shear cracking occurred near the end of load testing at an applied shear of approximately 118 Kips.

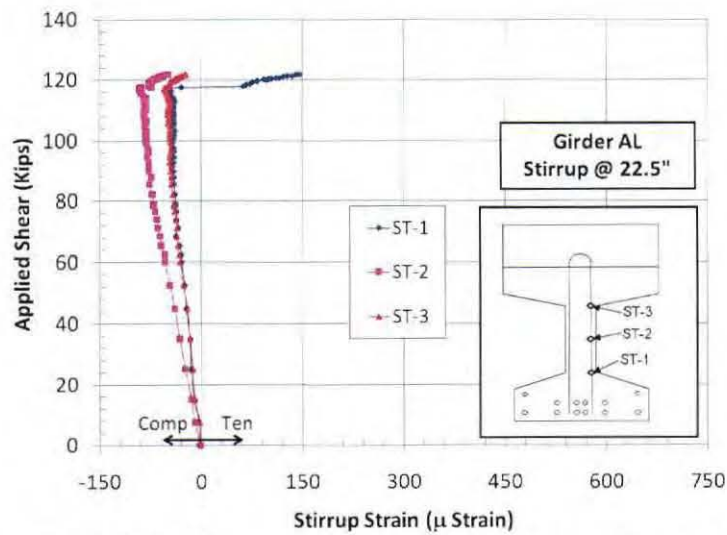


Figure 7.44: Measured Strain along Stirrup @ 22.5" – Girder AL

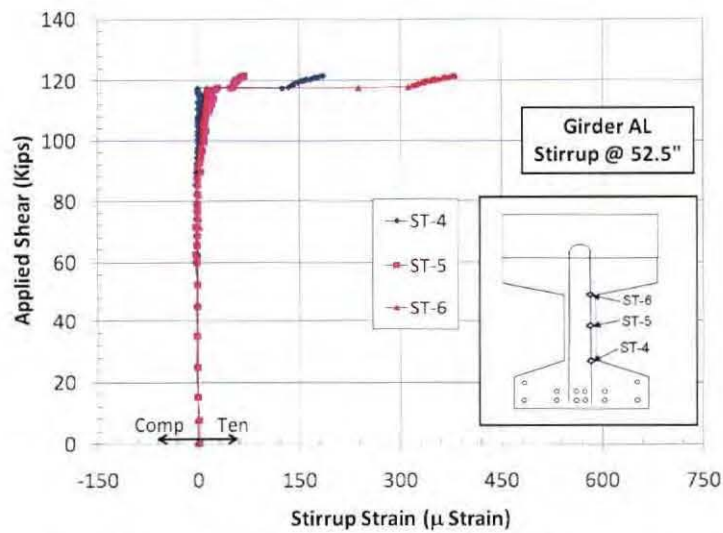


Figure 7.45: Measured Strain along Stirrup @ 52.5" – Girder AL

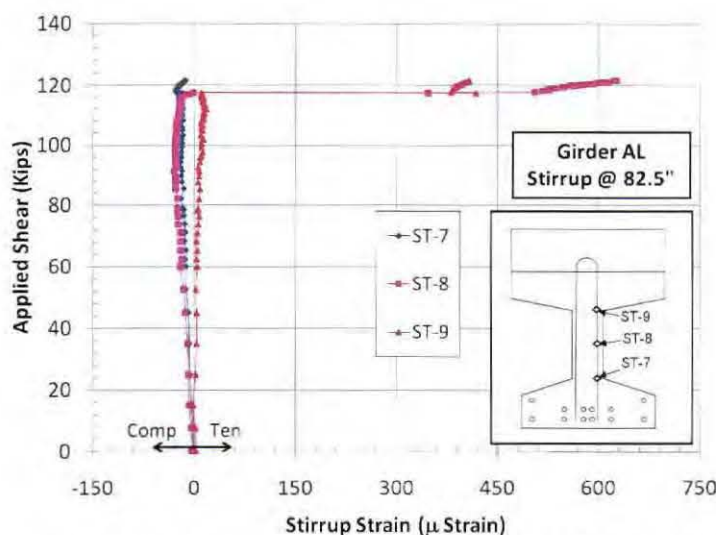


Figure 7.46: Measured Strain along Stirrup @ 82.5" – Girder AL

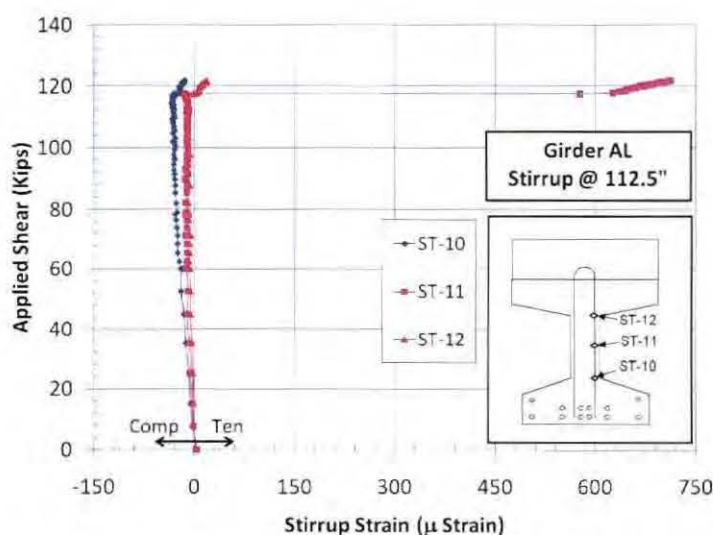


Figure 7.47: Measured Strain along Stirrup @ 112.5" – Girder AL

### 7.10.2 GIRDER BL EXPERIMENTAL RESULTS

Girder BL was cast with SCC and tested under monotonic increasing load. The load testing of Girder BL was performed on October 2, 2007. Figure 7.48 shows Girder BL at different stages during the test. The response of Girder BL was similar to that of Girder AL. Therefore, many of the observations and conclusions made during the testing of Girder AL were equally applicable to the testing of Girder BL. The first flexural tension crack occurred at mid-span at a load of 161.1 Kips and mid-span deflection of 0.367". The corresponding cracking moment was 1581 Kip-ft. As the load was increased, additional flexural and flexural-shear cracks developed within approximately the middle third of the girder, causing significant reduction in stiffness. It was observed that the flexural cracks occurred at the locations of the transverse reinforcement. At a load of 245.5 Kips and a corresponding mid-span deflection of 4.02", the first shear cracks were detected in the girder web. At the end of the test, the shear cracks were located between 6 and 12 feet from the south end and between 8-12 feet from the north end of the specimen. Girder BL failed in flexure at an ultimate load of 247.3 Kips and a corresponding mid-span deflection of



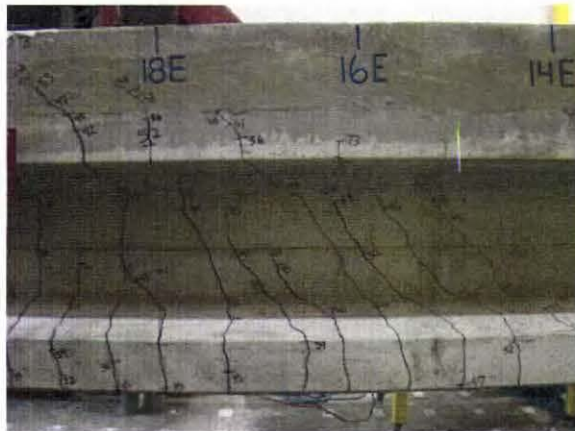
5.09". The flexural failure was manifested by crushing of the compression concrete at mid-span. Following the conclusion of the test, the cracks were surveyed and mapped. The crack maps of Girder BL are provided in Appendix E.



(a) Before Loading



(b) First Flexural Cracks at Load = 161 Kips



(c) Flexural and Flexural-Shear Cracks



(d) Diagonal Shear Cracks at Load = 245 Kips



(e) Girder BL Shortly before Failure



(f) Crushing of Compression Concrete at Failure

Figure 7.48: Girder BL at Different Stages during the Test

### 7.10.2.1 Measured Load–Deflection

Figure 7.49 shows the measured load–deflection plot. The load–deflection response was almost linear up to the point corresponding to the first flexural crack. As the load was increased, the additional flexural and flexural–shear cracks caused significant reduction in stiffness. Past the point of first flexural crack, the load–deflection response became non-linear.

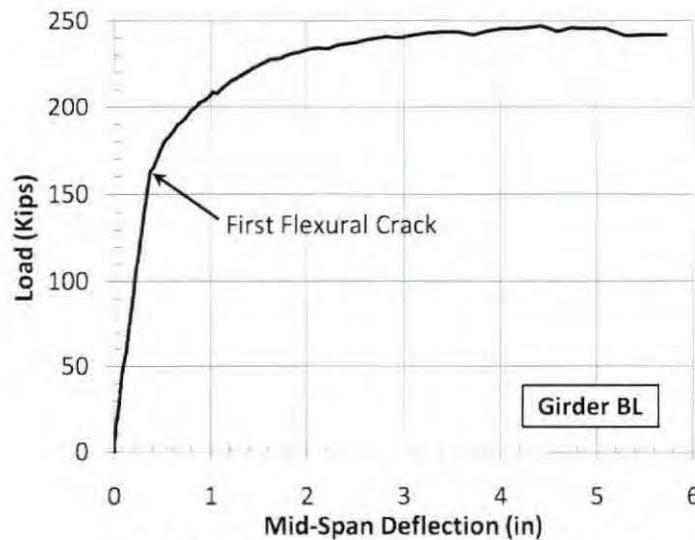


Figure 7.49: Measured Load-Deflection – Girder BL

### 7.10.2.2 Measured Strand Strain

Strand strains were measured at mid-span and at quarter-span. Figure 7.50 shows a plot of the measured strand strain at mid-span resulting from the externally applied load only. The plot does not include strain due to the prestressing force, the girder dead load, or the composite deck dead load. Prior to initiation of the first crack, the strand strain increased approximately linearly with an increase in the applied moment. At the cracking moment of 1581 Kip-ft, the measured strand strain increased significantly.

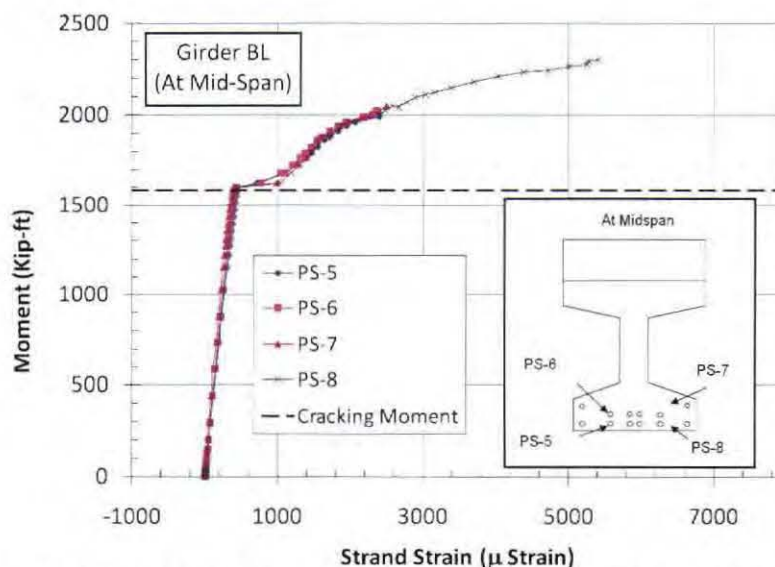
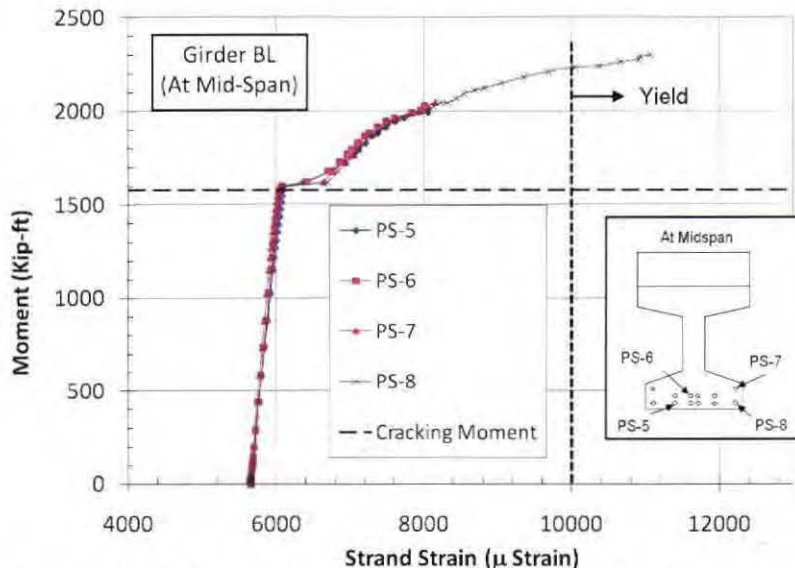


Figure 7.50: Measured Strand Strain at Mid-Span Resulting from External Load – Girder BL



Prior to the application of the actuator's load, the average measured strain in the prestressing strands was 5658 micro-strain. Therefore, the measured strain values shown in Figure 7.51 were increased by 5658 micro-strain to account for the strain due to prestressing and self-weight. Figure 7.51 shows a plot of the externally applied moment versus the measured strand strain at mid-span, including the strain due to prestressing and self-weight at. The prestressing strands had a yield strain of 1% or 10,000 micro-strain. As shown in Figure 7.51, the strain in some of the prestressing strands reached the yield strain at a moment of 2236 Kip-ft, corresponding to an actuator load of approximately 228 Kips.



**Figure 7.51: Measured Strand Strain at Mid-Span Resulting from All Loads – Girder BL**

The strain gages at quarter-span were placed on the same four strands that were instrumented at mid-span. Figure 7.52 shows a plot of the measured strand strain at quarter-span resulting from the externally applied moment only. This plot does not include strain due to the prestressing force, the girder dead load, or the composite deck dead load. The measured results indicate the following

1. The strain increased approximately linearly with an increase in the bending moment.
2. The measured strain values were consistent with the location of the strands relative to the bottom of the girder. For the same load, higher strain values were exhibited by the strands that were located closer to the outermost tensile fiber.
3. At a moment of approximately 1205 Kip-ft, corresponding to an actuator load of 245.5 Kips, the strands at quarter-span experienced a sudden increase in strain. This increase in the strain coincided with the formation of the diagonal shear cracks at and close to the quarter-span. The increase in the tensile strain reflects the shear-flexure interaction. Park and Paulay (1975) showed that the formation of diagonal shear cracks increase the tension in the flexural reinforcement.



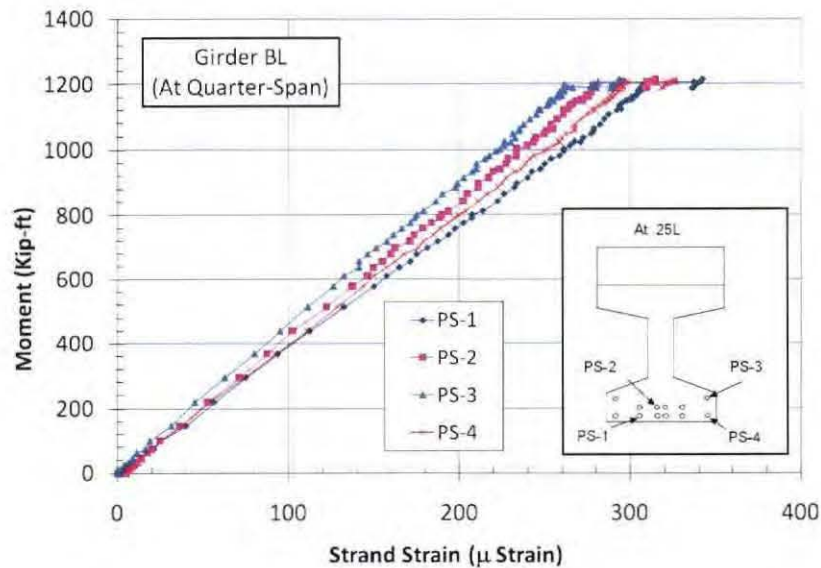


Figure 7.52: Measured Strand Strain at Quarter-Span Resulting from External Load – Girder BL

Figure 7.53 shows the measured strand strain at quarter span after the initial strain due to prestress and the specimen's self-weight are added to the strain resulting from the externally applied load. The maximum strain at quarter-span was approximately 6000 micro-strain which indicates that the strands at quarter-span remained significantly below the yield strain during the test.

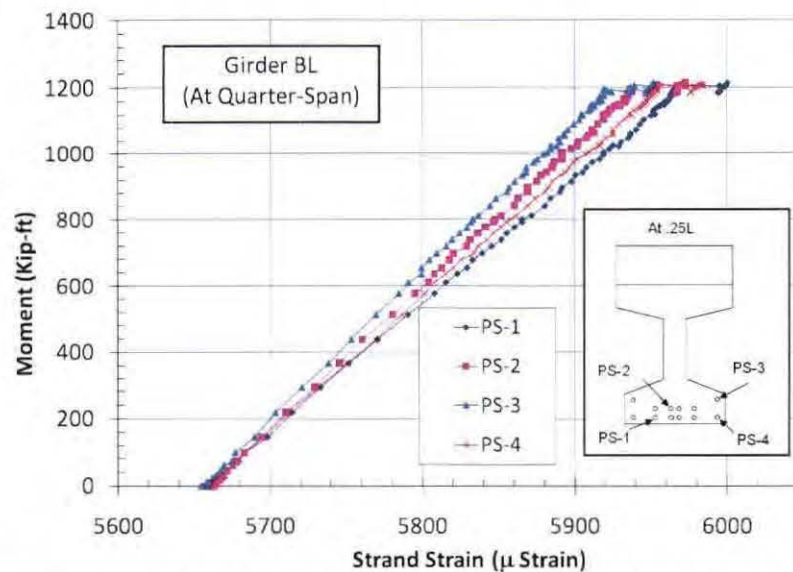


Figure 7.53: Measured Strand Strain at Quarter-Span Resulting from All Loads – Girder BL

### 7.10.2.3 Measured Concrete Strain

Figure 7.54 shows a plot of the measured concrete strain at mid-span resulting from the externally applied moment only. Figure 7.55 shows the measured concrete strain after the initial strains due to prestressing and self-weight were calculated and added to the measured strain. The concrete strains due to prestressing and self-weight were relatively small compared to the strains due to the applied moment at mid-span. At the first flexural crack, which occurred at a load of 161.1 Kips (or moment of 1581 Kip-ft), gages EM-8 and EM-9 did not register any increase in tensile strain. A possible explanation for the lack

could be the fact that a crack did not intersect and engage gages EM-8 and EM-9, but rather occurred on either side of them. The cracks propagated upward as they engaged strain gages EM-10 and EM-11 in sequence. Gages EM-12 and EM-13 remained in compression throughout the load test.

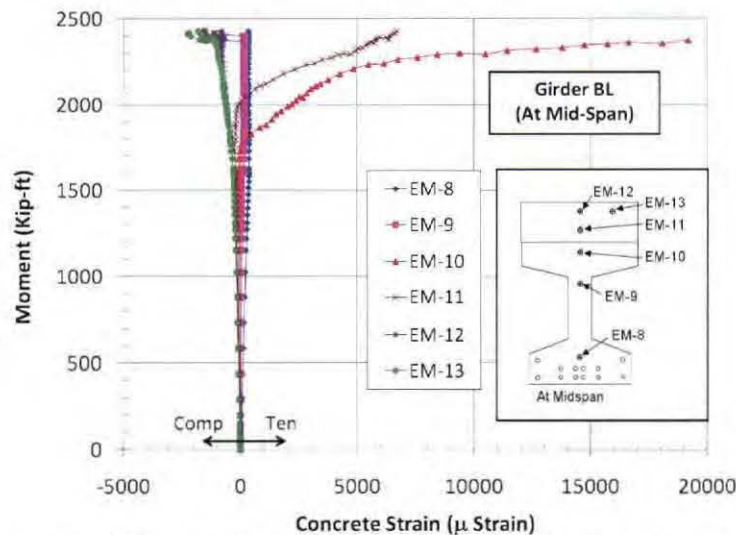


Figure 7.54: Measured Concrete Strain at Mid-Span Resulting from External Load – Girder BL

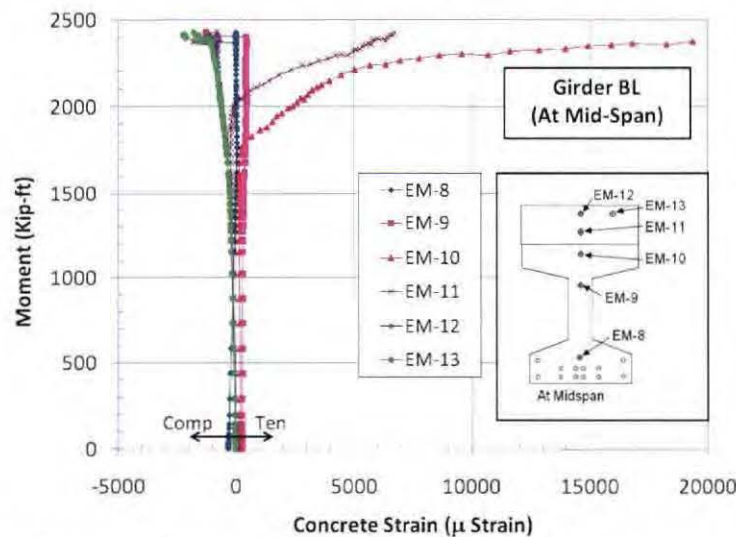


Figure 7.55: Measured Concrete Strain at Mid-Span Resulting from All Loads – Girder BL

The embedded strain gages at quarter-span were placed at the same relative locations as the embedded strain gages at mid-span. Figure 7.56 shows a plot of the measured concrete strain at quarter-span resulting from the externally applied moment only. Figure 7.57 shows the measured concrete strain after the initial strains due to prestressing and self-weight were calculated and added to the measured strain. The measured strain increased approximately linearly with an increase in the moment. This suggests that flexural cracking did not occur at quarter-span. The variation among the strain gage readings was consistent with the locations of the gages. Gages EM-6 and EM-7, which were located at the same depth, exhibited nearly identical compressive strains.

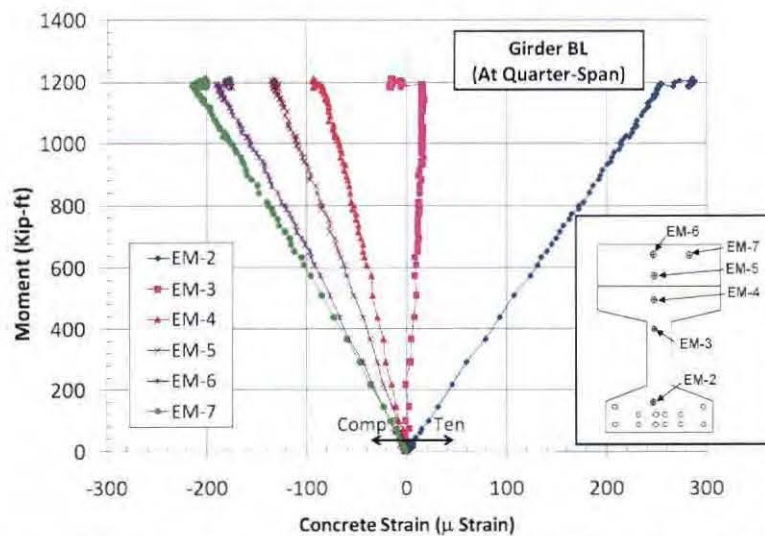


Figure 7.56: Measured Concrete Strain at Quarter-Span Resulting from External Load – Girder BL

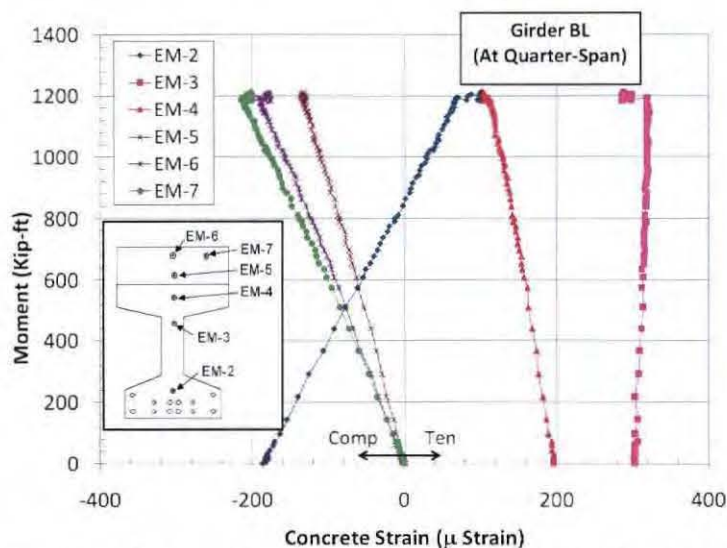


Figure 7.57: Measured Concrete Strain at Quarter-Span Resulting from All Loads – Girder BL

#### 7.10.2.4 Measured Top and Bottom Strains at Mid-Span

Girder BL was instrumented with a longitudinal LVDT attached to the bottom flange of the girder. The purpose of the LVDT was to detect the first flexural crack at mid-span. Girder BL was tested before Girder AL. The decision to add a longitudinal LVDT along the top flange was made after Girder BL was tested. Without the top LVDT, a strain profile could only be constructed using the strain from the bottom LVDT and the concrete-embedded strain gages. Figure 7.58 shows the applied moment versus the strain at the bottom LVDT location. The curve shows approximately linear Moment-Strain relationship until the point of first flexural crack.



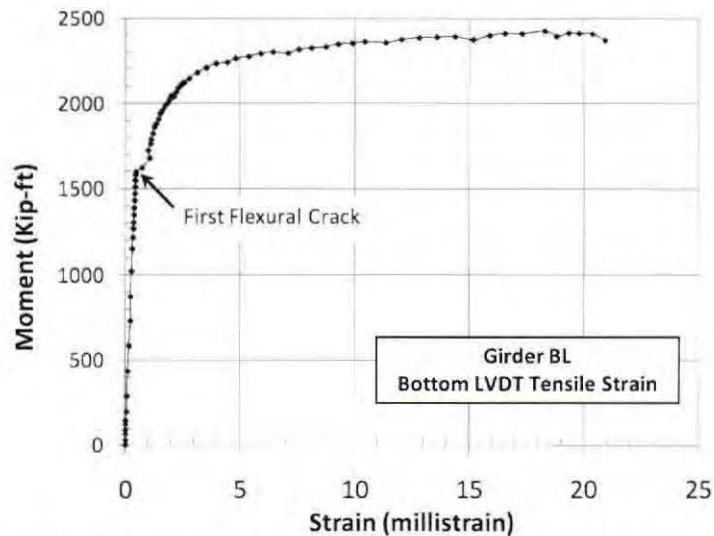


Figure 7.58: Measured Compressive Strain along Bottom Horizontal LVDT at Mid-Span – Girder BL

#### 7.10.2.5 Measured Strain in the Shear Reinforcement

Plots of the applied shear force versus stirrup strain are shown in Figure 7.59, Figure 7.60, Figure 7.61, and Figure 7.62 for the stirrups at 22.5", 52.5", 82.5", and 112.5" from the north end of the girder, respectively. The applied shear force does not include the shear due to self-weight of the specimen. For each stirrup, readings from three strain gages were collected. A sharp increase in at least one strain gage indicates the development of a web-shear crack that crosses the stirrup. The lack of sudden increase in strain in Figure 7.59, 7.60, and 7.61 indicates that web-shear cracking did not intersect any of the stirrups at 22.5", 52.5", and 82.5". The lack of cracking at those locations can be verified by viewing the crack maps for Girder BL in Appendix E. Figure 7.62, however, indicates that a web-shear crack had developed and intersected the stirrup located at 112.5" at an applied shear of approximately 123 Kips. This result is also consistent with the crack map shown in Appendix E.

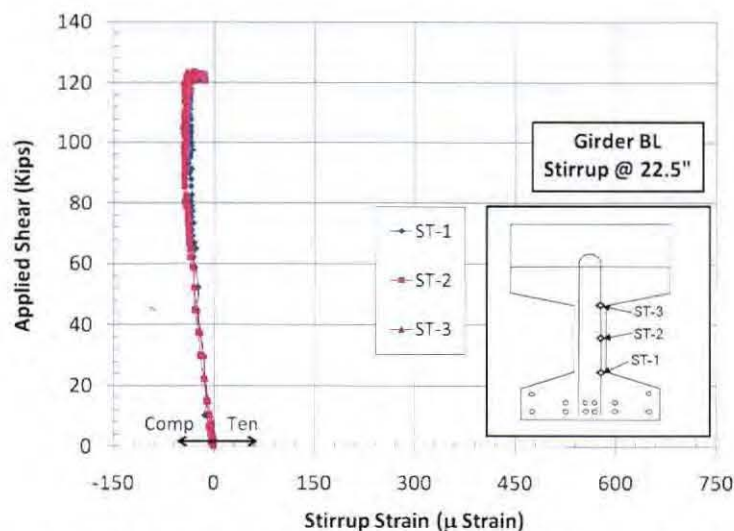


Figure 7.59: Measured Strain along Stirrup @ 22.5" – Girder BL

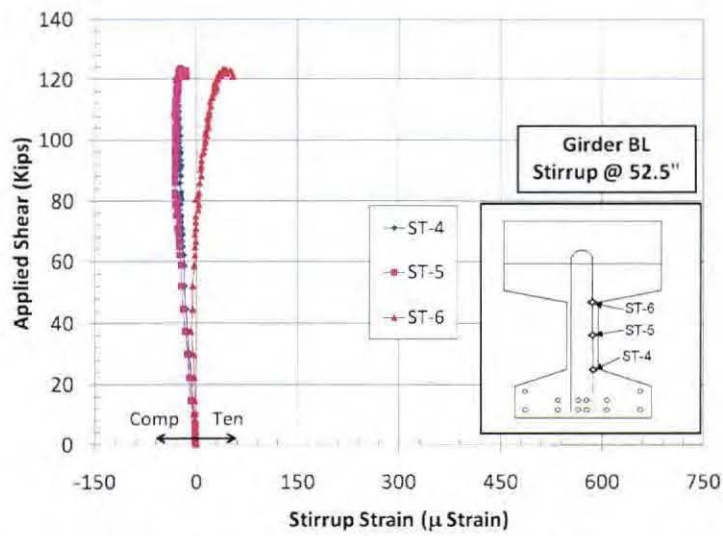


Figure 7.60: Measured Strain along Stirrup @ 52.5" – Girder BL

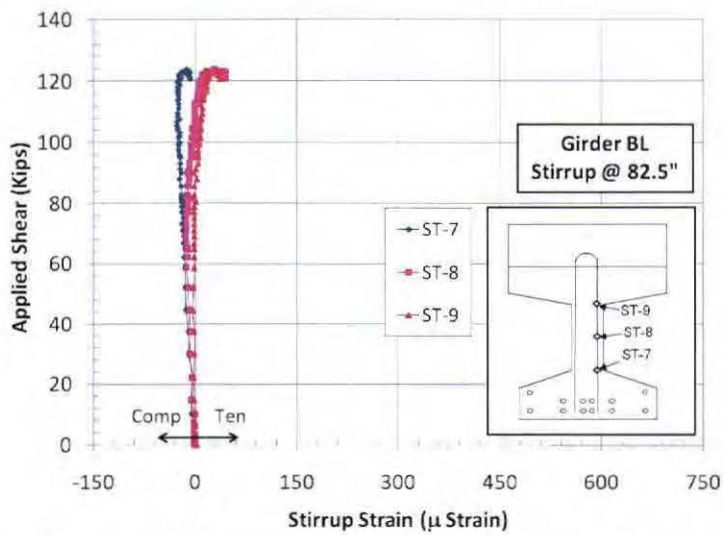


Figure 7.61: Measured Strain along Stirrup @ 82.5" – Girder BL

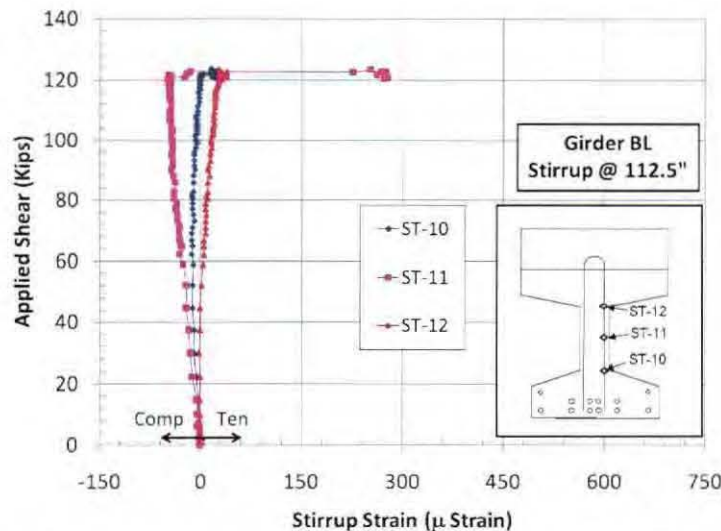


Figure 7.62: Measured Strain along Stirrup @ 112.5" – Girder BL

### 7.10.3 GIRDER CL EXPERIMENTAL RESULTS

Girder CL was cast with SCC and tested under increasing cyclic loads. The purpose for the cyclic loading was to investigate the effect of load cycling on stiffness degradation and strength of the girder. The load testing of Girder CL was performed on October 23, 2007. The specimen was subjected to eight load cycles. Load cycles 1, 2, and 3 were load-controlled and reached load maxima of approximately 50 Kips, 100 Kips, and 150 Kips, respectively. The remaining cycles were displacement-controlled and reached mid-span deflection maxima of approximately 0.5", 0.9", 1.3", 2.0", and past 2.0" until failure. During the first three load cycles, Girder CL did not experience any cracking. The first flexural crack occurred at mid-span during the fourth load cycle at a load of 152.8 Kips and mid-span deflection of 0.317". The cracking load corresponded to a mid-span moment of 1499 Kip-ft. As the load was increased, additional flexural and flexural-shear cracks developed within approximately the middle third of the girder, causing significant reduction in stiffness. It was observed that the flexural cracks occurred at the locations of the transverse reinforcement. At a load of 219 Kips and a corresponding mid-span deflection of 1.47", the first diagonal shear cracks were detected in the girder web within 6 feet from the south support. At the end of the test, the shear cracks were located 10 feet from the south end and between 2-12 feet from the north end of the specimen. Flexural failure occurred at a load of 241 Kips and mid-span deflection of 6.01". Figure 7.63 shows Girder CL at different stages during the test.

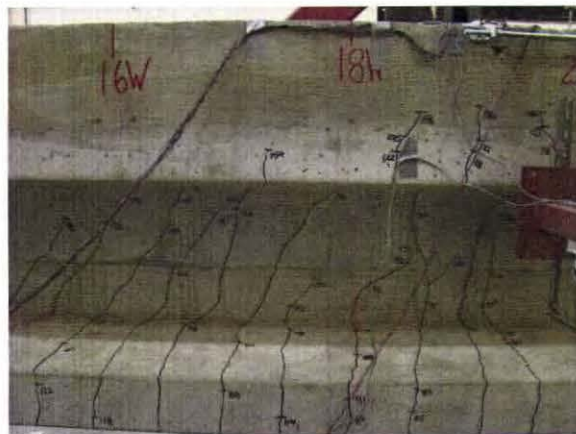




(a) Before Loading



(b) First Flexural Cracks at Load = 153 Kips



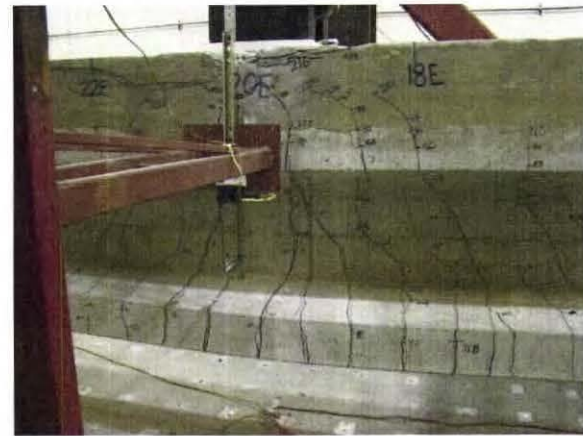
(c) Flexural and Flexural-Shear Cracks



(d) Diagonal Shear Cracks at Load = 219 Kips



(e) Diagonal Shear Cracks at Load = 232 Kips



(f) Crushing of Compression Concrete at Failure

Figure 7.63: Girder CL at Different Stages during the Test

#### 7.10.3.1 Measured Load-Deflection

Figure 7.64 shows the measured cyclic load-deflection plot. The envelope of the cyclic response curve is shown in Figure 7.65. The load-deflection response was almost linear up to the point corresponding to the first flexural crack. As the load was increased, the additional flexural and flexural-shear cracks

caused significant reduction in stiffness. Past the point of first flexural crack, the load–deflection response became non-linear.

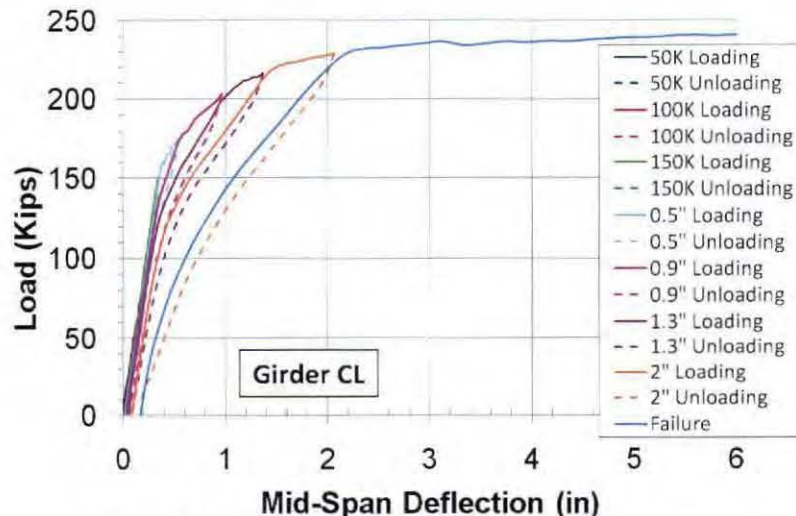


Figure 7.64: Measured Cyclic Load-Deflection – Girder CL

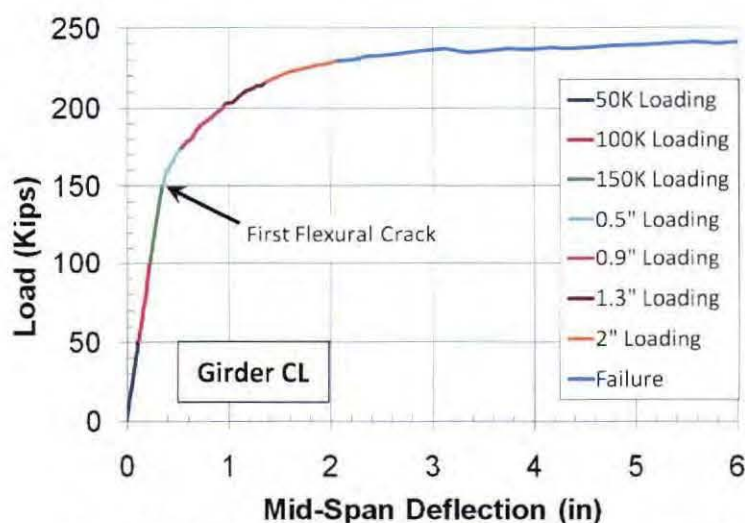


Figure 7.65: Measured Load-Deflection Envelope – Girder CL

### 7.10.3.2 Measured Strand Strain

Strand strains were measured at mid-span and at quarter-span. Figure 7.66 shows a plot of the measured strand strain at mid-span resulting from the externally applied load only. The plot does not include strain due to the prestressing force, the girder dead load, or the composite deck dead load. Prior to initiation of the first crack, the strand strain increased approximately linearly with an increase in the applied moment. At the cracking moment of 1565 Kip-ft, the measured strand strain increased significantly.



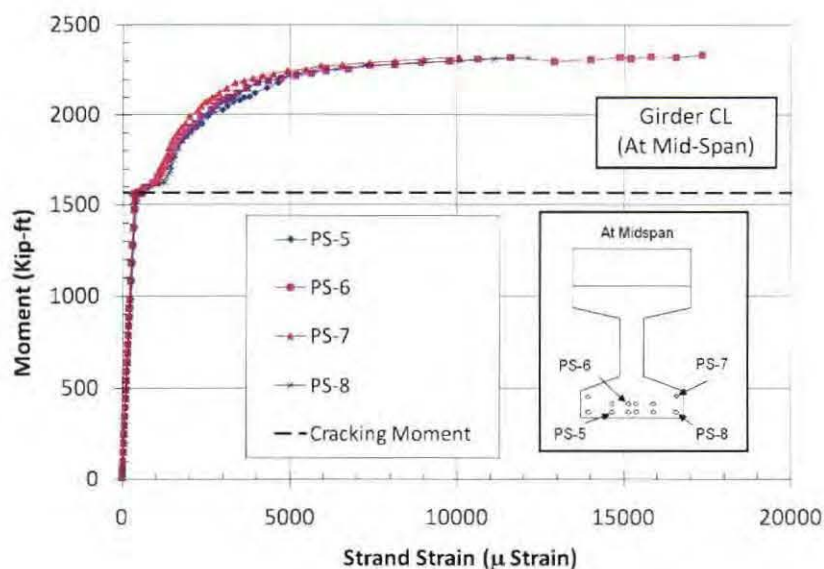


Figure 7.66: Measured Strand Strain at Mid-Span Resulting from External Load – Girder CL

Prior to the application of the actuator's load, the average measured strain in the prestressing strands was 5730 micro-strain. Therefore, the measured strain values shown in Figure 7.66 were increased by 5730 micro-strain to account for the strain due to prestressing and self-weight. Figure 7.67 shows a plot of the externally applied moment versus the measured strand strain at mid-span, including the strain due to prestressing and self-weight at. The prestressing strands had a yield strain of 1% or 10,000 micro-strain. As shown in Figure 7.67, the strain in some of the prestressing strands reached the yield strain at a moment of 2152 Kip-ft, corresponding to an actuator load of approximately 219.3 Kips.

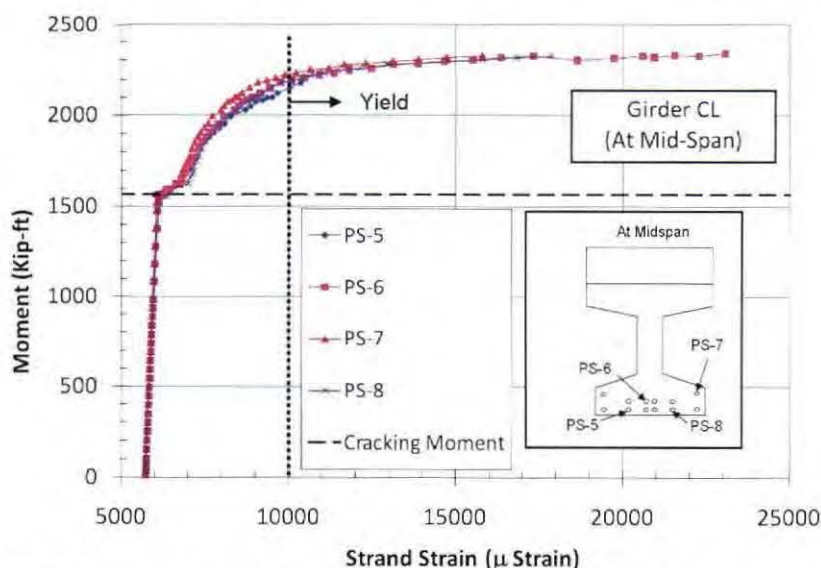


Figure 7.67: Measured Strand Strain at Mid-Span Resulting from All Loads – Girder CL

The strain gages at quarter-span were placed on the same four strands that were instrumented at mid-span. Figure 7.68 shows a plot of the measured strand strain at quarter-span resulting from the externally applied moment only. This plot does not include strain due to the prestressing force, the girder dead load, or the composite deck dead load. The measured results indicate the following



1. The strain increased approximately linearly with an increase in the bending moment.
2. The measured strain values were consistent with the location of the strands relative to the bottom of the girder. For the same load, higher strain values were exhibited by the strands that were located closer to the outermost tensile fiber.
3. At a moment of approximately 1140 Kip-ft, corresponding to an actuator load of approximately 234 Kips, the strands at quarter-span experienced a sudden increase in strain. This increase in the strain coincided with the formation of the diagonal shear cracks at and close to the quarter-span. The increase in the tensile strain reflects the shear-flexure interaction. Park and Paulay (1975) showed that the formation of diagonal shear cracks increase the tension in the flexural reinforcement.

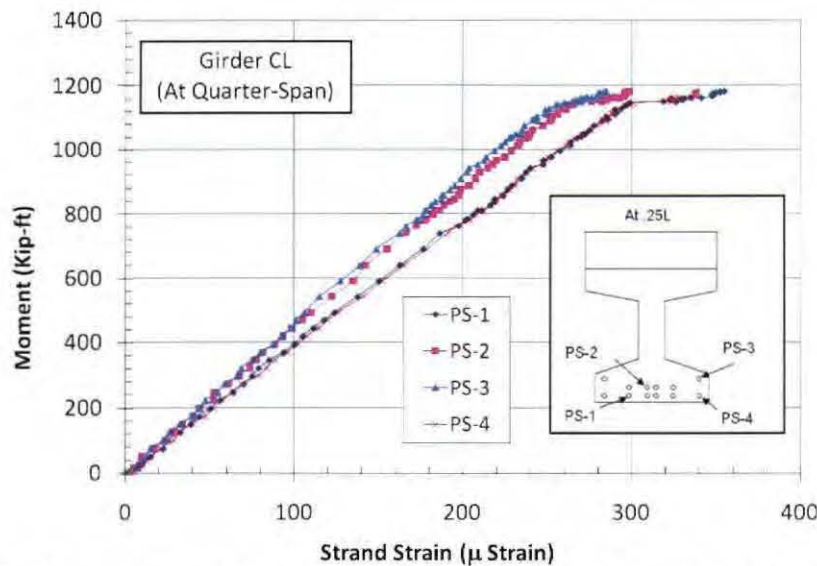


Figure 7.68: Measured Strand Strain at Quarter-Span Resulting from External Load – Girder CL

Figure 7.69 shows the measured strand strain at quarter span after the initial strain due to prestress and the specimen's self-weight are added to the strain resulting from the externally applied load. The maximum strain at quarter-span was approximately 6085 micro-strain which indicates that the strands at quarter-span remained significantly below the yield strain during the test.

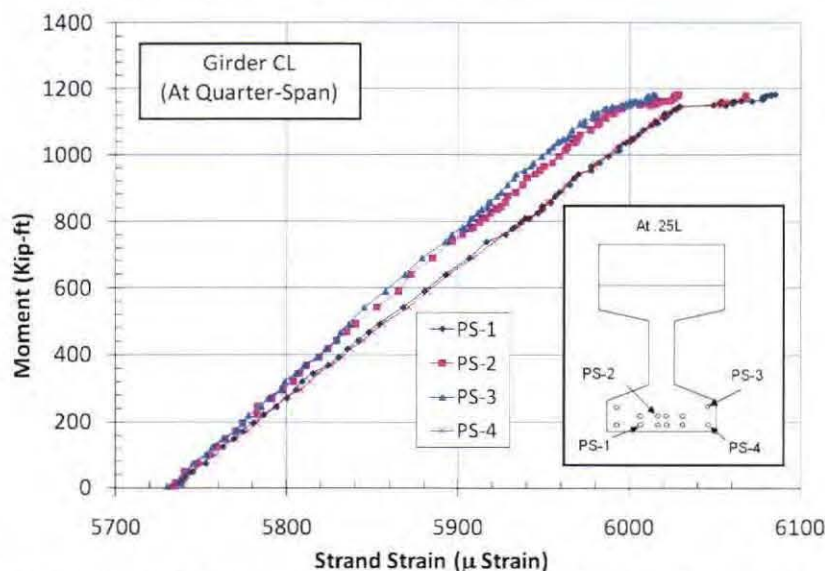


Figure 7.69: Measured Strand Strain at Quarter-Span Resulting from All Loads – Girder CL

### 7.10.3.3 Measured Concrete Strain

Figure 7.70 shows a plot of the measured concrete strain at mid-span resulting from the externally applied moment only. Figure 7.71 shows the measured concrete strain after the initial strains due to prestressing and self-weight were calculated and added to the measured strain. Figure 7.71 indicates that gages EM-8 and EM-9 experienced initial compressive strains and gage EM-10 experienced initial tensile strain. Contrary to what was expected, the initial section cracking did not cause substantial change in measured strain in gages EM-8, EM-9, EM-10, or EM-11. A probable reason could be that a crack did not intersect and engage the embedded gages, but rather occurred on either side of them. Gages EM-12 and EM-13 remain in compression throughout the load test. The significant increase in the compressive strain in EM-12 and EM-13 at a load of 236.8 kips indicates the initiation of concrete crushing in the deck.

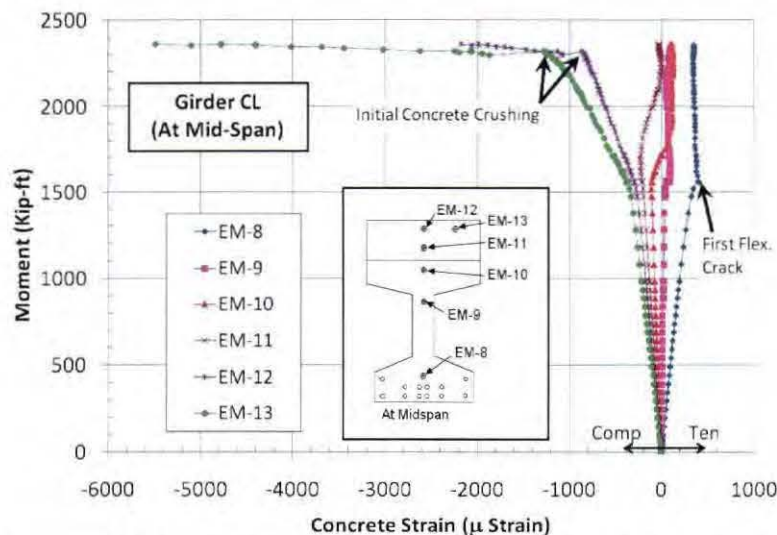


Figure 7.70: Measured Concrete Strain at Mid-Span Resulting from External Load – Girder CL

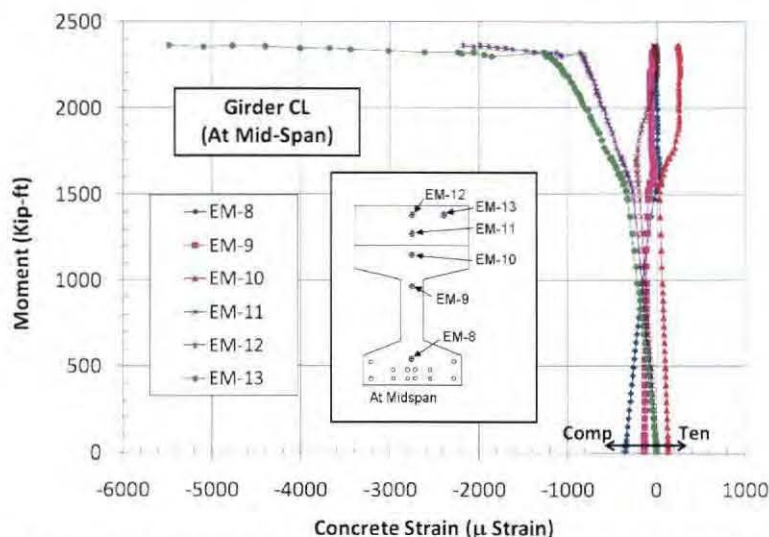


Figure 7.71: Measured Concrete Strain at Mid-Span Resulting from All Loads – Girder CL

The embedded strain gages at quarter-span were placed at the same relative locations as the embedded strain gages at mid-span. Figure 7.72 shows a plot of the measured concrete strain at quarter-span

resulting from the externally applied moment only. Figure 7.73 shows the measured concrete strain after the initial strains due to prestressing and self-weight were calculated and added to the measured strain. The measured strain increased approximately linearly with an increase in the moment. This suggests that flexural cracking did not occur at quarter-span. The variation among the strain gage readings was consistent with the locations of the gages. Gages EM-6 and EM-7, which were located at the same depth, exhibited approximately equal compressive strains.

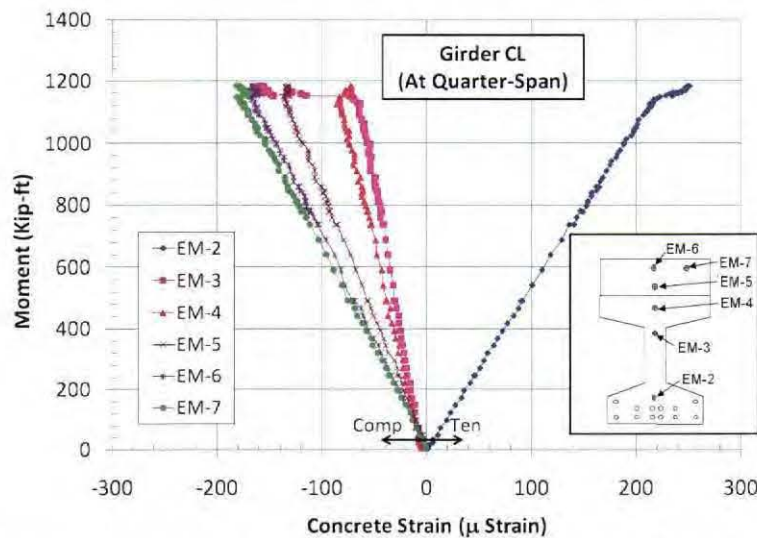


Figure 7.72: Measured Concrete Strain at Quarter-Span Resulting from External Load – Girder CL

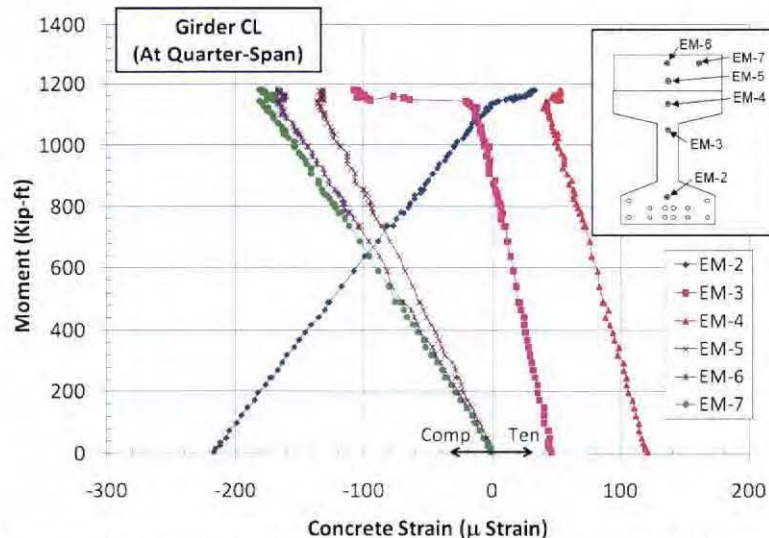


Figure 7.73: Measured Concrete Strain at Quarter-Span Resulting from All Loads – Girder CL

#### 7.10.3.4 Measured Top and Bottom Strains at Mid-Span

Girder CL was instrumented with LVDTs attached horizontally to the top and bottom of the girder at mid-span. The measurements obtained from the LVDTs were used to evaluate the section curvature, monitor the outermost compressive concrete strain, and detect the first flexural crack at the bottom of the section. Figure 7.74 and Figure 7.75 show the applied moment versus the strain at the top and the bottom LVDT locations, respectively. The top LVDT showed few erratic data points which may have been due to



momentary sticking of the LVDT plunger. The plots in Figure 7.74 and Figure 7.75 show approximately linear Moment-Strain relationships until the point of first flexural crack.

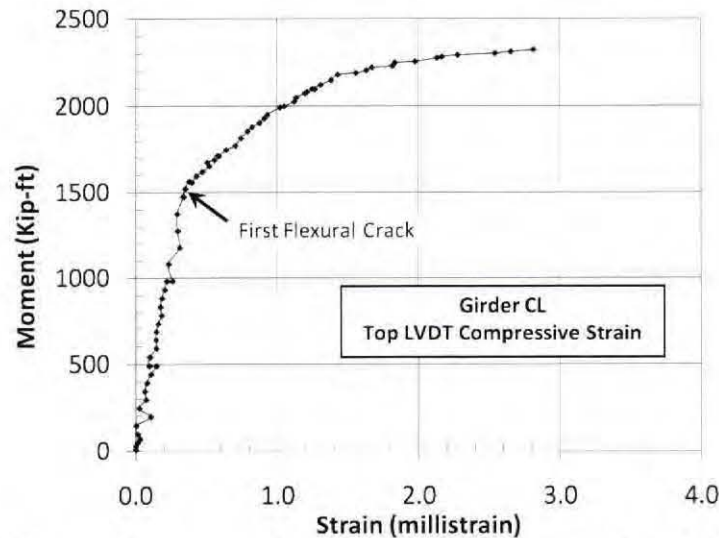


Figure 7.74: Measured Compressive Strain along Top Horizontal LVDT at Mid-Span – Girder CL

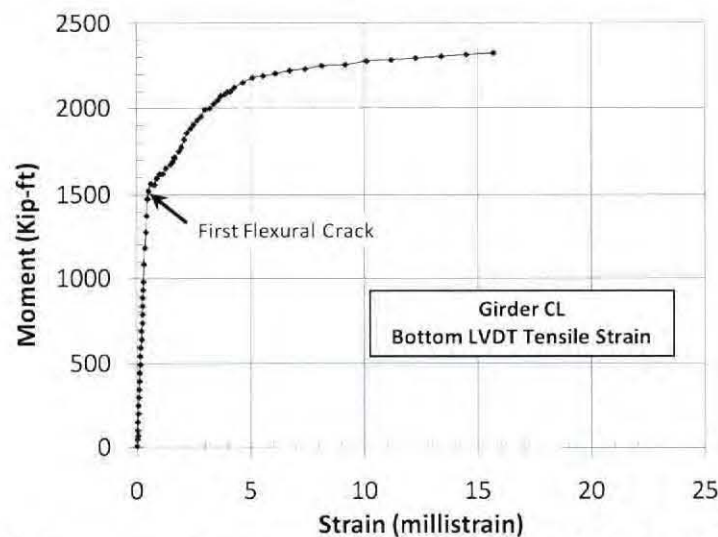


Figure 7.75: Measured Tensile Strain along Bottom Horizontal LVDT at Mid-Span – Girder CL

#### 7.10.3.5 Measured Strain in the Shear Reinforcement

The plots of applied shear force versus stirrup strain are shown in Figure 7.76, Figure 7.77, Figure 7.78, and Figure 7.79 for the stirrups at 22.5", 52.5", 82.5", and 112.5" from the north end of the girder, respectively. The applied shear force does not include the shear due to self-weight of the specimen. For each stirrup, readings from three strain gages were collected. A sharp increase in at least one strain gage indicates the development of a web shear crack that crosses the stirrup. The lack of sudden increase in strain in Figure 7.76 indicates that web-shear cracking did not intersect the stirrups at 22.5". Figure 7.77, Figure 7.78, and Figure 7.79 indicate that web-shear cracks had developed and intersected the stirrups located at 52.5", 82.5" and 112.5" at an applied shear of approximately 119 Kips.

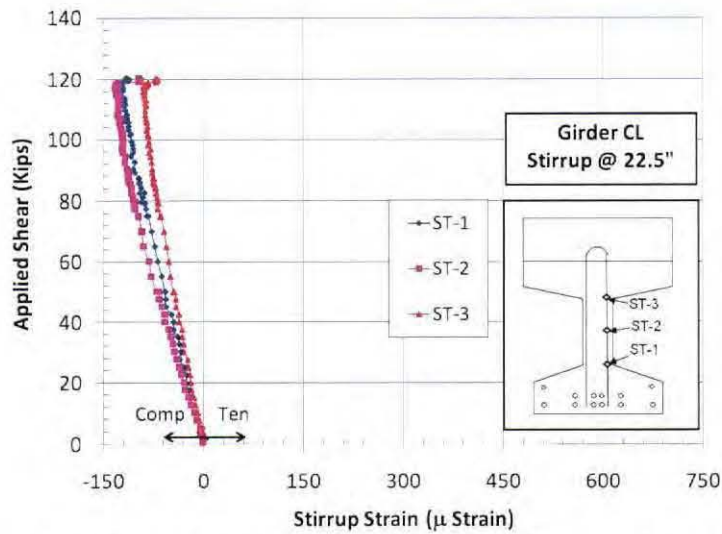


Figure 7.76: Measured Strain along Stirrup @ 22.5" – Girder CL

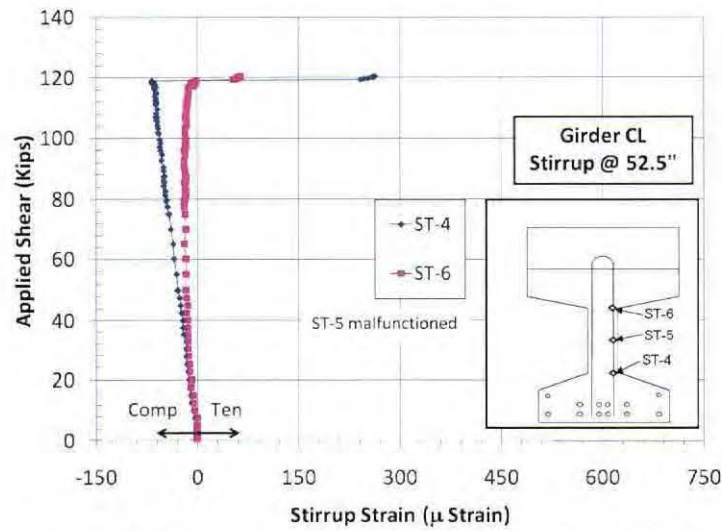


Figure 7.77: Measured Strain along Stirrup @ 52.5" – Girder CL

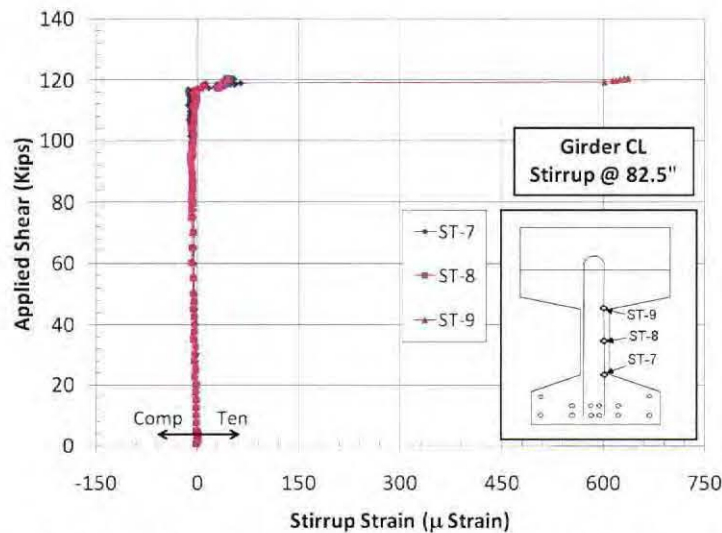


Figure 7.78: Measured Strain along Stirrup @ 82.5" – Girder CL

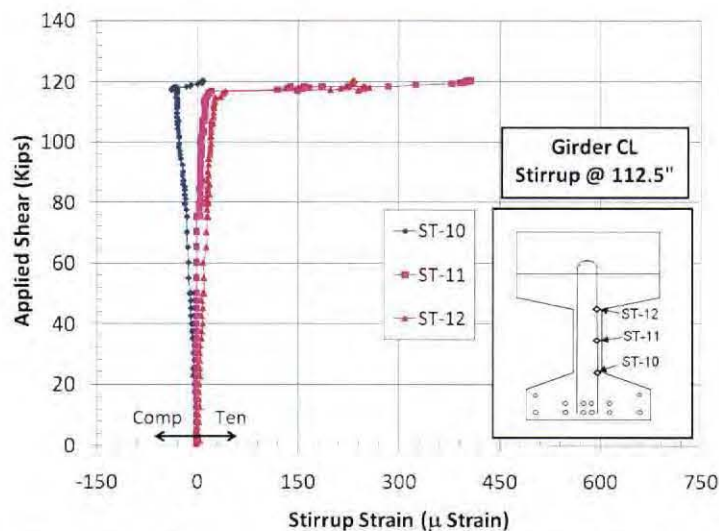


Figure 7.79: Measured Strain along Stirrup @ 112.5" – Girder CL

## 7.11 ANALYSIS OF FLEXURAL BEHAVIOR AND STRENGTH

This section presents an analysis of the flexural behavior of the girders. The analysis includes a comparison of the load-deflection characteristics of the three specimens, the effect of cyclic loading on the effective stiffness, and analytical evaluation of the flexural response, cracking moment, flexural strength, and flexural rigidity.

### 7.11.1 MEASURED LOAD-DEFLECTION CHARACTERISTICS

A comparison of the load-deflection test results indicates a significant similarity among the three specimens despite the small variation in concrete strength from one specimen to another. Table 7.20 presents a summary of the measured cracking moment, flexural strength, and the corresponding mid-span deflections. Figure 7.80 shows the measured load-deflection curves for the three girders plotted together on the same graph. The plots clearly show that the differences in stiffness, strength, and ductility among the three specimens were relatively small.



The pre-cracking effective stiffness, defined as the ratio of the load at first flexural crack to the corresponding mid-span deflection, was 453 Kip/in, 439 Kip/in, and 415 Kip/in for Girder AL, Girder BL, and Girder CL, respectively. Therefore, the measured pre-cracking effective stiffness of Girder BL was only 3.1 percent lower than that of control girder (Girder AL). However, the measured pre-cracking stiffness of Girder CL was 8.4 percent lower than that of Girder AL. It should be noted that Girder CL was subjected to three load cycles at increasing maximum load prior to the initiation of the first flexural crack, while Girder AL and Girder BL were subjected to increasing monotonic loads.

The load carrying capacities of the three girders were nearly identical. The measured ultimate load of Girder BL was 1.5 percent higher, while the measured ultimate load of Girder CL was 1.1 percent lower, than that of Girder AL.

**Table 7.20: Comparison of Measured Cracking Moments and Flexural Strengths**

	Girder AL	Girder BL	Girder CL
Load at 1 <sup>st</sup> Flexural Crack (Kips)	156.9	161.1	159.4
Deflection at 1 <sup>st</sup> Flexural Crack (in)	0.346	0.367	0.384
Ultimate Load (Kips)	243.6	247.3	241.0
Deflection at Ultimate Load (in)	5.46	5.09	6.01

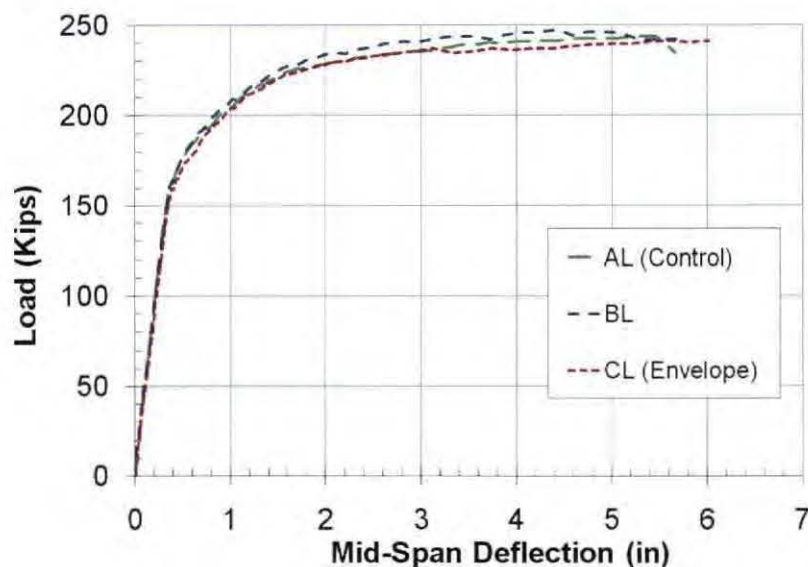


**Figure 7.80: Comparison of Measured Load-Deflection Relationships**

### 7.11.2 EFFECTIVE STIFFNESS UNDER CYCLIC LOADING

The effect of the maximum applied load on the stiffness of the girder was determined based on the measured load-deflection envelope shown in Figure 7.57. For each load cycle, the effective stiffness was determined as the slope of the secant joining the origin to the point at the end of the load cycle segment. Table 7.21 presents a summary of the measured effective stiffness. The results show that the effective stiffness decreased with an increase in the maximum applied load. It is well known that flexural cracking of concrete results in stiffness reduction. Section 9.5.2 of the ACI code (2008) relates the post-cracking effective moment of inertia to the maximum moment applied at the section. However, the results presented in Table 7.21 indicate that even during the pre-cracking load cycles, the effective stiffness

decreased with an increase in the maximum load reached during the load cycle. The reduction in stiffness at the pre-cracking conditions may be the result of concrete internal micro-cracking and/or slippage of the prestressing strands. Table 7.21 also shows the rate of effective stiffness degradation, which was determined as the ratio of the change in stiffness to the change in the maximum load reached between successive cycles. For the pre-cracking load cycles, the rate of stiffness degradation increased with an increase in the maximum load. For the post-cracking load cycles, the stiffness degradation rate was significantly higher than the pre-cracking degradation rate with an average rate of 4.48 Kip/in/Kip.

**Table 7.21: Measured Effective Stiffness**

Load Cycle	Effective Stiffness, $K_e$ (Kip/in)	Effective Stiffness Degradation Rate (Kip/in/Kip)
50 Kips <sup>‡</sup>	528.5	
100 Kips <sup>‡</sup>	508.6	0.398
150 Kips <sup>‡</sup>	482.1	0.530
0.5 in.	349.7	5.10
0.9 in.	224.5	5.21
1.3 in.	166.6	3.62
2.0 in.	114.8	3.70
Failure	40.5	5.71

<sup>‡</sup> Pre-cracking load cycles

### 7.11.3 ANALYTICAL EVALUATION OF FLEXURAL BEHAVIOR

The analytical flexural response was obtained using the computer program Response-2000 (Bentz and Collins 2000). The program input includes the cross-sectional dimensions, material properties for concrete, reinforcement, and prestressing strands, and the amount and location of reinforcement. Response-2000 also allows the user to define a composite deck by applying a strain discontinuity to the section. After specifying the required inputs, the user may solve a sectional response or a member response. The sectional response provides stress and strain profiles and a full moment-curvature plot for the section. The member response requires input with regards to the span length, the load location, and the type of supports. Solving the member response yields a full load-deflection plot as well as the deflection and curvature distribution along the length of the member.

#### 7.11.3.1 Load-Deflection Relationships

The analytical load-deflection relationships were calculated and compared to the measured values. The analytical and experimental results are plotted in Figure 7.81, 7.82, and 7.83 for Girder AL, BL, and CL, respectively.

In all three girders, the theoretical pre-cracking effective stiffness was lower than the respective measured effective stiffness. Table 7.22 presents a comparison between the theoretical and measured values. The ratio of the theoretical to the measured pre-cracking effective stiffness was 0.75, 0.71, and 0.84 for Girder AL, Girder BL, and Girder CL, respectively. After the point of first flexural crack, the analytical model resulted in instantaneous stiffness values higher than the respective experimental values.

The theoretical ultimate loads obtained from Response-2000 were in excellent agreement with the measured values. Table 7.23 presents a comparison between the theoretical and measured values. The theoretical and the respective measured ultimate loads were nearly identical for all three specimens.

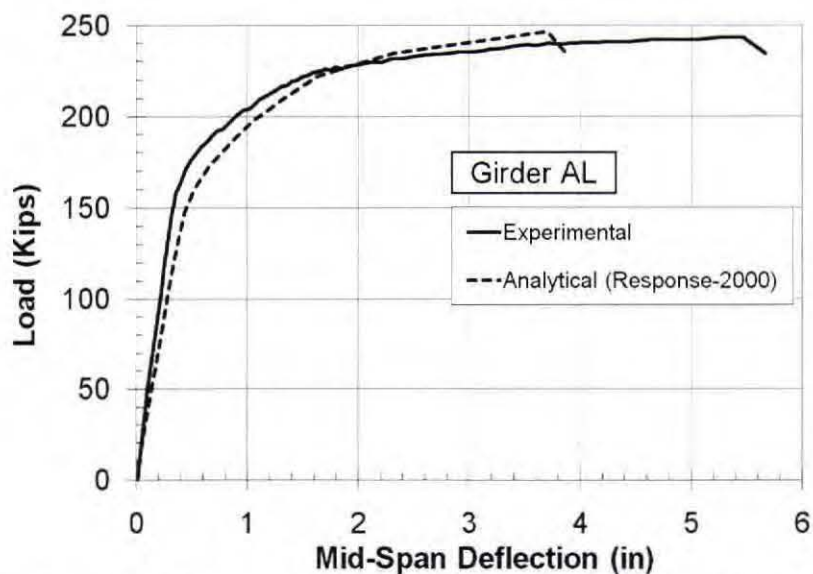


Figure 7.81: Analytical and Experimental Load-Deflection – Girder AL

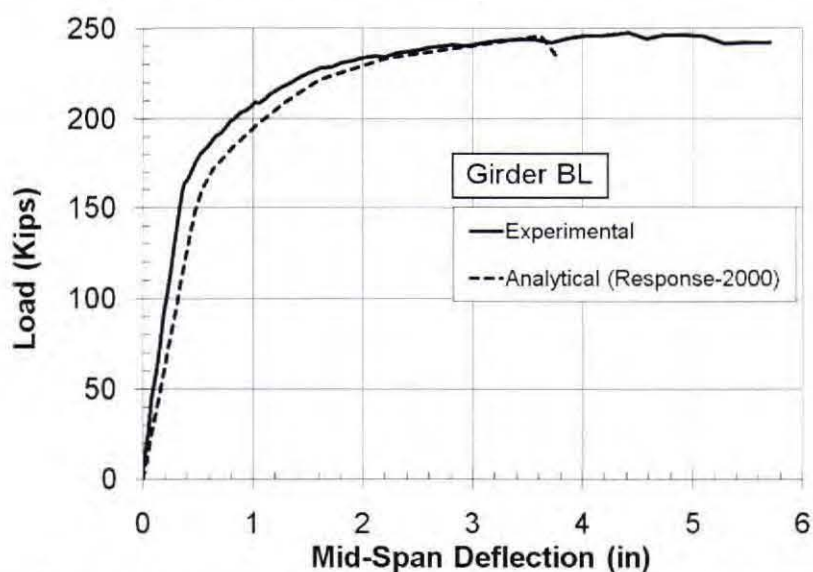


Figure 7.82: Analytical and Experimental Load-Deflection – Girder BL



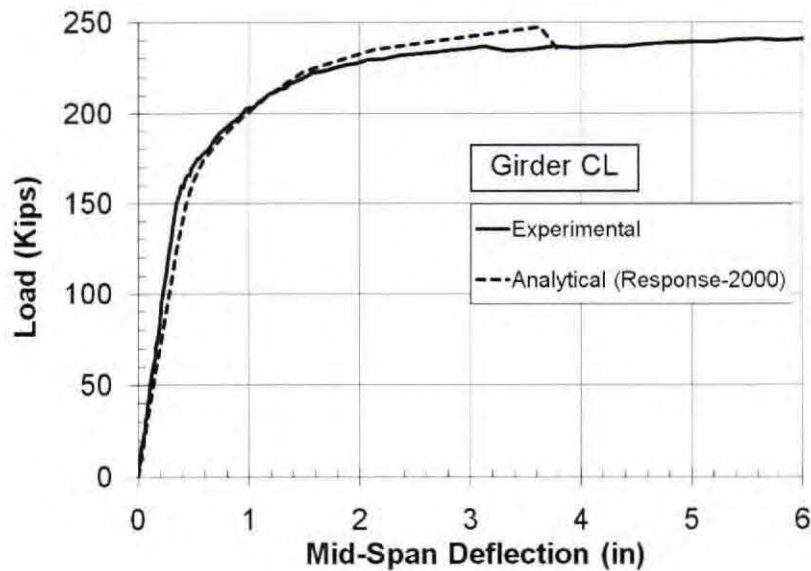


Figure 7.83: Analytical and Experimental Load-Deflection – Girder CL

Table 7.22: Comparison of Theoretical<sup>†</sup> and Measured Pre-Cracking Effective Stiffness

	Theoretical $K_e$ (Kip/in)	Measured $K_e$ (Kip/in)	Theoretical / Measured
Girder AL	338	453	0.75
Girder BL	313	439	0.71
Girder CL	347	415	0.84

<sup>†</sup> As determined by Response-2000

Table 7.23: Comparison of Theoretical<sup>†</sup> and Measured Ultimate Loads

	Theoretical Ultimate Load (Kips)	Measured Ultimate Load (Kips)	Theoretical / Measured
Girder AL	246.6	243.6	1.01
Girder BL	246.0	247.3	0.99
Girder CL	247.3	241.0	1.03

<sup>†</sup> As determined by Response-2000

### 7.11.3.2 Moment-Curvature Relationships

The analytical moment-curvature relationships were calculated and compared to the measured values. The analytical relationships were determined using Response-2000. The experimental relationships were determined using measured strains. Knowing the measured strain values  $\epsilon_1$  and  $\epsilon_2$  at two different elevations along the section height and the distance  $h$  between these two elevations, the experimental curvature  $\phi$  can be determined as  $\phi = (\epsilon_1 + \epsilon_2)/h$ . The experimental strain values were obtained from the top and bottom horizontal LVDT measurements shown in Figure 7.42 and Figure 7.43 for Girder AL and in Figure 7.74 and Figure 7.75 for Girder CL. Girder BL was fitted with only a bottom horizontal LVDT. Therefore, the strain profile for Girder BL was constructed using the strain values obtained from the bottom LVDT and strain gage EM-13 that was embedded in the deck concrete. The analytical and the experimental moment-curvature relationships are shown in Figure 7.84, Figure 7.85, and Figure 7.86 for Girder AL, Girder BL and Girder CL, respectively. It should be noted that in order to avoid damaging the

LVDTs at high deformations, they were removed from the test set up prior to the end of the test. Thus, the experimental measurements shown in the moment-curvature plots were terminated prematurely.

For Girder AL and Girder CL, the experimental and analytical moment-curvature relationships were in excellent agreement. However, the experimental curvature of Girder BL was significantly lower than the analytical curvature for most of the experimental data range. It is believed that the horizontal LVDTs provided a more realistic average strain than the embedded gages. This is due to the fact that the gage length of the LVDT spanned across several flexural cracks, whereas the embedded gage readings may have reflected localized effects.

The theoretical ultimate moment obtained from Response-2000 was 2,420 Kip-ft, 2,414 Kip-ft, and 2,427 Kip-ft for Girder AL, Girder BL, and Girder CL, respectively. A comparison of analytical and experimental flexural strength is covered in Section 7.11.3.4.

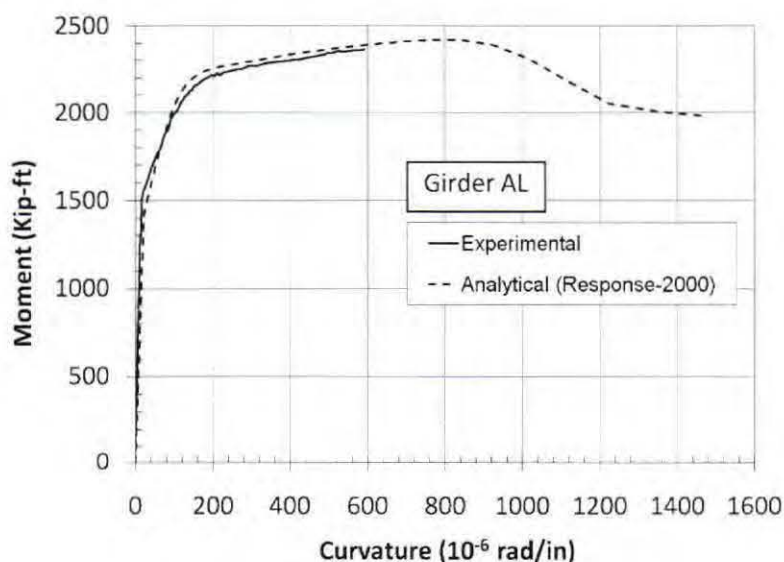


Figure 7.84: Analytical and Experimental Moment-Curvature – Girder AL

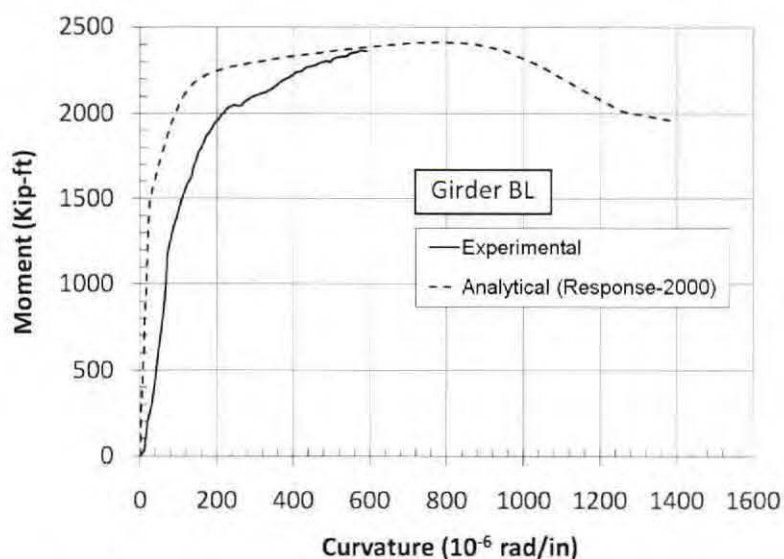


Figure 7.85: Analytical and Experimental Moment-Curvature – Girder BL

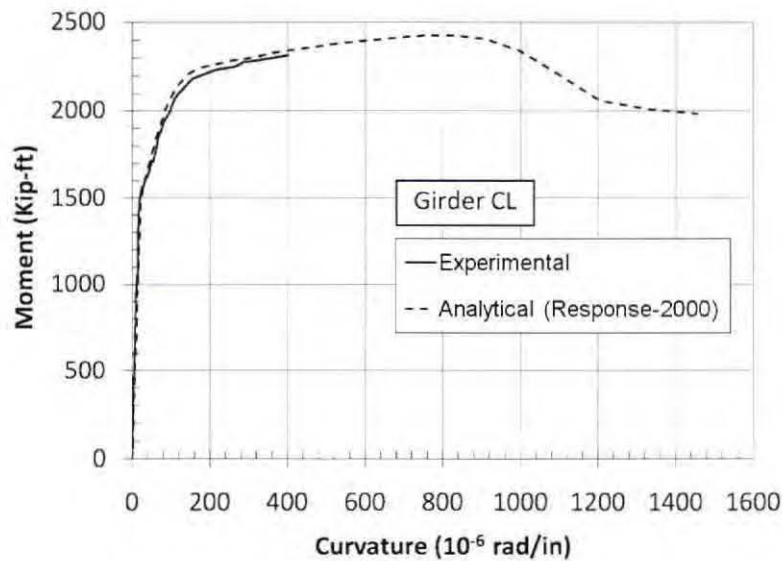


Figure 7.86: Analytical and Experimental Moment-Curvature – Girder CL

### 7.11.3.3 Cracking Moment

The cracking moment,  $M_{cr}$ , was determined analytically according to the ACI 318 code (2008) and the AASHTO LRFD Bridge Design Specifications (2007) methods. The equations for the cracking moment were presented by Equation 5.40 and Equation 5.46. The measured concrete strength was used for determining the analytical cracking moment. The measured and the theoretical cracking moments are summarized in Table 7.24. The results show an excellent agreement between the measured and the analytical values. Girder AL measured cracking moment was 2.4% and 3.3% lower than the values calculated using the AASHTO-LRFD and ACI methods, respectively. Girder BL measured cracking moment was 3.5% and 2.6% higher than the values calculated using the AASHTO-LRFD and ACI methods, respectively. Girder CL measured cracking moment was 1.1% and 2.0% lower than the values calculated using the AASHTO-LRFD and ACI methods, respectively..

Table 7.24: Analytical and Measured Cracking Moment

	Girder AL	Girder BL	Girder CL
$M_{cr, ACI}$ (Kip-ft)	1592	1541	1597
$M_{cr, LRFD}$ (Kip-ft)	1578	1528	1582
$M_{cr, Measured}$ (Kip-ft)	1540	1581	1499
$M_{cr, Measured} / M_{cr, ACI}$	0.97	1.03	0.94
$M_{cr, Measured} / M_{cr, LRFD}$	0.98	1.04	0.95

### 7.11.3.4 Flexural Strength

The nominal flexural strengths of the girders were determined using the ACI 318 (2008) and the AASHTO LRFD Bridge Design Specifications (2007). The methods for determining the nominal flexural strength were covered in Section 5.7. Table 7.25 summarizes the calculated nominal flexural strengths, the calculated ultimate moment by Response-2000, and the measured ultimate moments. The measured results were in excellent agreement with the analytical values obtained from the code methods



and the computer program. The ratio of the measured to the analytical flexural strength varied between 0.94 and 1.03.

**Table 7.25: Analytical and Measured Flexural Strength**

	Girder AL	Girder BL	Girder CL
$M_{n, ACI}$ (Kip-ft)	2365	2360	2369
$M_{n, LRFD}$ (Kip-ft)	2356	2351	2359
$M_{max, Response-2000}$ (Kip-ft)	2420	2414	2427
$M_{max, Measured}$ (Kip-ft)	2390	2427	2365
$M_{max, Measured} / M_{n, ACI}$	1.01	1.03	1.00
$M_{max, Measured} / M_{n, LRFD}$	1.01	1.03	1.00
$M_{max, Measured} / M_{max, Response-2000}$	0.99	1.01	0.97

### 7.11.3.5 Flexural Rigidity for Deflection Calculations

Flexural rigidity is defined as the product of the modulus of elasticity,  $E$ , and the moment of inertia,  $I$ . In this study, the experimental flexural rigidity of the test specimens was determined indirectly using the measured load-deflection values. The experimental rigidities were then compared to the analytical flexural rigidities calculated using the ACI code prescribed  $I$  and  $E$ .

For the purpose of calculating the deflection of simply supported reinforced concrete beams, the ACI code (2008) permits the use of the concrete elastic modulus and the effective moment of inertia at mid-span. The concrete elastic modulus is given by Equation 5.2. The effective moment of inertia is given in the ACI code by the following equation.

$$I_e = \left( \frac{M_{cr}}{M_a} \right)^3 I_g + \left[ 1 - \left( \frac{M_{cr}}{M_a} \right)^3 \right] I_{cr} \leq I_g \quad (7.1)$$

where

- $I_e$  = effective moment of inertia, in<sup>4</sup>
- $M_{cr}$  = cracking moment, Kip-in (or lb-in)
- $M_a$  = maximum moment in a member at the stage deflection is computed, Kip-in (or lb-in)
- $I_g$  = gross moment of inertia, in<sup>4</sup>
- $I_{cr}$  = moment of inertia of the cracked section, in<sup>4</sup>

Thus, for an applied moment of less than or equal to the cracking moment, the effective moment of inertia would be equal to the gross moment of inertia of the concrete section. When the applied moment is greater than the cracking moment, the effective moment of inertia is reduced below the gross moment of inertia in accordance with Equation 7.1. AASHTO (2007) adopted the ACI method for the effective moment of inertia.

The experimental flexural rigidities were obtained using the measured load-deflection and the theoretical deflection of elastic beams. For a simply supported beam with a point load applied at mid-span, the mid-span deflection can be obtained using the following equation.

$$\Delta = \frac{PL^3}{48EI} \quad (7.2)$$

where

- $\Delta$  = mid-span deflection, in
- $P$  = applied load, Kips (or lbs)
- $L$  = span length of the member, in
- $EI$  = flexural rigidity, Kip-in<sup>2</sup> (or lb-in<sup>2</sup>)

Rearranging Equation 7.2 for  $EI$ , the following equation is obtained.

$$EI = \frac{PL^3}{48\Delta} \quad (7.3)$$

The experimental and analytical effective rigidities are shown in Figure 4.87, Figure 4.88, and Figure 4.89 for Girder AL, Girder BL, and Girder CL, respectively. Unlike the code model which assumes constant pre-cracking rigidity, the experimental pre-cracking rigidity decreased with an increase in the moment at the mid-span. In all three specimens, the pre-cracking measured rigidity was higher than the respective analytical effective rigidity. Therefore, the code model provides a conservative estimate of the pre-cracking rigidity. A conservative estimate of the rigidity results in overestimation of deflection.

For moments higher than the service load moments, the flexural response becomes non-linear and, therefore, the code approach for calculating beam deflections would not be applicable. For service load moments that are greater than the cracking moment, the experimental rigidity was similar to the analytical rigidity for Girder AL, slightly higher than the analytical rigidity for Girder BL, and slightly lower than the analytical rigidity for Girder CL. In general, the code approach provided an acceptable and conservative estimate for the flexural rigidity in all cases except for the post-cracking loads under load cycling conditions (Girder CL). Had the analytical cracking moment of Girder CL been equal to or less than the experimental cracking moment, the experimental post-cracking segment of the rigidity curve of Girder CL would have been in excellent agreement with the theoretical curve. However, the code's overestimate of the flexural rigidity in the case of Girder CL would still result in reasonable estimates of deflections.

To assess the effect of the mid-span moment on the experimental effective rigidity, the trends of the pre-cracking and the post-cracking experimental rigidity data points were superimposed on each of the effective rigidity plots. The trend lines  $EI_1$  and  $EI_2$  correspond to the pre-cracking and the post-cracking experimental effective rigidities, respectively.  $EI_1$  was developed for the data points within a moment of 500 Kip-ft and the cracking moment, while  $EI_2$  was developed for the data points between the cracking moment and a moment of 2,000 Kip-ft. The selection of the range limits was based on estimates of the service load moments that the girder would be subjected to during its service life. A summary of the experimental rigidity change rates with respect to the applied moment is shown in Table 7.25. The cracked section rigidity change rate was between 8.0 to 8.9 times that of the corresponding un-cracked section. The un-cracked rigidity change rate of Girder AL was 1.10 and 1.28 times that of Girder BL and Girder CL, respectively, while the cracked rigidity change rate of Girder AL was 1.13 and 1.17 times that of Girder BL and Girder CL, respectively. In conclusion, Girder AL had the highest un-cracked and cracked section rigidity change rates. However, the three girders exhibited fairly similar rigidity change



rates for both un-cracked and cracked sections. The effect of cracking on the rigidity change rate was similar among the three girders.

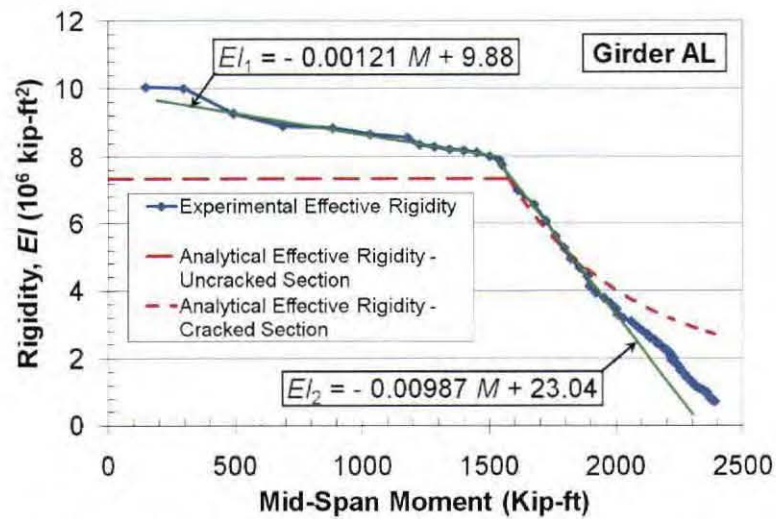


Figure 7.87: Analytical and Experimental Flexural Rigidity – Girder AL

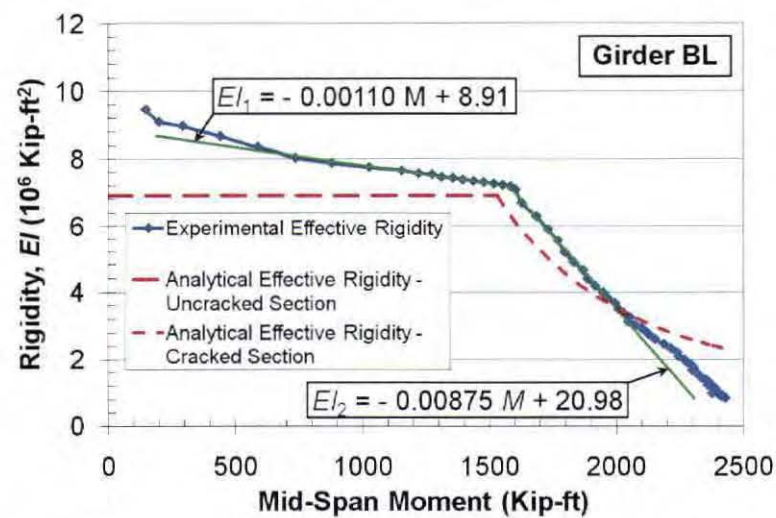


Figure 7.88: Analytical and Experimental Flexural Rigidity – Girder BL



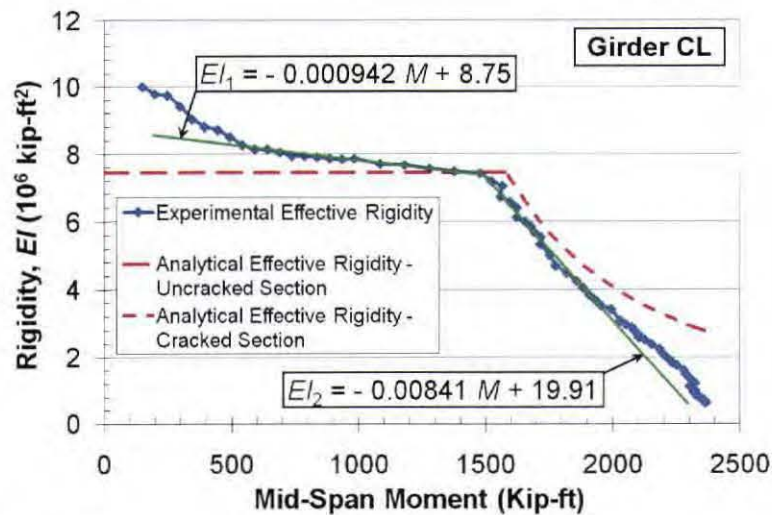


Figure 7.89: Analytical and Experimental Flexural Rigidity – Girder CL

Table 7.26: Analytical and Measured Flexural Strength

	Girder AL	Girder BL	Girder CL
$EI_1$ Slope (Kip-ft <sup>2</sup> /Kip-ft)	1210	1100	942
$EI_2$ Slope (Kip-ft <sup>2</sup> /Kip-ft)	9870	8750	8410
$(EI_2 \text{ Slope}) / (EI_1 \text{ Slope})$	8.2	8.0	8.9

## 7.12 ANALYSIS OF CONCRETE SHEAR STRENGTH

In this study, the experimental concrete shear strength was evaluated and compared to the analytical concrete shear strength obtained using the provisions of the ACI code (2008) and the simplified procedure of the AASHTO LRFD (2007). The code provisions were covered in Section 5.8 of this report. This section covers the evaluation of the experimental and analytical shear strength values and compares the experimental and analytical results.

### 7.12.1 EXPERIMENTAL EVALUATION OF CONCRETE SHEAR STRENGTH

The measured strain in the stirrups before and after the development of the inclined shear cracks were used to determine the concrete experimental shear strength,  $V_c$ . The measured stirrup strains were presented in Section 7.10 of this report.

As mentioned before, each instrumented stirrup was fitted with three strain gages. When an inclined shear crack develops and intersects a stirrup, the strain gage on the stirrup leg that is closest to the shear crack will most likely register the highest strain among the three gages. Therefore, the largest of the three strain values that occurred immediately after cracking was used to determine the axial stress in the stirrup. The number of stirrups that intercept a shear crack was determined experimentally by measuring the average angle of inclination of the shear cracks. The measured shear crack angle of inclination was found to be 35°. Figure 7.90 shows the angle measurement of an inclined shear crack. For a web height of 15.5" and a stirrup spacing of 7.5", the inclined shear crack would intersect an average of 2.94 stirrups. For a #5 U-stirrup, the total steel area that crosses an inclined shear crack would be 1.82 in<sup>2</sup>. Knowing the area of the shear reinforcement and the corresponding axial stress, the portion of the shear force that is

carries by the shear reinforcement was determined. The concrete shear capacity was then determined at the location of each instrumented stirrup by subtracting the force carried by the stirrups from the applied shear force at the time of cracking.



Figure 7.90: Inclination Angle of a Shear Crack

The experimental evaluation of the concrete shear capacity is presented in Table 7.27, Table 7.28, and Table 7.29 for Girder AL, Girder BL, and Girder CL, respectively. The applied shear forces shown in the tables include the shear due to the self-weight of the specimen. In some cases, the specimen failed in flexure prior to the development of the shear cracks at all instrumented stirrup locations. For such cases, the measured shear strain in the stirrups was negligible since the shear reinforcement was not mobilized. When the strain in the shear reinforcement is negligible, it can be assumed that the entire shear force is carried by the concrete.

Table 7.27: Concrete Experimental Shear Capacity – Girder AL

	@ 22.5" <sup>†</sup>	@ 52.5" <sup>†</sup>	@ 82.5" <sup>†</sup>	@ 112.5" <sup>†</sup>
Applied Shear (Kips)	133.8	131.6	129.4	127.2
Measured Stirrup Strain ( $\mu$ Strain)	62.5	312.4	504.5	625.8
Shear Force Carried by Stirrups (Kips)	3.3	16.3	26.3	32.7
Shear Force Carried by Concrete (Kips)	130.5	115.3	103.1	94.5

<sup>†</sup> Measured from the end of the girder

Table 7.28: Concrete Experimental Shear Capacity – Girder BL

	@ 22.5" <sup>†</sup>	@ 52.5" <sup>†</sup>	@ 82.5" <sup>†</sup>	@ 112.5" <sup>†</sup>
Applied Shear (Kips)	138.7	136.5	134.4	132.2
Measured Stirrup Strain ( $\mu$ Strain)	-	-	-	226.4
Shear Force Carried by Stirrups (Kips)	-	-	-	11.8
Shear Force Carried by Concrete (Kips)	138.7	136.5	134.4	120.4

<sup>†</sup> Measured from the end of the girder



**Table 7.29: Concrete Experimental Shear Capacity – Girder CL**

	@ 22.5" <sup>†</sup>	@ 52.5" <sup>†</sup>	@ 82.5" <sup>†</sup>	@ 112.5" <sup>†</sup>
Applied Shear (Kips)	135.3	133.1	130.9	128.7
Measured Stirrup Strain ( $\mu$ Strain)	-	241.7	601.0	378.4
Shear Force Carried by Stirrups (Kips)	-	12.6	31.4	19.8
Shear Force Carried by Concrete (Kips)	135.3	120.5	99.5	108.9

<sup>†</sup> Measured from the end of the girder

Following the development of inclined shear cracks, the stirrups experienced increased strain with an increase in the applied shear. The change in the applied shear and the corresponding measured change in the force carried by the shear reinforcement are summarized in Table 7.30, Table 7.31, and Table 7.32 for Girder AL, Girder BL, and Girder CL, respectively. The results show that, in most of the cases, the increase in the force carried by the shear reinforcement was higher than the corresponding increase in the applied shear. This could be explained by the fact that as the shear force increased, the shear crack widened. This caused a decrease in the shear force carried by the concrete and an increase in the force carried by the shear reinforcement.

**Table 7.30: Change in Stirrup Force Following Development of Web-Shear Cracking – Girder AL**

	@ 22.5" <sup>†</sup>	@ 52.5" <sup>†</sup>	@ 82.5" <sup>†</sup>	@ 112.5" <sup>†</sup>
Increase in Applied Shear Force (Kips)	3.85	3.85	3.85	3.85
Change in Shear Force Carried by Shear Reinforcement (Kips)	4.37	3.63	6.33	4.49

<sup>†</sup> Measured from the end of the girder

**Table 7.31: Change in Stirrup Force Following Development of Web-Shear Cracking – Girder BL**

	@ 22.5" <sup>†</sup>	@ 52.5" <sup>†</sup>	@ 82.5" <sup>†</sup>	@ 112.5" <sup>†</sup>
Increase in Applied Shear Force (Kips)	0.81	0.81	0.81	0.81
Change in Shear Force Carried by Shear Reinforcement (Kips)	-	-	-	1.35

<sup>†</sup> Measured from the end of the girder

**Table 7.32: Change in Stirrup Force Following Development of Web-Shear Cracking – Girder CL**

	@ 22.5" <sup>†</sup>	@ 52.5" <sup>†</sup>	@ 82.5" <sup>†</sup>	@ 112.5" <sup>†</sup>
Increase in Applied Shear Force (Kips)	1.13	1.13	1.13	1.13
Change in Shear Force Carried by Shear Reinforcement (Kips)	-	1.11	1.84	1.48

<sup>†</sup> Measured from the end of the girder

### 7.12.2 COMPARISON OF EXPERIMENTAL AND ANALYTICAL CONCRETE SHEAR STRENGTH

The nominal shear strength of the concrete was calculated using the provisions of the ACI code (2008) and the simplified procedure of the AASHTO LRFD (2007). The experimental results obtained above and the analytical results are summarized and compared in Table 7.33. The experimental values reported in the highlighted cells are lower bound estimates of the shear strength since no shear cracks had developed at the respective locations.

The results indicate that the AASHTO simplified method resulted in highly conservative estimates of the concrete nominal shear strength. The ratio of the experimental to the AASHTO nominal shear strength



varied between 1.44 and 2.40. On the other hand, the ACI method resulted in overestimation of the nominal shear strength in some cases. The ratio of the experimental to the ACI nominal shear strength varied between 0.86 and 1.42. It should be noted that when a strength reduction factor  $\phi$  of 0.75 is applied to the ACI nominal shear strength values, all of the design shear strength ( $\phi V_c$ ) values would be well below the corresponding experimental shear strength values.

**Table 7.33: Comparison of Experimental<sup>†</sup> and Analytical Shear Strength**

	Location <sup>†</sup> (in)	Experimental $V_c$ (Kips)	AASHTO <sup>‡</sup> $V_c$ (Kips)	ACI $V_c$ (Kips)	Exp. $V_c$ / AASHTO $V_c$	Exp. $V_c$ / ACI $V_c$
AL	22.5	130.5	63.1	107.4	2.07	1.22
	52.5	115.3	64.0	108.3	1.80	1.06
	82.5	103.1	64.8	109.2	1.59	0.94
	112.5	94.5	65.5	109.9	1.44	0.86
BL	22.5	138.7*	57.9	97.5	2.40	1.42
	52.5	136.5*	58.8	98.4	2.32	1.39
	82.5	134.3*	59.6	99.3	2.25	1.35
	112.5	120.3	60.3	100.0	2.00	1.20
CL	22.5	135.3*	63.6	108.2	2.13	1.25
	52.5	120.5	64.6	109.2	1.87	1.10
	82.5	99.5	65.4	110.1	1.52	0.90
	112.5	108.9	66.0	110.8	1.65	0.98

<sup>†</sup> Measured from girder end

<sup>‡</sup> AASHTO LRFD simplified method

\* Lower bound estimate of experimental  $V_c$

## 8 PRESTRESSED QUARTZITE-AGGREGATE SCC GIRDERS

### 8.1 INTRODUCTION

In 2006-2007 the primary investigators of this study performed load testing of three full-scale prestressed girders made with quartzite aggregate. One of the girders was cast with conventional concrete, while the other two were cast with SCC. For ease of reference, those three girders will be referred to as the quartzite-aggregate girders, while the three specimens covered in Chapter 7 will be referred to as the limestone-aggregate girders. The testing of the quartzite-aggregate girders was part of a separate study to investigate the structural performance of prestressed SCC girders made with quartzite aggregate. Quartzite aggregates are normally used for the production of concrete in eastern South Dakota. Funding for the quartzite-aggregate girders study was provided by the College of Engineering at SDSU and Gage Brothers Concrete Products Inc. of Sioux Falls, SD.

The experimental data that have been generated on the performance of the quartzite-aggregate and the limestone-aggregate SCC girders will enable SDDOT to assess the structural performance of prestressed SCC bridge girders made with the two main coarse aggregate types used in the state. The final report on the quartzite-aggregate girders was not complete at the time of writing of this report. However, it will be made available to SDDOT upon its completion. This chapter presents a brief description of the test specimens and a summary of the experimental results that were obtained from the quartzite-aggregate girders study.

### 8.2 SPECIMEN DESCRIPTION, INSTRUMENTATION, AND TEST SET UP

The quartzite-aggregate girder specimens were almost identical in cross section, span, instrumentation, and test set up to the limestone-aggregate girder specimens covered in Chapter 7. Similar to the limestone-aggregate girder specimens, the cross section used for the quartzite-aggregate girder specimens was a MnDOT 36M and the span length was 40'. The two main differences between the limestone- and the quartzite-aggregate girders were the shear reinforcement spacing and the distribution and location of the twelve prestressing strands. The #5 U-stirrups in the quartzite-aggregate girders were spaced at 5" center-to-center. Figure 8.1 presents a cross section of a quartzite-aggregate girder specimen showing the distribution of the prestressing strands. The non-prestressed reinforcement details were similar to those shown in Figure 7.3 except that the #4 reinforcement in the bottom flange was placed at 5" center-to-center. The specified concrete strength at release and at 28 days was 6,500 psi and 7,000 psi, respectively. The specified tendon jacking force was 40,500 lbs, corresponding to an initial jacking force of 486,000 lbs.

A total of three quartzite-aggregate girders were fabricated. One girder was cast with a conventional concrete mix used by the SDDOT for bridge girders. This girder was labeled Girder A and served as the control specimen. The other two girders were cast with an SCC concrete mix and were labeled Girder B and Girder C. The control girder concrete mix and the SCC mix proportions are shown in Table 8.1. Type C Flyash was used in the SCC mix due to a cement shortage in 2006.

The concrete decks were reinforced with two mats of WWF4x4-W5xW5 welded wire fabric. The bottom mat was located 2" above the top of the girder, while the top mat was located 5" above the top of the



girder. The deck concrete had a specified 28-day concrete strength of 5,000 psi. The mix design is shown in Table 8.2.

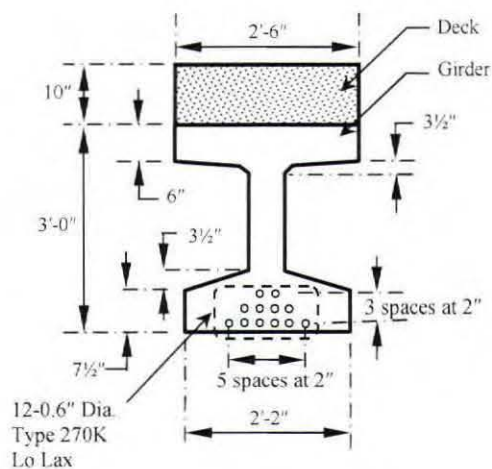


Figure 8.1: Cross Section of the Quartzite-Aggregate Girder

Table 8.1: Control and SCC Quartzite-Aggregate Mix Proportions

	Control Mix	SCC Mix
SD Type III Cement (lb)	755	630
Type C Flyash (lb)	-	140
Fine Aggregate (lb)	1100	1420
1/2" x 20 Sioux Quartzite (lb)	-	1420
3/4" Sioux Quartzite Size #1A (lb)	1720	-
Water (Gal)	31.4	32.0
ADVA Cast 540 (oz)	90	115
DARATARD (oz)	15	-
DARAVAIR M (oz)	4	1
VMA (oz)	-	22
W/C Ratio	0.35	0.36
Yield (yd <sup>3</sup> )	1.00	1.01

Table 8.2: Deck Concrete Mix Proportions

	Deck Mix
SD Type III Cement (lb)	635
Type C Flyash (lb)	105
Concrete Sand (lb)	1240
3/4" x 4 Quartzite (lb)	1650
Water (Gal)	30
DARACEM 19 (oz)	118
W/C Ratio	0.34
Yield (yd <sup>3</sup> )	1.00



The instrumentation plan was almost similar to that used for the limestone-aggregate girders covered in Section 7.3. Surface-mounted strain gages were placed on the prestressing tendons and the steel stirrups, and embedment strain gages were placed in the concrete. Once in place for testing, the girder specimens were also instrumented with several LVDTs and wire displacement transducers.

The girders were fabricated at the Gage Bothers Concrete Products Inc. facility in Sioux Falls, SD. Fabrication of the three girders was done simultaneously on the same prestressing bed between July 18 and July 25, 2006. The strands were tensioned on July 18, the girder concrete was placed on July 20, and the prestress transfer was done on July 25. The decks were constructed between July 28 and July 30, 2006. All three girders were delivered to the Lohr Structures Laboratory on August 7, 2006.

The test set up was similar to that used for the limestone-aggregate girders and described in Section 7.5.1. Girder A (control specimen) and Girder C were tested under increasing monotonic load until failure. Girder B was subjected to fatigue cyclic loading for a total of 1,500,000 load cycles before it was subjected to an increasing monotonic load until failure.

## 8.3 EXPERIMENTAL RESULTS

This section presents the experimental data including measured material properties, transfer length, load-deflection characteristics, flexural strength, and behavior under shear stresses.

### 8.3.1 MEASURED MATERIAL PROPERTIES

The compressive strength of the girder concrete was tested on the day of prestress release, at 28 days, and on the day of testing of the girder specimen. Table 8.3 presents a summary of the measured girder concrete strength. The compressive strength of the deck concrete was tested at 28 days and on the day of testing of the girder specimens. Table 8.4 shows the deck concrete compressive strength.

**Table 8.3: Measured Girder Concrete Compressive Strength – Quartzite-Aggregate Girders**

	Measured Concrete Strength (psi)		
	Girder A (Control)	Girder B (SCC)	Girder C (SCC)
@ Release	6,730	7,120	6,500
@ 28 Days	7,540	7,853	7,480
@ Day of Testing	7,570 <sup>†</sup>	9,130 <sup>‡</sup>	8,230 <sup>*</sup>

<sup>†</sup> Tested 99 days after casting

<sup>‡</sup> Tested 141 days after casting at the start of fatigue loading

<sup>\*</sup> Tested 130 days after casting

**Table 8.4: Measured Deck Concrete Compressive Strength – Quartzite-Aggregate Girders**

	Measured Concrete Strength (psi)		
	Girder A	Girder B	Girder C
@ 28 Days	7,540	7,853	7,480
@ Day of Testing	7,570 <sup>†</sup>	9,130 <sup>‡</sup>	8,230 <sup>*</sup>

<sup>†</sup> Tested 99 days after casting

<sup>‡</sup> Tested 141 days after casting at the start of fatigue loading

<sup>\*</sup> Tested 130 days after casting

The prestressing strands were 7-wire, 0.6"-diameter, 270 Ksi low relaxation type strands. The strand tensile properties were obtained from the mill certificate and were the same as those used for the strands in the limestone-aggregate girders study. The strand load versus strain relationship is shown in Figure 7.21. The strand had a cross sectional area of 0.218 in<sup>2</sup> and a modulus of elasticity of 29,000 Ksi. Yielding of the strand was assumed to occur at 1% elongation. The load at yield was 54,972 lbs. The ultimate load was 60,828 lbs and occurred at 8% elongation.

### 8.3.2 TRANSFER LENGTH

Similar to the method presented in Section 7.7.1, the strand strain measurements at prestress transfer were used to determine the experimental transfer length. The strain gages along the potential transfer length of Girder C malfunctioned. Therefore, only the measurements from Girder A and Girder B were used to establish the experimental transfer length. The measured strand strain versus the distance from the girder end for Girder A and Girder B are shown in Figures 8.2 and 8.3, respectively. Also shown are the 95% AMS lines as explained by Russell and Burns (1997) and presented in Section 5.4.3 of this report. Using the 95% AMS method, the transfer lengths for Girder A and Girder B were determined to be 27.5" and 28.0", respectively. These values were well within the AASHTO-LRFD (2007) transfer length requirement of 60 times the strand diameter (36").

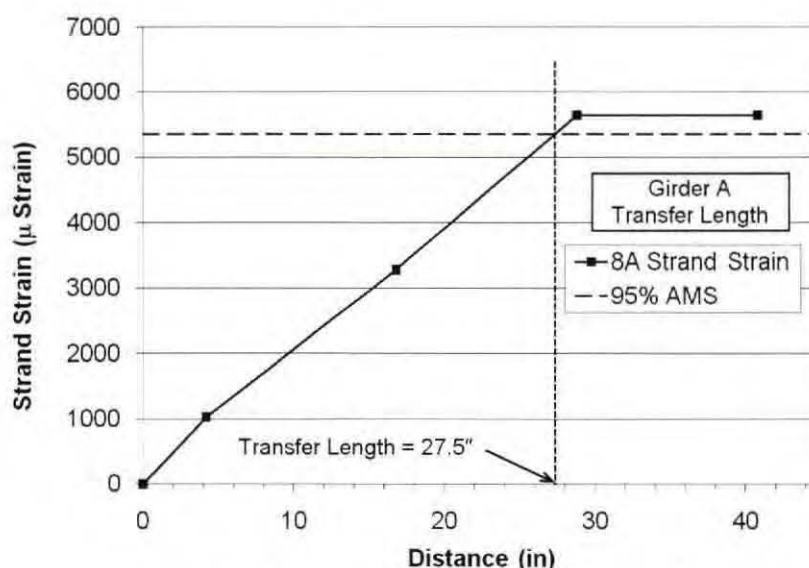


**Figure 8.2: Measured Transfer Length for Girder A**



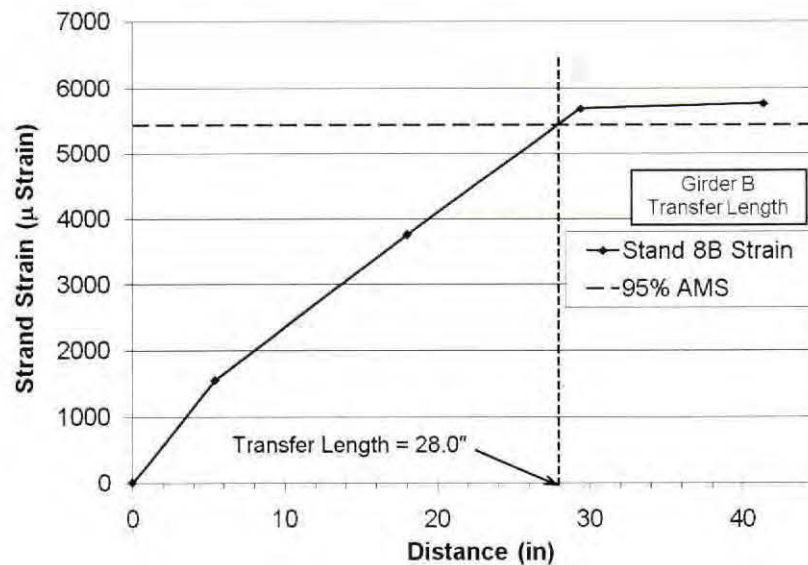


Figure 8.3: Measured Transfer Length for Girder B

### 8.3.3 LOAD TESTING RESULTS

The experimental results presented in this section include general description of the behavior of the specimens during the load tests, the load-deflection characteristics of the girder specimens, the effect of cyclic loading on stiffness degradation, and evaluation of the load-deflection responses of the quartzite-aggregate girders as compared to the limestone-aggregate girders.

#### 8.3.3.1 Girder A (Control Specimen)

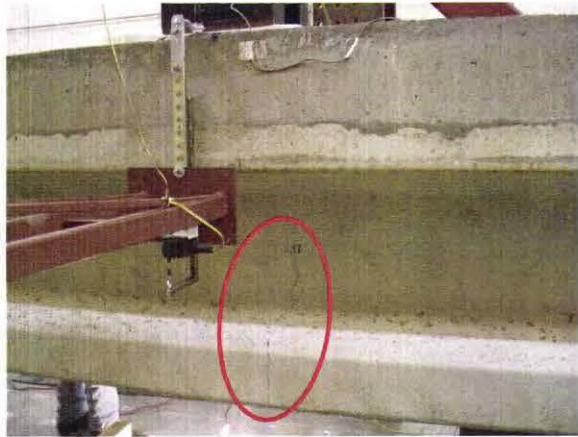
Prior to the day of testing, Girder A was preloaded to 103.6 Kips. The corresponding mid-span deflection was 0.256". The girder was then immediately unloaded. The purpose for the preloading cycle was to verify the stability of the test set up and the adequacy of the loading system. The full load test of Girder A was performed on October 25, 2006. The loading was applied under displacement-controlled conditions.

Figure 8.4 shows Girder A at different stages during the test. Figure 8.5 presents the measured load-deflection relationship. The first flexural tension crack at mid-span was noticed at a load of 141 Kips and mid-span deflection of 0.338". The corresponding moment at mid-span was 1393 Kip-ft. However, it was later observed from the measured load-deflection curve that the girder experienced a reduction in stiffness at a lower load of 135 Kips and a corresponding mid-span deflection of 0.338". Therefore, the cracking moment must have occurred at a load between 135 and 141 Kips. As the load was increased, additional flexural and flexural-shear cracks developed in the girder. In general, the location of the flexural cracks coincided with the location of the transverse reinforcement in the bottom flange.

The first visible diagonal shear crack was observed at a load of 190 Kips. The crack was located at 9' from north end of the girder. At higher loads, additional diagonal shear cracks were developing in the girder within a distance of approximately 12' from each end.

Girder A failed in flexure at a load of 251.6 Kips and mid-span deflection of 6.690". The failure was initiated by crushing of the compression concrete at the top of the deck.





(a) First Flexural Crack at Load  $\approx 141$  Kips



(b) Development of Flexural-Shear Cracks



(c) Development of Diagonal Shear Cracks



(d) Crushing of Compression Concrete at Failure

Figure 8.4: Girder A at Different Stages during the Test

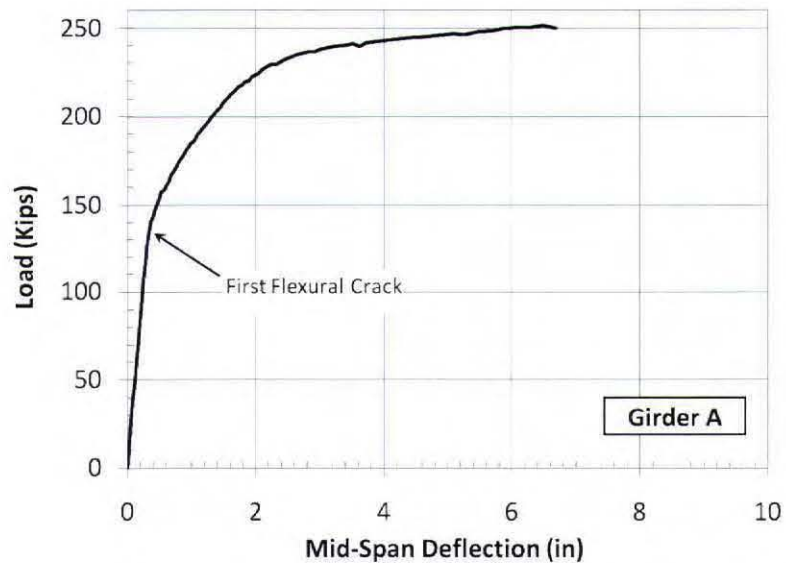


Figure 8.5: Measured Load-Deflection – Girder A

### 8.3.3.2 Girder C

Girder C was tested on November 28, 2006. The loading was monotonic and was applied under displacement controlled conditions.

Figure 8.6 shows Girder C at different stages during the test. Figure 8.7 presents the measured load-deflection relationship. The first flexural tension crack at mid-span was occurred at a load of 143 Kips and mid-span deflection of 0.323". The corresponding moment at mid-span was 1417 Kip-ft. As the load was increased, additional flexural and flexural-shear cracks developed in the girder. In general, the location of the flexural cracks coincided with the location of the transverse reinforcement in the bottom flange.

Multiple diagonal shear cracks appeared at a load of 188 Kips. The cracks were located between 6' and 12' from each end of the girder. At higher loads, additional diagonal shear cracks developed in the girder and extended longitudinally along the web-top flange interface.

Girder C failed in flexure at a load of 251.5 Kips and mid-span deflection of 7.02". The failure was initiated by crushing of the compression concrete at the top of the deck.



(a) First Flexural Crack at Load = 143 Kips



(b) Development of Flexural-Shear Cracks



(c) Development of Diagonal Shear Cracks



(d) Crushing of Compression Concrete at Failure

Figure 8.6: Girder C at Different Stages during the Test



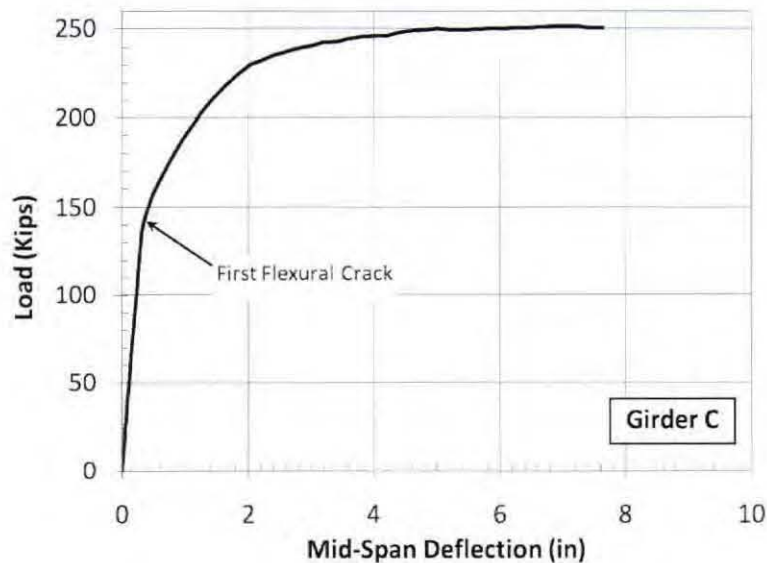


Figure 8.7: Measured Load-Deflection – Girder C

### 8.3.3.3 Girder B

Girder B was subjected to fatigue loading for a total of 1,500,000 load cycles before it was subjected to increasing monotonic load until failure. The purpose for the fatigue loading was to examine the effects of repeated loads on the stiffness and strength of the girder. The fatigue testing started on December 15, 2006 and was completed on February 6, 2007. The loading was performed at a rate of one cycle per second. The load cycles were divided into four groups. For each group, the load oscillated between two specific load limits. The upper load limit in each load group was selected so as to induce a predetermined nominal stress level at the outermost tensile fiber. Table 8.5 summarizes the load cycles performed and the corresponding load limits, nominal stress level targets at the bottom of the girder, and the measured change in the outermost strand tensile stress due to the applied load range.

Table 8.5: Fatigue Loading Protocol and Corresponding Strand Stresses

Load Cycle (x 1000)	Load Limit (Kips) (Range)	Nominal Tensile Stress <sup>†</sup>	Measured Change in Strand Stress (psi)
0 – 300	9.0 – 44.9 (35.9)	Compression	2,345
300 – 600	57.7 – 94.5 (36.8)	0	2,330
600 – 1,100	77.9 – 113.9 (36.0)	$3 \sqrt{f'_c}$	2,730
1,100 – 1,500	96.2 – 131.1 (34.9)	$6 \sqrt{f'_c}$	3,950

<sup>†</sup> At the bottom of the girder

The first two groups of load cycles were selected so that no tensile stresses would develop at the bottom of the girder. The last two groups of load cycles were designed to induce tensile stresses at the bottom of the girder. The first group represented service load levels at which the stress at the bottom fiber would be compressive. The upper load in the second group would result in approximately zero-stress at the bottom fiber. The upper load in the third group would induce a maximum tensile stress of approximately  $3 \sqrt{f'_c}$  in



the bottom fiber of the girder. This stress level corresponds to one-half the maximum tensile stress for bonded reinforcement allowed by AASHTO Standard Specifications (AASHTO 2002). The final group would induce a maximum tensile stress of approximately  $3\sqrt{f'_c}$  in the bottom fiber of the girder.

The measured change in the strand stress for the first two groups of cycles was nearly equal. This was expected as the load ranges for the first two groups were nearly the same and the section was still uncracked. Prior to the start of the third group of cycles (600,000-1,100,000) a hairline flexural crack appeared at the bottom flange of the girder. This crack was likely caused by a spike in the load during the set up for the third group of load cycles (600,000-1,100,000). During the application of the final load group, the flexural crack that started in the previous load group was progressively extending into the web.

During the fatigue testing, the girder stiffness was measured after every 36,000 load cycles. The stiffness tests were performed under monotonic loads reaching the upper load limit of the load group under consideration. Figure 8.8 presents the monotonic load tests that were performed to measure the stiffness of the girder. The four clusters of lines correspond to the four cyclic load groups. Figure 8.8 indicates that the stiffness of the girder reduced as the upper load limit within a load group increased. However, the stiffness variation within the same load group was not as significant except for the fourth load group where the girder was subjected to repeated loads that exceeded the cracking load.

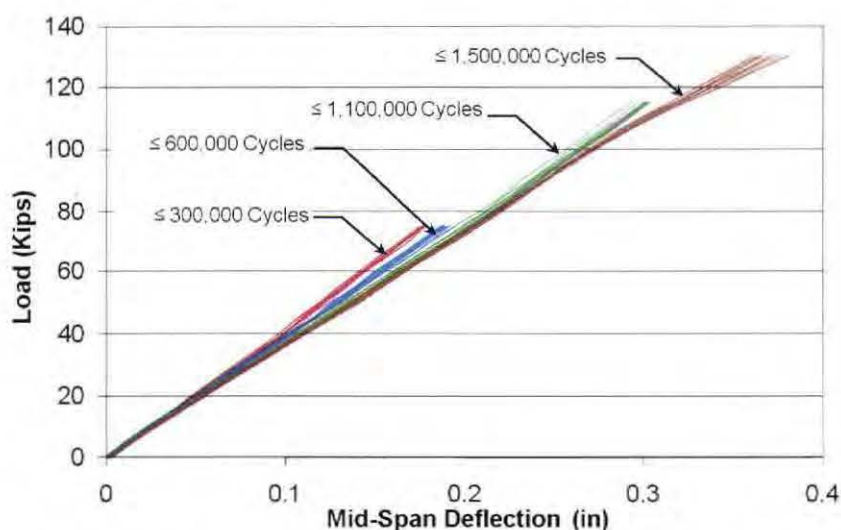


Figure 8.8: Measured Stiffness under Fatigue Loading – Girder C

The measured stiffness values are plotted in Figure 8.9 against the number of load cycles. Also shown in the figure are the trend straight lines for each load cycle cluster. The change in the average stiffness from one cluster to another reflects the effect of the upper load limit on the girder stiffness, while the change in the slope of the trend lines demonstrates the effect of the upper load limit on the stiffness degradation rate. The average stiffness and stiffness degradation for the four load groups are summarized in Table 8.6. The results demonstrate that

1. the average stiffness decreased with an increase in the upper load limit,
2. the change in the average stiffness per unit load increment in the upper load limit decreased with an increase in the upper load limit, and
3. the stiffness degradation with the number of applied load cycles increased with an increase in the upper load limit.

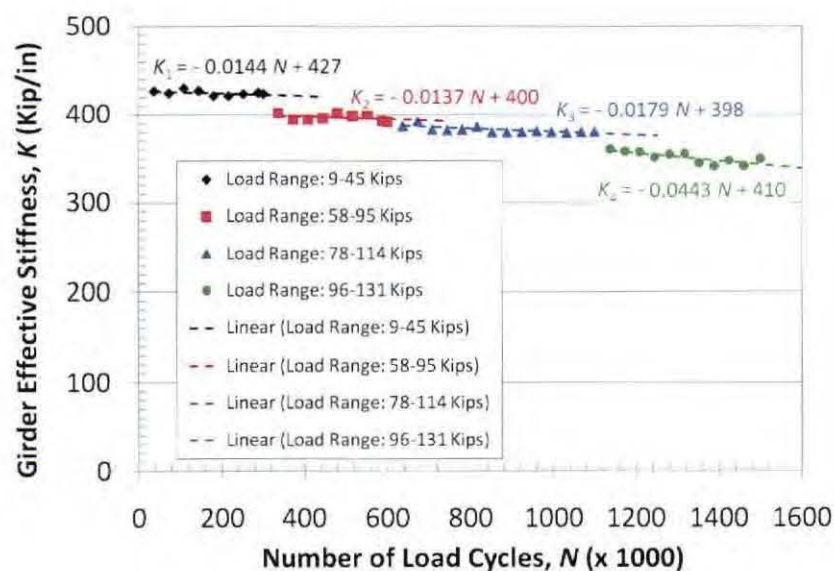


Figure 8.9: Girder Stiffness Degradation – Girder C

Table 8.6: Average Fatigue Stiffness and Stiffness Degradation

Load Cycle (x 1000)	Average Stiffness (Kip/in)	Change in Average Stiffness per Unit Load Increment (Kip/in/Kip)	Stiffness Degradation (Kip/in/1000cycles)
0 – 300	424.7	N.A.	0.0144
300 – 600	397.4	8.56	0.0137
600 – 1,100	382.8	2.26	0.0179
1,100 – 1,500	351.4	1.83	0.0443

Following the fatigue load testing, Girder B was subjected on March 20, 2007 to increasing monotonic load until failure. The load was applied under displacement-controlled conditions.

Figure 8.10 shows Girder B at different stages during the monotonic load test. Figure 8.11 presents the measured load-deflection relationship. Prior to applying the monotonic load, the fatigue loading had already caused few flexural and flexural shear cracks to develop close to the mid-span. However, it was possible to determine from the measured strain at the girder bottom the load at which the flexural crack at mid-span started to open. The load at the beginning of crack opening was approximately 115 Kips. The kink in the load-deflection curve at 147 Kips was assumed to correspond to the cracking load.

At a load of approximately 157 Kips and a corresponding displacement of 0.552, multiple flexural-shear and web-shear cracks developed in the girder. In general, the location of the flexural cracks coincided with the location of the transverse reinforcement in the bottom flange. It was also observed that a crack had developed longitudinally along the web-top flange interface, similar to the crack that developed in Girder C.

Girder B failed in flexure at a load of 257.9 Kips and mid-span deflection of 8.93". The failure was initiated by crushing of the compression concrete at the top of the deck.





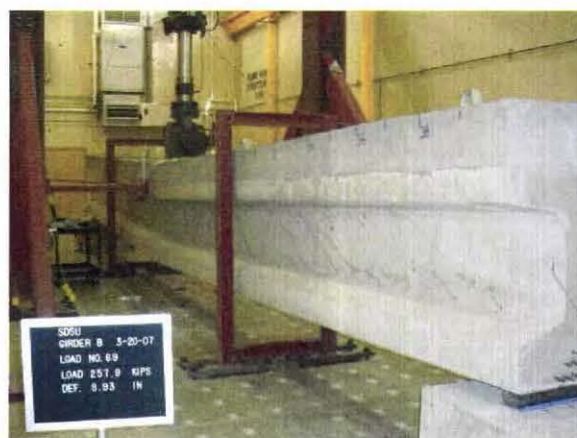
(a) Flexural Crack prior to Loading



(b) Development of Flexural-Shear Cracks



(c) Development of Diagonal Shear Cracks



(d) Crushing of Compression Concrete at Failure

Figure 8.10: Girder B at Different Stages during the Monotonic Load Test

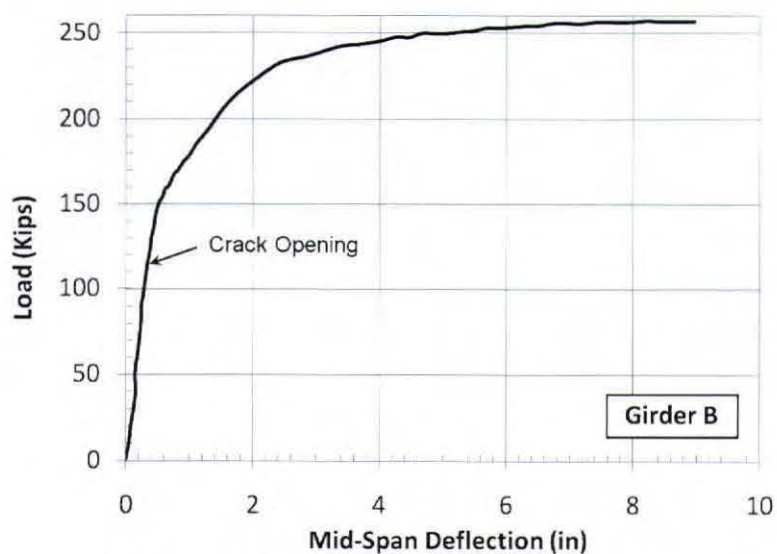


Figure 8.11: Measured Load-Deflection – Girder B



### 8.3.3.4 Performance Assessment of the Quartzite-Aggregate Girders

The measured load-deflection curves for the three girder specimens are plotted in Figure 8.12. All three specimens exhibited similar load-deflection characteristics in terms of stiffness and strength. Girder B displayed a slightly lower “elastic” stiffness than the other two specimens. The lower stiffness was due to the fatigue loading that was applied to the girder. Table 8.7 presents a summary of the measured cracking moments, flexural strengths and shear force at first observed web-shear crack. The test results demonstrate that there are no noticeable difference in the performance of quartzite-aggregate SCC and conventional concrete girders.

A more detailed analysis will be available upon the completion of the report on the quartzite-aggregate girders study.

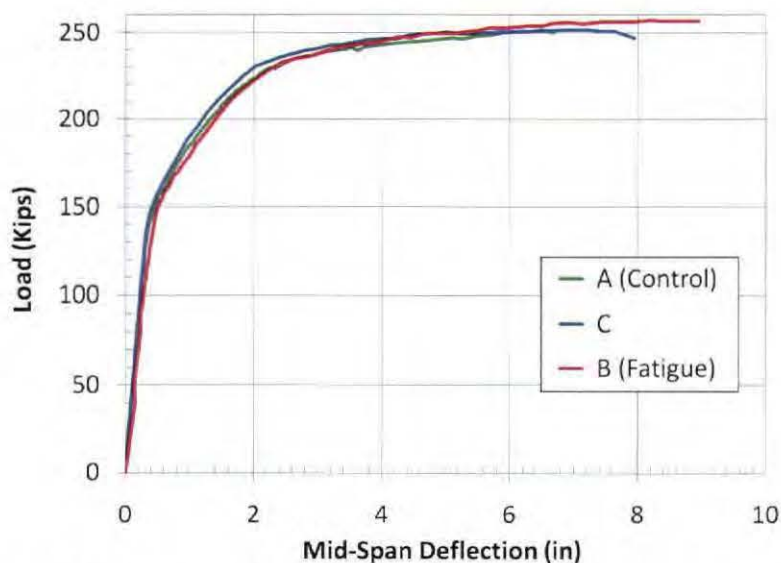


Figure 8.12: Measured Load-Deflection – Quartzite-Aggregate Girders

Table 8.7: Measured Cracking Moment, Flexural Strength, and Shear Force at First Web-Shear Crack

	Girder A	Girder B	Girder C
Cracking Moment (Kip-ft)	1393	1451 <sup>†</sup>	1417
Flexural Strength (Kip-ft)	2484	2546	2484
Shear @ 1 <sup>st</sup> Web-Shear Crack (Kips)	95	78.5	94

<sup>†</sup> Based on observed stiffness change in the monotonic load-deflection curve

### 8.3.3.5 Comparative Evaluation of Quartzite- and Limestone-Aggregate Girders

The load-deflection curves for the three quartzite-aggregate and three limestone-aggregate girders are plotted in Figure 8.13. The results show that the two types of girders exhibited similar “elastic” stiffness and ultimate strength. The main difference between the two types was the lower stiffness that the quartzite-aggregate girders exhibited in the middle segment of the load-deflection curve between the end of the “elastic” segment and the beginning of the “plastic” segment.

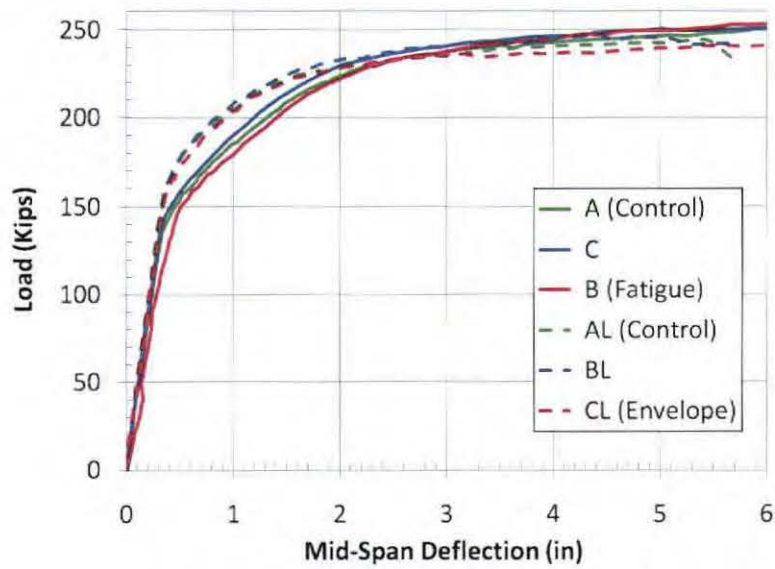


Figure 8.13: Measured Load-Deflection – Quartzite-Aggregate and Limestone-Aggregate Girders

## 9 EVALUATION OF SCC FOR PRESTRESSED BRIDGE GIRDERS

This chapter presents an evaluation of self-consolidating concrete (SCC) for use in prestressed bridge girder applications. Topics discussed in this chapter include constructability, finish quality, structural performance, and economic evaluation of SCC prestressed girders, and development of special provisions for use of SCC in prestressed applications.

### 9.1 CONSTRUCTABILITY

One of the advantages to using SCC for prestressed structural applications is the increased production efficiency and ease of placement and consolidation. During this study, the placement of each SCC girder required a crew of two workers and one vibrator. Although SCC does not require vibration to consolidate, the past experience gained by primary investigators of this study suggest that a “burst” of vibration (approximately two seconds) at each girder end might be necessary to ensure the release of any trapped air pockets during casting. In contrast, the placement of the conventional concrete girder required a crew of five workers and three vibrators. The placement time of a conventional concrete girder was found to be three to four times that of a SCC girder. Through personal interviews of the precast plant management and field personnel, it was found that placement of SCC is overwhelmingly preferred by the industry over placement of conventional concrete due to the substantially reduced effort to place SCC.

SCC may be very sensitive to variations in constituent materials. Therefore, greater care must be taken when producing SCC than that required for conventional concrete. During this study, segregation was not an issue. However, four SCC batches were rejected due to low air content.

During the construction of the test specimens, concrete was transported from the batch plant to the prestressing bed using a 2-yd<sup>3</sup> hopper. Each girder required approximately 6 yd<sup>3</sup> of concrete. Due to the limited capacity of the hopper, multiple batches were required to cast each girder. The casting process would have been more efficient if concrete was discharged into the form directly from the drum of a concrete mixer truck. The truck's capacity would eliminate the need for multiple batching and would allow for a continuous pour of the entire girder.

### 9.2 FINISHED PRODUCT

A superior finished product is often achieved with SCC. When conventional concrete is used, “bugholes” and other surface imperfections often occur. Such imperfections require finishing and patching of a member after removal of the forms. During this study, minor surface blemishes were repaired in all three girders. The imperfections, which occurred mainly at the interface between successive concrete lifts, were the result of the delay in transporting successive batches to the prestressing bed. Casting each girder in one continuous pour may have prevented the development of those imperfections.

In general, it was observed that the SCC girders were of a better finished surface quality than the conventional concrete girders. This observation was consistent with a previous study on SCC girders made with quartzite aggregates (Wehbe et al. 2007a).



### 9.3 MATERIAL AND STRUCTURAL PERFORMANCE

The performance of the SCC material and the SCC girders were covered in details in Chapter 6 and Chapter 7, respectively. Following is a brief evaluation of the suitability of SCC for prestressed applications in South Dakota.

The work performed in this study has demonstrated the ability to produce stable SCC mixtures in the laboratory and at the batch plant using South Dakota local aggregates. The hardened SCC properties followed trends similar to those of conventional concrete. Thus, strength growth, modulus of rupture, and modulus of elasticity of SCC can be determined using the empirical equations that are commonly used with conventional concrete. The shrinkage of SCC was found to be lower than that of conventional concrete of the same w/c ratio.

The strand transfer lengths in the SCC specimens were found to be comparable to that of the control specimen. The AASHTO transfer length requirement of 60 times the strand diameter was determined to be adequate for use with prestressed SCC girders.

The calculated and measured effective prestress values for the SCC and the conventional concrete girders were in excellent agreement. The calculated effective prestress was performed in accordance with four different methods. The ratio of the measured effective prestress to the calculated effective prestress varied between 0.98 and 1.13. All four models resulted in reasonable estimates of the total prestress losses. However, the calculated prestress losses based on the AASHTO LRFD Bridge Design Specifications and the 1975 PCI Committee on Prestress Losses were virtually identical to the measured prestress losses.

The SCC and the conventional concrete girders exhibited identical stiffness and strength characteristics. The current code equations and methods resulted in highly accurate estimates of the cracking moments and flexural strengths of the SCC and the conventional concrete girders. The measured concrete shear strengths of the SCC specimens were higher than that of the control specimen. The simplified method used by AASHTO for calculating the shear strength of concrete resulted in conservative estimates for the shear strength of the SCC and the conventional concrete girders.

In conclusion, the use of SCC did not compromise the performance and strength of the prestressed girders. Therefore, SCC similar to that used in this study can be specified for prestressed bridge girders.

### 9.4 ECONOMIC EVALUATION

The economic evaluation of using SCC for prestressed applications can be separated into three main categories: raw material costs, production costs, and finished product improvement costs. Since only three girders were constructed in this study, the generated economic data were limited in scope which did not allow for detailed comparison of the production costs of conventional and SCC prestressed girders. However, a preliminary economic evaluation was performed based on discussions with industry personnel and the results of past research projects on SCC by the primary investigators of this study and by others.

Typically, a SCC mix requires select aggregate size and shape, high cement content, and some specialty admixtures such as high-range water-reducing (HRWR) admixtures and viscosity-modifying admixtures (VMA). These requirements increase the unit cost of a SCC mix. SCC mixes often require smaller, more

rounded coarse aggregates and additional fine aggregates. To obtain the specific aggregates necessary to produce SCC, producers may have to pay an average of 8-12% more for raw materials. The use of a VMA can increase the cost of a concrete mix by approximately 2%, but also can result in some savings by allowing a larger variety of aggregates to be used and minimizing the impact of varying aggregate moisture contents (Martin 2003). A previous study reported that the production of SCC in South Dakota can increase material cost by approximately 26% (Boushek 2007).

The increase in the cost of raw materials is partially offset by improved production efficiency, reduced equipment cost, and increased worker safety. One particular case study reported a 20% reduction in concrete placing time and a 32% reduction in labor required to cast a double-tee member when compared to using conventional concrete. An average reduction in labor has been estimated to be about 30% when using SCC, regardless of the application (Martin 2003).

In addition to the benefits associated with production costs, SCC has been proven to reduce the number of surface imperfections on the finished concrete surface. Such imperfections require finishing and patching of a member which can lead to added production cost. An improved finished product is consistently achieved with SCC, thus reducing the finishing and patching expenses.

In conclusion, there are cases where the member geometry or reinforcement congestion may render SCC as the only viable choice despite the added material nominal cost, while in other cases the choice to use SCC may be based on expediency and the ability of the contractor or the pre-caster to meet production rate demands. Irrespective of the case, allowing the contractor or producer the freedom to select SCC may result in cost savings for the client.

## **9.5 SPECIAL PROVISIONS**

Based on the work performed in this study, the work performed in previous studies (Boushek 2007, Wehbe et al. 2007a), and discussions with SDDOT and industry personnel, special provisions for the use of SCC for precast/prestressed bridge girders have been developed. Those provisions are presented in Appendix F of this report.



## 10 SUMMARY, CONCLUSIONS, AND RECOMMENDATIONS

### 10.1 SUMMARY

Recent studies have shown that the use of self-consolidating concrete (SCC) results in improved finished quality, increased production efficiency, and reduced labor cost. Because of the favorable properties that SCC exhibits, the Federal Highway Administration and the precast concrete industry have been promoting the research and development of SCC for structural applications in bridges.

The use of SCC for prestressed applications is relatively new to local designers and producers in South Dakota. Because of the lack of data on the performance of SCC using South Dakota aggregates, there is hesitancy by local engineers and producers to design and fabricate prestressed SCC bridge girders. If SCC is properly specified and used, it has the potential to yield more economical and higher quality prestressed concrete products than conventional concrete. To take advantage of this new technology, there was a need to study production feasibility and structural performance of prestressed SCC bridge girders made with South Dakota aggregates. Proportioning, behavior, and properties of SCC are highly dependent on the coarse aggregates physical properties. Two types of aggregates, crushed limestone and quartzite, are frequently used in preparing concrete for SDDOT bridges.

In 2007 researchers at South Dakota State University (SDSU) concluded an experimental study on three full-scale prestressed bridge girders. One of the three girders was cast using conventional concrete and used as a control specimen, while the other two girders were cast using SCC. The SCC mix was made with quartzite coarse aggregate that is commonly used in eastern South Dakota. The results of the study showed that the structural performance of the prestressed SCC girders was similar to that of the control prestressed girder. It was also observed that the SCC girders had a better finished surface than the conventional concrete girder.

Crushed limestone is commonly used for concrete production in western South Dakota. In order to assure the applicability of prestressed SCC concrete statewide, a study was designed to investigate the performance of prestressed SCC bridge girders made with limestone aggregates and to develop draft specifications, acceptance criteria, mix qualifications, and guidelines for use by SDDOT for prestressed SCC applications. The study covered in this report involved material testing of SCC mixtures and structural testing of full-scale prestressed bridge girders.

Three mix designs were developed based on varying the w/c ratio and using different curing methods. The design mix was provided by Cretex Concrete Products West, Inc. The design mix had a w/c ratio of 0.33. The three w/c ratios used in this research were 0.33, 0.35, and 0.37. The three mixes were moist cured and the design mix was also heat cured. The fresh properties of the three SCC mix designs were measured to evaluate the feasibility of producing SCC made with limestone coarse aggregate. The fresh SCC properties that were measured in this study include slump flow, visual stability index (VSI), T20, J-ring spread, L-box, and column segregation. The hardened properties of the SCC mixes were measured to evaluate the performance of SCC made with limestone coarse aggregate. The hardened SCC properties that were measured in this study include compressive strength, flexural strength, modulus of elasticity, hardened visual stability index (HVSI), and shrinkage.



Three full-scale prestressed girders were fabricated at Cretex Concrete Products West, Inc. in Rapid City, SD. Two of the girders were cast with SCC and one was cast with conventional concrete to serve as a control specimen. Design of the girders included instrumentation capable of measuring instantaneous and time-dependent structural responses. The girders were tested until failure. The control specimen and one of the SCC specimens were tested under increasing monotonic load until failure. The other SCC specimen was tested under increasing cyclic loading until failure. The evaluation of SCC for use in prestressed bridge girder applications included analysis of transfer length, prestress losses, camber, flexural behavior and strength, flexural rigidity, and shear strength.

## 10.2 CONCLUSIONS

Based on the experimental and analytical studies covered in this report, the following conclusions can be drawn.

### SCC Material Behavior

1. The laboratory tests and the large-scale batches prepared by South Dakota concrete producers showed that stable SCC mixtures can be produced using South Dakota local aggregates.
2. A new parameter named the normalized amount of superplasticizer and defined as the ratio of the amount of superplasticizer to the w/c ratio was introduced in this study. The normalized amount of superplasticizer was found to be a parameter that affects the slump spread, blocking potential, and air content of SCC mixtures. For the SCC mixtures included in this study, it was found that an increase in the normalized amount of superplasticizer resulted in linear increase in slump flow, linear decrease in blocking potential, and linear increase in the required amount of air entraining admixture to maintain a constant air content in SCC mixtures having different w/c ratios but otherwise the same amount of constituent materials.
3. The effects of the w/c ratio on strength and strength growth of SCC are similar to those of conventional concrete.
4. The effect of heat curing on the strength growth of SCC is similar to that of conventional concrete.
5. The modulus of rupture and the modulus of elasticity of SCC can be determined using the ACI code empirical equations used for conventional concrete.
6. Similar to conventional concrete, the shrinkage strain of the SCC mixes increased with an increase in the w/c ratio.
7. The conventional concrete mix with w/c ratio of 33% exhibited significant shrinkage during the first 24 hours. The measured shrinkage strain at 24 hours was 42% of the total measured shrinkage strain at 94 days. The significant initial shrinkage may be attributed to autogenous shrinkage which normally occurs in concrete mixtures with w/c ratios below that required for complete hydration. Normally, a w/c of 0.42 is considered to be the minimum ratio for complete hydration. The high fluidity and set retarding properties of the SCC mixtures may have prevented autogenous shrinkage from taking place at the same rate experienced by conventional concrete mix.
8. At a w/c ratio of 0.33, the conventional concrete mix exhibited higher shrinkage strain than the SCC mix. This was mainly due to the higher initial shrinkage strains that the conventional mix exhibited during the first 24 hours. However, at higher ages, the rates of strain increase with time for the two mixtures were practically similar.
9. The ACI 209 shrinkage model was generally in good agreement with the measured shrinkage strain of the SCC mixes. However, it underestimated the strains of the SCC mixes with w/c ratios of 35% and 37% during the initial 24 hours. For the conventional concrete mix, the model resulted in significant underestimation of the initial shrinkage strains, but was in good agreement with the measured strain at 94 days.

### SCC Girders Behavior

10. A transfer length of 60 times the strand diameter (60 db) is adequate for prestressing strands in SCC girders.

11. The prestress losses in the SCC girders were similar to those in the conventional concrete girder. Current code methods for determining prestress losses can be used for prestressed SCC girders.
12. The load-deflection responses of the SCC girders were extremely similar to that of the conventional concrete girder. The specimens exhibited similar flexural stiffness, cracking strength, and nominal strength.
13. The code methods for determining flexural stiffness, cracking strength, and nominal strength of prestressed concrete girders can be used for SCC girders.
14. The effective flexural stiffness of prestressed girders decrease with an increase in the maximum applied load even at pre-cracking loads.
15. The AASHTO-LRFD simplified method for determining the nominal shear capacity of prestressed girders resulted in conservative estimates of the shear strength for both SCC and conventional concrete girders.

### **General**

16. The surface finish of the SCC girders was in general better than that of the conventional concrete girder.
17. The large concrete production facilities in Sioux Fall and Rapid City possess the capabilities and expertise to supply SCC on a commercial scale.

## **10.3 IMPLEMENTATION AND RECOMMENDATIONS**

In this study it was shown that the fabrication of prestressed SCC in South Dakota is feasible and that the performance of SCC bridge girders using South Dakota local aggregates is similar to that of conventional concrete. SCC has the added advantage of enhanced finished quality and increased production efficiency. Given the option of using SCC, the precast industry may select SCC over conventional concrete for the fabrication of prestressed bridge girder, or other precast elements, at no additional cost to the client. The use of SCC may even be more cost effective to the fabricator and the client under certain circumstances. However, successful production of a SCC mix is highly dependent on the type of aggregate used. Therefore, proportioning of a SCC mix to meet target performance levels may require a trial-and-error approach. The "Special Provisions" Based on the preceding discussion, the following recommendations are made.

1. The South Dakota Department of Transportation should permit the use of SCC for the production of prestressed bridge girders and probably for other cast-in-place and precast applications.
2. The concrete producer should be responsible for the design of a SCC mix to meet the client's stated performance levels. The special provisions that were developed in this study set performance levels and acceptance criteria for SCC mixtures when used for the fabrication of prestressed/precast elements for bridge structures in South Dakota.
3. It is recommended that a showcase bridge be constructed by SDDOT using SCC for parts of the substructure and the superstructure. The bridge can be instrumented for data collection over an extended period of time. Monitoring of such a bridge would provide valuable information on the long-term performance of SCC bridge structures.



## REFERENCES

- American Association of State and Highway Transportation Officials (AASHTO). (2007). AASHTO LRFD Bridge Design Specifications, 4th Edition, Washington, D.C.
- American Association of State Highway and Transportation Officials (AASHTO). (2005). "Draft: standard method of test for static segregation of hardened self-consolidating concrete cylinders." AASHTO.
- American Association of State Highway and Transportation Officials (AASHTO). (2002). Standard Specifications for Highway Bridges, 17th Edition, Washington, D.C.
- American Concrete Institute (ACI). (2008). Building code requirements for structural concrete and commentary, ACI 318-08 and ACI 318R-05, ACI, Farmington Hills, Mich.
- American Concrete Institute (ACI) Committee 237. (2007). Self-Consolidating Concrete, ACI 237R-07, ACI, Farmington Hills, Mich.
- American Concrete Institute (ACI) Committee 209. (2005). Prediction of Creep, Shrinkage, and Temperature Effects in Concrete Structures, ACI 209.1R-05, ACI, Detroit, Michigan.
- American Society of Civil Engineers (ASCE). (2001). "2001 Report Card for America's Infrastructure," 1015 15th Street, NW, Washington DC 20005; [www.asce.org/reportcard](http://www.asce.org/reportcard).
- American Society for Testing and Materials (ASTM). (2006). Annual book of ASTM standards, Section 4 construction, Volume 04.02 concrete and mineral aggregates, ASTM, Philadelphia, Pennsylvania.
- Attiogbe, E. K., See, H. T., and Daczko, J. A. (2005). "Engineering properties of self-consolidating concrete." Proc., First North American Conference on the Design and Use of Self-Consolidating Concrete, Hanley-Wood, LLC, Addison, Illinois, 331-336.
- Barnes, R. W., Grove, J. W., and Burns, N. H. (2003). "Experimental Assessment of Factors Affecting Transfer Length." ACI Structural Journal, 100(6), 740-748.
- Bentz, E. C., and Collins, M. P. (2000). "Response-2000 – Reinforced Concrete Section Analysis Program Using the Modified Compression Field Theory." v. 1.0.5, University of Toronto, Toronto, ON, Canada.
- Berke, N. S., Cornman, C. R., Jeknavorian, A. A., Knight, G. F., and Wallevik, O. (2003). "The effective use of superplasticizers and viscosity modifying agents in self-consolidating concrete." Proceedings, The First North American Conference on the Design and Use of Self-Consolidating Concrete, Hanley-Wood, LLC, Addison, Illinois, pp 165-169.
- Bonen, D., and Shah, S. P. (2005). Fresh and hardened properties of self-consolidating concrete." Progress in Structural Engineering Materials, 7(1), 14-26.
- Boushek, A. L. (2007). "Self-Consolidating Concrete for Box Culverts in South Dakota Using Local Aggregates." M.S. Thesis. South Dakota State University, Brookings, SD.
- Buckner, C. D. (1995). "A Review of Strand Development Length for Pretensioned Concrete Members." PCI Journal, 40(2), 84-105.



Center for Advanced Cement-Based Materials (ACBM). (2005). "The Proceedings of the 2nd North American Conference on the Design and Use of Self-Consolidating Concrete," Chicago, October 30-November 2, 2005.

Center for Advanced Cement-Based Materials (ACBM). (2003). "Notes from the 1st North American Conference on the Design and Use of Self-Consolidating Concrete," Chicago, November 2, 2003.

Collepari, M., Borsoi, A., Collepari, S., and Troli, R. (2005). "Strength, shrinkage and creep of SCC and flowing concrete." Proceedings, The Second North American Conference on the Design and Use of Self-Consolidating Concrete (SCC), Hanley-Wood, LLC, Addison, Illinois, pp 911-919.

Federal Highway Administration (FHWA) (2005). "Self-Consolidating Concrete Workshop," Proceedings, Las Vegas, NV, November 16, 2005.

Federal Highway Administration (FHWA). (1988). "Prestressing Strand for Pretension Applications—Development Length Revisited," FHWA, Memorandum, Chief, Bridge Division, Washington, D.C.

Girgis, A. F. M., and Tuan, C. Y. (2005). "Bond Strength and Transfer Length of Pretensioned Bridge Girders Cast With Self-Consolidating Concrete." *PCI Journal*, 50(6), 72-87.

Goodier, C. I. (2003). "Development of self-compacting concrete." *Proc. of the Institution of Civil Engineers: Structures and Buildings*, 156(4), 405-413.

Hamilton, III, H. R., Labonte, T., and Ansley, M. H. (2005). "Behavior of Pretensioned Type II AASHTO Girders Constructed with Self-Consolidating Concrete." *Ned H. Burns Symposium on Historic Innovations in Prestressed Concrete*, ACI, Farmington Hills, MI.

Hegger, J., Rauscher, S., Kommer, B., and Gortz, S. (2005). "Shear strength of concrete beams made of self-consolidating concrete." Proceedings, The Second North American Conference on the Design and Use of Self-Consolidating Concrete (SCC), Hanley-Wood, LLC, Addison, Illinois, pp 495-501.

Illinois Department of Transportation. (2004). "Quality control/quality assurance program addendum for precast concrete products using self-consolidating concrete."

Kosmatka, S. H., Kerkhoff, B., and Panarese, W. C. (2002). *Design and control of concrete mixtures*, 14th Ed., Portland Cement Association (PCA), Skokie, Illinois.

Martin, D. J. (2003). "Economic Impact of SCC in Precast Applications." *Proc., First North American Conference on the Design and Use of Self-Consolidating Concrete*, Hanley-Wood, LLC, Addison, IL, 147-152.

Michigan Department of Transportation. (2005). "Special Provision for Production of Prestress Beams with Self-Consolidating Concrete."

Mindess, S., Young, J.F., and Darwin, D. (2003). *Concrete*, 2nd Ed., Prentice-Hall, Inc., Upper Saddle River, New Jersey.

Naito, C. J., Parent, G., and Brunn, G. (2006). "Performance of Bulb-Tee Girders Made with Self-Consolidating Concrete." *PCI Journal*, 51(6), 72-85.

Nawy, E. G. (2006). *Prestressed Concrete: A Fundamental Approach*, 5th Edition, Prentice Hall, Upper Saddle River, NJ.

North Carolina Department of Transportation. (2005). "Self-consolidating concrete for precast and prestressed concrete (special)."

Nowak, A. S., Laumet, P., Czarnecki, A. A., Kaszynska, M., Szerszen, M. M., and Podhoreck, P. J. (2005). "US-specific self-consolidating concrete for bridges." University of Michigan, Ann Arbor, Michigan.

Park, R., and Paulay, T. (1975). "Reinforced Concrete Structures." John Wiley and Sons.

Precast/Prestressed Concrete Institute (PCI). (2004). PCI Design Handbook, Precast and Prestressed Concrete, MNL-120-04, 6th Edition, PCI, Chicago, IL.

Precast/Prestressed Concrete Institute (PCI). (2003). Interim Guidelines for the use of self-consolidating concrete in precast/prestressed concrete institute member plants, TR-6-03, PCI, Chicago, Illinois.

Precast/Prestressed Concrete Institute (PCI) Committee on Prestress Losses. (1975). "Recommendations for Estimating Prestress Losses." PCI Journal, 20(4), 43-75.

Russell, B. W., and Burns, N. H. (1997). "Measurement of Transfer Lengths on Pretensioned Concrete Elements." Journal of Structural Engineering, 123(5), 541-549.

Wehbe, N., Sigl, A., and Zemlicka, J. (2007a). "Strength and Serviceability of Prestressed SCC Bridge Girders Made with Quartzite Aggregates," presented at the American Concrete Institute Spring 2007 Convention, Atlanta, GA. April 23, 2007.

Wehbe, N., Sigl, A., and Boushek, J. (2007b). "Structural Applications of Self-Consolidating Concrete," Interim Report SD2005-13-I, South Dakota Department of Transportation, Pierre, SD. July 2007.

## APPENDIX A: AGGREGATE TESTING DATA

**Table A.1: ASTM C 29 for Rapid City Limestone**

ASTM C29, "Standard Test Method for Bulk Density ("Unit Weight") and Voids in Aggregate"

Test sample	Coarse
Date	7/19/2007

### Data

Mass of measure (kg) =	3.53
Mass of measure + water (kg) =	10.56
Mass of water (kg) =	7.03
Water temperature (°F) =	74
Water density at this temperature (kg/m <sup>3</sup> ) =	997.4575
Volume of measure (m <sup>3</sup> ) =	0.007048

Mass of measure (kg) =	3.53
Mass of aggregate + measure (kg) =	14.45
Mass of aggregate sample (kg) =	10.92
Bulk density of sample (kg/m <sup>3</sup> ) =	1549.393
Bulk density of sample (lb/ft <sup>3</sup> ) =	96.72547

### Summary of results

Bulk density of sample (kg/m <sup>3</sup> ) =	1549.393
Bulk density of sample (lb/ft <sup>3</sup> ) =	96.72547



**Table A.2: ASTM C 127 for Rapid City Limestone**

ASTM C 127, "Standard Test Method for Density, Relative Density (Specific Gravity), and Absorption of Coarse Aggregate"

Test Sample 7.1  
Rapid City Limestone

---

Data

Mass of bowl, g =	336.57
Mass of bowl + SSD aggr., g =	2456.32
Mass of SSD aggr., g =	2119.75
Mass of oven dry aggr., g =	2104.96
Absorption, % =	0.70
<hr/>	
Mass of oven dry sample in air, g =	2104.96
Mass of SSD sample in air, g =	2119.75
Apparent mass of saturated sample in water, g =	744.00
Specific gravity of SSD sample =	1.54
Density, kg/m <sup>3</sup> =	1536.94
Density, lb/ft <sup>3</sup> =	95.95

---

Summary of Results

Specific gravity of SSD sample =	2.54
Density (SSD), kg/m <sup>3</sup> =	1536.94
Density (SSD), lb/ft <sup>3</sup> =	95.95
Absorption, % =	0.70

**Table A.2: ASTM C 127 for Rapid City Limestone (continued)**

ASTM C 127, "Standard Test Method for Density, Relative Density (Specific Gravity), and Absorption of Coarse Aggregate"

Test Sample 7.2  
Rapid City Limestone

Data

Mass of bowl, g =	282.72
Mass of bowl + SSD aggr., g =	1953.30
Mass of SSD aggr., g =	1670.58
Mass of oven dry aggr., g =	1659.51
Absorption, % =	0.67

Mass of oven dry sample in air, g =	1659.51
Mass of SSD sample in air, g =	1670.58
Apparent mass of saturated sample in water, g =	587.00
Specific gravity of SSD sample =	1.54
Density, $\text{kg/m}^3$ =	1537.87
Density, $\text{lb/ft}^3$ =	96.00

Summary of Results

Specific gravity of SSD sample =	2.54
Density (SSD), $\text{kg/m}^3$ =	1537.87
Density (SSD), $\text{lb/ft}^3$ =	96.00
Absorption, % =	0.67

**Table A.2: ASTM C 127 for Rapid City Limestone (continued)**

ASTM C 127, "Standard Test Method for Density, Relative Density (Specific Gravity), and Absorption of Coarse Aggregate"

Test Sample 7.3  
Rapid City Limestone

Data

Mass of bowl, g =	237.21
Mass of bowl + SSD aggr., g =	2335.54
Mass of SSD aggr., g =	2098.33
Mass of oven dry aggr., g =	2085.48
Absorption, % =	0.62

Mass of oven dry sample in air, g =	2085.48
Mass of SSD sample in air, g =	2098.33
Apparent mass of saturated sample in water, g =	735.00
Specific gravity of SSD sample =	1.54
Density, $\text{kg/m}^3$ =	1535.27
Density, $\text{lb/ft}^3$ =	95.84

Summary of Results

Specific gravity of SSD sample =	2.54
Density (SSD), $\text{kg/m}^3$ =	1535.27
Density (SSD), $\text{lb/ft}^3$ =	95.84
Absorption, % =	0.62



**Table A.3: ASTM C 136 for Rapid City Limestone**

ASTM C 136, "Standard Test Method for Sieve Analysis of Fine and Coarse Aggregates"

Test Sample

Sieve	Size (in)	Sieve Wt. Only (kg)	Sieve + Retained Sample Wt. (kg)	Retained Sample Wt. (kg)	Percent Retained on Sieve (%)	Percent Passing Sieve (%)
1"	1	7.24	0	0.00	0.0	100.0
3/4"	0.75	7.22	0.00	0.00	0.0	100.0
1/2"	0.5	7.33	0.00	0.00	0.0	100.0
3/8"	0.375	7.17	7.18	0.01	0.3	99.7
No. 4	0.1870079	7.28	10.01	2.73	76.7	23.0
Pan	0	7.28	8.10	0.82	23.0	0.0

Total Retained 3.56 100.0

**Table A.4: ASTM C 29 for Rapid City Sand**

ASTM C29, "Standard Test Method for Bulk Density  
("Unit Weight") and Voids in Aggregate"

Test sample	Fine
Date	7/20/2007

Data

Mass of measure (kg) =	3.53
Mass of measure + water (kg) =	10.56
Mass of water (kg) =	7.03
Water temperature (°F) =	74
Water density at this temperature (kg/m <sup>3</sup> ) =	997.4575
Volume of measure (m <sup>3</sup> ) =	0.007048

Mass of measure (kg) =	3.53
Mass of aggregate + measure (kg) =	14.97
Mass of aggregate sample (kg) =	11.44
Bulk density of sample (kg/m <sup>3</sup> ) =	1623.174
Bulk density of sample (lb/ft <sup>3</sup> ) =	101.3314

Summary of results

Bulk density of sample (kg/m <sup>3</sup> ) =	1623.174
Bulk density of sample (lb/ft <sup>3</sup> ) =	101.3314

**Table A.5: ASTM C 128 for Rapid City Sand**

ASTM C 128, "Standard Test Method for Density, Relative Density (Specific Gravity), and Absorption of Fine Aggregate"

Test Sample 7.4  
Rapid City Sand

---

Data

Mass of flask, g =	188.73
Mass of flask + water to calibration, g =	687.74
Mass of flask + SSD aggr. + water, g =	1004.16
Mass of SSD aggr., g =	508.34
Specific gravity of SSD sample =	2.65
SSD Density, kg/m <sup>3</sup> =	2642.09
SSD Density, lb/ft <sup>3</sup> =	164.94

Mass of oven dry aggr., g =	502.55
Mass of SSD aggr., g =	508.34
Absorption, % =	1.15

---

Summary of Results

Specific gravity of SSD sample =	2.65
Density, kg/m <sup>3</sup> =	2642.09
Density, lb/ft <sup>3</sup> =	164.94
Absorption, % =	1.15



**Table A.5: ASTM C 128 for Rapid City Sand (continued)**

ASTM C 128, "Standard Test Method for Density, Relative Density (Specific Gravity), and Absorption of Fine Aggregate"

Test Sample 7.5  
Rapid City Sand

Data

Mass of flask, g =	188.73
Mass of flask + water to calibration, g =	687.74
Mass of flask + SSD aggr. + water, g =	1000.10
Mass of SSD aggr., g =	504.52
Specific gravity of SSD sample =	2.63
SSD Density, kg/m <sup>3</sup> =	2618.96
SSD Density, lb/ft <sup>3</sup> =	163.49
Mass of oven dry aggr., g =	498.22
Mass of SSD aggr., g =	504.52
Absorption, % =	1.26

Summary of Results

Specific gravity of SSD sample =	2.63
Density, kg/m <sup>3</sup> =	2618.96
Density, lb/ft <sup>3</sup> =	163.49
Absorption, % =	1.26

**Table A.5: ASTM C 128 for Rapid City Sand (continued)**

ASTM C 128, "Standard Test Method for Density,  
Relative Density (Specific Gravity), and  
Absorption of Fine Aggregate"

Test Sample 7.6  
Rapid City Sand

Data

Mass of flask, g =	188.73
Mass of flask + water to calibration, g =	687.74
Mass of flask + SSD aggr. + water, g =	1008.93
Mass of SSD aggr., g =	518.14
Specific gravity of SSD sample =	2.63
SSD Density, kg/m <sup>3</sup> =	2624.24
SSD Density, lb/ft <sup>3</sup> =	163.82
Mass of oven dry aggr., g =	512.24
Mass of SSD aggr., g =	518.14
Absorption, % =	1.15

Summary of Results

Specific gravity of SSD sample =	2.65
Density, kg/m <sup>3</sup> =	2642.09
Density, lb/ft <sup>3</sup> =	164.94
Absorption, % =	1.15

**Table A.6: ASTM C 136 for Rapid City Sand**

ASTM C 136, "Standard Test Method for Sieve Analysis of Fine and Coarse Aggregates"

Test Sample

Rapid City Sand

Data

Sieve	Size ( $\mu\text{m}$ )	Sieve Wt. Only (g)	Sieve + Retained Sample Wt. (g)	Retained Sample Wt. (g)	Percent Retained on Sieve (%)	Percent Passing Sieve (%)	Min. SD DOT % Passing Req't (%)	Max. SD DOT % Passing Req't (%)
3/8"	9500			0.00	0.0	100.0	100	100
No. 4	4750	765.03	770.45	5.42	1.3	98.7	95	100
No. 8	2360	687.99	730.37	42.38	10.5	88.2		
No. 16	1180	648.31	721.40	73.09	18.1	70.1	45	85
No. 30	600	592.69	691.01	98.32	24.4	45.7		
No. 50	300	548.94	640.26	91.32	22.6	23.1	10	30
No. 100	150	522.05	595.55	73.50	18.2	4.9	2	10
No. 200	75	513.60	529.55	15.95	4.0	0.9		
Pan	0	492.43	493.57	1.14				
Wash	0			2.57	0.9	0.0		

Total Sample Weight 403.69 100.0

Sample Wt. Before Washing & Sieving 401

Percent Difference Between Sample Wt.  
Before Sieving and Wt. Retained on  
Sieves (%) 0.67

Sieve	Size ( $\mu\text{m}$ )	Percent Retained on Sieve (%)	Cumulative Percent Retained on Sieve (%)	
3/8"	9500	0.0	0.0	0
No. 4	4750	1.3	1.3	0.0134261
No. 8	2360	10.5	11.8	0.1184077
No. 16	1180	18.1	29.9	0.2994625
No. 30	600	24.4	54.3	0.5430157
No. 50	300	22.6	76.9	0.7692289
No. 100	150	18.2	95.1	0.9512993
No. 200	75	4.0	99.1	
Pan	0			
Wash	0	0.9	100.0	

Fineness Modulus 2.69



## APPENDIX B: ADMIXTURE LITERATURE

### Concrete

#### PRODUCT INFORMATION



## ADVA® Cast 555

Superplasticizer for Precast Concrete ASTM C494, Type F

#### Description

ADVA® Cast 555 is a high efficiency polycarboxylate based superplasticizer. ADVA Cast 555 has been formulated to impart maximum desired workability without segregation to concrete, and to achieve high early compressive strength as required by the precast industry. ADVA Cast 555 is optimized for the production of Self-Consolidating Concrete (SCC) in precast/prestressed applications.

ADVA Cast 555 is formulated to comply with ASTM C494 as a Type F admixture and meets the provisional requirements. One year ASTM will be complete in June 2006.

#### Uses

ADVA Cast 555 is recommended for use in precast and prestressed production in Self-Consolidating Concrete and conventional applications.

#### Self-Consolidating Concrete Applications:

Self-Consolidating Concrete produced with ADVA Cast 555 has unique advantages over conventional flowing concrete.



- **Lower SCC Viscosity:** flow properties of SCC are enhanced, reducing SCC viscosity with no change in stability or segregation resistance.
- **Self Placement:** vibration can be eliminated because SCC is highly flowable and will change shape under its own weight to self level and self consolidate within formwork.
- **High Cohesion:** the window of acceptable mix designs to maintain cohesive SCC's is increased, allowing for the production of SCC that is flowable and yet highly cohesive. Bleeding is significantly reduced.
- **No Blocking:** SCC can pass freely through narrow openings and congested reinforcement without aggregate "blocking" behind obstructions that stop the flow of concrete.

**GRACE**  
Construction Products

Self-Consolidating Concrete produced with ADVA Cast 555 provides the following benefits:

- Reduced labor and improved productivity through faster and easier concrete placement with no vibration
- The highest quality surface finish, eliminating/reducing the need for surface touch ups
- Improved labor safety; reduced plant noise levels and improved work environment
- Reduced wear and tear on forms by eliminating vibration
- Achievement of complete consolidation throughout concrete elements, even in thin walled, highly reinforced units
- Increased production flexibility by enabling use of form geometry and form orientations in which placement of conventional concrete mixes would be difficult or impossible

#### Conventional Concrete Applications:

- ADVA Cast 555 superplasticizer can produce concrete with extremely high levels of workability without segregation.
- ADVA Cast 555 may be used to produce concrete with very low water/cement ratios while maintaining normal levels of workability.

- ADVA Cast 555 is ideal for use in precast and prestressed applications where concrete needs to achieve high early strength along with high levels of workability.
- ADVA Cast 555 provides superior concrete surface finish characteristics with reduced bugholing.

#### Dosage Rates

ADVA Cast 555 is an easy to dispense liquid admixture. Dosage rates can be adjusted to meet a wide spectrum of concrete performance requirements. Addition rates for ADVA Cast 555 can vary with the type of application, but will normally range from 540 to 1400 mL/100 kg (8 to 20 fl oz/100 lbs) of cement. Should conditions require using more than the recommended addition rate, please consult your Grace Representative.

For Self-Consolidating Concrete applications, pre-placement testing is recommended to determine the optimum admixture addition rate and mix design. Factors that influence optimum addition rate include other concrete mix components, aggregate gradations, form geometry, and reinforcement configurations. Please consult your local Grace Construction Products representative for assistance with developing mix designs for Self-Consolidating Concrete.

#### Compatibility with Other Admixtures

ADVA Cast 555 is compatible in a concrete mix with all Grace admixtures, including all air entraining agents. Each admixture should be added separately into the mix.

#### Dispensing Equipment

A complete line of accurate, automatic dispensing equipment is available.

#### Packaging

ADVA Cast 555 is available in bulk, delivered by metered trucks, in 1041 L (275 gal) totes, and 210 L (55 gal) drums. ADVA Cast 555 will freeze at approximately 0°C (32°F) but will return to full functionality after thawing and thorough mechanical agitation.

#### Specifications

ADVA Cast 555 is supplied as a ready to use brown liquid, one liter weighs approximately 1.07 kg (one gallon weighs approximately 8.90 lbs). ADVA Cast 555 contains no intentionally added chlorides.

The superplasticizer shall be ADVA Cast 555 as manufactured by Grace Construction Products, Cambridge, MA.

North American Customer Service: 1-877-4AD-MIX1 (1-877-423-6491)



Visit our web site at: [www.graceconstruction.com](http://www.graceconstruction.com)

W. R. Grace & Co.-Conn. 62 Whittemore Avenue Cambridge, MA 02140

ADVA and the ADVA logo are registered trademarks of W. R. Grace & Co.-Conn.

We hope the information here will be helpful. It is based on data and knowledge considered to be true and accurate and is offered for the user's consideration, acceptance and reliance only. We do not warrant the truth or its content. Please read all instructions, recommendations or suggestions in conjunction with the product of sale which apply to all goods supplied by us. No insurance, compensation or damages is provided for any use which would infringe any patent or copyright. W. R. Grace & Co.-Conn., 62 Whittemore Avenue, Cambridge, MA 02140. In Canada: Grace Canada, Inc., 244 Common Road, West Ajax, Ontario, Canada L1B 1G7.

This product may be covered by patents or pending patents.

Copyright 2001 W. R. Grace & Co.-Conn. DCA-311C Printed in U.S.A. 1201 FA2NPLM

**GRACE**  
Construction Products



## PRODUCT INFORMATION

## Daratard® 17

Initial Set Retarder ASTM C494, Type B and Type D

**Description**

Daratard® 17 admixture is a ready-to-use aqueous solution of hydroxylated organic compounds. Ingredients are factory premixed in exact proportions to minimize handling, eliminate mistakes and guesswork. Daratard 17 admixture weighs approximately 1.17 kg/L (10.2 lbs/gal).

**Uses**

Daratard 17 retards the initial and final set of concrete. At the usual addition rate of 19.5 mL/100 kg (3 fl oz/100 lbs) cement it will extend the initial setting time of portland cement concrete by 2 to 3 hours at 21°C (70°F). Daratard 17 is used wherever a delay in setting time will insure sufficient delivery, placement, vibration or compaction time, such as in:

- Hot Weather Concreting
- Transit Mix Concrete
- Prestressed Concrete

Daratard 17 is also used in special applications, as in bridge decks where it extends plastic characteristics of the concrete until progressive deflection resulting from increasing loads is completed.

**Water-Reducing Properties**

Along with set retardation, Daratard 17 provides water-reduction (typically 8 to 10%) in a concrete mix. This water-reducing action of Daratard 17 produces greater plasticity and workability in the fresh concrete and the strength and permeability of the hardened concrete are measurably improved. Daratard 17 is designed for use on jobs where high temperatures or extended setting times are the prime factors. It is recommended only when the primary purpose is to delay and control the setting time of concrete. When time and

temperature are not major considerations, Grace Construction Product's water-reducing admixtures such as WRDA® with HYCOL® should be used.

**Compatibility with Other Admixtures**

Daratard 17 is compatible in concrete with all commercial air-entraining admixtures, such as Daravair®. Due to the slight air-entraining properties of Daratard 17, itself, the addition rate of Daravair may be reduced by about 25%. Each admixture should be added separately.

**GRACE**  
Construction Products



#### Addition Rates

Addition rates for Daratard 17 will range from 130 to 520 mL/100 kg (2 to 8 fl oz/100 lbs) of cement. The amount to be used will depend upon the degree of retardation required under job conditions. Longer setting times or higher temperatures will require higher addition rates. Conversely, the addition rate will be lower for shorter extensions of time.

#### Dispensing Equipment

A complete line of accurate, automatic dispensing equipment is available. Daratard 17 may be introduced to the mix with the sand or with the water.

#### Packaging

Daratard 17 is available in bulk, delivered by metered tank trucks, and 210 L (55 gal) drums. Daratard 17 will freeze at about -2°C (28°F), but will return to full strength after thawing and thorough agitation.

#### Architects' Specification for Concrete Retarding Admixture

Concrete shall be designed in accordance with ACI Standard Recommended Practice for Selecting Proportions for Concrete (ACI 211.1).

The set-retarding/water-reducing admixture shall comply with ASTM Designation C494, Type D admixture, and shall be Daratard 17, as manufactured by Grace Construction Products, or equal. Certification of compliance shall be made available on request. It shall be used in strict accordance with the manufacturer's recommendations.

The addition rate shall be adjusted to produce the specified retardation of the concrete mix at all temperatures.

North American Customer Service: 877-4AD-MIX1 (877-423-6491)

Visit our web site at: [www.graceconstruction.com](http://www.graceconstruction.com)

W. R. Grace & Co.-Conn. 62 Whittemore Avenue Cambridge, MA 02140

Daratard, Daratard 17, RT-40 and HYCOL are registered trademarks of W. R. Grace & Co.-Conn.

We hope the information here will be useful. It is based on data and knowledge considered to be true and accurate and is offered for the user's convenience, interpretation and application, but we do not warrant the results to be obtained. Please read all instructions, recommendations or regulations in conjunction with the installation of this product, apply to all goods supplied by us. No statement, recommendation, or warranty is intended for any use which would violate any patent or copyright. W. R. Grace & Co.-Conn., 62 Whittemore Avenue, Cambridge, MA 02140. In Canada, Grace Canada Inc., 234 Common Road, West Ajax, Ontario, Canada L1W 1G1.

This product may be covered by patents or patents pending.

Copyright 2002 W. R. Grace & Co.-Conn. RT-40 Printed in U.S.A. 4/04 FAL/FIM

**GRACE**  
Construction Products

# DARACEM 19

## High-range water-reducing admixture

ASTM C494 Type A and F, and ASTM C1017 Type I

### Product Description

Daracem® 19 is an aqueous solution of a modified naphthalene sulfonate. Daracem 19 is a superior dispersing admixture having a marked capacity to disperse the cement agglomerates normally found in a cementwater suspension. The capability of Daracem 19, in this respect, exceeds that of normal water-reducing admixtures. It is a low viscosity liquid manufactured for use as received. Daracem 19 contains no added chloride. Daracem 19 is formulated to comply with *Specifications for Chemical Admixtures for Concrete*, ASTM C494 as a Type A and Type F admixture, and ASTM C1017 as a Type I admixture. One gallon of Daracem 19 weighs approximately 10 lbs (1.2 kg/L).

### Uses

Daracem 19 produces concrete with extremely workable characteristics referred to as high slump. Daracem 19 also allows concrete to be produced with very low water/cement ratios at low or normal slumps. Daracem 19 is ideal for use in prestress, precast, bridge deck or any concrete where it is desired to keep the water/cement ratio to a minimum and still achieve the degree of workability necessary to provide easy placement and consolidation. Daracem 19 will also fluidize concrete, making it ideal for tremie concreting or other applications where high slumps are desired.

### Addition Rates

Addition rates of Daracem 19 can vary with type of application, but will normally range from 6 to 20 fl oz/100 lbs (390 to 1300 mL/100 kg) of cement. In most instances the addition of 10 to 16 fl oz/100 lbs (650 to 1040 mL/100 kg) of cement will be sufficient. At a given water/cement ratio, the slump required for placement can be controlled by varying the addition rate. Should job site conditions require using more than recommended addition rates, please consult your Grace representative.

### Product Advantages

- Can produce high slump flowable concrete with no loss in strength
- Can produce low water/cement ratio concrete and therefore, high strengths
- Concrete produced with Type I

cement may be substituted for normal concrete produced with Type III cement to achieve early strengths

- \* At high slump, exhibits no significant segregation in comparison to concrete without a superplasticizer at the same slump

### **Compatibility with Other Admixtures and Batch Sequencing**

Daracem 19 is compatible with most Grace admixtures as long as they are added separately to the concrete mix, usually through the water holding tank discharge line. However, Daracem 19 is not recommended for use in concrete containing ADVA® superplasticizers or MIRA® 92. In general, it is recommended that Daracem 19 be added to the concrete mix near the end of the batch sequence for optimum performance. Different sequencing may be used if local testing shows better performance. Please see Grace Technical Bulletin TB-0110, *Admixture Dispenser Discharge Line Location and Sequencing for Concrete Batching Operations* for further recommendations. Daracem 19 should not come in contact with any other admixture before or during the batching process, even if diluted in mix water.

Pretesting of the concrete mix should be performed before use, and as conditions and materials change in order to assure compatibility, and to optimize dosage rates, addition times in the batch sequencing and concrete performance. For concrete that requires air entrainment, the use of an ASTM C260 airentaining agent (such as Daravair® or Darex® II AEA) is recommended to provide suitable air void parameters for freeze-thaw resistance. Darex AEA is not recommended. Please consult your Grace representative for guidance.

### **Packaging & Handling**

Daracem 19 is available in bulk, delivered by metered tank trucks, and in 55 gal (210 L) drums.

It will begin to freeze at approximately 32°F (0°C), but will return to full strength after thawing and thorough agitation.

In storage, and for proper dispensing, Daracem 19 should be maintained at temperatures above 32°F (0°C).

### **Dispensing Equipment**

A complete line of accurate, automatic dispensing equipment is available.



# DARAVAIR® 1000

## Air-entraining admixture

ASTM C260

### Product Description

Daravair® 1000 is a liquid air-entraining admixture that provides freeze-thaw resistance, yield control, and finishability performance across the full range of concrete mix designs. Daravair 1000 is a clean, light-orange product designed to generate specification-quality air systems. Based on a high-grade saponified rosin formulation, Daravair 1000 is chemically similar to vinsol-based products, but with increased purity and supply dependability. Daravair 1000 weighs approximately 8.5 lbs/gal (1.02 kg/L). Daravair 100 does not contain intentionally added chloride.

### Uses

Daravair 1000 air-entraining admixture may be used wherever the purposeful entrainment of air is required by concrete specifications. Formulated to perform across the entire spectrum of production mixes, Daravair 1000 generates quality, freeze-thaw resistant air systems in concrete conditions that include the following:

- Low slump
- Paving
- Central mix
- Extruded slip form
- Mixes containing hot water and accelerators
- Precast
- High cement factor
- Fly ash and slag
- Superplasticizers
- Manufactured sands

### Performance

Air is incorporated into the concrete by the mechanics of mixing and stabilized into millions of discrete semi-microscopic bubbles in the presence of a specifically designed airentraining admixture such as Daravair 1000.

These air bubbles act much like flexible ball bearings increasing the mobility, or plasticity and workability of the concrete. This can permit a reduction in mixing water with no loss of slump. Placeability is improved. Bleeding, plastic shrinkage and segregation

are minimized.

Through the purposeful entrainment of air, Daravair 1000 markedly increases the durability of concrete to severe exposures particularly to freezing and thawing. It has also demonstrated a remarkable ability to impart resistance to the action of frost and de-icing salts as well as sulfate, sea and alkaline waters.

#### **Product Advantages**

- Rapid air build suitable for short mix cycles
- Can be used in wide spectrum of mix designs

#### **Addition Rates**

There is no standard addition rate for Daravair 1000. The amount to be used will depend upon the amount of air required for job conditions, usually in the range of 4 to 8%. Typical factors which might influence the amount of air-entraining admixture required are temperature, cement, sand gradation, and the use of extra fine materials such as fly ash and microsilica. Typical Daravair 1000 addition rates range from  $\frac{1}{2}$  to 3 fl oz/100 lbs (30 to 200 mL/100 kg) of cement. Pretesting of concrete should be performed to confirm dosage rates required to achieve desired concrete performance.

The air-entraining capacity of Daravair 1000 is usually increased when other concrete admixtures are contained in the concrete, particularly water-reducing admixtures and water-reducing retarders. This may allow up to  $\frac{2}{3}$  reduction in the amount of Daravair 1000 required.

#### **Mix Adjustment**

Entrained air will increase the volume of the concrete making it necessary to adjust the mix proportions to maintain the cement factor and yield. This may be accomplished by a reduction in water requirement and aggregate content.

#### **Compatibility with Other Admixtures and Batch Sequencing**

Daravair 1000 is compatible with most Grace admixtures as long as they are added separately to the concrete mix. In general, it is recommended that Daravair 1000 be added to the concrete mix near the beginning of the

batch sequence for optimum performance, preferably by “dribbling” on the sand. Different sequencing may be used if local testing shows better performance. Please see Grace Technical Bulletin TB-0110, *Admixture Dispenser Discharge Line Location and Sequencing for Concrete Batching Operations* for further recommendations. Daravair 1000 should not be added directly to heated water. Pretesting of the concrete mix should be performed before use, and as conditions and materials change in order to assure compatibility, and to optimize dosage rates, addition times in the batch sequencing and concrete performance. Please consult your Grace representative for guidance.

### Packaging & Handling

Daravair 1000 is available in bulk, delivered by metered tank trucks and in 55 gal (210 L) drums. **Daravair 1000 will freeze at about 30°F (-1°C) but its air-entraining properties are completely restored by thawing and thorough mechanical agitation.**

### Dispensing Equipment

A complete line of accurate automatic dispensing equipment is available. These dispensers can be located to discharge into the water line, the mixer, or on the sand.

### Specifications

Concrete shall be air entrained concrete, containing 4 to 8% entrained air. The air contents in the concrete shall be determined by the pressure method (ASTM Designation C231) or volumetric method (ASTM Designation C173). The air-entraining admixture shall be a completely neutralized rosin solution, such as Daravair 1000, as manufactured by Grace Construction Products, or equal, and comply with *Standard Specification for Air-Entraining Admixtures* (ASTM Designation C260). The air-entraining admixture shall be added at the concrete mixer or batching plant at approximately  $\frac{1}{2}$  to 3 fl oz/100 lbs (30 to 200 mL/100 kg) of cement, or in such quantities as to give the specified air contents.

**[www.graceconstruction.com](http://www.graceconstruction.com)**

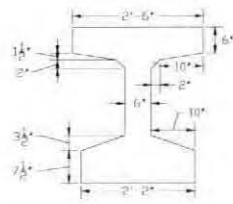
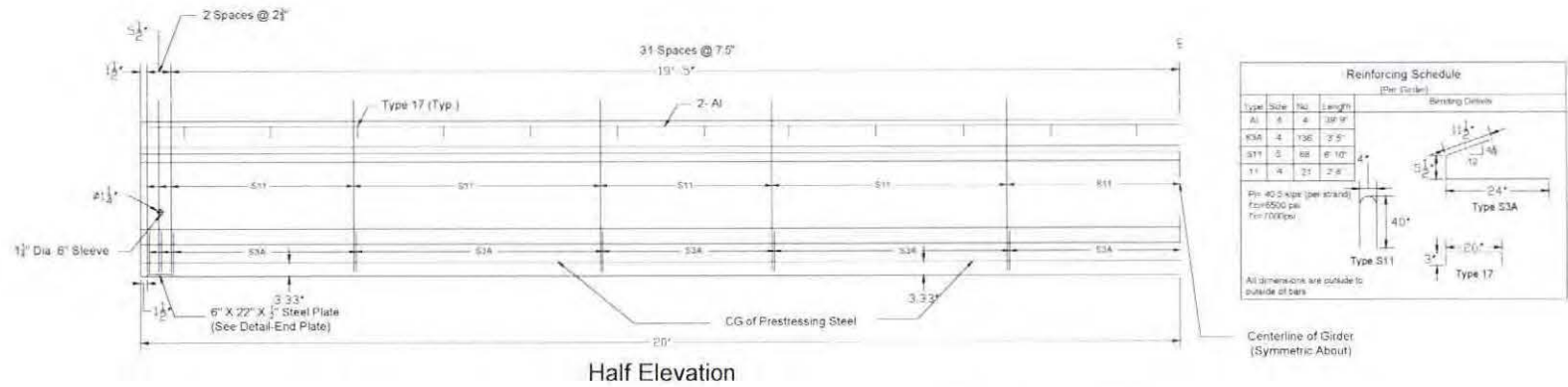
**North American Customer Service: 1-877-4AD-MIX1 (1-877-423-6491)**

Daravair is a registered trademark of W. R. Grace & Co.-Conn.

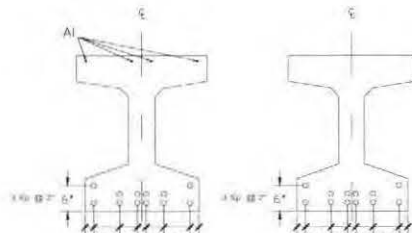
We hope the information here will be helpful. It is based on data and knowledge considered to be true and accurate and is offered for the users' consideration, investigation and verification, but we do not warrant the results to be obtained. Please read all statements, recommendations or suggestions in conjunction with our conditions of sale, which apply to all goods supplied by us. No statement, recommendation or suggestion is intended for any use which would infringe any patent or copyright. W. R. Grace & Co.-Conn., 62 Whittemore Avenue, Cambridge, MA 02140. In Canada, Grace Canada, Inc., 294 Clements Road, West, Ajax, Ontario, Canada L1S 3C6.



This product may be covered by patents or patents pending. Copyright 2007, W. R. Grace & Co.-Conn.  
AIR-7F Printed in U.S.A. 11/07 FA/LI/IM

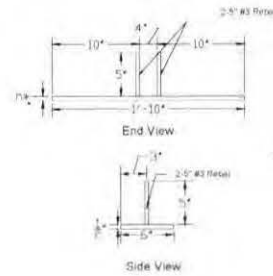


Type 36M Girder

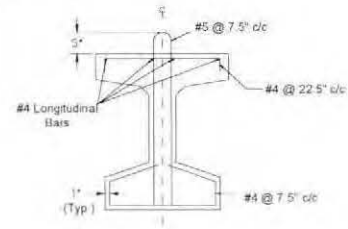


Mid-Span Section

End Section



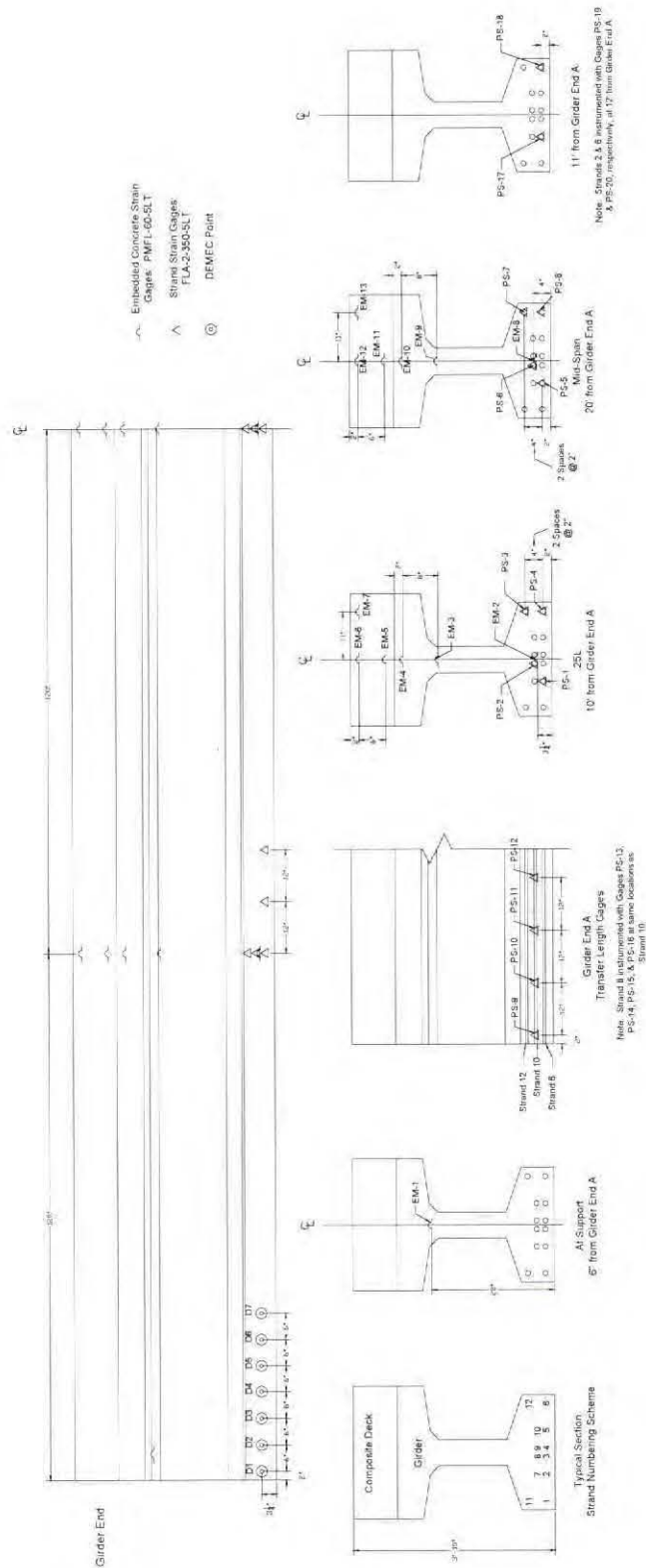
End Plate



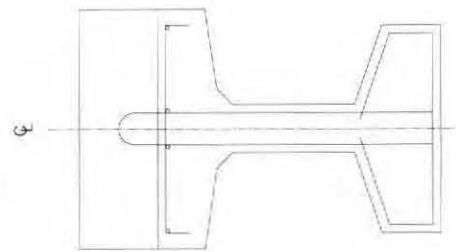
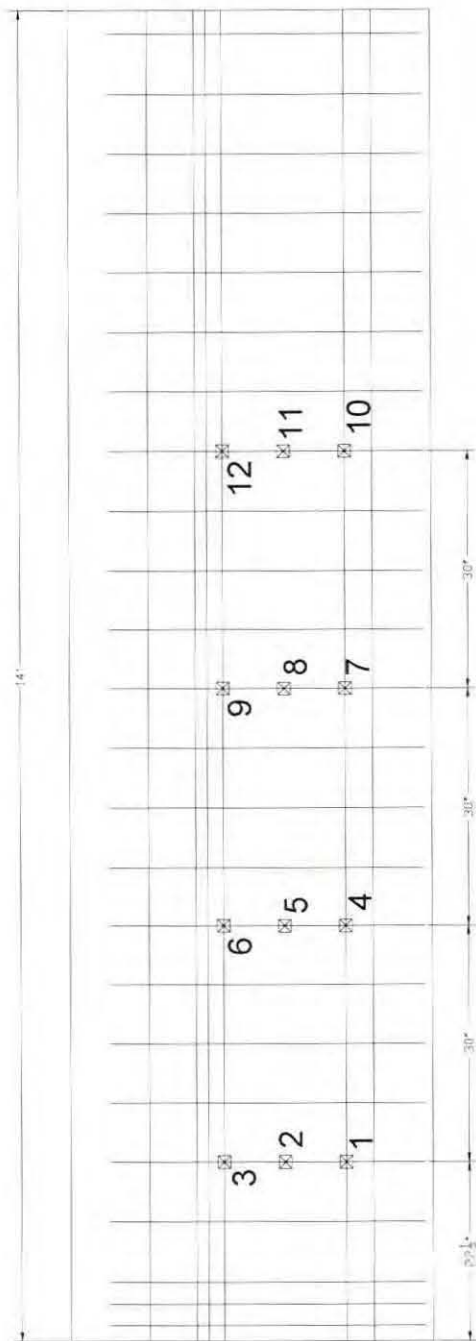
Stirrup Details

40' Girders  
(12-0.6" Dia. Type 270K Low Lax Strands)

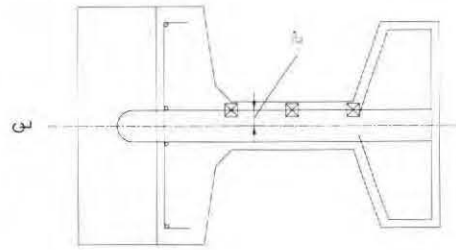
# APPENDIX D: GIRDER INSTRUMENTATION DETAILS







Typical  
Cross-Section



Cross-Section @ 22  $\frac{1}{2}$  ",  
52  $\frac{1}{2}$  ", 82  $\frac{1}{2}$  ", & 112  $\frac{1}{2}$  "

Stirrup Gage  
FLA-6-350-5LT



Table D.1 Girder AL Strain Gage Locations

Number	Type	DESIGN LOCATION			ACTUAL LOCATION		
		X (in)*	Y (in)*	Z (in)*	X (in)*	Y (in)*	Z (in)*
EM-1A-L	Embedded	7.5	28.5	0	6.75	28.5	0
EM-2A-L	Embedded	120	3.25	0	120	5.75	0
EM-3A-L	Embedded	120	26	0	120	25.75	0
EM-4A-L	Embedded	120	34	0	120	33.5	0
EM-5A-L	Embedded	120	38	0	120	38	0
EM-6A-L	Embedded	120	44	0	121.25	42.75	0
EM-7A-L	Embedded	120	44	11	121.25	42.75	11.5
EM-8A-L	Embedded	240	3.25	0	240	5.75	0
EM-9A-L	Embedded	240	26	0	240	26	0
EM-10A-L	Embedded	240	34	0	240	33.75	0
EM-11A-L	Embedded	240	38	0	240	38	0
EM-12A-L	Embedded	240	44	0	240	42.5	0
EM-13A-L	Embedded	240	44	11	240	42.5	11.5
PS-1A-L	Strand	120	2	-5	120.25	2	-5
PS-2A-L	Strand	120	4	-1	120	4	-1
PS-3A-L	Strand	120	6	11	120	6	11
PS-4A-L	Strand	120	2	11	120.5	2	11
PS-5A-L	Strand	240	2	-5	240	2	-5
PS-6A-L	Strand	240	4	-1	240.25	4	-1
PS-7A-L	Strand	240	6	11	240.25	6	11
PS-8A-L	Strand	240	2	11	240.25	2	11
PS-9A-L	Strand	2	4	5	2	4	5
PS-10A-L	Strand	14	4	5	14	4	5
PS-11A-L	Strand	26	4	5	26	4	5
PS-12A-L	Strand	38	4	5	38	4	5
PS-13A-L	Strand	2	4	-1	2	4	-1
PS-14A-L	Strand	14	4	-1	14	4	-1
PS-15A-L	Strand	26	4	-1	26	4	-1
PS-16A-L	Strand	38	4	-1	38	4	-1
PS-17A-L	Strand	132	2	-5	132.25	2	-5
PS-18A-L	Strand	132	2	11	132.25	2	11
PS-19A-L	Strand	144	2	-5	144	2	-5
PS-20A-L	Strand	144	2	11	144	2	11
ST-1A-L	Stirrup	22.5	11	2	22.5	11	2
ST-2A-L	Stirrup	22.5	18.75	2	22.5	18.75	2
ST-3A-L	Stirrup	22.5	26.5	2	22.5	26.5	2
ST-4A-L	Stirrup	52.5	11	2	23	11	2
ST-5A-L	Stirrup	52.5	18.75	2	23	18.75	2
ST-6A-L	Stirrup	52.5	26.5	2	23	26.5	2
ST-7A-L	Stirrup	82.5	11	2	83.25	11	2
ST-8A-L	Stirrup	82.5	18.75	2	83.25	18.75	2
ST-9A-L	Stirrup	82.5	26.5	2	83.25	26.5	2
ST-10A-L	Stirrup	112.5	11	2	113	11	2
ST-11A-L	Stirrup	112.5	18.75	2	113	18.75	2
ST-12A-L	Stirrup	112.5	26.5	2	113	26.5	2

\*Gage location is measured from centerline of bottom of Girder AL. Positive is right, negative is left when looking down girder from instrumented end.

Table D.2 Girder BL Strain Gage Locations

Number	Type	DESIGN LOCATION			ACTUAL LOCATION		
		X (in)*	Y (in)*	Z (in)*	X (in)*	Y (in)*	Z (in)*
EM-1	Embedded	7.5	28.5	0	7.75	28.25	0
EM-2	Embedded	120	3.25	0	120	6	0
EM-3	Embedded	120	26	0	120	26	0
EM-4	Embedded	120	34	0	120	34	0
EM-5	Embedded	120	38	0	120	38	0
EM-6	Embedded	120	44	0	121.5	43	0
EM-7	Embedded	120	44	11	121.5	43	11
EM-8	Embedded	240	3.25	0	240.5	6	0
EM-9	Embedded	240	26	0	240.5	26	0
EM-10	Embedded	240	34	0	240.5	33.5	0
EM-11	Embedded	240	38	0	240	38	0
EM-12	Embedded	240	44	0	241.5	43	0
EM-13	Embedded	240	44	11	241.5	43	11
PS-1	Strand	120	2	-5	120	2	-5
PS-2	Strand	120	4	-1	120	4	-1
PS-3	Strand	120	6	11	120.25	6	11
PS-4	Strand	120	2	11	120.25	2	11
PS-5	Strand	240	2	-5	239.25	2	-5
PS-6	Strand	240	4	-1	239.5	4	-1
PS-7	Strand	240	6	11	239.5	6	11
PS-8	Strand	240	2	11	239.5	2	11
PS-9	Strand	2	4	5	2.25	4	5
PS-10	Strand	14	4	5	14	4	5
PS-11	Strand	26	4	5	26	4	5
PS-12	Strand	38	4	5	38	4	5
PS-13	Strand	2	4	-1	2	4	-1
PS-14	Strand	14	4	-1	14	4	-1
PS-15	Strand	26	4	-1	26	4	-1
PS-16	Strand	38	4	-1	38	4	-1
PS-17	Strand	132	2	-5	132	2	-5
PS-18	Strand	132	2	11	132.25	2	11
PS-19	Strand	144	2	-5	144	2	-5
PS-20	Strand	144	2	11	144	2	11
ST-1	Stirrup	22.5	11	2	22	11	2
ST-2	Stirrup	22.5	18.75	2	22	18.75	2
ST-3	Stirrup	22.5	26.5	2	22	26.5	2
ST-4	Stirrup	52.5	11	2	51.25	11	2
ST-5	Stirrup	52.5	18.75	2	51.25	18.75	2
ST-6	Stirrup	52.5	26.5	2	51.25	26.5	2
ST-7	Stirrup	82.5	11	2	81	11	2
ST-8	Stirrup	82.5	18.75	2	81	18.75	2
ST-9	Stirrup	82.5	26.5	2	81	26.5	2
ST-10	Stirrup	112.5	11	2	112	11	2
ST-11	Stirrup	112.5	18.75	2	112	18.75	2
ST-12	Stirrup	112.5	26.5	2	112	26.5	2

\*Gage location is measured from centerline of bottom of Girder BL. Positive is right, negative is left when looking down girder from instrumented end.



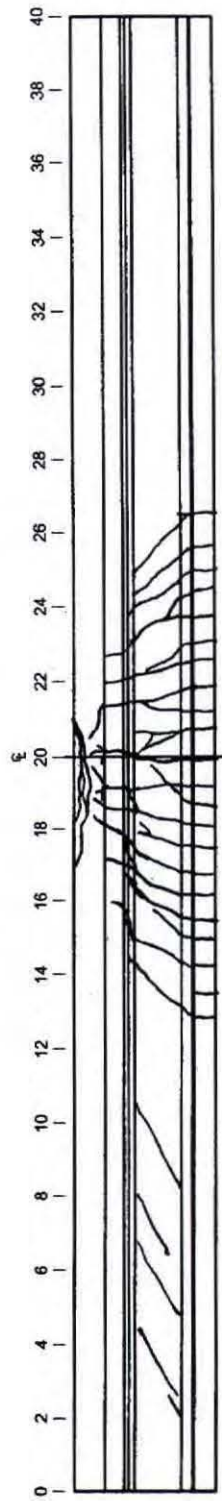
Table D.3 Girder CL Strain Gage Locations

Number	Type	DESIGN LOCATION			ACTUAL LOCATION		
		X (in)*	Y (in)*	Z (in)*	X (in)*	Y (in)*	Z (in)*
EM-1	Embedded	7.5	28.5	0	7.5	28.5	0
EM-2	Embedded	120	3.25	0	120.25	6	0
EM-3	Embedded	120	26	0	120.25	25.5	0
EM-4	Embedded	120	34	0	120.25	33.75	0
EM-5	Embedded	120	38	0	120	38	0
EM-6	Embedded	120	44	0	119	42.5	0
EM-7	Embedded	120	44	11	119	42.5	11
EM-8	Embedded	240	3.25	0	240	6.25	0
EM-9	Embedded	240	26	0	240	25.75	0
EM-10	Embedded	240	34	0	240	34	0
EM-11	Embedded	240	38	0	240.5	38	0
EM-12	Embedded	240	44	0	241	43	0
EM-13	Embedded	240	44	11	241	43	11
PS-1	Strand	120	2	-5	120	2	-5
PS-2	Strand	120	4	-1	119.5	4	-1
PS-3	Strand	120	6	11	120.5	6	11
PS-4	Strand	120	2	11	120	2	11
PS-5	Strand	240	2	-5	239.5	2	-5
PS-6	Strand	240	4	-1	239.5	4	-1
PS-7	Strand	240	6	11	240	6	11
PS-8	Strand	240	2	11	240	2	11
PS-9	Strand	2	4	5	2	4	5
PS-10	Strand	14	4	5	14	4	5
PS-11	Strand	26	4	5	26	4	5
PS-12	Strand	38	4	5	38	4	5
PS-13	Strand	2	4	-1	2	4	-1
PS-14	Strand	14	4	-1	13.5	4	-1
PS-15	Strand	26	4	-1	26	4	-1
PS-16	Strand	38	4	-1	38	4	-1
PS-17	Strand	132	2	-5	132	2	-5
PS-18	Strand	132	2	11	132	2	11
PS-19	Strand	144	2	-5	144	2	-5
PS-20	Strand	144	2	11	144	2	11
ST-1	Stirrup	22.5	11	2	21	11	2
ST-2	Stirrup	22.5	18.75	2	21	18.75	2
ST-3	Stirrup	22.5	26.5	2	21	26.5	2
ST-4	Stirrup	52.5	11	2	50.75	11	2
ST-5	Stirrup	52.5	18.75	2	50.75	18.75	2
ST-6	Stirrup	52.5	26.5	2	50.75	26.5	2
ST-7	Stirrup	82.5	11	2	81	11	2
ST-8	Stirrup	82.5	18.75	2	81	18.75	2
ST-9	Stirrup	82.5	26.5	2	81	26.5	2
ST-10	Stirrup	112.5	11	2	110.25	11	2
ST-11	Stirrup	112.5	18.75	2	110.25	18.75	2
ST-12	Stirrup	112.5	26.5	2	110.25	26.5	2

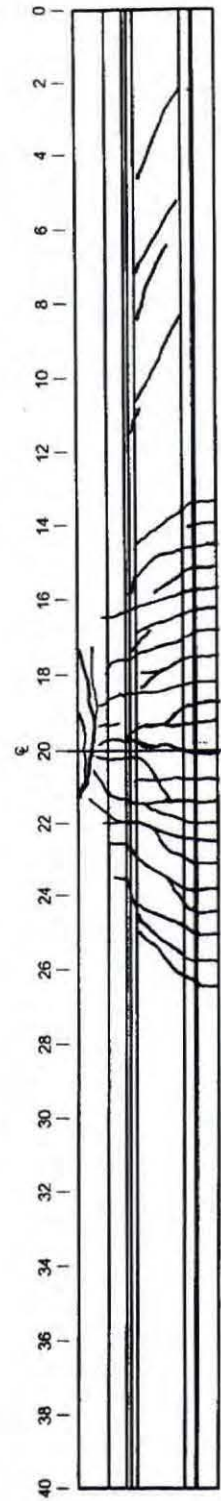
\*Gage location is measured from centerline of bottom of Girder CL. Positive is right, negative is left when looking down girder from instrumented end.

## APPENDIX E: CRACK MAPS

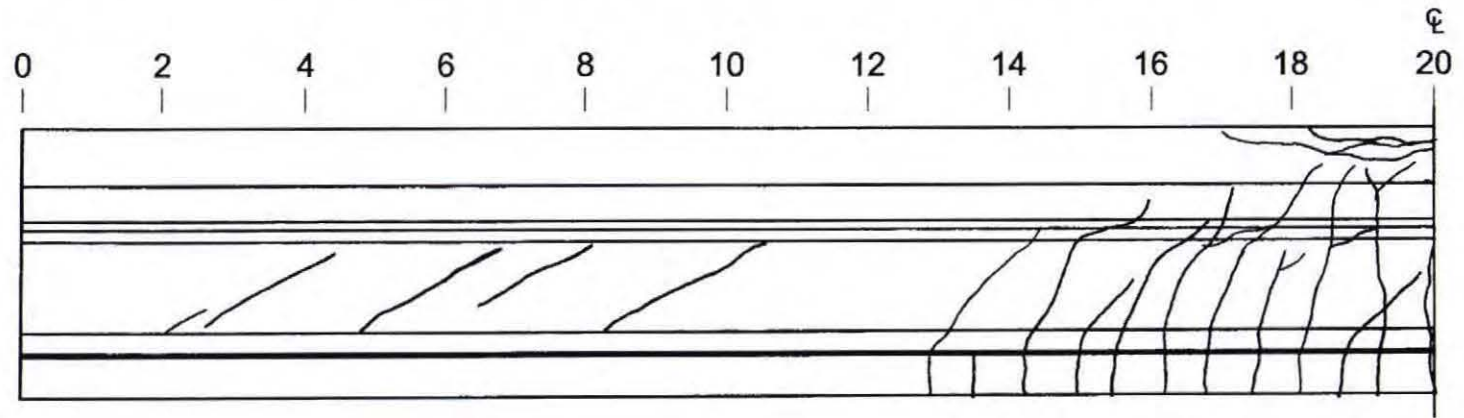
Girder A-L West Side Crack Map



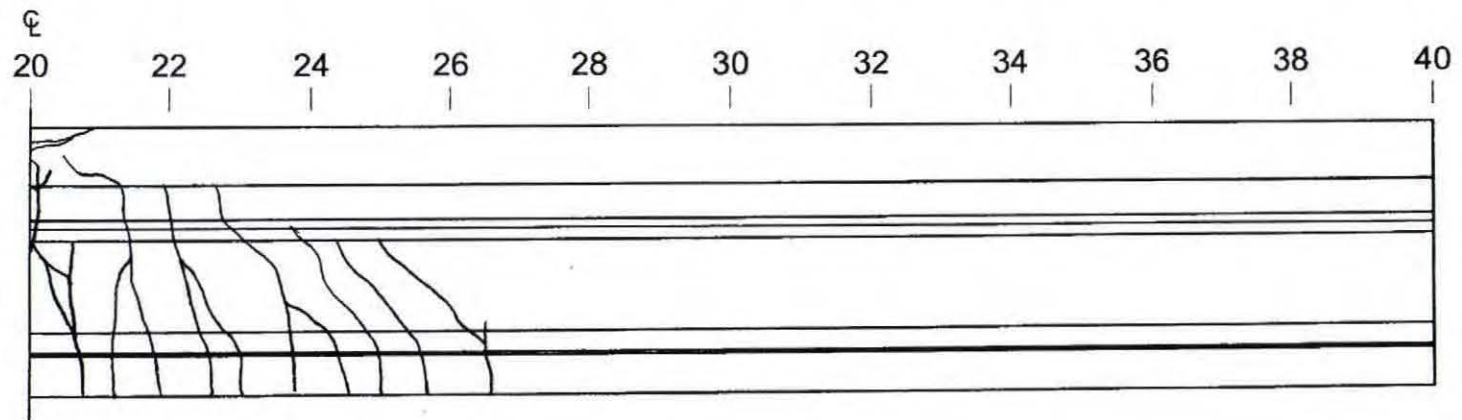
Girder A-L East Side Crack Map



## Girder A-L West Side-North End Crack Map

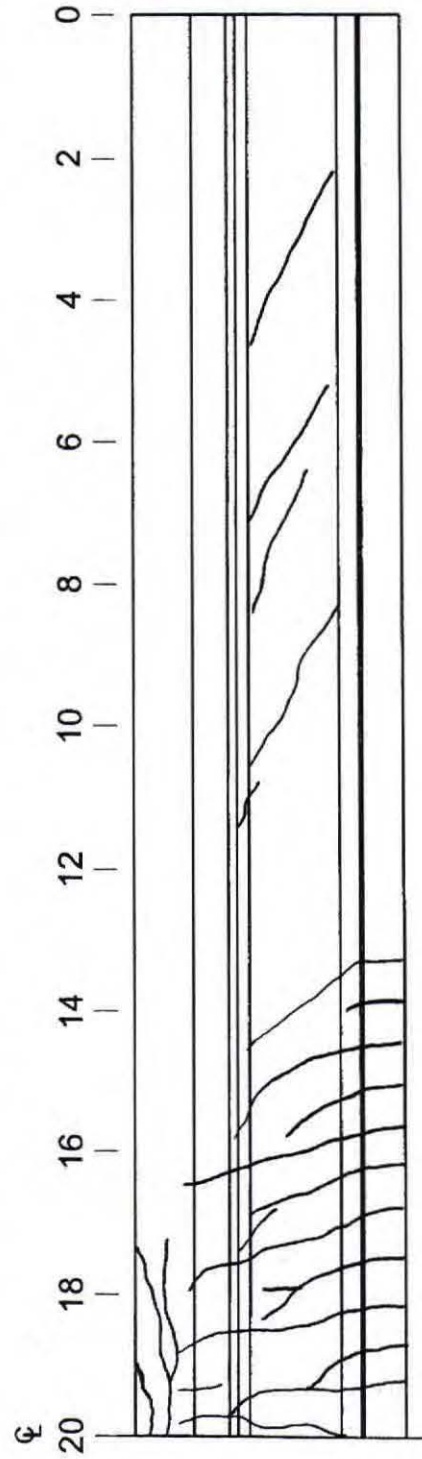


## Girder A-L West Side-South End Crack Map

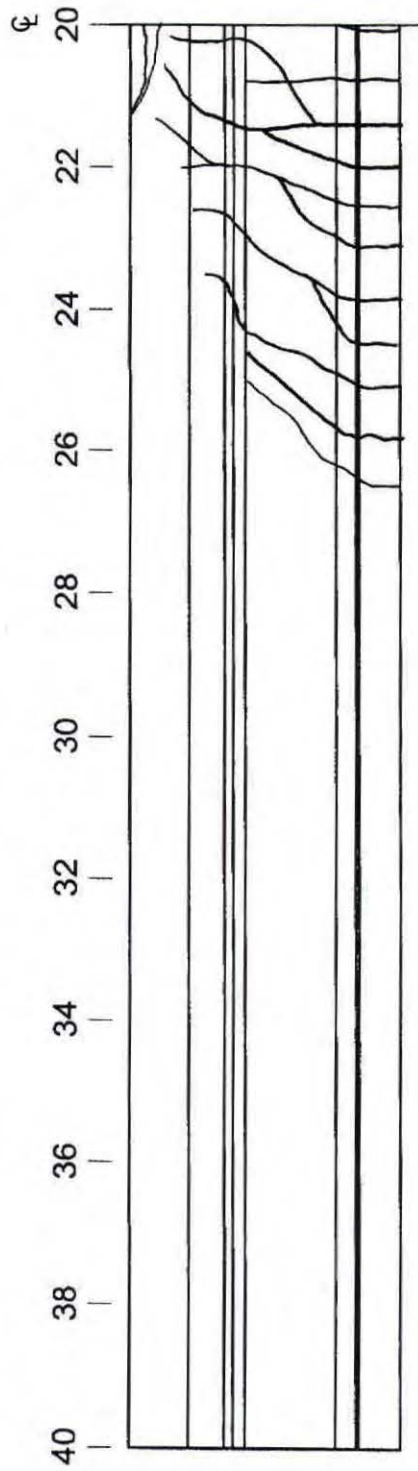




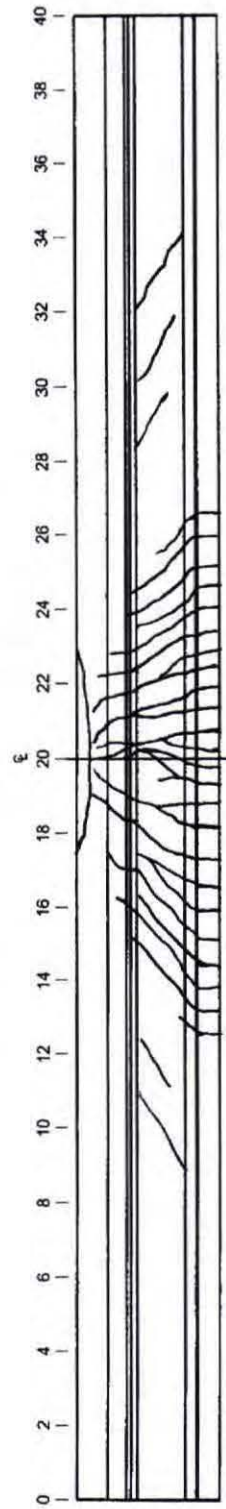
# Girder A-L East Side-North End Crack Map



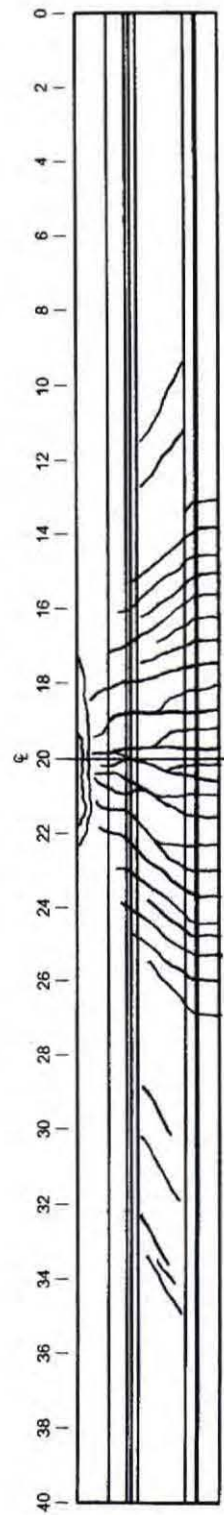
# Girder A-L East Side-South End Crack Map



Girder B-L West Side Crack Map

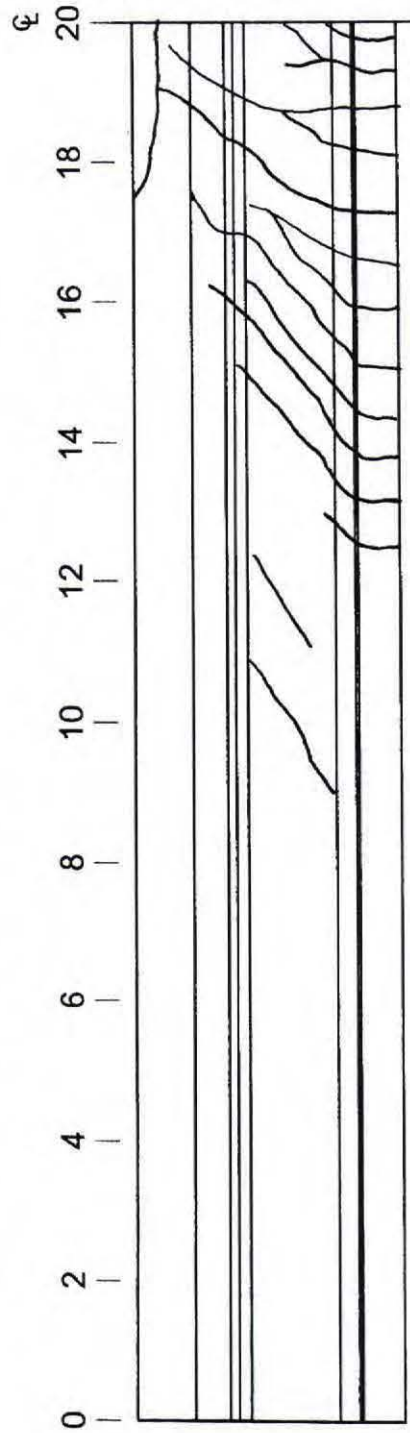


Girder B-L East Side Crack Map

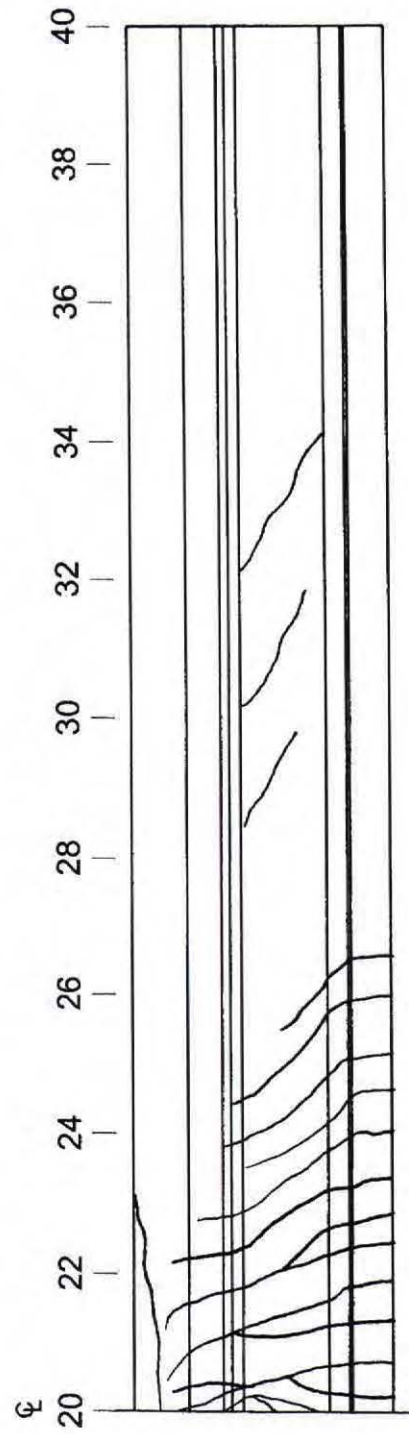




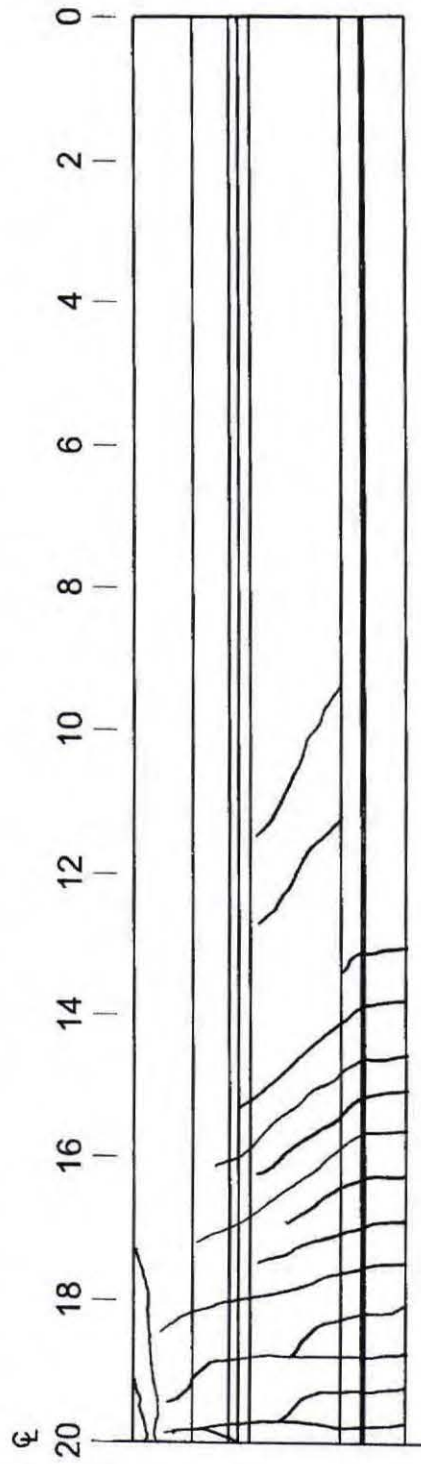
# Girder B-L West Side-North End Crack Map



# Girder B-L West Side-South End Crack Map

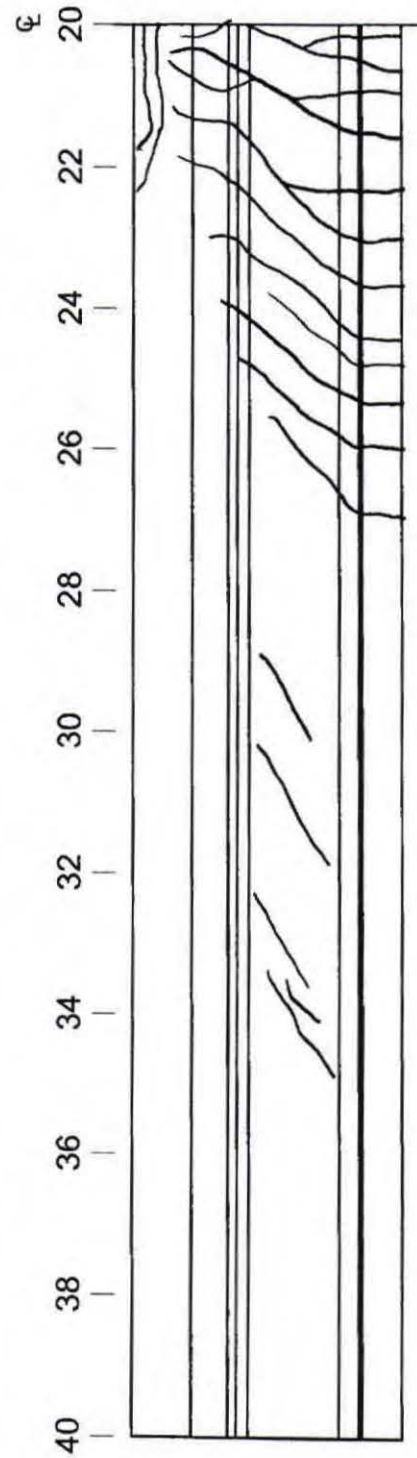


# Girder B-L East Side-North End Crack Map

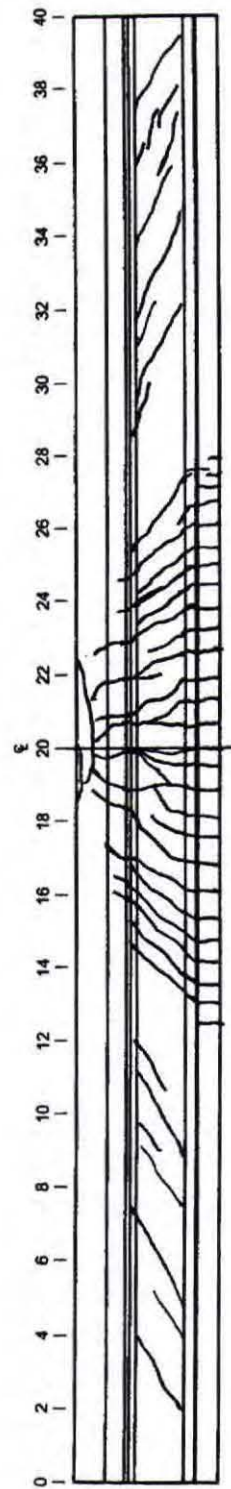




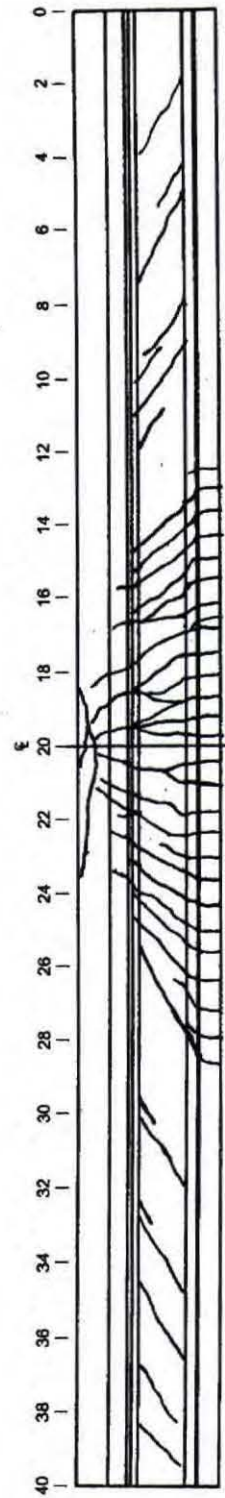
# Girder B-L East Side-South End Crack Map



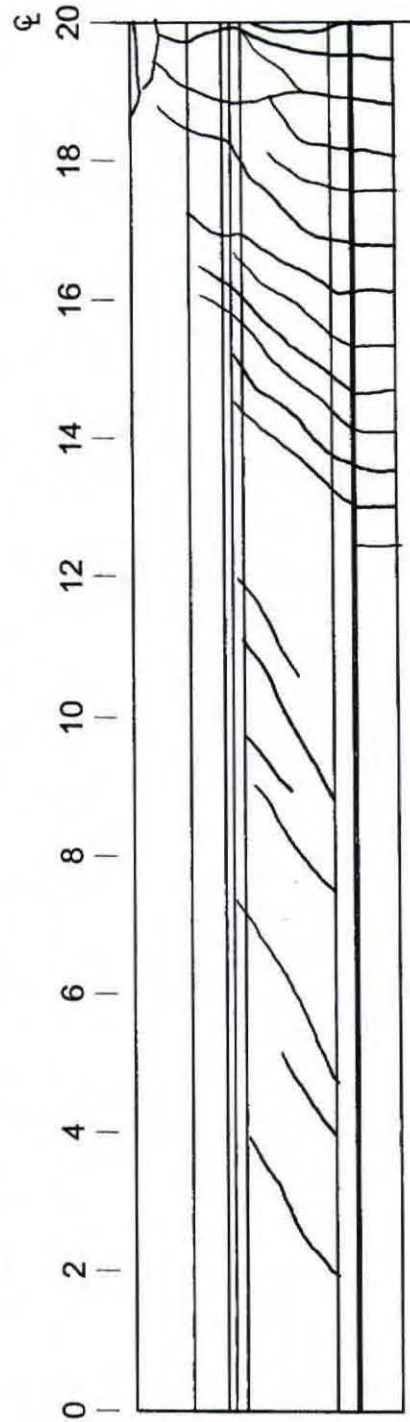
Girder C-L West Side Crack Map



Girder C-L East Side Crack Map

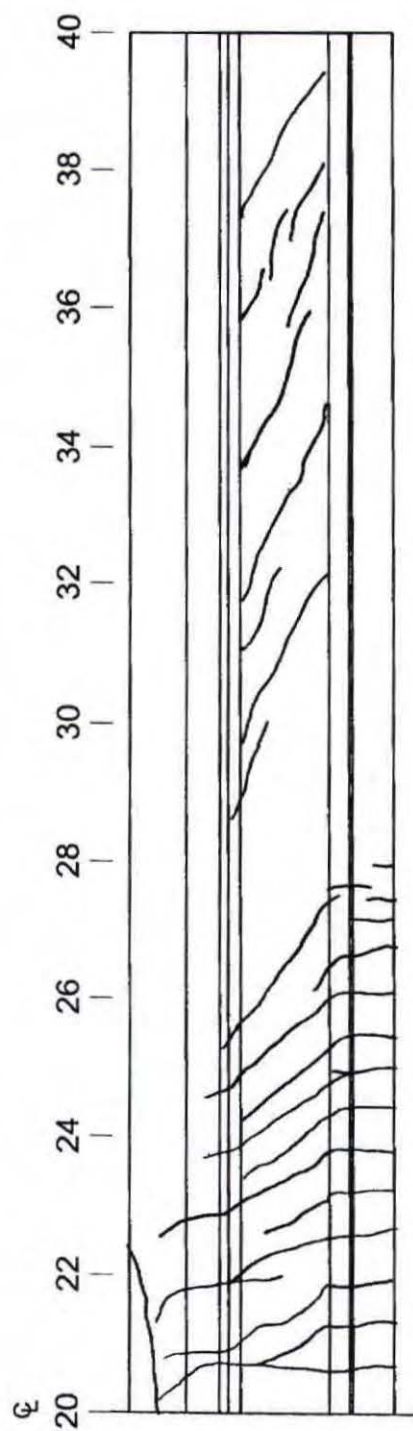


# Girder C-L West Side-North End Crack Map

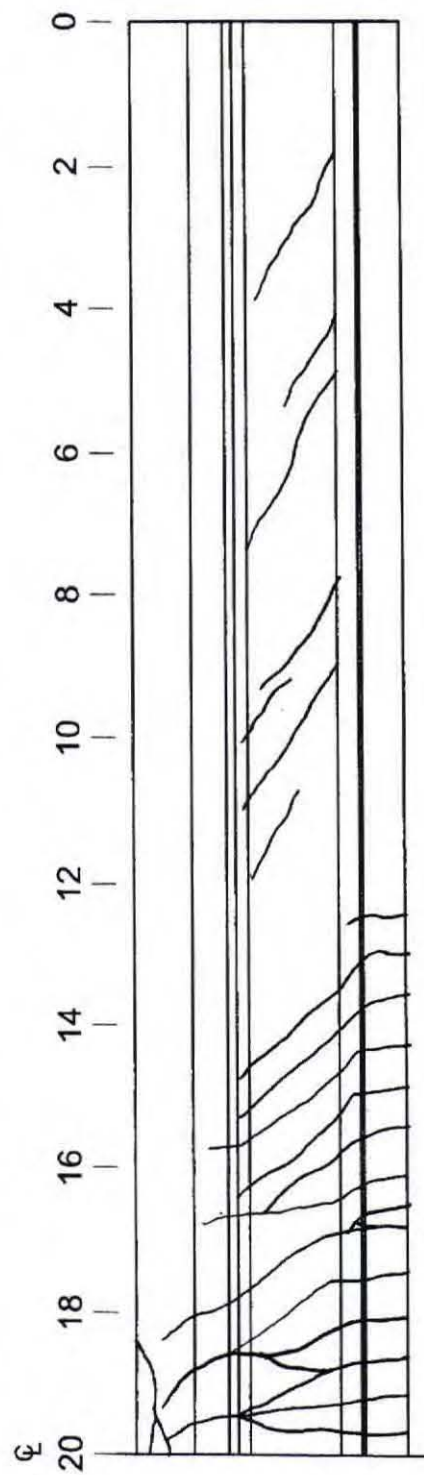




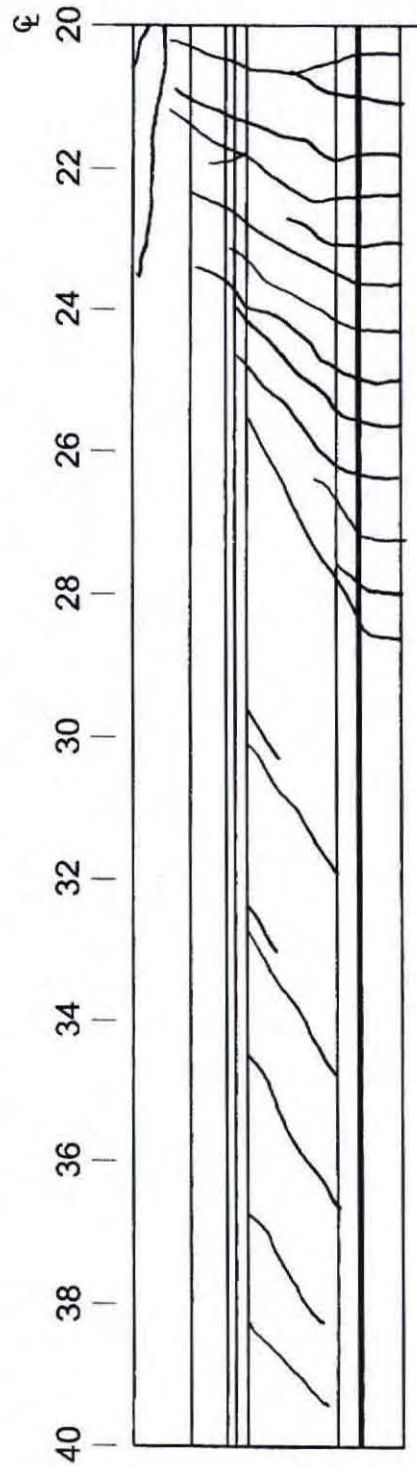
# Girder C-L West Side-South End Crack Map



# Girder C-L East Side-North End Crack Map



# Girder C-L East Side-South End Crack Map





## APPENDIX F: SPECIAL PROVISIONS

### STATE OF SOUTH DAKOTA DEPARTMENT OF TRANSPORTATION

#### SPECIAL PROVISION FOR SELF-CONSOLIDATING CONCRETE (SCC) FOR PRECAST/PRESTRESSED BRIDGE GIRDERS

November 17th, 2008

---

Delete Section 560 from the Standard Specifications in its entirety and replace it with the following revised specification:

##### 560.1 DESCRIPTION

This work consists of furnishing and installing precast and prestressed self-consolidating concrete (SCC) items.

##### 560.2 MATERIALS

###### A. Concrete:

1. **Fine Aggregate:** Section 800.
2. **Coarse Aggregate:** Course aggregate for SCC shall meet the requirements of Section 820 with the following exceptions:

Course aggregate used in SCC shall be either quartzite or limestone aggregate conforming to the following gradation requirements:

Sieve Size	Percent Passing	
	Quartzite	Limestone
5/8 inch (16.0 mm)	100	
1/2 inch (12.5 mm)	90 to 100	100
3/8 inch (9.50 mm)	70 to 90	90 to 100
No. 4 (4.75 mm)	0 to 30	0 to 20
No. 8 (2.36 mm)	0 to 15*	0 to 5*

\* The combined mixture of fine and coarse aggregate shall be such that not more than 1.5 percent passes the No. 200 (75  $\mu$ m) sieve.

3. **Water:** Section 790.
4. **Admixtures:** Section 751 and 752. The Contractor may use viscosity modifying admixtures (VMA) to attain the desired SCC performance. VMA for use in SCC must meet the requirements of ASTM C 1017.

5. **Cement:** Section 750. Type I/II Portland Cement shall be used for all SCC. No substitutions will be allowed.

**B. Pretensioning Reinforcement:** Section 1010.

**C. Reinforcing Steel:** Section 1010.

**D. Drainage Fabric:** Section 831.1 – Type A.

### 560.3 CONSTRUCTION REQUIREMENTS

**A. General Requirements:** The Contractor shall satisfy the following for all precast/prestressed SCC items.

1. **Fabrication:** Fabricators shall be on the approved fabricators list prior to fabricating precast and prestressed SCC items.

2. **Concrete Mix Requirements:** The Contractor shall submit a concrete job mix design for approval ten working days prior to fabrication. The mix design shall include all aggregate sources, admixtures proposed for use.

- a. **Minimum Cementitious Content:** The SCC shall contain a minimum cementitious content of 700 pound per cubic yard (415 Kilograms per cubic meter).

- b. **Maximum Water Cementitious Ratio:** The mix design shall establish a maximum water cementitious ratio for all SCC produced. This maximum water cement ratio shall never exceed 0.37

- c. **Minimum Course Aggregate Content:** Minimum course aggregate content shall be 40 percent of the aggregate content.

- d. **Entrained Air Content Range:** The SCC shall contain an entrained air content of between 4.5 and 7.5 percent. The procedure for testing of entrained air content shall be performed as described in SD 403 with the following exceptions:

The air content meter bucket shall be filled in one continuous lift. Rodding of the concrete shall not be permitted. Light tamping by hand on the side of the bucket may be allowed to remove cavities and large air bubbles.

- e. **Slump Flow at Time of Placement:** The slump flow at time of placement for SCC shall be between twenty and twenty-eight inches (20" - 28") when tested according to ASTM C 1611/C 1611M - 05, filling procedure B (inverted mold).

- f. **Visual Stability Index (VSI) at Time of Placement:** The VSI of the SCC at the time of placement shall not exceed 1 when tested according to ASTM C 1611/C 1611M - 05.

- g. **Difference between J-Ring Spread and Slump Flow Spread:** The difference between the J-Ring spread and the slump flow spread shall not be greater than 2.0 inches. The J-Ring spread shall be tested according to ASTM C 1621/C 1621M - 06. The slump flow spread shall be tested according to ASTM C 1611/C 1611M - 05, filling procedure B (inverted mold).

- h. **Minimum 28 Day Compressive Strength:** The SCC shall obtain a minimum 28 day compressive strength equal to or greater than the minimum compressive strength

specified. The procedure for filling molds and beams shall be performed as described in SD 405 with the following exceptions:

The concrete cylinder molds shall be filled in one continuous lift. Rodding of the concrete shall not be permitted. Light tamping by hand on the side of the mold may be allowed to remove cavities and large air bubbles.

The absolute volume of mix proportions shall yield 27.0 to 27.25 cubic feet.

All mix designs and any modifications thereto, including changes in admixtures, shall be submitted with mix design. Mix design data and test results shall be recorded on a DOT Form 24 and submitted to the Engineer.

Equipment and methods used for batching, mixing, and transporting of concrete shall be approved by the Engineer.

3. **Shop Drawings:** Fifteen days prior to fabrication, the Contractor shall furnish shop drawings for Department review. The shop drawings shall consist of fabrication details including reinforcing steel and spacer placement and configurations, total quantities for the complete structure, and all information necessary for fabrication and erection.

Shop drawings for prestressed SCC items shall also include the method and sequence of stressing.

4. **Forms:** The forms shall be designed to withstand the fluid pressure of the concrete without distortion. The forms shall be mortar tight and free from warp.

The form area in contact with the concrete shall be treated with an approved form oil or wax before the form is set in position. The forms shall be thoroughly cleaned of all other substances.

5. **Concrete Cure:** The concrete shall be cured by low pressure steam, radiant heat, or as specified in Section 460.3 N. When curing in accordance with Section 460.3 N, the concrete temperature requirements of Section 460.3 O shall apply.

Low pressure steam or radiant heat curing shall be done under an enclosure to contain the live steam or the heat and prevent heat and moisture loss. The concrete shall be allowed to attain initial set before application of the steam or heat. The initial application of the steam or heat shall be three hours after the final placement of concrete to allow the initial set to occur. When retarders are used, the waiting period before application of the steam or radiant heat shall be five hours. When the time of initial set is determined by ASTM C 403, the time limits described above may be waived.

During the waiting period, the minimum temperature within the curing chamber shall not be less than 50° F (10° C) and live steam or radiant heat may be used to maintain the curing chamber between 50° F (10° C) and 80° F (27° C). During the waiting period the concrete shall be kept moist.

Application of live steam shall not be directed on the concrete forms causing localized high temperatures. Radiant heat may be applied by pipes circulating steam, hot oil, hot water, or by electric heating elements. Moisture loss shall be minimized by covering exposed concrete surfaces with plastic sheeting or by applying an approved liquid membrane curing compound to exposed concrete surfaces. The top surface of concrete members for use in composite construction shall be free of membrane curing compound residue unless suitable mechanical means for full bond development are provided.



During the initial application of live steam or radiant heat, the concrete temperature shall increase at an average rate not exceeding 40° F (22° C) per hour until the curing temperature is reached. The maximum concrete temperature shall not exceed 160° F (71° C). The maximum temperature shall be held until the concrete has reached the desired strength. After discontinuing the steam or radiant heat application, the temperature of the concrete shall decrease at a rate not to exceed 40° F (22° C) per hour until the concrete temperature is within 20° F (11° C) of the ambient air temperature. The Contractor will not be required to monitor this cool down temperature when the ambient air temperature is 20° F (11° C) or above.

The test cylinders shall be cured with the unit, or in a similar manner (similar curing method and concrete curing temperature, as approved by the Concrete Engineer) as the unit, until minimum compressive strength has been obtained

6. **Surface Finish and Patching:** If a precast or prestressed item shows stone pockets, honeycomb, delamination or other defects which may be detrimental to the structural capacity of the item, it will be subject to rejection at the discretion of the Engineer. Minor surface irregularities or cavities, which do not impair the service of the item, and which are satisfactorily repaired will not constitute cause for rejection. Repairs shall not be made until the Engineer has inspected the extent of the irregularities and has determined whether the item can be satisfactorily repaired. If the item is deemed to be repairable, the repair method and procedures shall be agreed upon by the Department and fabricator prior to the work commencing.

Depressions resulting from the removal of metal ties or other causes shall be carefully pointed with a mortar of sand and cement in the proportions, which are similar to the specific class of concrete in the unit. A sack rub finish is required on prestressed beams except for the bottom of the bottom flange and the top of the top flange. A sack rub finish is also required on sloped surfaces of box culvert end sections.

**B. Precast Box Culverts:** The following shall apply to box culverts:

1. **Design:** Precast concrete box culverts shall conform to AASHTO M 259 or M 273. Configurations in variance with those provided by AASHTO will be accepted provided the AASHTO materials, design, fabrication specification and the requirements of this Section are complied with.

Box culvert end sections (inlet or outlet) materials, design, and fabrication shall conform to AASHTO Standard Specifications for Highway Bridges and Materials Specifications.

Precast box culverts shall be designed to specified load conditions. The Design Engineer of the structure must be registered in the State of South Dakota. The design shall conform to the AASHTO design requirements for the depth of fill, including surfacing, etc., as well as live load or specified loading. The specified live load shall apply to all barrel sections.

Minimum reinforcing steel clear cover shall be 1 inch (25mm) for all member faces. The exception to this is that box culverts covered by a fill of less than 2 feet (0.6 m) shall have a minimum reinforcing steel clear cover of 2 inches (50 mm) in the top of the top slab.

The Contractor shall furnish a checked design with the shop drawings. A checked design includes the design calculations, and check design calculations performed by an independent Engineer.

A checked design for barrel sections will not be required to be submitted if the proposed fabrication dimensions and reinforcement conform to AASHTO M 259M or M 273M. A checked design for the end sections and special sections will be required.

- 2. Fabrication:** The Contractor shall notify the Engineer seven days prior to fabrication.

Limite vibrating may be allowed when necessary, as approved by the engineer.

The minimum length of precast section shall be four feet. (1200 mm)

Welding of reinforcing steel will not be permitted.

Joint ties shall be provided on all sections.

Steel wire bar supports shall be used to maintain proper reinforcement location and concrete cover. Cutting of reinforcement and bending to the form surface, for support, will not be permitted. Steel wire bar supports, in contact with the casting forms, shall be stainless steel, hot dipped galvanized, or plastic tipped extending at least ½ inch (13 mm) from the form surface.

The surface temperature of forms and reinforcing steel (that come in contact with the concrete being placed) shall be raised to a temperature above freezing prior to concrete placement. All deleterious material shall be removed from the forms prior to concrete placement.

The dry casting method of fabrication for precast concrete box culverts will not be allowed.

The precast units shall have sufficient strength to prevent damage to the units during removal of the forms and yarding. Precast units shall have a minimum concrete compressive strength of 800 psi (5.5 MPa) prior to form removal. Precast units shall have a minimum concrete compressive strength of 3000 psi (21 MPa) prior to yarding. The Engineer may approve a different minimum concrete strength for form removal and yarding, based upon fabricator demonstrated results or as shown on design details submitted and approved with the shop plans.

The fabricator shall make a minimum of one group of test cylinders for each class of concrete for each day's production, not to exceed 150 cubic yards (125 cubic meters) per group of cylinders.

At a minimum, a group of test cylinders shall consist of the following:

- a. Two test cylinders are required for the 28 day compression test.
- b. Two additional cylinders will be required for determining concrete strength, when the Contractor desires to make delivery and obtain acceptance by the Department prior to the 28 day compression test.

Acceptance of the precast units shall be in accordance with Section 460.3 B. The precast units will be accepted when the minimum design concrete compressive strength requirements have been met. Accepted precast units represented by that test group of cylinders may be delivered to the project and will not require the 28 day cylinder test.

- 3. Installation:** Box culvert installation shall conform to the approved shop drawings and the following:

- a. **Foundation:** Foundation preparation shall be in accordance with Sections 420, 421, and 450. The foundation shall be shaped to provide a satisfactory template section and density.



- b. **Transverse Joints:** The floor joint between adjacent sections shall be sealed with a preformed mastic along the floor to the top of the haunches. Fabric shall be placed along the top and walls, to provide a minimum of 2 ½ feet (750 mm) of fabric centered on the joint. Transverse joints in the fabric shall be overlapped at least two feet (600 mm). Sufficient adhesive shall be required along the edge of the fabric to hold it in place while backfilling. The lift holes shall be plugged with an approved non-shrink grout or as shown on the approved shop drawings.

The maximum allowable gap at any point between adjacent sections of box culvert shall be 1" (25 mm).

- c. **Joint Ties:** Each section shall be tied to adjacent sections with joint ties as shown on the approved shop drawings.
- d. **Backfilling:** Backfilling shall conform to Section 450. Hand compaction methods may be required for satisfactory compaction under and adjacent to corners with radius and between culverts on multiple installations.

**C. Prestressed Concrete:** The following shall apply to all prestressed SCC products:

1. **General:** The Contractor shall notify the Engineer at least seven days prior to fabrication to permit inspection of the forms and reinforcement by Department personnel.

The Contractor shall have a PCI Level II Certified technician, skilled in the prestressing method used, available to provide assistance and instruction in the use of the prestressing equipment and installation of materials.

Prestressing shall be by the pretensioning method. All common or similar elements shall be prestressed using the same method.

The Contractor shall prevent damage to prestressing steel that weakens the prestressing steel or may cause failure under stress. Nicking, kinking, or twisting of the prestressing steel will not be permitted. Sparks or pieces of molten metal from welding or burning equipment shall not contact any prestressing steel. The use of prestressing steel as a ground for welding equipment will not be permitted. The cutting of surplus tendons by burning will be permitted providing the burning is done rapidly and neatly. The term "prestressing steel" shall be that portion of the prestressing tendons, which will be incorporated in the work.

2. **Forms:** Forms shall comply with Section 423.3 and the following:

Joints in sectional forms shall have a tight fit without excessive offset.

Forms shall be set on a rigid foundation and the soffit form shall be a plane surface at right angles to the vertical axis of the beam.

The beams shall be accurately cast to the dimensions shown in the plans or in the shop drawings. Requests for minor shape changes to accommodate the available forms shall be accompanied by design calculations.

3. **Steel Units:** Reinforcement and tendons shall be placed in the position specified and securely held during the placing and setting of the concrete. The distances between the forms and steel shall be maintained by metal bar chairs, spacers, hangers, and precast mortar or concrete blocks of approved shape and dimensions. Metal devices in contact with the forms shall be galvanized. Distances between layers of units shall be maintained



by metal spacers, precast mortar, or concrete blocks. Welding of reinforcement or tendons will not be allowed.

Loose rust, dirt, oil, or other foreign substances shall be removed from the prestressing tendons before the side forms are erected.

The hold down devices for deflected strands shall provide for the removal of the device for a distance of one inch (25 mm) or more from the exposed face of the concrete and the resulting hole patched with mortar. As an alternative, the device shall rest on the bottom form and remain in place after concrete placement. When the hold down devices are to remain in place, the portion of the devices in contact with the forms shall be galvanized for a minimum distance of one inch (25 mm).

#### 4. Tensioning:

- a. **Equipment:** Equipment, tools, and machinery used in the work shall be adequate for the purpose for which they are to be used and shall be appropriately maintained.

In all methods of tensioning, the stress induced in the prestressing elements shall be measured both by jacking gages and by elongation of the elements. The results shall check as specified in paragraph two below. Means shall be provided for measuring the elongation of reinforcement to the nearest 1/16 inch (whole millimeter). Stressing devices, whether hydraulic jacks or screw jacks, shall be equipped with accurate calibrated pressure gages, rings, or other devices applicable to the type of jack being used. Jacks, gages, and pumps shall be calibrated as a unit by a competent laboratory under conditions similar to operating conditions. A dated, certified calibration curve shall be furnished for each combination used. Calibration of jacks, gages, and load cells shall be repeated annually or after an overhaul. Recalibration will be required for all equipment that produces erratic results during tensioning operations.

The sensitivity and accuracy of the gages shall be such that at final elongation the total load on the jack(s) can be accurately determined within a tolerance of five percent of the total indicated stress at that time.

- b. **General Procedures:** The tensioning procedure shall be conducted so the indicated stress on the tendons based on gage pressures and the indicated stress based on the corresponding elongation of the tendons may be measured and compared at any time. When the two indicated stresses, corrected for friction loss, differ by five percent or less, the tendons shall be stressed so the lower of the two indicated stresses is equal to the required tension in the tendon. If the difference exceeds five percent, tensioning operations shall cease until the source of the discrepancy has been determined and corrected. Alternate stressing procedures shall be approved by the Engineer prior to fabrication.

Tendons shall be tensioned to produce the forces shown in the plans, or on the approved working drawings with appropriate allowances for all losses. Losses to be provided for shall be as specified in Section 9.16 of Division I, Design, of the AASHTO Standard Specifications for Highway Bridges. The maximum temporary stress (jacking stress) and the stress in the steel before loss due to creep and shrinkage shall not exceed the values allowed in Section 9.15 of Division I, Design, of the AASHTO Specifications.

Each strand shall be given an initial tension of such magnitude and shall be supported at such intervals that the strand is straightened and the slack removed before jacking is started. Strands tensioned as a group shall have the same initial tension and all strands in the group shall be from the same manufacturer.



The tensioning of deflected strands shall be done so that the final tension in all parts of the strand is uniform and means shall be provided to reduce frictional forces at the bend points to a minimum. Hold down devices shall contain rollers to aid in minimizing the effects of friction.

Tension elongation measurements shall be corrected for losses as determined in the field due to slippage of wedges or anchorages, and friction, to obtain the required prestress force in the strands after anchorages are set.

Appreciable changes in elongation of the strands due to a temperature differential in the strands between the tensioning and time of concrete placement shall be considered in the final elongation measurements to obtain the required prestress force at the time of casting. The change in elongation due to temperature shall be based on 1/8 inch per 100 feet (3 mm per 30 meters) of strand length for each 15° F (10.0° C) variation in temperature. Temperature corrections shall be performed as per PCI standards and details of temperature corrections shall be submitted prior to fabrication.

5. **Placement of Concrete:** The surface temperature of the forms and reinforcing steel, which come into contact with the concrete being placed, shall be raised to a temperature above freezing prior to concrete placement. All deleterious material shall be removed from the forms prior to concrete placement.

Beams shall be cast in an upright position and the concrete shall be placed in continuous lifts not exceeding one half the depth of the beam. A continuous flow of concrete from end to end of the beam may be permitted provided segregation of the concrete is not taking place. Cold joints or initial set between lifts will not be allowed.

The rate of placement shall be maintained at a minimum rate such that no cold joints exist in the beam.

Limited vibrating may be allowed, when necessary, as approved by the Engineer.

The top surface of the beam shall be float finished to seal the surface and depress the coarse aggregate. After finishing and prior to initial set, the top surface shall be given a transverse grooving. The grooves shall be approximately 1/4 inch (6 mm) deep by 1/4 inch (6 mm) wide at one inch (25 mm) spaces. The top surface of the outside edges of the top flange shall be finished with a concrete edging tool for the full length of the beam. The edging tool shall be of sufficient size to produce a smooth finish for approximately the outside 3 inches (75 mm) of flange top width. In addition, a smooth spot shall be left at the span tenth points.

6. **Form Removal:** When side forms are removed from the curing chamber before the curing cycle (including temperature cooling process) is complete, only the minimum area of the curing chamber enclosure shall be removed and remain uncovered at any one time. The open area in the enclosure shall be immediately closed as each form section is removed. The enclosure shall not remain open for more than 60 minutes.

When the Contractor elects to remove the beams from the casting bed during the cooling process, appropriate measures shall be taken to keep the beams warm during moving operations, and shall immediately resume the cooling process at the storage area.

7. **Curing:** The Contractor shall provide all approved continuous recording thermometers located in each enclosure and curing chamber. Two recording thermometers shall be provided for each casting chamber having a casting bed length of 100 feet (30 meters) or less. For each additional 100 feet (30 meters) or less in the length of the casting bed,

within each chamber, an additional thermometer shall be provided. The thermometers shall record temperatures at intervals not to exceed 15 minutes and have an accuracy of plus or minus 5° F (3° C).

Complete temperature recording charts for all cures shall be submitted to the Engineer prior to acceptance of the beams. If the records indicate that the specified temperature and time element pertaining to the curing are not being complied with, the affected beams will be subject to rejection.

Curing shall be maintained until the concrete has gained sufficient strength for prestress transfer.

8. **Prestress Transfer:** For pretensioned beams, the prestress transfer shall not be made until the control cylinders, cured with the beams, indicate that the concrete has reached the compressive strength specified in the plans, or as amended by the approved shop drawings.

Detensioning shall be accomplished after the steam or radiant heat curing has been discontinued and before the concrete temperature drops below 65° F (18° C).

The prestress transfer sequence shall keep the lateral eccentricity of the prestress to a minimum and shall prevent cracking in the top flange of the beams.

In addition, the prestress transfer shall be made in accordance with the following:

When steam or other added heat is used for cure, the prestress transfer shall be made while the concrete in the beams is still warm and moist.

The prestress transfer may be made by the gradual release of hydraulic jacks, by heating exposed portions of individual strands to failure, or shall be completed as detailed in approved production procedures.

When heating of individual strands is employed, it shall be subject to the following:

Heating of each individual strand shall be done simultaneously on the strand at a minimum of two locations along the casting bed. The sequence of heating each strand along the bed, the sequence of prestress transfer between individual strands, and the sequence of release of the hold downs for deflected strands for the prestress transfer shall be such that no deleterious effect will result. A schedule of the proposed prestress transfer operations shall be submitted with the shop drawings.

Heating shall be done with a large, low oxygen flame along the strand for a minimum distance of five inches (125 mm). The application of heat shall be controlled so that failure of the first wire in the strand does not occur for at least five seconds after heat is applied, followed by gradual elongation and failure of the remaining wires. If the release is not gradual and damages the beam, this method of release shall be discontinued.

9. **Tolerances:** Dimensional tolerances of the completed beams shall not exceed the dimensional tolerances specified in the current edition of Prestressed Concrete Institute Manual for Quality Control for Plants and Production of Precast Prestressed Concrete Products.

10. **Handling, Storage, Transportation, and Installation:** Pretensioned beams may be moved from the casting bed to the storage yard after the prestress transfer strength has been reached but shall not be removed from the casting yard or installed until they have



reached the specified minimum design compressive strength, as indicated by the test cylinders cured with the beams.

Prestressed beams shall remain in an upright position at all times. The beams shall be supported during storage, lifting, and transportation at only two points. During lifting and transporting, each point shall be not farther from the end of the beam than the depth of the beam. During storage, the points shall not be farther from the end of the beam than one third the depth of the beam.

The prestressed concrete beams shall be installed and fastened in accordance with the details shown in the plans.

**D. Frequency of Testing:** Sampling and testing by the Department shall be in accordance with the Materials Manual with the following exceptions:

**1. First Three Truckloads:** The fresh (plastic) concrete tests listed in Section 460.3 T.2 shall be performed on the concrete from the first three truckloads of any individual concrete placement. Sampling of the concrete for this application shall be at the beginning of the batch after 5 gallons of concrete has been discharged from the mixing drum. The slump flow spread and the J-Ring spread tests shall be performed concurrently or subsequently with no more than two minutes elapsed time between the slump flow spread and the J-Ring spread tests.

**2. Subsequent Truckloads:** After the first three truckloads, fresh (plastic) concrete tests shall be performed on the concrete from all subsequent truckloads at the following frequency:

**a. Slump Flow Spread:** Slump flow spread shall be tested at a rate of every conveyance.

**b. J-Ring Spread:** J-Ring spread shall be tested at a rate of one out of every two conveyances.

The slump flow spread and the J-Ring spread tests shall be performed on the same conveyance. The slump flow spread and the J-Ring spread tests shall be performed concurrently or subsequently with no more than two minutes elapsed time between the slump flow spread and J-ring spread tests.

**c. Entrained Air Content:** Entrained air content shall be tested at a rate of one out of every four conveyances.

**d. Unit Weight:** Unit weight shall be tested at a rate of one out of every four conveyances.

**e. Temperature:** Temperature shall be tested at a rate of every conveyance.

#### 560.4 METHOD OF MEASUREMENT

**A. Prestressed Concrete Beam:** Measurement of prestressed beams will not be made. Plans quantity will be used for payment.

**B. Furnishing Precast Box Culvert:** Measurement for furnishing precast box culverts will not be made. Plans quantity shall be used for payment.

- C. Installing Precast Box Culvert:** Measurement for installing precast box culvert will not be made. Plans quantity shall be used for payment
- D. Furnishing Precast Box Culvert End Sections:** Furnishing precast box culvert end sections will be measured per each. One end section will be considered to be all of the individual pieces required to construct one end of the box culvert.
- E. Installing Precast Box Culvert End Sections:** Installing precast box culvert end sections will be measured per each. One end section will be considered to be all of the individual pieces required to construct one end of the box culvert.

#### **560.5 BASIS OF PAYMENT**

- A. Prestressed Concrete Beam:** Prestressed concrete beams will be paid at the contract unit price per foot (meter). Payment will be full compensation for furnishing and installing the prestressed concrete beam, and all other incidentals.
- B. Furnishing Precast Box Culvert:** Furnish precast box culvert will be paid for at the contract unit price per 0.1 foot (0.1 meter). Payment will be full compensation for furnishing the box culvert, joint seal mastic, drainage fabric, and joint ties.
- C. Installing Precast Box Culvert:** Installing precast box culvert will be paid for at the contract unit price per 0.1 foot (0.1 meter). Payment will be full compensation for precast box culvert installation and will include compensation for foundation preparation, backfilling, and all other incidentals.
- D. Furnishing Precast Box Culvert End Sections:** Furnishing precast box culverts will be paid for at the contract unit price per each.
- E. Installing Precast Box Culvert End Sections:** Installing precast box culvert end sections will be paid for at the contract unit price per each.

\* \* \* \* \*